DESIGN AND DEVELOPMENT OF A PARTICULATE EMISSION MONITOR

A thesis submitted to the University of London for the degree of Doctor of Philosophy

by

Stylianos Gerazounis

Department of Chemical Engineering
University College London
Torrington Place
London WC1E 7JE

April 2000

ProQuest Number: U643987

All rights reserved

INFORMATION TO ALL USERS
The quality of this reproduction is dependent upon the quality of the copy submitted.

In the unlikely event that the author did not send a complete manuscript
and there are missing pages, these will be noted. Also, if material had to be removed,
a note will indicate the deletion.

ABSTRACT

In the last two decades, numerous studies have revealed that atmospheric particulates and especially those emitted by diesel engined vehicles pose a serious health and environmental hazard.

This thesis describes the design and development of a co-axial capacitance transducer as well as the ancillary solids dispersion production unit for the on-line measurement of particulates concentration in air in real time basis. The primary application of the device is as a particulate monitor for diesel engine exhausts although the reported experimental results also evaluate and establish its feasibility for monitoring solids/gas dispersions during their pneumatic conveying.

Briefly, the transducer comprises two different diameter metallic cylindrical electrodes placed co-axially within one another so that an annulus is formed. The latter constitutes the sensing volume of the capacitance transducer following the application of a voltage between the two electrodes.

The principle of the operation of the device relies on the fact that the effective dielectric constant of a solids-gas dispersion driven between the electrodes is proportional to the concentration of the entrained solids. In practice therefore, the concentration of a test powder is determined by measuring capacitance and referring to a previously prepared calibration chart.

The feasibility and reliability of the transducer have been verified by conducting a series of experiments investigating its performance characteristics in response to changes in a number of design and operating parameters in conjunction with different powders of various size, density, and electrical properties.

The design parameters investigated include variations in electrode diameters, length and separation distance. The various operating parameters on the other hand deal with

changes in air relative humidity (8 - 78 %), temperature (20 °C - 100 °C), flow velocity (6.5 - 15 ms^{-1}), solids flow pattern (e.g. from homogeneous to slug flow) as well as variations in the frequency of the applied voltage (1-100 kHz).

The results indicate that the transducer's sensitivity increases with a decrease in the separation distance between the two cylindrical electrodes, whereas the electrodes' length has no profound effect on it. On the other hand, the effective dielectric constant, ε_{eff} of all solids-gas dispersions tested was found to be directly proportional to the solids concentration and unaffected by variations in air humidity, air velocity, electric field frequency, and solids flow regime. However, ε_{eff} for dispersions of insulating powders, in contrast to that of conducting powders, was found to be dependent on the respective dielectric constant of the solid particles as well as their size. Furthermore, in the case of mixtures of two insulating powders simultaneously dispersed in air, ε_{eff} was found to be dependent not only to the total solids concentration but also on the volumetric ratio of the two powders in the mixture. The transducer's baseline capacitance (zero solids concentration) varied linearly with the average surface temperature of the cylindrical electrodes. Finally, a 'temperature capacitor coefficient' was calculated in order to account for the effect of temperature on capacitance. This was found to be in close agreement with the coefficient of thermal expansion of the electrodes' material of construction (c.f. 0.0001/°C with 0.00012/°C).

To my father up there...

(I know he would have loved to see this)

... and to the rest of my beloved family down here

ACKNOWLEDGEMENTS

LIST OF CONTENTS

C H A P T E R 3.   REVIEW OF TECHNIQUES FOR MONITORING AMBIENT AND VEHICULAR PARTICULATE POLLUTANTS

CHAPTER 4.   CAPACITANCE TECHNIQUE FOR
                       CONCENTRATION MEASUREMENTS

C H A P T E R 5. DESIGN AND DEVELOPMENT OF SOLIDS DISPERSIONS UNIT

C H A P T E R 6. RESULTS AND DISCUSSION

C H A P T E R 7 CONCLUSIONS AND SUGGESTIONS FOR FUTURE WORK

CHAPTER   1

INTRODUCTION

Black smoke released into the atmosphere by motor vehicles as well as industrial and house stacks is often the most obvious form of air pollution that we routinely encounter. The smoke is mainly composed of particulate matter; tiny solid or liquid particles in the range of 0.005 - 100 μm in diameter suspended in air (Baird, 1995).

Recent studies have shown that such pollutants have a significant effect on human health as well as the environment generally.

The majority of researchers (see for example U.N., 1979; WHO, 1979; Willeke, 1980; Baird, 1995; Sawyer, 1997; DETR, 1998) agree that particles smaller than 10 μm (**PM_{10}** , abbreviation for Particulate Matter less than 10 μm in aerodynamic diameter see section 3.3.1) impose the greatest health hazard to human beings rather than the larger ones. They are capable of penetrating deep into the lungs, where their physical presence can increase the airway resistance and susceptibility to infection and consequently reduce lung function (Willeke, 1980; Baird, 1995). A survey compiled by Sawyer (1997) in the US, indicates 1 % increase in mortality in days when the concentration of PM_{10} increases by 10 $\mu g/m^3$. Furthermore, atmospheric particulates have been associated with increase in allergic disorders such as asthma, eczema; while ongoing research investigates the possible association of these particulates with lung cancer (DETR, 1998; Pepelko, 1999).

Additionally, fine particles change the light transmission characteristics of the urban atmosphere (decreased visibility) with a subsequent impact on the fundamental physical and chemical properties of the atmosphere (Elsom, 1992). Heat transfer rates, electrostatic properties, precipitation formation and other phenomena are significantly affected by fine particulate pollutants (Larson et al., 1989).

Other studies (U.N., 1979) have revealed that fine particles, especially those containing sulphate or nitrate, have long-term impacts on the acidity of fresh water and soil as well as on vegetation.

Finally, atmospheric particulates are responsible for the soiling of buildings, which is both cosmetically unpleasant and causes erosion of stones and corrosion of metal works. Mansfield (1992) estimated that in the UK, for the year 1990-91, the cleaning cost for the buildings facade was £79 million.

There are two major categories of atmospheric particle sources. These include natural sources such as dust storms, soil and rock debris, volcanic activities etc. and man-made sources such as combustion in domestic and industrial processes, incineration, traffic and alike. The estimated global emissions of particles smaller than 20 μm resulting from natural sources range from 421 - 1850 million tons per year, whereas emissions from man-made sources is 237 - 756 million tons per year (Buffle et al., 1992). Clearly, on a global scale the contribution of natural sources is immense; however, in the context of the urban air pollution, this contribution is dwarfed in comparison to the amount of particles originated by human activities (U.N., 1979).

Particulates emitted by vehicles and more specifically from diesel-engined automobiles have attracted special attention due to their high concentration, size distribution (they are within the respirable range), and chemical composition (absorbed carcinogenic and toxic hydrocarbons). Diesel particulates account for around 20% of the total UK emissions for PM_{10} per year (DETR, 1999).

The first legislation of its kind officially declaring maximum allowable concentrations of particulates in ambient atmosphere and from individual (stationary and mobile) emission sources was introduced by the Environmental Protection Agency (EPA) in United States in 1971 (Light, 1988). In the UK on the other hand, the last review of the air quality standards for particles was on the 29th October 1998, where it was recommended that the maximum concentration of PM_{10} particles

measured on an average of 24 hours should be 50 $\mu g/m^3$. These standards are to be reviewed in 2003 (DETR, 1998).

Countries world wide have established monitoring networks for the surveillance of air pollution in order to determine the air quality effects on human health as well as the environment (Harrison, 1986, Couling, 1993). These networks employ a number of different methods comprising means for sampling and measuring ambient as well as source particulate pollutants. Over the years, a large number of methods have been developed, the choice though depends crucially upon the purpose of monitoring.

However, at present, there is no satisfactory method for monitoring particulate matter emitted from exhaust pipes of vehicles in an on-line manner. Until recently, the Department of Transport and Environment had three ongoing projects (S026F/VB, S140A/VB, S260H/VB) (www.detr.gov.uk, 2000) investigating alternative means of testing smoke emissions from exhaust pipes of vehicles on an on line basis. The completion date was set for the end of 1998. However, as yet, no results on the findings have been published.

The objective of this study is to establish the operational feasibility and performance characteristics of a specially constructed capacitance transducer for the on-line measurement of particulates concentration in air in real time basis. The ultimate aim is to introduce the technique as a routine testing procedure for automobile particulate emissions in the light of forthcoming review of the existing legislation regarding particulate emissions in 2003.

The technique works on the basis of the fact that the effective dielectric constant (ratio of solids/air mixture capacitance to the capacitance of pure air) of a solids/air dispersion driven through a capacitance cell is directly related to the concentration of the entrained solid particles. In practice therefore, the concentration of a test powder is determined by measuring capacitance and referring to a previously prepared calibration chart.

The transducer basically comprises two metallic cylinders of different diameters placed coaxially within one another so that an annulus is formed. The latter constitutes the sensing volume of the capacitance transducer when a voltage is applied between the inner and the outer cylinder.

It is noted that particulate concentrations emitted from diesel engined vehicles are very small, approximately 20-200 mg/m^3 (Bosch,1996; Bagyi, 1998) with 92% (mass percentage)of the particles smaller than 2.5 μm in diameter (USEPA, 1985). Despite this, the feasibility of operation of the transducer is, in the main, investigated in conjunction with considerably larger particles, primarily in the 90 – 1200 μm size range. In fact during the course of this work several successful attempts were made in measuring glass ballotini particles between 1-50 μm. However, they were not systematically studied due to technical problems associated with dispersing fine particles in a controllable manner, using the existing experimental rig. On the other hand, there is nothing to suggest fundamental problems which will prevent measuring much smaller particles by using the particular or an improved design probe based on the same principle.

Also, in the light of the additional application of the same transducer for monitoring solids concentration during pneumatic conveying, the results reported for the 'large size particles' (i.e. 90 – 1200 μm) are particularly pertinent.

This thesis is presented in seven chapters.

Chapter 2 deals with a literature review of the air particulate pollution problem. In particular, the adverse effects of atmospheric particulates especially those relating PM$_{10}$, on human health as well as the environment are described in detail with special reference to particles emitted by diesel powered vehicles. The latter are of great importance due to their chemical and physical characteristics which are extensively studied. The chapter also reviews existing and forthcoming legislation in United States, United Kingdom and European Union concerning ambient and vehicular

particulate pollutants. The chapter concludes with a discussion on future trends in particulates in diesel emissions and air quality issues.

Chapter 3 is divided into two main parts. The first part contains a review of existing techniques for sampling and measuring ambient particulate pollutants. Part two describes the most commonly used instruments for measuring particulates from vehicle exhausts. The chapter concludes by highlighting the need for the development of an instruments for testing particulate emissions from exhaust pipes of vehicles, on an on line and in real time basis taking into account both operational and economic considerations.

Chapter 4 starts with a theoretical overview on dielectric materials and capacitive systems. This is followed by a basic description of the principle of operation and the design details of the capacitance transducer. The latter includes determination of the appropriate dimensions, shape and material of construction for the capacitor's electrodes. The chapter concludes with an overview of the most commonly used electronic circuits for measuring capacitance. The important electronic and operational specifications of the LCR (L: inductance; C: capacitance; R: resistance) meter used in the present study to measure capacitance is given in Appendix A.

Chapter 5 starts with an extensive review of the available techniques for generating particulates aerosols of controlled concentration together with the associated design and operating requirements for maintaining the particles in a suspended fully developed flow prior to measurement. The design and development of the appropriate equipment used in this study for generating solid/air dispersions for subsequent concentration measurement using the capacitance transducer is then presented in the light of the above findings. This is followed by a description of the experimental procedures, materials and ancillary equipment used in this study.

The results of extensive experiments elucidating the performance characteristics of the capacitance transducer are presented in Chapter 6. The aim of these experiments is to establishing the feasibility and reliability of the coaxial capacitance transducer in

measuring solids concentration in gas streams as well as identifying the effects of a number of design and operating parameters on the transducer's performance. The design parameters include the transducer's overall dimensions, namely electrode diameters, length and separation distance. The various operating parameters on the other hand deal with different particulate properties (e.g. size, electrical properties, density, and flow pattern), particulate concentrations, ambient conditions (e.g. humidity and temperature), and variations in the frequency of the applied voltage.

Chapter 7 presents a general conclusion on the main findings of the thesis as well as suggestions for future work.

CHAPTER 2

LITERATURE SURVEY

2.1. Introduction: Particulates In Air Pollution

Particulates are tiny solid or liquid particles in the range of 0.005 µm to 100 µm in diameter suspended in air and are usually invisible to the naked eye. However, these particles collectively form an atmospheric aerosol that restricts visibility and is noticeable as black smoke released into the atmosphere by motor vehicles, house and/or industrial stacks. The above is the most obvious form of air pollution that we routinely encounter (Baird, 1995).

Air pollution has been a lingering problem in British cities for centuries. From the middle 19th century, especially during winter time, the atmospheres over large British cities were covered by the so called "pea-soup" fogs or smogs (from the words smoke and fog). These were mainly attributed to smoke and sulphur dioxide emissions from the widespread combustion of coal in domestic and industrial applications. However, the effects of such smogs on human health were first realised in 1952 when during a four day pollution episode approximately 4000 people died in the Greater London (Elsom, 1992; Harisson, 1994). This incident led to Parliament proposing the First Clean Air act in 1956 to control the burning of smoky fuels in towns and cities. The implementation of this legislation led to a dramatic reduction in concentrations of black smoke and sulphur dioxide in the atmosphere over the next 30 years. This trend is shown in figure 2.1, where the black smoke concentration was recorded for three large UK cities, during 1961-1994 (DETR, 1998).

This decline is primarily attributed to a number of measures such as the use of cleaner fuels, especially natural gas instead of coal, the relocation of factories and power stations outside cities, and the use of tall stacks (Harrison, 1994).
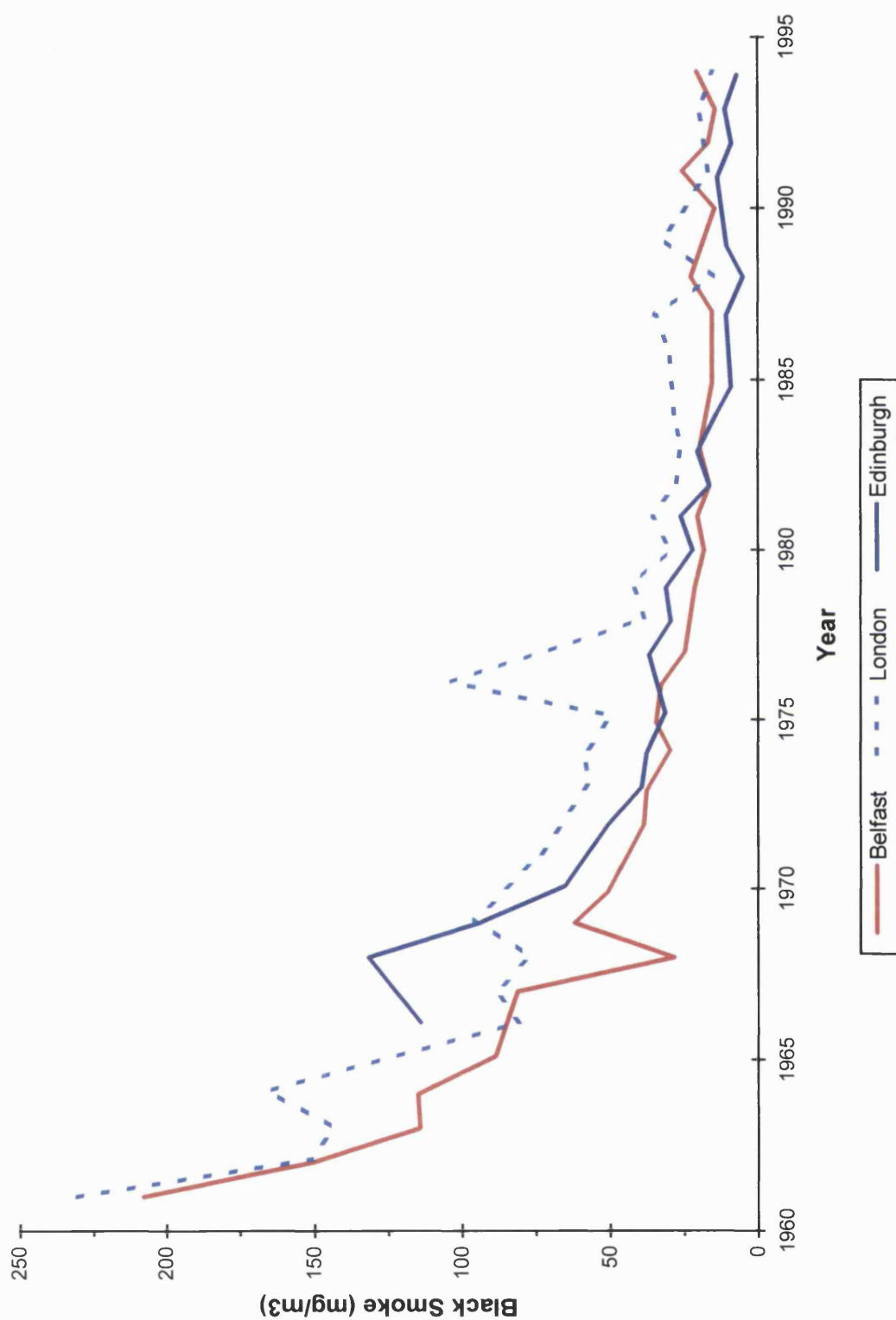
Figure 2.1. Annual average concentrations of smoke at three UK urban sites between 1961 - 1994. (DETR, 1998).

The resulting improvement in air quality with respect to airborne particles and SO_2 had convinced scientists and the public that the urban pollution problem had been solved. However, developments in the last 20 years have raised new concerns leading to a review of the problem. This is mainly due to an increase in traffic volume in cities unveiling different forms of air pollution (DETR, 1998; Harrison, 1994). Furthermore, numerous studies have revealed that the accompanying particulates suspended in the exhaust fumes, especially those between 0.01 μm to 10μm, introduce serious health hazard and environmental problems even at concentrations far lower than those recorded during the 1950s and 1960s (U.N., 1979; DETR, 1998).

This chapter contains an extensive review of the literature on the effects of particulate air pollution on human health as well as the environment. Particular attention is paid to particulates emitted by automobiles, specially those emitted by diesel engines as their concentration is high and they are within the respirable size range. Finally, a review of the existing air quality standards for atmospheric particulates in the United Kingdom, European Union, and United States is given.

2. 2. Health and Environmental Effects of Particulate Pollutants

2.2.1. Health Effects

The health effects of atmospheric aerosols have been the subject of great interest in the last two decades. The impact of the atmospheric aerosols on human health is a function of their physical and chemical characteristics (U.N., 1979; DETR, 1998). Therefore, any toxicological appraisal of particulate pollutants should specify these two parameters.

The most important physical characteristic of the atmospheric particulates is their size. This characteristic determines the ability of particles to remain suspended in air as well as the degree of their penetration into the human respiratory system. Thereafter once retained, the particles' chemical characteristics determine the biological effect (U.N.,1979; DETR, 1998).

Much research has been carried out in order to determine the size range of particulates that impose the greatest health hazard for human beings. The majority of researchers agree that the particles smaller than 10 μm, are of principal concern to human health than the larger ones. These particles are called **PM$_{10}$** abbreviation for **Particulate Matter** less than 10 μm in aerodynamic diameter (see section 3.3.1, figure 3.2) (see for example U.N., 1979; WHO, 1979; Willeke, 1980; Baird, 1995; Sawyer, 1997; DETR, 1998).

Baird (1995) reports several reasons justifying the above. These are :

(i) Particles of size larger than 10 μm settle down quickly and hence human exposure to them via inhalation is reduced. The settling velocity of particles increases with the square of their diameter. For example, a particle half a diameter of another, falls four times more slowly. Therefore, fine particles with diameter less than 3 μm usually remain airborne for days or weeks.

(ii) The human respiratory system acts as a highly effective filter for coarse particles, trapping a large percentage of those inhaled particles with an aerodynamic diameter greater than 10 μm. The larger particles trapped in the nose and in the throat are removed via the mucociliary system. However, it is the particles below 3 μm that have the greatest likelihood of reaching the furthest parts of the lung, where their presence can increase airway resistance and susceptibility to infection, and consequently reduce lung function. Figure 2.2 shows the retention of particles in the lungs as a function of particle size. Under severe exposure, fibrosis, silicosis and other patho-physiological changes can occur.

(iii) The surface area per unit mass of large particles is smaller than that of small ones; thus, gram for gram, their ability to carry adsorbed gas molecules to any part of the respiratory system and thereby to catalyse chemical and biochemical reactions, is correspondingly smaller.

(iv) Particulate collection devices such as electrostatic precipitators and baghouse filters that are commonly used to remove particulates from air are efficient only for coarse particles. Therefore, although a device may remove 95% of the total particulate mass, the reduction of the surface area and of the respirable particles is a much lower fraction.
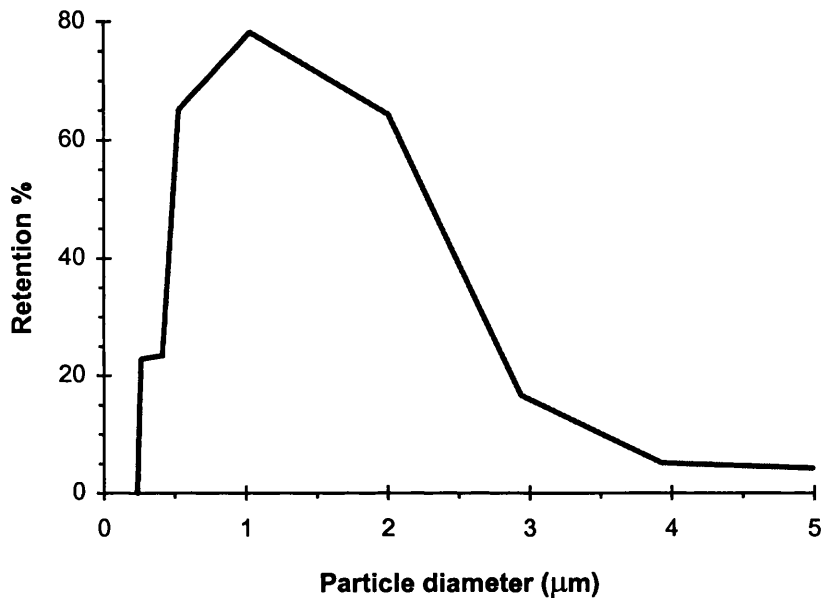
Figure 2.2. Retention of particles in the lungs (U.N., 1979).

In the last two decades, numerous studies investigating the possibility of associating particulate air pollution with mortality, morbidity and lung related problems have been conducted in the UK (see for example Anderson et al., 1991; Walters et al., 1994; Higgins et al. 1985) as well as in the US (see for example Speizer, 1989; Dockery et al.,1993; Pope et al. 1995). Consequently, the World Health Organisation (WHO) appointed a group of experts to analyse these studies and to calculate the excess numbers of deaths and incidents of ill-health possibly associated with different concentrations of PM_{10}. Compiled results of this investigation are shown in table 2.1 (WHO, 1995).

Table 2.1. Summary of short-term exposure-response relationship of PM_{10} with different health effect indicators.

HEALTH EFFECT INDICATOR	Estimated change in daily average PM_{10} concentration needed for a given effect (in $\mu g/m^3$)
Daily mortality:	
5% change	50
10% change	100
20% change	200
Hospital admissions for respiratory conditions:	
5% change	25
10% change	50
20% change	100
Numbers of asthmatic patients using extra bronchodilators:	
5% change	7
10% change	14
20% change	29
Numbers of asthmatic patients noting exacerbation of symptoms:	
5% change	10
10% change	20
20% change	40

The above results, which illustrate a dose-response relationship between particulate air pollution and excess mortality and health deterioration, have led some researchers to speculate that the association might be causal. However, till date, no convincing biological hypothesis establishing causative association exists. A recent extensive study undertaken by the Expert Panel on Air Quality Standards (DETR, 1998) have reached the following conclusions on the basis of available evidence:

a) All the available studies, even though they have not shown identical results, illustrate the same overall pattern establishing the hypothesis that the effect of PM_{10} pollution episodes on mortality is by determining the time of death of those who are susceptible due to pre-existing disease. The Panel considers it possible during pollution episodes that inhalation of particles could cause lung-inflammation and consequently fatal cardiovascular and pulmonary illness in susceptible individuals.

However, the possibility of the cause and development of these diseases by a prolonged exposure to air pollution, should not be dismissed.

b) Numerous studies record a rise in the occurrence of allergic disorders such as asthma, eczema, and hay fever in cases of unfavourable environmental conditions. This increase is more pronounced amongst young children in big cities in the United Kingdom and other countries with a western lifestyle. The Panel have considered that particulate pollutants might have been in part responsible for this rise in allergic diseases but there is not clear evidence proving causality.

c) Finally the Panel have reviewed laboratory studies investigating possible association of lung cancer with exposure to particulates coming from diesel exhausts. The laboratory work involved long term exposure of two strains of rat to high concentration of diesel particulates. The results indicate an increase of malignant and benign tumours which is in proportion with the particle concentration .

Particulate matter emitted from motor vehicles is of great importance because it is close to the ground and within the breathing zone (WHO, 1979). The problem is more severe in urban areas and especially near busy roads. Indicative is the study conducted by London Scientific Services (LSS) that measured particles concentrations at four different sites in London over the years 1986-1989. Roadside concentration are about 2.5-3 times higher than at the rest of the monitoring sites (LSS, 1989). This fact therefore, has a direct impact on human beings, animals and soils.

Chemical substances that have been traced onto diesel particulates have raised considerable concern. Tests on hydrocarbons derived from diesel particulates show a high level of toxicity (Collier, 1994). Some of the compounds, namely the polycyclic aromatic compounds (PAH's) such as benzo(a)pyrene, pyrene, anthracene, are known to be carcinogenic and others have been found to be mutagenic (Clayton et al.,1992). Furthermore, there is some evidence (Faulkner et al., 1979) that the high particulate level of diesel exhaust can increase the pulmonary retention time of substances such as benzo(a)pyrene, thereby increasing the chance of absorption by the body .

Sulphuric and sulphate compounds are two of the substances commonly attached to atmospheric particulates and especially to those from diesel exhausts. These compounds are known to have an impact on the physiology and morphology of the lung and may cause permanent lung damage in extreme exposures (U.N., 1979).

The most recent assessment of possible health hazards associated to diesel particulates conducted by Environmental Protection Agency (EPA) (Pepelko, 1999) has concluded that diesel exhaust particulates is "highly likely" to be carcinogenic. This is based on epidemiological studies suggesting that lung cancer occurrence increases about 33-47% in occupational exposure to diesel exhaust fumes. The EPA "believes" that the cancer hazard is also applicable to environmental (i.e. ambient) exposures, even though none of the studies examined by EPA confirmed that (Pepelko, 1999).

Finally, a report by the World Health Organisation (1979) associates air particulate pollution with annoyance of the public. Annoyance is defined as "a feeling of displeasure associated with any agent or condition believed to affect adversely an individual or a group" (WHO, 1979). The public identifies traffic as the major source of these nuisance effects; although, other activities such as construction and demolition can contribute locally. This survey reports that 50% of the persons interviewed believed that particulate pollution was a general nuisance when annual concentration of particulates reached $230\mu g/m^3$, and 33%, when the concentration reached 150 $\mu g/m^3$. In the same survey 20-30% of the people responded, blamed the vehicle derived pollution for these effects.

2.2.2. Environmental Effects

Along with the direct effects of fine particulate matter on human health, atmospheric particulate pollutants in general may affect the environment in various ways. As a result, the human health is degraded indirectly and the general human welfare is affected.

The loss of atmospheric visibility defined as the greatest distance at which a black object can be seen against the horizon, is one of the most obvious impacts of air pollution (Willeke, 1980). Air pollution reduces visibility due to light absorption by gases and particles and light scattering by particles. The latter is the predominant mechanism and it is most effective for particles with diameters similar to the wavelength of visible light i.e. 0.1-1 μm (Elsom, 1992). Vehicular particulates are believed to contribute a great deal since their size range coincides with the one mentioned above. Clarke et al. (1987) estimated that the light absorption coefficient at the side of the road was three times that on the rooftop 30 m above the road, highlighting the significance of particulates originated by traffic.

Extreme visibility reduction results in the formation of fogs where particulates play a crucial role by acting as nuclei for the condensation of fog droplets. The effect of fogs is such that prior to the implementation of environmental laws (circa 1956) in Europe and North America , many urban areas received only 50% of their potential sunshine in the winter (Elsom, 1992; Larson et al., 1989). However, following the implementation of the Clean Air Act (1956) the frequency of fog occurrence has decreased in all urban, coastal and rural locations in the UK (Lee, 1994).

Soiling of buildings remains a big problem despite the dramatic reductions in the concentration of particulate pollutants in the last three decades. This is mainly due to the increase of the volume of the diesel-engined vehicles which are the main emitters of very fine carbonaceous particles in urban areas. Diesel particulates because of their hydrocarbon content are more sticky than the soil particles and therefore more likely to adhere to surfaces. Furthermore, they are much less wettable than other particles, and thus less readily removed by rain. The soiling of the buildings' facades is not only a cosmetic problem but practical as well. Nitrogen and sulphur oxides are easily absorbed on the surface of the adhered particles and enhance the erosion of building stones and the corrosion of metals. Mansfield (1992) estimated that in the UK, for the year 1990-91, the cleaning cost for the buildings' facade was £79 million.

The effect of particulate pollution on vegetation is such that it can hinder plants growth. The effect is more profound on leafy vegetable crops where it causes a damage commonly known as "silver-leaf"; a shiny, oily effect on the leaf's lower surface (Hodges, 1977). Particles depositing on the plant's leaves plug their pores and as a result the absorption of CO_2 as well as the sunlight reaching the interior of the leaf are reduced (Elsom, 1992). The extent of the problem is more severe in urban vegetation (e.g. amenity trees in public parks or alongside roads and plants and flowers in private gardens). Studies have shown a clear decrease in yield of exposed crop plants when moving from the suburbs into central London. In the UK prior to implementation of the Clear Air Act very few trees were able to grow in urban areas, whereas today there is a greater diversity of trees (Schwela et al., 1999).

It has been shown (U.N.,1979) that fine particles, especially when they contain sulphate or nitrate, are the principle conveyors of acid in the atmosphere with long-term impacts on the acidity of fresh water and soil. This affects the productivity of natural and agricultural soils and consequently the health of several animal species (Bower, 1994).

Atmospheric aerosols are believed to influence the earth's climate directly through the reflection and absorption of solar radiation and indirectly through the modification of the clouds' lifetime and optical properties. However, the exact net effect is yet to be determined. Theoretical model calculations by Preining (1993) indicate that sulphate aerosols due to light scattering may have a net positive effect upon global warming as opposed to greenhouse gases. On the other hand, carbonaceous particles emitted by diesel engines have an adverse effect on global warming due to the fact that elemental carbon absorbs visible light instead of scattering it (Willeke, 1980; Preining 1993). However, our comprehension of climatic change phenomena in association with atmospheric particulates is incomplete and more research is necessary in order to determine their contribution towards global warming or cooling (Elsom, 1992).

Finally, the presence of fine particulates in the atmosphere will alter the fundamental chemical, physical and electrostatic characteristics of the atmosphere (U.N., 1989).

Particles acting like nuclei for larger aerosol droplets promote liquid phase chemical reactions. They may also have some catalytic activity. A very important factor during these phenomena is the shape of the atmospheric particulates because it determines the absorption surface area of the particles. The latter may act as sites for heterogeneous conversion of atmospheric pollutants into other more hazardous compounds (Willeke, 1980).

2.3. Sources of Particulate Matter

A report conducted by the World Health Organisation (WHO, 1979) identifies two major categories of atmospheric particulate sources. The first include the natural sources and the second the man-made sources. The estimated global emissions of particles smaller than 20 μm resulting from natural sources range from 421 to 1850 million tons per year, whereas emissions from man-made sources is 237 to 756 million tons per year (Buffle et al., 1992). Clearly, on a global scale the contribution of the natural sources is immense, however, in the context of urban air pollution this contribution is dwarfed by particles originated by human activities (U.N., 1979).

2.3.1. Natural Sources

The contribution of natural sources include phenomena such as volcanic activity, dust storms, forest fires, soil and rock debris, sea salt, and secondary particulate matter resulting from reactions of gaseous emissions. Soil dust blowing into the air by the action of the wind on dry loose surfaces is the most commonly encountered form of environmental particulate matter. It is estimated that suspension of "surface soils" introduces 150 million tonnes of dust per year to the Northern hemisphere and about twice this if the Sahara desert is included. The presence of such particles is witnessed on every day basis because of their deposition onto surfaces such as windows and window sills, cars, washing and indoor fabrics (QUARG,1996).

Sea salt particles suspended in the air is another form of atmospheric aerosol very frequently encountered especially in countries like UK, which is totally surrounded by

sea. These particles are originated by the evaporation of the water from tiny sea droplets generated by the breaking of the waves. During the winter months an increase in salt particles concentration is observed but this is mainly due to the use of salt for de-icing the roads. Vehicles travelling at high speed suspend the salt particles in the air (QuARG,1996).

Some of these naturally made particulate matter are generally rather coarse to remain in suspension for long periods and hence they have rather limited atmospheric lifetime and travelled distance (WHO, 1979). However, cases of dust particles carried from North Africa to the UK or sea salt particles been traced even at the most inland of UK locations show that this is not always the case. However, in the context of this work and particularly in relation to urban areas, these sources will not be considered further.

2.3.2. Man-made sources

Combustion of fossil fuels and industrial processes such as mining, quarrying, construction and demolition are amongst the prime sources of particulate emissions. Table 2.2 gives the UK emissions inventory of particles smaller than 10 μm, by emission source in 1996, as estimated by The Department of the Environment (DETR, 1999).

Combustion of fuel (especially coal) for domestic/industrial applications and for power generation and transport has been the major contributor to suspended particulate matter in urban areas (U.N., 1979; Elsom, 1992). The chemical and physical characteristics of the emitted particles differ depending on their source. More specifically, coal burning processes generate mainly fly-ash which consists of fine particles of mineral material contained in coal. Combustion of volatile fuels on the other hand, emit carbon based particles with high content of absorbed hydrocarbons, whereas diesel fuels lead to fine carbonaceous particles with a mixture of hydrocarbons and sulphates. Waste incineration as well as metallurgical processes involving combustion form fine metal-rich particles (Hildemann et al., 1991).

28

Table 2.2. Estimated UK emissions for PM_{10} by emission source, 1996, thousands tonnes/year (http://www.aeat.co.uk/netcen/airqual/emissions/pm10.htm, 2000).

Source	1970	1980	1990	1991	1992	1993	1994	1994
1. Public power etc.	**41**	**58**	**39**	**40**	**39**	**39**	**37**	**15%**
Coal	38	57	38	38	38	38	36	14%
Fuel Oil	3	1	1	1	1	1	1	1%
Other	0	0	0	1	0	0	0	0%
2. Commercial, Residential, Institutional Comb.	**226**	**97**	**45**	**46**	**42**	**42**	**33**	**13%**
Domestic	210	88	39	41	37	37	28	11%
Other	16	9	6	5	5	5	5	2%
3. Industrial Plants/ Processes with Comb.	**131**	**60**	**46**	**46**	**44**	**45**	**44**	**18%**
Refineries	10	10	6	6	6	7	7	3%
Iron and Steel	56	17	21	21	20	20	21	8%
Other	65	33	19	19	18	18	16	7%
4. Non-Combustion Processes	**63**	**63**	**63**	**63**	**63**	**63**	**63**	**25%**
Construction	4	4	4	4	4	4	4	1%
Industrial processes	30	30	30	30	30	30	30	12%
Mining & Quarrying	29	29	29	29	29	29	29	12%
5. Extraction /Distribution of Fossil Fuels	**0**	**0**	**0**	**0**	**0**	**0**	**0**	**0%**
6. Solvent Use	**0**	**0**	**0**	**0**	**0**	**0**	**0**	**0%**
7. Road Transport	**45**	**53**	**68**	**69**	**68**	**66**	**65**	**26%**
Petrol Exhaust	11	15	17	16	14	13	12	5%
Diesel Exhaust	32	35	47	49	49	49	49	20%
Non-Exhaust	2	3	4	4	4	4	4	1%
8. Other Transport	**20**	**9**	**7**	**7**	**7**	**7**	**6**	**3%**
9. Waste Treatment & Disposal	**2**	**1**	**1**	**1**	**1**	**1**	**1**	**0%**
10. Agriculture	**2**	**1**	**1**	**1**	**1**	**1**	**1**	**0%**
TOTAL (ktonnes)	**531**	**342**	**270**	**273**	**264**	**264**	**250**	**100%**

Source :Economic Council of Europe (UNECE), October 1998

Particles generated during construction and demolition processes constitute another form of urban particulate pollution routinely encountered. Mechanical break-up of materials, surface abrasion, loading/unloading, and uncovered soil stockpiles generate uncontrolled "fugitive" particle emissions. These emissions are inversely proportional to the moisture and silt content of the soil. Even though it is difficult to quantify these sources due to their nature and lack of information, it is believed to have a substantial impact on local air quality (DETR, 1999).

Agriculture is another source of airborne particulates in the atmosphere through activities such as land preparation, fertilising, harvesting and stubble burning. The very nature of these emissions make it hard to be estimated. However harvesting is expected to contribute the most since it is done when the crops are dry, favouring particles suspension by the blowing wind (DETR, 1999).

Road transport is known to contribute appreciable amounts of fine particulate matter to the atmosphere in several ways: dust from the wear of tyres as well as dust from the road, particulates rich in lead compounds from the exhaust pipes of petrol-engined vehicles, and black smoke from diesel powered vehicles (Rogge, 1993; Baird, 1995; Wolfgang et al., 1993;).

Table 2.3. Increase in emissions from road transport in the UK, from 1980-1990. (DTE, 1992).

Pollutant	% Increase
Volatile Organic Compounds (VOC's)	12
Carbon Monoxide (CO)	46
Nitrogen Oxides (NOx)	72
Sulphur Dioxide (SO_2)	50
Carbon Dioxide (CO_2)	43
Black Smoke	**75**

As has been already mentioned, the Clean Air Act enforcement brought a dramatic decrease in atmospheric particulate concentration. However, recent studies in the United Kingdom and United States have drawn attention to an increasing contribution of road transport and especially diesel vehicles to urban pollution (DETR, 1998). This

trend is mainly attributed to the steadily increasing number of vehicles. In the UK, from 1980 to 1990 only, the vehicle number increased by 28% to almost 25 million vehicles resulting in a significant rise in concentration of many air pollutants as illustrated in table 2.3 (DTE, 1992). The alarming increase of diesel generated particulate pollution in urban areas, prompts us to have a more thorough investigation on the possible reasons for this trend, the nature of diesel particulates and its future trends.

2.4. Diesel Vehicles Exhaust Particulate Emissions

2.4.1. Overview of Particulate Emissions Inventories in UK with respect to diesel vehicles

The most recent study undertaken by the Department of Environment and Transport reveals that during 1996 in the UK, diesel vehicles contributed 17 % to emissions inventory of particles smaller than 10 µm, 24% of particles smaller than 2.5 µm, and 50% of particles less than 0.1 µm (DETR, 1998).
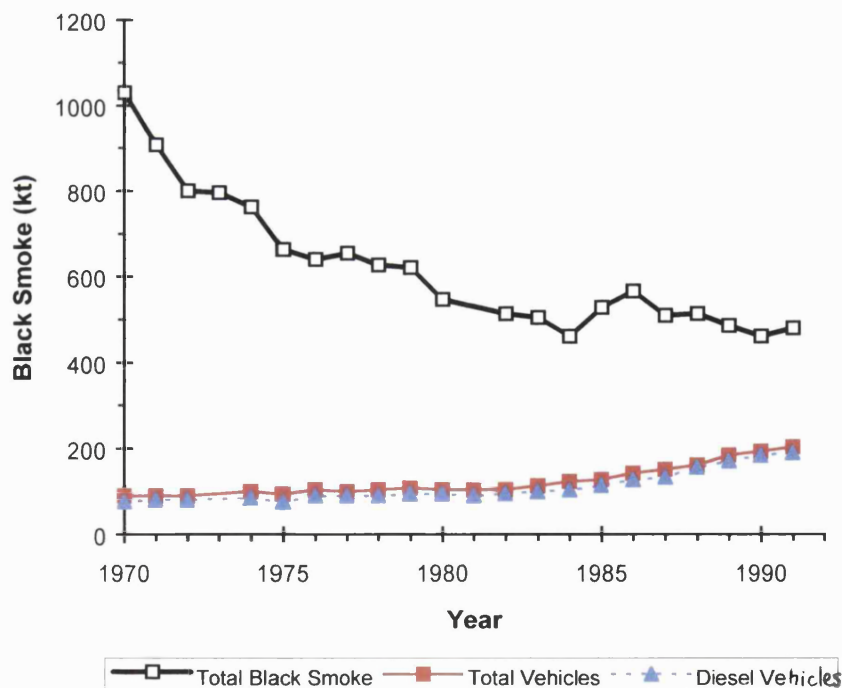
Figure 2.3. UK Black smoke emissions between 1970-1991 (DETR, 1999).

The relative importance of the diesel vehicular emissions in the last decades is highlighted in figure 2.3. This graph shows the trends in total UK emissions of black smoke together with the total vehicular emissions and diesel only emissions, for the period 1970-1991. It can be seen that the total black smoke emissions in 1991 are half of that in 1970 due to the implementation of the Clean Air Act, whereas the diesel generated emissions are steadily increasing over the same period, accounting for almost the total vehicular emissions (Eggleston, 1992).

These trends are largely attributed to the following two factors:

a) A steadily increased number of diesel vehicles on the roads due to a strong campaign during the '70s and 80s by the motor industry and governments (especially in US) to promote diesel vehicles as a cheap alternative to petrol vehicles. This move was part of a general energy conservation policy caused by the high fuel prices and the steadily decreasing oil reserves (Faulkner et al., 1979; Willeke, 1980). In line to this policy the US Federal Government issued a regulation requiring the average fuel mileage for each auto manufacturer to be at least 27.5 mi /gal by the year 1985 favouring the diesel vehicles which are much more economical than petrol vehicles (25-75% better fuel mileage compared to a gasoline engine). Furthermore, they have reduced maintenance requirements as well as higher durability than petrol engines (Faulkner et al., 1979).

The composition, temperature and volumetric flowrate of the exhaust gases produced by diesel engines are listed in table 2.4 (BOSCH, 1996).

Furthermore, comparative exhaust emission data for diesel and petrol automobiles listed in table 2.5, show that the former have lower gaseous emissions -carbon monoxide, hydrocarbons, and nitrogen oxides than the latter (Howitt, 1987; Bretschneider et al., 1987; Farrow et al., 1993). Consequently, at the time, increasing the number of diesel vehicles was perceived as a potential environmental strategy to reduce emissions of carbon oxides (the principal greenhouse gases) from the road transport sector. A study undertaken by the World Wide Fund for Nature (WWF)

shows that due to lower COx emissions, the total global warming per kilometre travelled, is 20% lower from a diesel car than from a petrol car (WWF, 1993).

Table 2.4. Composition , temperature and volumetric flowrate of exhaust gases from diesel engines (BOSCH, 1996).

Component		at idle	at maximum output
Nitrous oxides (NO_x),	ppm	50-250	600-2500
Hydrocarbons (HC),	ppm C_1	50-500	150
Carbon monoxide (CO),	ppm	100-450	350-2000
Carbon dioxide (CO_2),	% vol/vol	3.5	12-16
Water vapour,	% vol/vol	2-4	15
Oxygen ,	% vol/vol	18	2-20
Nitrogen etc.,	% vol/vol	residual	residual
Particulates,	mg/m^3	20	200
Exhaust gas temperature, (just after the engine's exhaust valve)	°C	100-200	550-700
Exhaust gas temperature *, (at the end of the tailpipe)	°C	35-50	80-120
Volumetric flow rate *, (2 Litres, 4 stroke car engine)	l/min	(600 revs/min) 510	(5000 revs/min) 4000

* (Nightingale, 1999)

Table 2.5. Comparative urban emissions for petrol and diesel passenger cars.

Vehicle Type	Average on-Road Emissions (g/km)			
	CO	Hydrocarbons	NOx	PM_{10}
Standard petrol (without catalyst)	27	2.8	1.7	not recorded
Petrol with catalyst	2	0.2	0.4	not recorded
Diesel	0.9	0.3	0.8	0.4

Ultimately, the campaign to promote the diesel vehicle as an environmental friendly and economical alternative to petrol cars resulted in a significant increase in car market penetration as shown in figure 2.4.
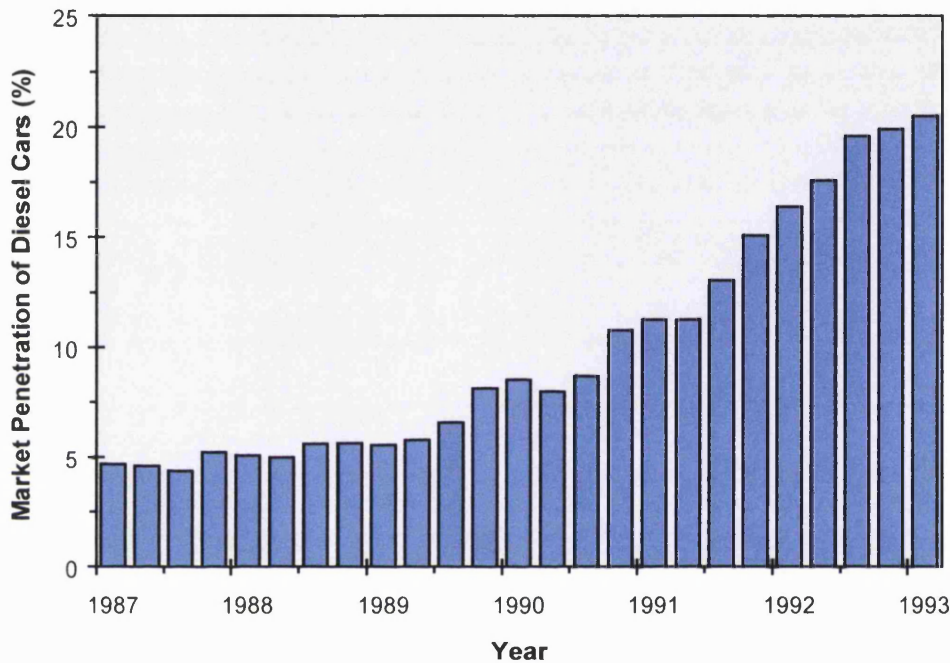
Figure 2.4. Growth in new market penetration of diesel cars (DETR, 1998).

b) Diesel vehicles emit particulate matter at much higher rate than petrol vehicles. Ironically, the reason that diesel engines produce high levels of particulates emissions is the same as that responsible for their superior economical performance, namely the efficient combustion process (Faulkner et al., 1979; Howitt, 1987).

The diesel engine, unlike the gasoline engine, does not have a spark plug to ignite the fuel-air mixture. It operates by compressing the air in the cylinder until it becomes very hot and then injecting the fuel into the hot compressed air where it ignites spontaneously (Lynn, 1976). Most of the fuel is burned in this process, but a small amount is cracked, polymerised, or partially oxidised into a large array of compounds including elemental carbon or soot. Various researchers report that diesel engines emit particulates at rates of 0.25 - 0.80 g / mile which are 50 -100 times greater than

the rates produced by engines using unleaded gasoline (Faulkner et al., 1979; Howitt 1987).

It is worth noting that these rates are not absolute since they vary depending on a range of factors such as engine design, pollution control provision, maintenance, driver behaviour, traffic conditions, vehicle speed, age and type of vehicle. However, they may be considered to be representative of the situation.

2.4.2. Characteristics of Diesel Exhaust Particles

2.4.2.1. Particle Size Distribution

Diesel engine exhaust particulates consist largely of agglomerates of very small carbon particles which have grown by coagulation into chain aggregates. (Faulkner, 1979; Willeke, 1980). Figure 2.5. shows a characteristic microscope photograph of diesel exhaust particulates collected in a high efficiency filter.
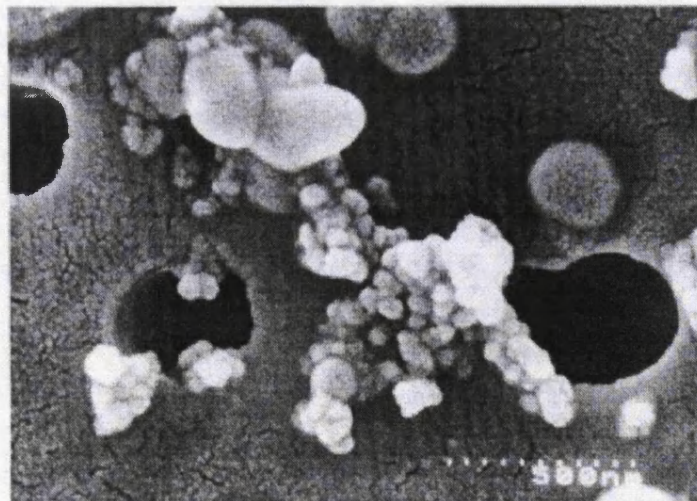
Figure 2.5. Example of various size agglomerates made of individual spherical particles. (The dark circles are the filter's pores about 0.5 μm in diameter) (Willeke, 1980)

The individual carbon particles are almost spherical, 0.01 μm in diameter whereas the produced agglomerates have a mass mean diameter that ranges from 0.05 to 0.30 μm (Williams et al., 1989; Burtscher et al., 1993).

A typical size distribution of diesel particulates is shown in figure 2.6. (DETR, 1996). The mass median diameter of 0.3 μm with 70% smaller than 1 μm is in good agreement with Willeke (1980) data. A similar survey undertaken by the Environmental Protection Agency in the US showed that diesel particles are smaller than 10 μm with 92% (mass percentage) of them smaller than 2.5 μm (USEPA, 1985). The density of the individual particles , which are primarily elemental carbon (see 2.4.2.2 below), is approximately 2000 kg/m^3, however the open structure of the formed agglomerates give rise to a very low density of 120 kg/m^3 (Faulkner, 1979).
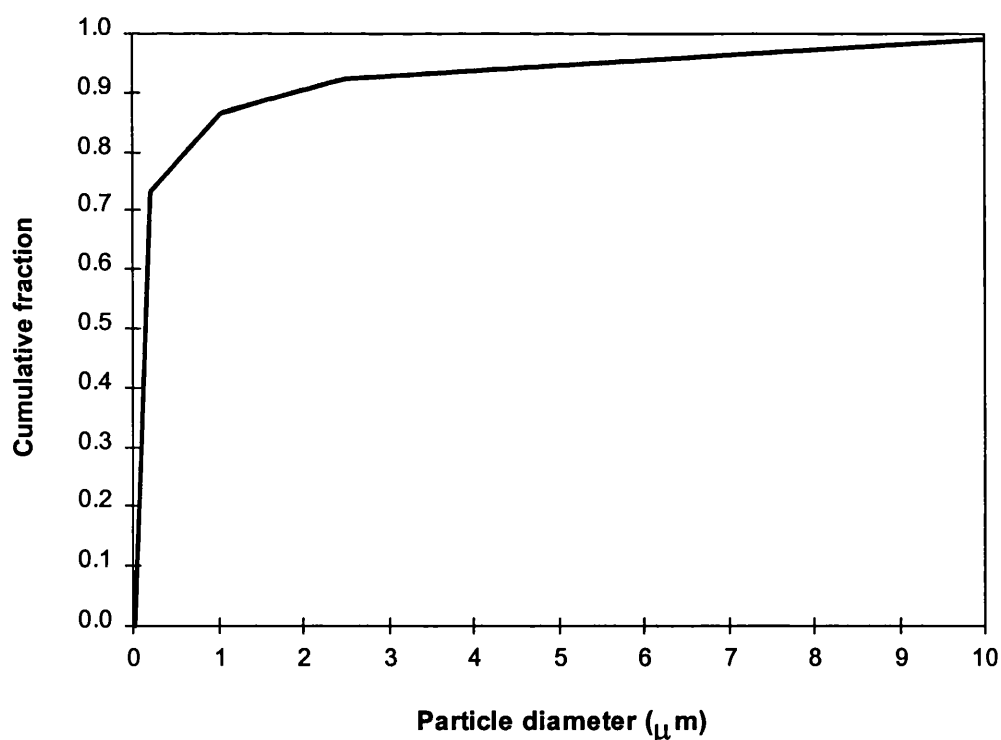
Figure 2.6. Size distribution of diesel particulates (QUARG,1996).

2.4.2.2. Particles Chemical Composition

The individual diesel particles consist primarily of elemental carbon containing quantities of adsorbed/condensed organic and sulphur compounds and other materials such as lubricant oil and unburned fuel (Willeke, 1980). In fact, environmental studies reveal that diesel emissions contribute 80-95 % to the total mass of particulate elemental carbon (PEC) in the atmosphere (Hamilton et al.,1991).

Diesel particles start their formation at high temperatures during the combustion process in the engine's cylinders. At this stage they consist only from carbon since the other compounds are in the vapour phase. However, along the exhaust tailpipe from the cylinder to the atmosphere, the temperature drops and as a result hydrocarbons, sulphate and other combustion by-products condense and absorb onto the particles' surface (Ahvlik et al., 1998).

Williams et al., (1989) conducted an extensive survey on particulate matter emitted by exhaust pipes of light duty diesel vehicles. More specifically, they found that the total carbon (TC) accounts for 75-85% of the particle mass. On average, 71% of the TC was present in non-volatile form (i.e. sooty or elemental carbon,(EC)) the remainder being contained in volatile organic carbon (VOC) due to the adsorbed hydrocarbons. The latter comprise a wide range of chemical compounds including hydrocarbons (alkanes, alkenes, aromatics) oxygenates (alcohols, aldeydes, acides) etc.

However, the work of various researchers (Postulka et al 1981; Williams et al., 1989) indicates that the distinction between these two forms of carbon varies. This is because the amount of hydrocarbons adsorbed onto the particles' surface is dependent not only on the combustion parameters of the engine but also on the fuel and lubricant oil composition as well as the sampling conditions when the particulates are collected (dilution ratio, temperature, pressure etc.).

Diesel particles also carry sulphate compounds due to the sulphur content of the diesel. The amount of sulphur in diesel varies according to the type of refined crude

oil as well as the extent of the desulphurisation. When diesel fuel is burnt, most of the sulphur is converted to SO_2 whereas a small amount produces SO_3. The latter combines with water and other compounds in the exhaust gases forming sulphuric acid and sulphates. In general, sulphates and water account for 10-15% of diesel particulates (RCEP, 1991).

2.5. Legislation

2.5.1. Historical Background

During the last decades, the role of the Government has become crucial in environmental issues related to vehicles. The recent improvements in the environmental performance of vehicles due to new technologies have been forced on manufacturers through legislation.

United Kingdom was the first country in the world to introduce air pollution laws in its Clean Air Act in 1956. However, since the 1960s it has been the US and specially the State of California, which has provided the model for standards of automotive emissions around the world (Nieuwenhuis et al., 1994). The main reason that California State has adopted such strong policies for vehicular emissions is that its market alone absorbs around 2 million new cars annually. This figure is similar in size to those from the large European markets such as UK, Italy, Germany and France (Nieuwenhuis et al., 1994).

On April 30, 1971 in response to the U.S. Congress requirement for protection of public health due to the severe air pollution episodes in Los Angeles, California, the Environmental Protection Agency (EPA) declared the first ambient air quality standards for particulate matter. Protection of public health is interpreted as protection against effects on soil, water, vegetation, materials, animals, weather, visibility, and personal health and well-being (Light, 1988). These standards are expressed in terms of the amount of "total suspended particulate" (TSP) matter as collected from the air by a high volume sampler, which effectively collects particulate matter up to nominal

diameter of 25 to 45 μm (Light, 1988). The designated primary standards of the 1971 Clean Air Act were, 75 μg/m^3 for annual geometric mean and 260 μg/m^3,as a maximum 24-hour averaged concentration not to be exceeded more than once a year.

The first legislation in the UK dealing with exhaust emission control was Regulation 61 of the Construction and Use Regulations   in 1971 . This states that "no person shall use a motor vehicle from which any smoke, visible vapour, grit, sparks, ashes, cinders or oily substance is emitted". Later in 1971, the development of the diesel engine for road use forced car manufacturers to obtain approval to a new British Standard controlling smoke, BS Au 141a: 1971 -BSI, 1971- in order to limit the "visible emissions". Eventually, these initial standards were integrated into the European Community legislation – Council Directive 70/220/EEC – and have since undergone thirteen amendments (last on 08/10/96 Commission Directive 96/69/EC) each progressively tightening up the initial exhaust emission limits, in response to growing environmental concerns.

2.5.2. Air Quality Standards for Particles

2.5.2.1 Justification of Air Quality Standards for Particles.

Air quality standards are based primarily on assessment of the effects of a specific pollutant upon human health. However, individual response to a given concentration of air pollution varies considerably amongst individuals. For example, people with pre-existing lung diseases are more sensitive to a given dose of airborne particulates than healthy people. Differences in response can also be due to age, sex and level of fitness. Hence, air quality criteria aim to minimise the health impact on sensitive groups of people.

Another factor that has to be taken into account while assessing adverse effects of air pollution on human health is the duration of the exposure. Therefore, in case of those pollutants for which long term exposure is thought to be of most importance, the air pollution criteria are based on concentration averaged over one year. Similarly, for

pollutants that short term exposure is believed to be more important, the concentrations are averaged over shorter times, varying from 10 minutes to 24-hours.

2.5.2.2. UK Air Quality Standards for Particles.

In the UK the Department of Environment and Transport has appointed the Expert Panel on Air Quality Standards as the official body responsible for setting the air quality criteria. The last review of the UK air quality standards for particles was on the 29th October 1998. The outcome of the Panel's review is focused in three points summarised below whereas the actual values of these standards are listed in table 2.6 (DETR, 1998).

a) The measurement of PM_{10} particles is recommended instead of the black smoke. The former measurement is believed to be more appropriate since it represents the particles that are most likely to penetrate into the human lungs, causing adverse health effects (see sections 2.2.1 and 3.3.1). Furthermore, most of the data available to the Panel are results of epidemiological studies that have been conducted using PM_{10} measurements.

b) The particles concentration measurements will be averaged over a 24-hour period. In the absence of any studies indicating shorter duration, the panel considered that a pollution episode of 24-hours minimum duration may cause acute health effects.

c) The recommended maximum concentration of PM_{10} particles has been set at 50 $\mu g/m^3$. It is the Panel's belief that at this concentration health effects on susceptible individuals are likely to be very small whereas the very large majority of individuals will be unaffected. Further reduction was considered to have a minimal effect. Indicative is the estimation that a rise from a 20 to 50 $\mu g/m^3$ daily average would result in just one extra patient in a population of one million being admitted to hospital with respiratory problems.

d) It is recommended that these standards should be reviewed after a maximum five years period in the light of any new data.

Table 2.6. UK Air quality standards and objectives.

Pollutant	Standard		Objective
	Concentration	**Measured as**	
Particles PM_{10}	50 µg/m^3	24 hours mean	99th percentile by 2005

* Ninety-nine (99%) percent of the 365 24hours mean values should be at or below this value (i.e. 50 µg m^{-3})

2.5.2.3. Air Quality Standards in European Community and US

In 1998 the member states of EU agreed on the "Daughter" Directive in order to protect the human health and the ecosystem. This directive which has two stages contains limiting values for major pollutants such as SO_2, NO_2, PM_{10} and lead. Table 2.7 shows the PM_{10} values. On the other hand,, table 2.8 contains the maximum allowable concentrations of PM_{10} set by the US National Ambient Air Quality Standards (NAAQS).

Table 2.7. EU "Daughter" Directive limiting values for PM_{10}.

	Averaging period	**Limit value**	**Compliance Date**
Stage I			
1. 24 hour limit value for the protection of human health	24 hours	50µg m^{-3} PM_{10} not to be exceeded more than 25 times per year	1 January 2005
2. annual limit value for the protection of human health	calendar year	30µg m^{-3} PM_{10}	1 January 2005
Stage II			
1. 24 hour limit value for the protection of human health	24 hours	50µg m^{-3} PM_{10} not to be exceeded more than 7 times per year	1 January 2010
2. annual limit value for the protection of human health	calendar year	20µg m^{-3} PM_{10}	1 January 2010

Table 2.8. US national ambient air quality standards for PM_{10} (NAAQS).

Primary Standards	Averaging Time	Secondary Standard
$50\mu g\ m^{-3}$	Annual arithmetic mean	same as primary

Table 2.9. EU emissions standards for diesel vehicles.

Passenger Cars	Driving Test Cycle: ECE15 & EUDC	
Tier	**Year**	PM_{10} (g/km)
Euro II	1999	0.10
Euro III	2000	0.05
Euro IV	2005	0.025
Light Duty Vehicles	Driving Test Cycle: ECE15 & EUDC	
Class	**Year**	PM_{10} (g/km)
I <1305 kg	1994	0.14
	2000	0.05
	2005	0.025
II <1305-1760 kg	1994	0.19
	2000	0.07
	2005	0.04
III > 1760 kg	1994	0.25
	2000	0.10
	2005	0.06
Heavy Duty Vehicles (Trucks and Buses)	Driving Test Cycle ESC& ETC	
Tier	**Year**	PM_{10} (g/kWh)
Euro II	1998	0.15
Euro III	2000	0.10
Euro IV	2005	0.02
Euro V	2008	0.02

2.5.3. Diesel Particulate Emission Standards

Diesel emissions control have been an environmental issue world wide. In the US, Europe and Japan essentially all lorries and buses operate with diesel engines whereas

the favourable price of diesel fuel relative to gasoline has resulted in a large number of diesel passenger cars as well. For example, in the UK (1996) the relative contribution of various types of vehicles to the total particulate matter (smaller than 10 μm) coming from diesel road transport was: heavy goods vehicles (HGV's) 58%, light good vehicles (LGV's) 20%, buses 12.% and passenger cars 10% (DETR, 1999).

Depending on the application of the diesel engine (i.e. trucks, buses, passenger cars) the allowable emission standards as well as the test driving cycles vary in order to reflect the different duty anticipated for the particular engine. In addition, the test cycles that the vehicles undergo during the emission inspection differ for various countries in order to simulate the local driving conditions imposed by the distinct terrain morphology (Heck, 1995). Table 2.9 summarises current and proposed emission standards in Europe.

2.6. Future Trends in Diesel Emissions and Air Quality Issues in Relation to Particulates

In most urban areas in the UK and especially the larger ones, road traffic is the major contributor to ground level concentration of most pollutants. Therefore, an assessment of future trends in urban air quality will strongly depend on trends in road traffic pollution. Future trends of atmospheric particulates, depend heavily on the relative contribution of diesel emissions since diesel vehicles are the principal particulate contributors(DETR, 1999).

The latest projection study for road transport exhaust emissions conducted by the Department of Transport and Environment was published in January 1999, using the most recent and detailed national data (DETR 1999).

The projections are based on traffic forecasts for different types of vehicles and roads from 1996 to 2026 and are provided by the National Road Traffic Forecasts. The composition of the vehicles fleet is estimated from predictions on new vehicles sales as well as the survival rates of the old vehicles. It is believed that the considerable

increase in diesel car sales over the recent years will be sustained. Therefore, the projections are based on the assumption of a 20% annual growth in new car market penetration. This rate will remain constant over the forecast period. Furthermore, the survival rate of the old vehicles has been assumed constant at the mean levels of recent years (DETR, 1999).

Another factor that has been taken into account was the impact of existing and future legislation affecting automotive emissions. The stimulus for the current study was based on the implementation of the proposed EC Directives (see section 2.6.3.) which aim to limit the PM_{10} concentrations emitted from the exhaust pipes of new diesel vehicles marketed after 2000. Furthermore, other pieces of legislation indirectly affecting the particulate emissions have been taken also into account. For example, the implementation of new EU fuel standards in 2000 and 2005 as well as the termination of leaded petrol by the year 2000 (DETR, 1999).

The projected emission of PM_{10} from road vehicles exhaust up to the year 2025 are shown in figures 2.7 and 2.8.
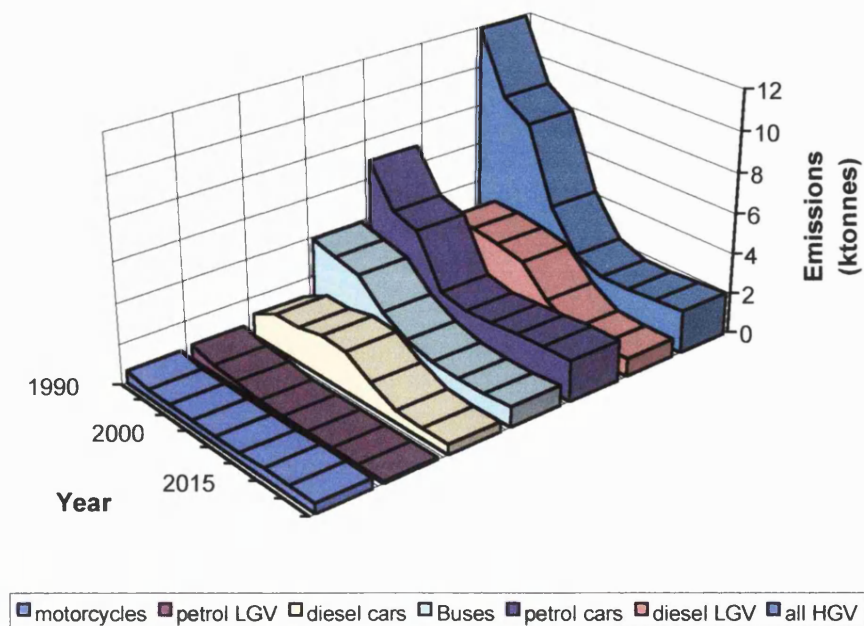
Figure 2.7 UK road transport future emissions for PM_{10} (DETR, 1999).
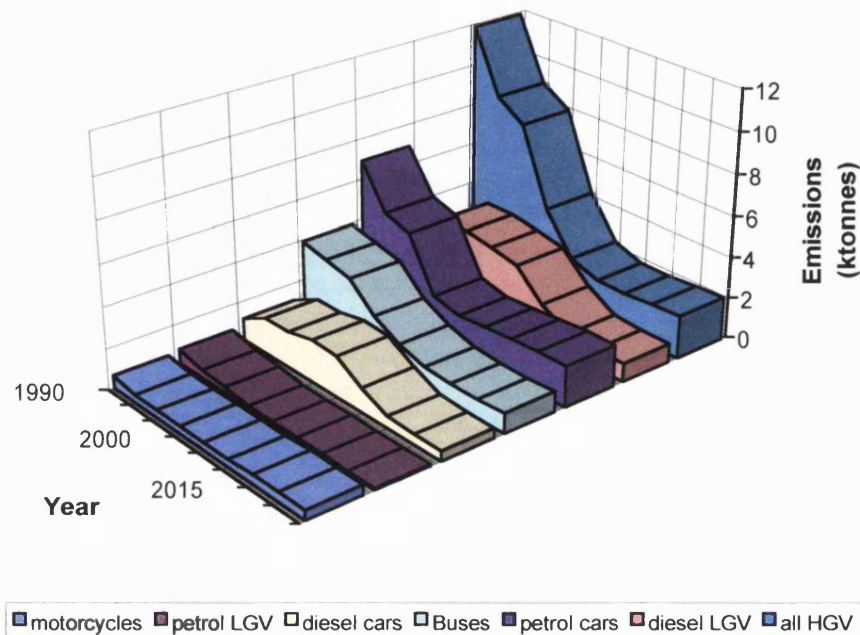
Figure 2.8 Urban UK road transport future emissions for PM_{10} (DETR, 1999).

These figures show the dominance of diesel vehicles as a the main source of PM_{10} emissions. However, there is an overall decrease mainly due to the penetration into the fleet of diesel vehicles meeting the tighter emissions standards compensating for the continuing growth in traffic over the same period. These results also highlight the constant decline of the petrol vehicular emissions attributed mainly to the use of the three-way catalyst as well as the decrease in the consumption of leaded petrol (DETR, 1999).

These projections are based on the current proposals (DETR, 1999) being negotiated by the member states of EU up to March 1998.

2.7. Conclusion

The chapter provided an up to date overview of the air particulate pollution issue. Until recently, public and scientific interest have focused on the harmful effects of the

'gaseous' pollutants emitted by vehicles. However, more recent studies have revealed that the accompanying particulates suspended in the exhaust fumes, especially those between 0.01 μm to 10μm, pose serious health hazard and environmental problems. Road traffic and more specifically diesel vehicles are the major contributors to the total suspended particulate matter in the atmosphere.

Consequently, various regulatory laws that aim to progressively decrease vehicular emissions and ultimately achieve "zero emissions" have been introduced. It is however clear that the successful implementation of such regulations crucially depends on the ability to effectively monitor, in an online manner, particulate emissions from various sources as well as those present in the ambient.

CHAPTER 3

REVIEW OF TECHNIQUES FOR MONITORING AMBIENT AND VEHICULAR PARTICULATE POLLUTANTS

3.1. Introduction

During the past two decades, environmental issues have caused growing concern amongst the public. Consequently Governments and regulators have taken action by introducing a growing amount of environmental legislation that impinge on the ability to obtain high quality measurements. The results of air pollution measurement are being used in a number of areas and frequently are compared with other data and regulatory limits in order to draw useful conclusions. Therefore, it is of great importance that measuring methods are selected carefully and are well characterised in terms of precision, accuracy, reliability, limitations and specificity for the pollutant in question.

This chapter is divided into parts. The first part contains a review of existing techniques for sampling and measuring ambient particulate pollutants. The second part describes the most commonly used instruments for measuring particulates from vehicle exhausts.

3.2. Ambient Particulate Monitoring Networks

Countries world wide have established monitoring networks for the surveillance of air pollution. The principal objective of such networks is the determination of air quality effects on human health as well as the environment (Harrison, 1986, Couling, 1993). The networks monitor compliance with National standards and *Eu* directives and create long-term databases of particulate pollution concentration and spatial distribution.

The latter provide essential information for studying air pollution phenomena and planning future environmental control strategies (AEA, 1998).

In the UK, the Smoke and Sulphur Dioxide Network was established in 1980. It comprises 204 sites whose locations are shown in figure 3.1.
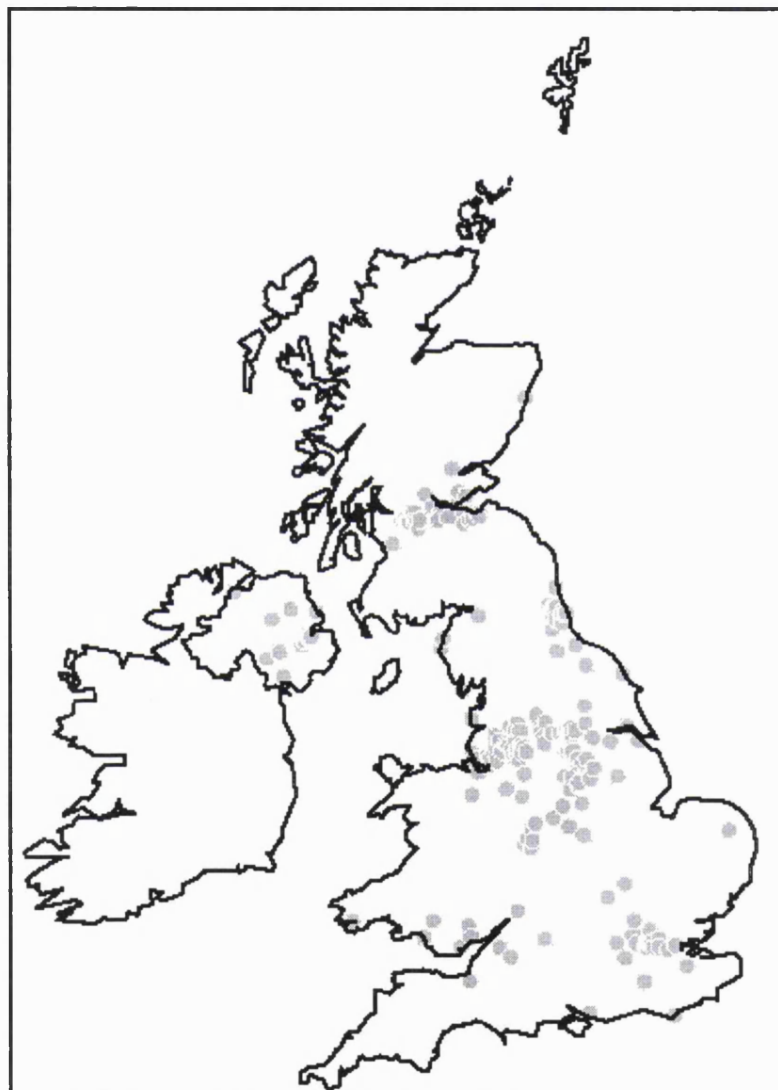
Figure 3.1. UK Smoke and SO_2 network sites for the year 1997-1998.

(http://www.aeat.co.uk/netcen/airqual/reports/smkso2/fig1.html)

Monitoring networks employ a number of different measuring systems. These systems comprise means for collecting a representative sample from the atmosphere (samplers) and means to measure the collected sample (measuring method) (Harrison, 1986). Over the years, a large number of methods for sampling and measuring ambient particulate matter have been developed. The choice though depends crucially upon the purpose of monitoring. The following represents a review of the existing sampling and measuring methods used for monitoring ambient particulates.

3.3. Ambient Particulate Sampling Systems

3.3.1. Particulate Sampling Standards

Historically, filter methods were the first samplers to be employed in order to measure what is termed "Total Suspended Particulate" (TSP), representing the material collected by the specific sampler regardless of the size (normally < 40 μm). However, as stated previously (section 2.2.1), the particles' potential health effects are related to their size. In early 1980's, the International Standards Organisation in ISO 7708 specified three new conventions for fractions of airborne particles that directly affect human health (Couling S., 1993). These conventions are shown in figure 3.2 and summarised in the following:

Inhalable: size range of the total airborne particles that can potentially be inhaled through the nose and/or mouth.

Thoracic: inhaled particles that can penetrate into respiratory tract beyond the larynx. Thoracic particles have a median aerodynamic diameter of 10 μm and geometric standard deviation of 1.5 μm.

Respirable: inhaled particles which can penetrate deep into the airways of the lungs (alveovar region). Respirable particles have median aerodynamic diameter of 2.5 μm and geometric standard deviation of 1.5 μm.
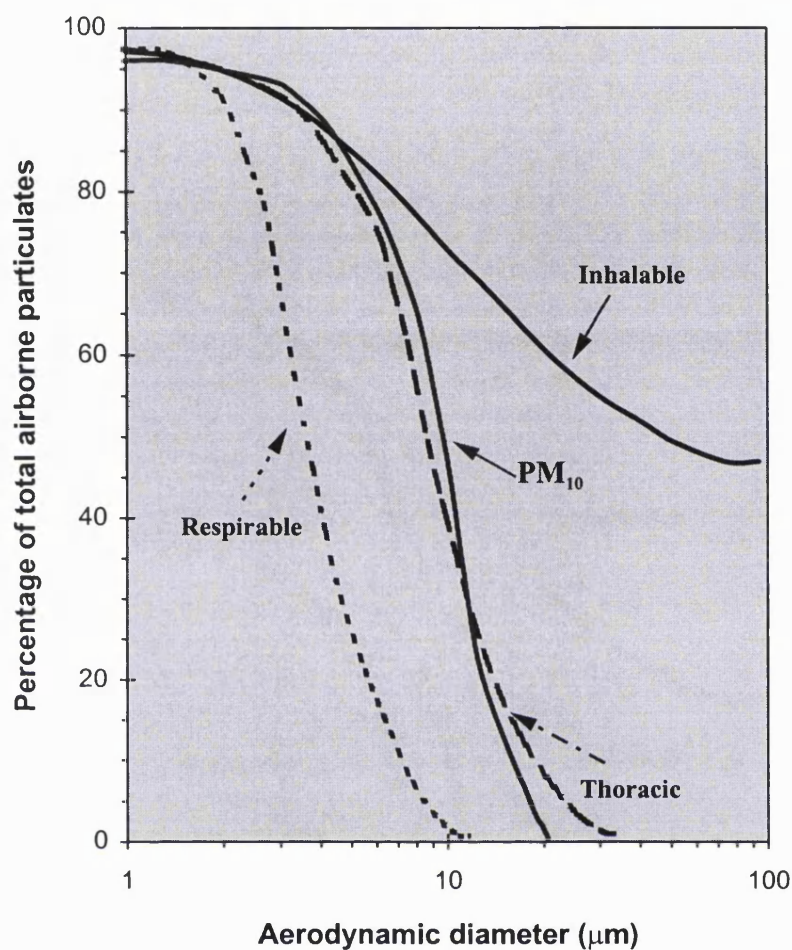
Figure 3.2. ISO 7708 Particle sampling conventions related to health (DETR, 1996)

In the US, EPA's equivalent of the thoracic aerosol fraction is known as PM_{10}, which represents the airborne particles with 50% cut-off size of 10 μm. PM_{10} differs slightly from the ISO definition since *the latter's* upper limit is higher at 26 μm as shown in figure 3.2. However, in practice this difference is thought to have a negligible result on their physiological effects (Harrison et al.,1986).

Subsequently, TSP measurements have been progressively sidelined by other sampling techniques as these do not meet the international requirements for particulate concentration measurements of a specific size range (Benarie M. 1976, DETR, 1998). The current focus of health related sampling of particulate is on PM_{10} since they represent the highest health hazard.

3.3.2. Description of the Sampling Systems

3.3.2.1. British Standards Suspended Particulate Sampler (BS 1747)

The suspended particulate or smoke sampler has been widely used in the UK since 1960's. It is the official sampler of the Basic Urban Network, and UK Smoke and the EC Directive 80/779/EEC Sulphur Dioxide Network (DETR 1998). This sampler is shown in figure 3.3a.The inlet which is protected by a mesh comprises an inverted glass funnel located more than 2.5m above the ground and 1m from the adjacent wall. The atmospheric air is drawn through the funnel using a suction pump at a sampling rate varying from 1 to 100 litres/min. The particles are collected on a 10 cm diameter filter placed 2m from the inlet (DETR, 1996). The amount of the collected material can be determined either with gravimetric or photometric methods (reflectance /transmittance) (Harrison et al., 1986; WHO, 1976). A minimum sample of 10 μg is considered to be adequate for the determination of particulate mass concentration, which will normally require a sampling period of 24h.

This sampler is commonly used in combination with a light reflectance method (see 3.3.3.2) to measure smoke concentration ($\mu g/m^3$). The efficiency curve presented in figure 3.3b shows that the sampled particles have maximum diameter of 30 μm with 50% cut-off size of 4.5 μm. The latter approximates the "respirable" fraction defined in IS 7708 and therefore it is often used as low volume (1-1.6 l/min) sampler for measuring $PM_{4.5}$ (Harrison, 1986).

This system requires a rather complicated housing arrangement since the measuring instruments (especially with the photometric method) are located indoors with a sampling line leading to the outside. Furthermore, the sampler must be calibrated rather frequently by trained personnel. However this type of sampler is inexpensive and incurs low operating costs (WHO 1976).
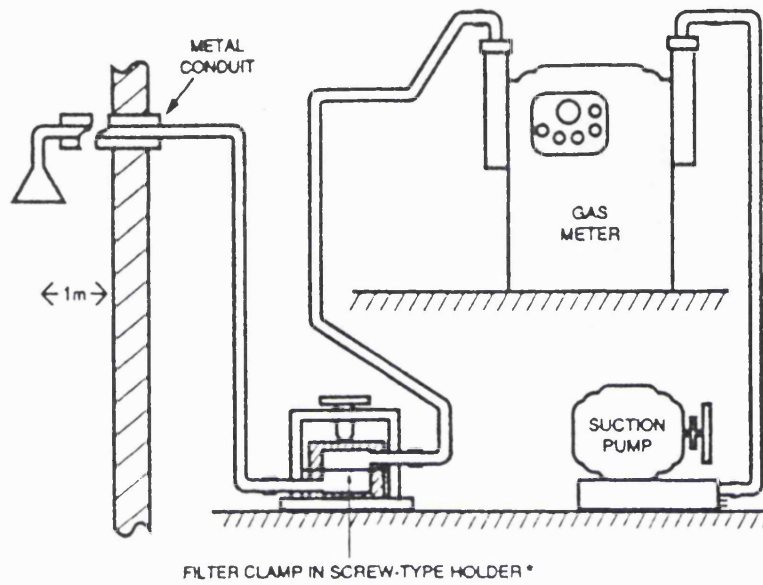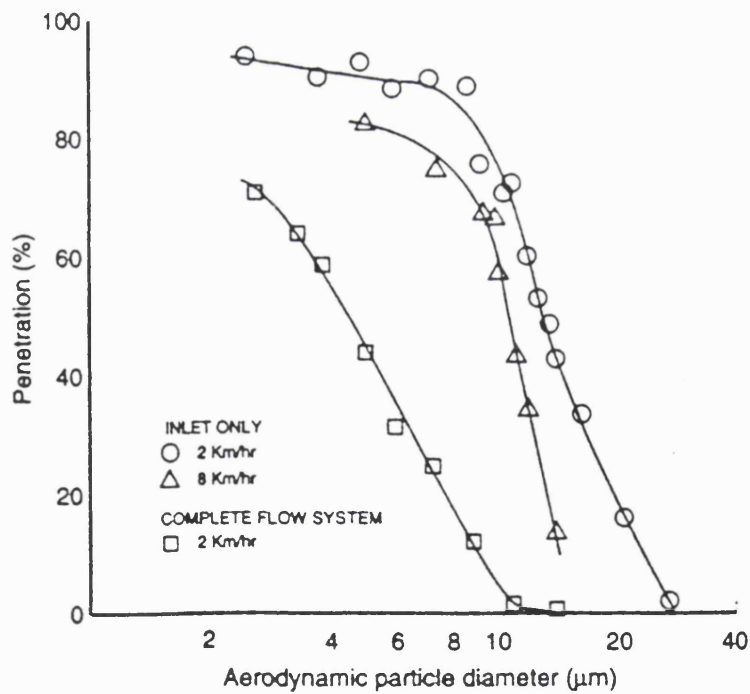
Figure 3.3. British black smoke sampler together with its sampling efficiency curves. (QUARG 1996).

3.3.2.2. High Volume Samplers

High volume samplers have been widely used in the US. The Graseby Andersen High Volume (Hi-Vol) sampler depicted in figure 3.4 is the official EPA sampler used for PM_{10} measurements by the US National Air Sampling Network (DETR 1996).

A high flowrate turbine blower draws ambient air through a fixed area gabled roof and a 20 x 25 cm rectangular filter at a constant flow rate varying from 0.16 to 0.12 m^3/min (WHO, 1976). Because of the special design and dimensions of the sampling slot, suspended particles having diameters between 0.1 to 100 μm are removed from the air. These particles are further fractionated to PM_{10} by a classifier (normally an impactor) and subsequently collected on the filter (DETR, 1996). The flow rate can be maintained constant despite all the variations in pressure drops on the filter by using electronic flow controllers (Harrison, 1986). The mass concentration (μg/m^3) of suspended particles in the air is defined by measuring the mass of the collected particulates (gravimetrically) and dividing it by the air sample volume measured by a gas meter. A routine sampling time is normally 24h.

The advantages of this method are first the maintenance of constant flow rate and constant sampling time. Second, the collection of large quantity of sample allows further chemical analysis of the particulates if required. Finally, this sampler is relatively inexpensive and easy to operate requiring minimal training (WHO, 1976). .

The main disadvantage of this method is that a clean filter has to be reloaded before every sampling period and retrieved immediately after. This will otherwise result in errors due to passive sampling or particles blowing by the wind. Furthermore, contamination or damage of the filter is possible when inserting or removing it from the sampler especially on windy rainy days. Also, the effect of humidity on the filter and the collecting sample has to be eliminated before proceeding to particulate mass measurement (Harrison, 1986).

High volume samplers can also be used for measuring total suspended particulate matter. The design of the apparatus is identical to that used for PM_{10} minus the fractionator between the inlet cover and the filter.

3.3.2.3. Sequential Filter Sampler (SFS)

The sequential filter sampler (SFS) is a multiple sampling device equipped with a medium volume PM_{10} inlet. Strictly speaking, SFS sampler is a semi-automatic apparatus which has been devised in order to eliminate difficulties arising from the frequent change of sampling filters. The main component of the system shown in figure 3.5, is a programmable timing motor which in predetermined time intervals (every 24h or every 3h) automatically changes the sampling lines. The motor moves through 1/8 of a revolution to move the upper slotted disc which connects the main air intake to each of the eight sampling lines. At the end of the sampling sequence filters and Drechsel bottles are removed for analysis and replaced with new ones.

3.3.2.4. M-Type Sampler

The M-type sampler is one of the oldest samplers, established in the UK during early 1970's. Its design resembles the BS Smoke Sampler described earlier. Figure 3.6.a is a schematic representation of the device. A filter placed in a 37 mm open-face holder is covered by a downwards-facing cylindrical hood which protects the filter from the rain and the wind. Because of this metal cover, large particles cannot be sampled and this is clear in the sampling efficiency curve shown in figure 3.6.b (QUARG, 1996).

The most important advantage of this method is that the filter is placed just off the sampler's inlet. Therefore, potential losses due to particles deposition on the walls during the transportation of the air sample between the inlet and the filter are eliminated. On the other hand the sampler performance is dependent strongly on the speed of the wind. However, at a speed of 6 m/sec it's sampling efficiency curve approximates that of the PM_{10}. Therefore, even though it's performance is not very

reliable it is still used as an indicative PM_{10} method when the results are averaged over longer time periods (i.e. few months to a year)(QUARG, 1996).

3.3.2.5. Automatic Tape Smoke Sampler

The automatic tape smoke sampler is used to obtain multiple samples over very short periods that cannot be taken with manually operated instruments (Harrison et al., 1986). This instrument uses filter paper which is coiled around two reels. The filter strip is held in a 2.5 cm clamp which can be released automatically by a timing motor of programmable periods. Air is drawn through the filter clamp for a specific time after which a solenoid automatically raises the clamp, whilst at the same time the filter reel is wound up one complete revolution exposing fresh piece of filter strip under the clamp. The solenoid is then deactivated, clamping the new filter paper again. At the end of sampling, the strip of filter paper is removed and the deposited particles are measured by light reflectance or beta attenuation (Harrison et al., 1986).

3.3.2.6. Diffusion Batteries

Diffusion batteries have been used to sample particles in a size range of approximately 0.006 to 0.2 μm. The separation of the particles from the sampled air is based on the fact that gases have diffusion coefficients which are generally orders of magnitude higher than those of particles (Keith, 1996). Furthermore, the diffusion coefficient of the separated particles decreases with increasing particle size, resulting in a fractional capture of particles through the battery.

Diffusion batteries consist of multiple layers made of a bundle of equal diameter capillary tubes (e.g. 14500 tubes of 0.2 mm diameter and 3.8 cm length) or equally spaced flat plates or very fine wire mesh. Air is drawn through a number of sampling ports and the particles depending on their diffusion coefficient penetrate through the battery's levels where they deposit and subsequently are measured using nucleus counters (Hinds, 1982).

The advantage of this technique is that it gives particle size distribution and is very efficient for measuring very small particles. However, the latter is one of the reasons that diffusion batteries have not been widely used in ambient measurements since at the moment the focus is on slightly bigger particles (minimum 2.5 μm).

3.3.2.7. Impingement Samplers

In impingement samplers, the solids-gas mixture is first accelerated though a jet and then directed to an abrupt obstruction where the particles, due to their high momentum, do not follow the abrupt change of direction of the gas streamlines but deposit on the obstruction (Hinds, 1982). Subsequent analysis of the particle size distribution may be made by gravimetric methods, macroscopic inspection, attenuation of radiation, or light scattering (Strauss, 1978).

Particle size distributions are normally calculated from experimental data by relating the mass collected on various impaction stages to the theoretical or empirical size cut points associated with those stage geometries (Strauss, 1978).

Three types of impingement samplers exist. These include a cascade impactor, virtual impactor and cyclone sampling system which are depicted in figure 3.7. A brief description of each technique is given in the following paragraphs.

(i) **Cascade impactors** . Cascade impactors use multiple stages in series so that the sampled particles are divided into sub-fractions of specific size with the finest particles (smaller than 0.3 μm) collected on a back-up filter. Figure 3.7.a shows a schematic representation of the device (Strauss, 1978, Lundgren et al., 1979).

Commercially available cascade impactors have 2-8 stages and can be used as high volume (0.6-1.1 m³/min) or low volume samplers (0.01-0.04 m³/min). The cut-off sizes of different stages can be determined theoretically or experimentally and are dependent on geometrical parameters and air flow velocity. It is therefore important

that the sampling flow rate is maintained constant during the entire sampling period (Harrison et al., 1986).

The use of impactors requires skill, experience and proper calibration in order to take accurate particle size distributions. Furthermore, it is important to collect sufficient mass of samples for further analysis. The latter might require long sampling times (Strauss, 1978). Cascade impactors suffer also from inlet and wall losses as well as re-entrainment losses occurring when particles bounce off overloaded collection surfaces. This problem can be reduced to a certain extent by coating the impaction surface with an inert adhesive material (Hinds, 1972).

(ii) **Virtual impactors** . The operating principle in a virtual impactor is the same as that of the conventional impactor i.e. based on inertial separation. As it can be seen in figure 3.7.b, the only difference is that in a virtual impactor the impaction plate of a conventional impactor is replaced by a region of relatively stagnant air. This virtual surface (which are practically deflected streamlines) is created in the cavity of collection probe so that the particles coming out of the nozzle do not impact in any surface but penetrate into the cavity. In the cavity the larger particles which remain airborne are removed by a small flow of air, known as minor flow, whereas the smaller ones that do not penetrate too deep into the cavity, reverse direction and exit the collection probe near the walls along with the majority of the air, known as the major flow (Marble et al.,1995). A device like this classifies the aerosol sample into two particle size fractions and therefore it is also called dichotomous sampler. Virtual impactors have similar size range to that of cascade impactors.

Marple et al. (1995) reports some of the advantages and disadvantages of using virtual impactors. In some applications, virtual impactor provides an ideal solution due to the following reasons: First, both the fine and the coarse particles remain airborne in the major and minor flow respectively. Therefore, is not necessary to stop the sampling operation in order to collect the different particle segments for further analysis.

Second, the cut-off characteristics of the virtual impactor can be as sharp and as accurate as those of the conventional impactor and far better than the corresponding characteristics of the cyclone.

Finally, by not having an impaction plate, the problem of particle re-entrainment causing errors in the size distribution is eliminated.

On the other hand the internal losses are greater in the virtual impactor than in the conventional one. Another inherent disadvantage of the virtual impactor is that the coarse particles segment contains a small fraction of fine particles.

(iii) **Cyclone Sampling Systems.** Cyclones have been used less frequently than impactors for obtaining particle size distribution measurements because they tend to be bulky and give poorer resolution. However, when larger samples are required or when continuous operation is needed cyclones are more suitable than impactors (Strauss, 1978).

Figure 3.7.c depicts the most commonly used design: the reverse flow cyclone. In this design the gas-solids mixture enters the top chamber tangentially and spirals down to the apex of the conical section. It then moves upward in a second, smaller diameter spiral, and exits at the top through a central vertical pipe. The solids move radially to the walls, and after the impaction slide down towards the bottom of the cyclone to the collection area (Coulson, 1991). Strauss (1978) reports a design by Chang (1974) comprising a system of parallel cyclones that separates particles into four size fractions. This system is used for in situ measurement of source emissions but because of its size a probe for sample extraction is used.
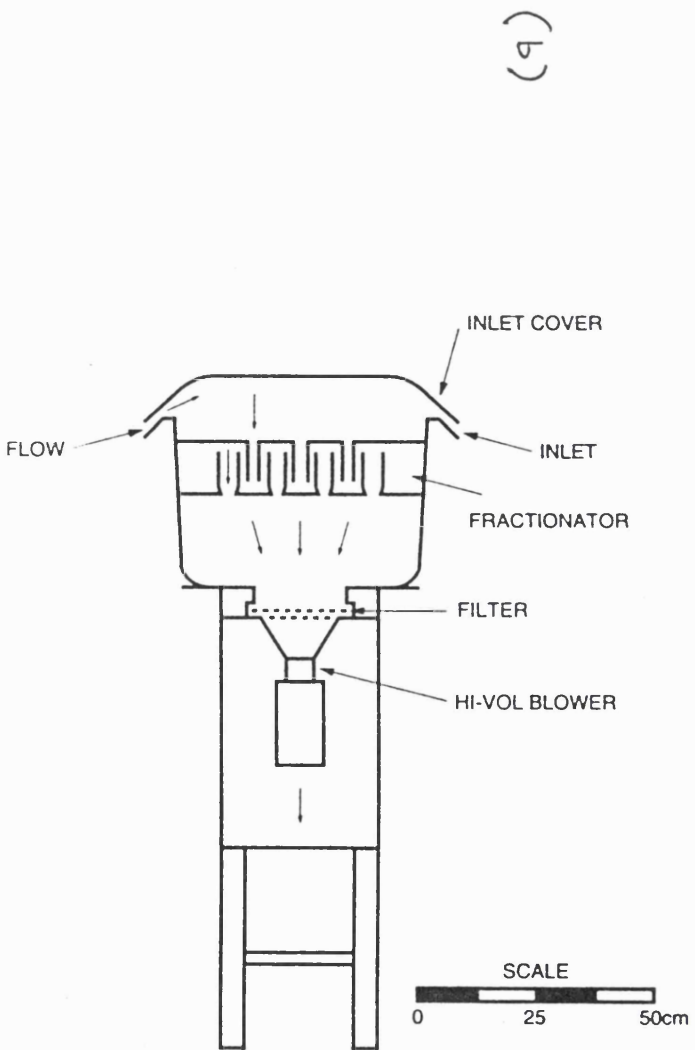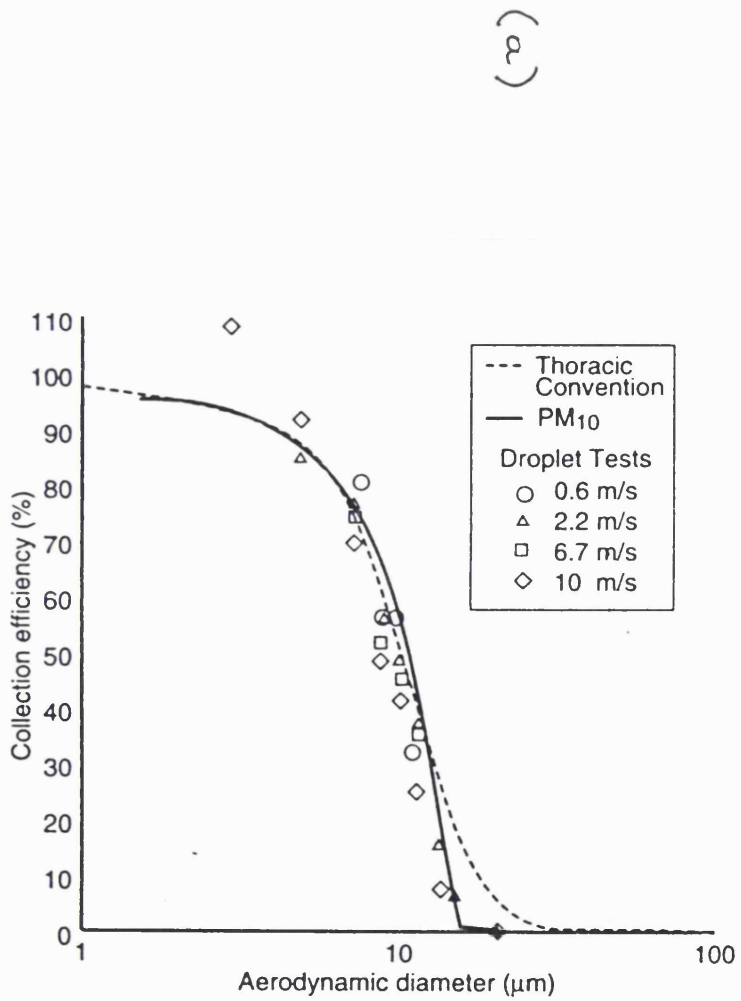
Figure 3.4. High volume PM$_{10}$ sampler together with its sampling efficiency curve. (QUARG, 1996).
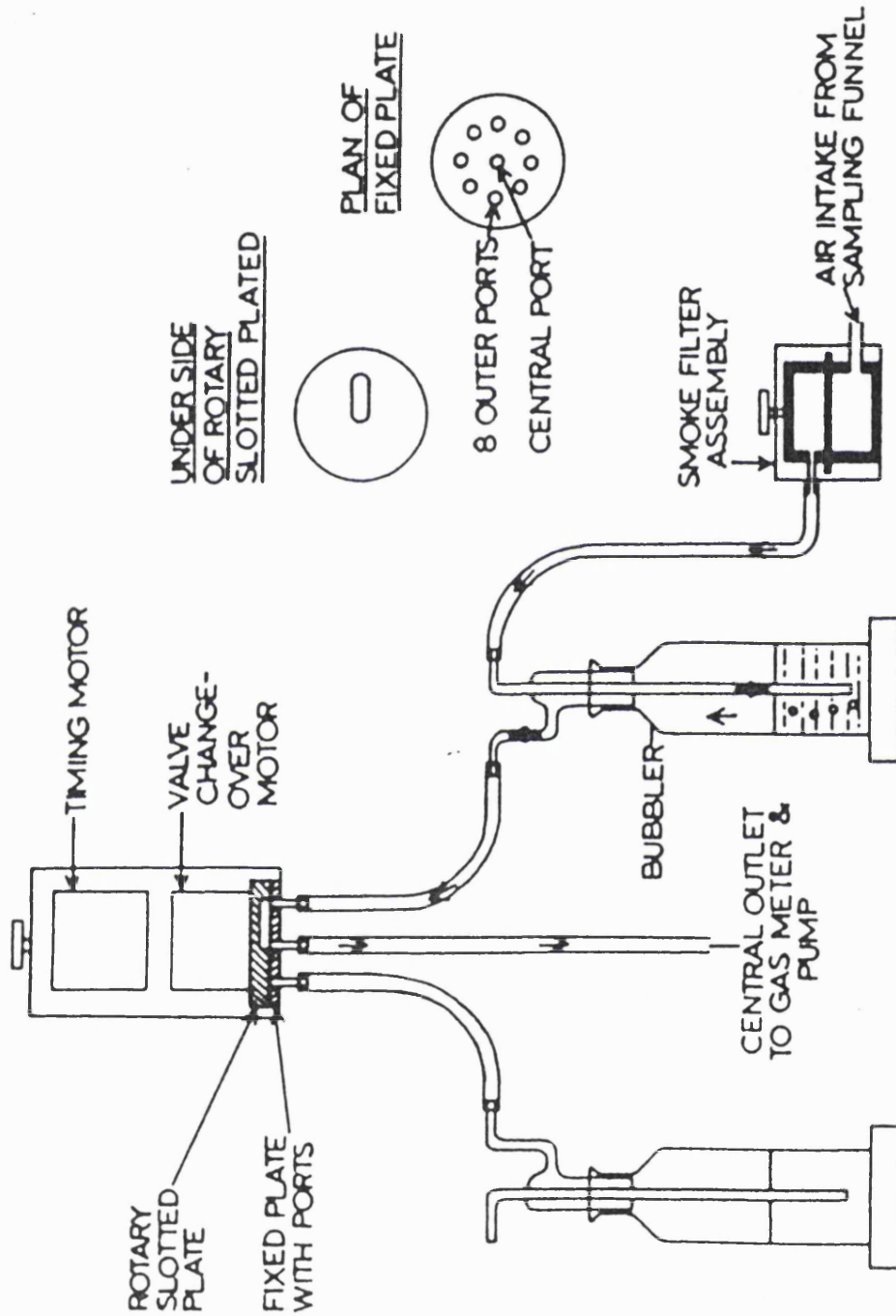
Figure 3.5. Sequential filter sampler (Harrison, 1986).

SECTIONAL VIEW - DIMENSIONS IN mm
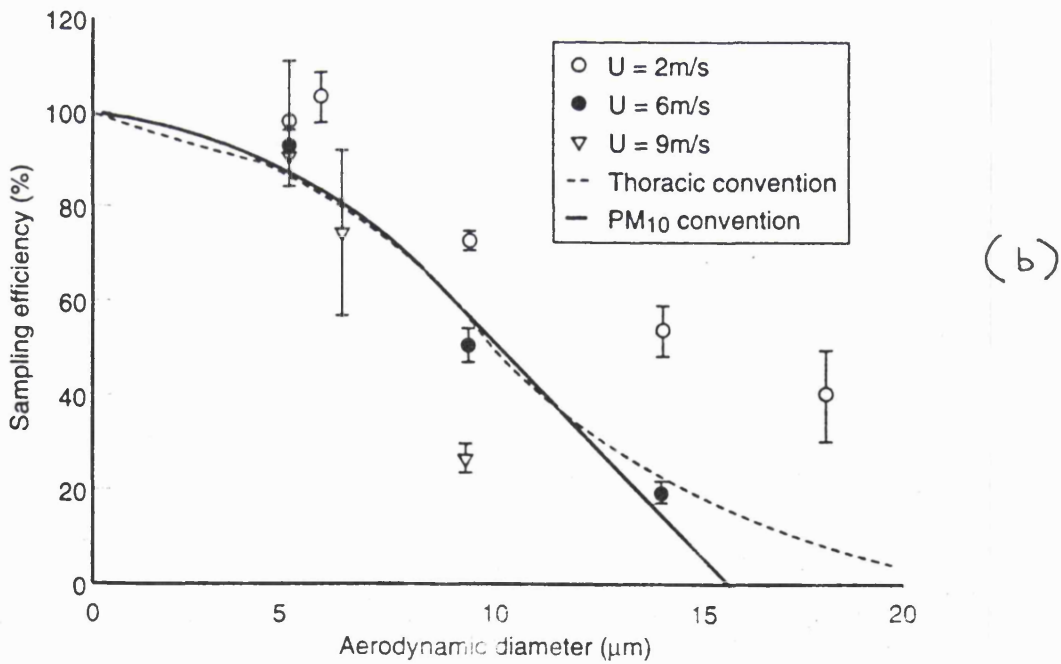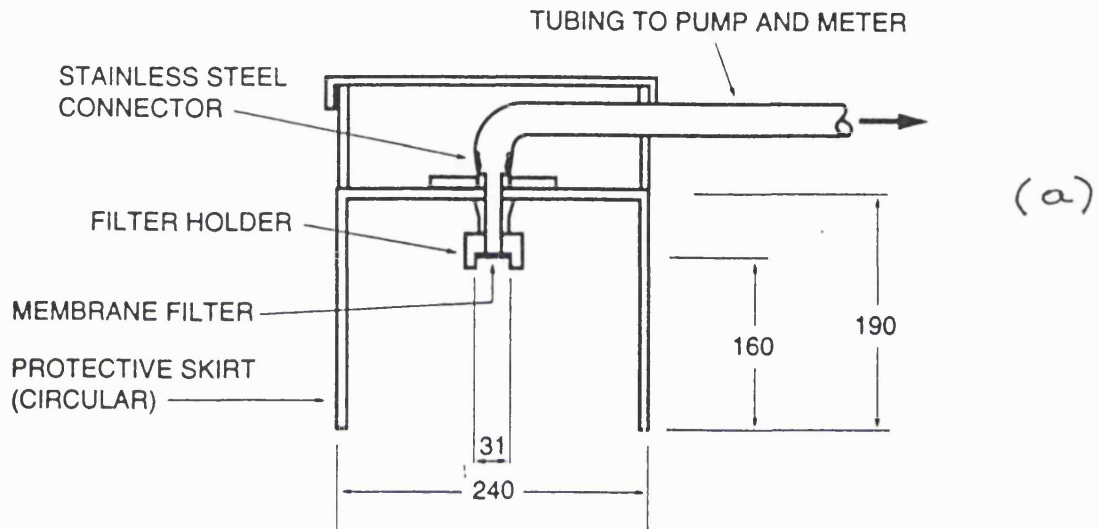
Figure 3.6. M-Type sampling head together with its sampling efficiency curve. (QUARG, 1996).

(a)

(c)

(b)
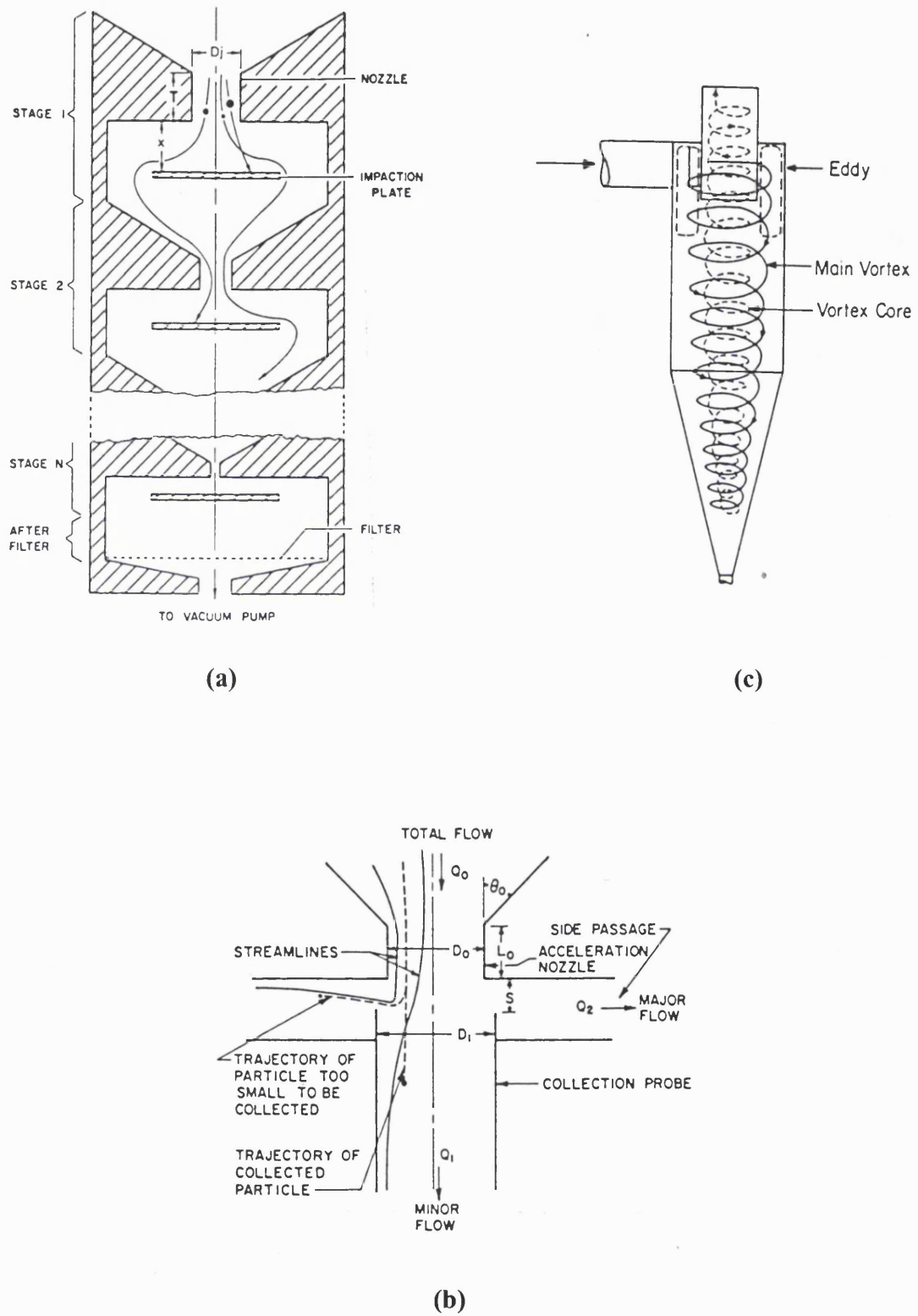
Figure 3.7. Impingement Samplers: a) cascade impactor b) virtual impactor
c) cyclone.

3.3.2.8. Deposit gauges

Deposit gauges are samplers used for monitoring the nuisance effects of airborne particulates. Deposition of dust is considered by people as a major nuisance, and therefore its measurement is considered to be indicative of the nuisance effects of particulate pollution. The two main designs of deposit gauges are briefly described below:

i) The British Standard Gauge (BS 1747). This is essentially a glass or plastic bowl into which the dust falls. Dust is washed down by rain into a large collecting bottle under the bowl. The sample is collected monthly for gravimetric determination and further chemical analysis. The major disadvantage of this gauge is that because it is shallow the deposited material can be blown out during dry periods (Harrison, 1986; Couling, 1993).

ii) French Standard Gauge (NF X43-006). This gauge is an improvement on the British standard model which prevents the dust from being blown out. It has a better aerodynamic design in order to minimise the generation of eddies during collection. Furthermore, the angles of the lower half of the gauge are steeper facilitating the descent of the particles into the collecting bottle. As a result, the particles spend less time resting in the collecting bowl reducing the possibility of being blown out by wind (Harrison, 1986; Couling, 1993).

3.3.3. Description of Methods for Measuring Atmospheric Particulates

3.3.3.1. Gravimetric

The most common method for determining the particulate mass deposited on a filter is the gravimetric method. This method has been selected by most of the workers as well as organisations such as EPA and WHO as the standard method for the determination of particulate concentrations (WHO, 1976, DETR 1996).

The only instrument required for this method is a high accuracy analytical balance that can weigh filters to a precision of 0.01 mg. The balance is located in a chamber or a room with controlled temperature ($\pm 1^\circ$ C) and humidity ($\pm$ 5% for a relative humidity 30 and 50%). The filter is left to equilibrate for at least 1h in this environment before each weighting. Three blank (control) filters and a reference mass of approximately the same weight as the filters should be weighed each time the sample filters are weighted.

Attention should be paid to the external conditions, especially humidity, during the measurements. Any change in humidity between initial and final weightings can cause serious errors. Hinds (1982) reports that a 47 mm PVC filter gained about 0.7 μg whereas a similar cellulose filter gained 28-35 μg for each one percent increase in relative humidity. Another source of error is static charge build-up. Therefore, it is common to have an alpha radiation source (e.g. polonium-210) near the filter in order to neutralise any accumulated charge (Hinds, 1982). Finally, the filters should be handled with care in sealed filter-holding cassettes in order to avoid contamination.

The main disadvantage of the gravimetric method for measuring particulate mass is the long time required not only to perform the measurement but also to condition the filter. Furthermore, the weighting requires controlled laboratory conditions. Therefore, the samples are either transported to a laboratory or a mini lab has to be set-up by the sampling site (WHO, 1976). These limitations make the method unsuitable for real-time or continuous measurements.

3.3.3.2. Light Reflectance

The light reflectance method has been widely used in the UK and is the standard measuring method (80/779/EEC) for measuring airborne particulates. Strictly speaking, the technique uses a reflectometer to assess the darkness of the stained filters and subsequently the black smoke mass concentration (μg/m^3) can be inferred using a calibration curve (QUARG, 1996).

The most important part of the reflectometer is the measuring head which consists of a light source and a photo sensor. It is tightly fitted into a masking disc which restricts the illumination only into a small hole of 0.5 inch diameter. This hole serves as a "window" through which the stained filter is examined. The beam generated by the light source is reflected upon the filter paper on to the photo sensor where it causes an electrical current detected by an amperemeter. The darker the stain, the lower the intensity of the reflected light (Harrison, 1986).

Even though the light reflectance method is suitable for most routine air pollution work, its accuracy is not very high. The main source of error is that the technique measures the darkness of the sample rather than mass concentration directly. Therefore, the nature of sampled particles and especially their optical properties affect greatly the measurements. For example two equal samples of crystalline matter and carbon rich matter will reflect different amount of light to the photo sensor resulting to an error (WHO, 1976). Consequently, one has to bear in mind that the measurement is mainly an indication of dark material in air, which may not be proportional to the total weight of suspended matter.

On the other hand the reflectometer can be integrated on the sampler making the results immediately available and thus eliminating errors arising from filter's manipulation. Furthermore, the cost to purchase and operate the apparatus is low (WHO, 1976).

3.3.3.3. Oscillating Microbalance

The operational principle of this technique is that the frequency of mechanical oscillation of any element such as a tapered glass tube or a piezoelectric crystal is directly proportional to the mass of the element. Any change in effective mass of the element due to particles deposition results in a change in its resonant frequency (Keith, 1996; Allen, 1997). Since Olin J.G., in 1971 first described the system, several commercial versions have been developed. In this section two of the most

widely used applications will be briefly described. These are: i) the Tapered Element Oscillating Microbalance (TEOM) ii) the Piezoelectric Microbalance.

i) Tapered Element Oscillating Microbalance (TEOM). The TEOM shown in figure 3.8 is built in a 16.7 l./min PM_{10} sampler and can measure continuous hourly values. The sampled air passes through a flow divider which directs a portion (3 l /min) of the total flow through a 16 mm diameter filter located on the narrow end of a hollow tapered glass tube (Keith, 1996). The wider end of the tube is fixed, while the narrow end oscillates in response to an applied electric field. As the particles are collected on the filter, the tube's natural frequency of oscillation decreases and this decrease is linearly proportional to the added mass. Subsequently, the PM_{10} concentration is calculated by comparing with experimentally determined frequency calibrations. An important detail of this system is that the inlet including the measuring system is kept at steady 50 °C to drive off any sampled water droplets. However, because of this temperature there is the risk of volatile material losses (QUARG, 1996). This instrument has been chosen by the Department of the Environment's for the Automatic Urban Network as well as by other organisations.

ii) Piezoelectric Microbalance. The piezoelectric microbalance has exactly the same operating characteristic as TEOM described above but instead of an oscillating filter mounted on a tapered tube it uses a quartz oscillating crystal. The most frequently used crystal is AT-cut quartz disk, about 13 mm diameter and 0.2 mm thick (Lundgen, 1979). The sensitivity of the sensor is about 200 Hz/μg and thus the minimum detectable mass is about 0.005 μg. The instrument collects particles in the size range of 0.01 to 10 μm at concentrations between 2 to 20000 μg/m^3 (Allen, 1997).

FLOW ———→   ←——— FLOW

SAMPLING HEAD

HEATED-AIR INLET

FILTER CARTRIDGE

ELECTRONIC
FEEDBACK SYSTEM

MICROPROCESSOR

TAPERED
ELEMENT

TO FLOW CONTROLLER
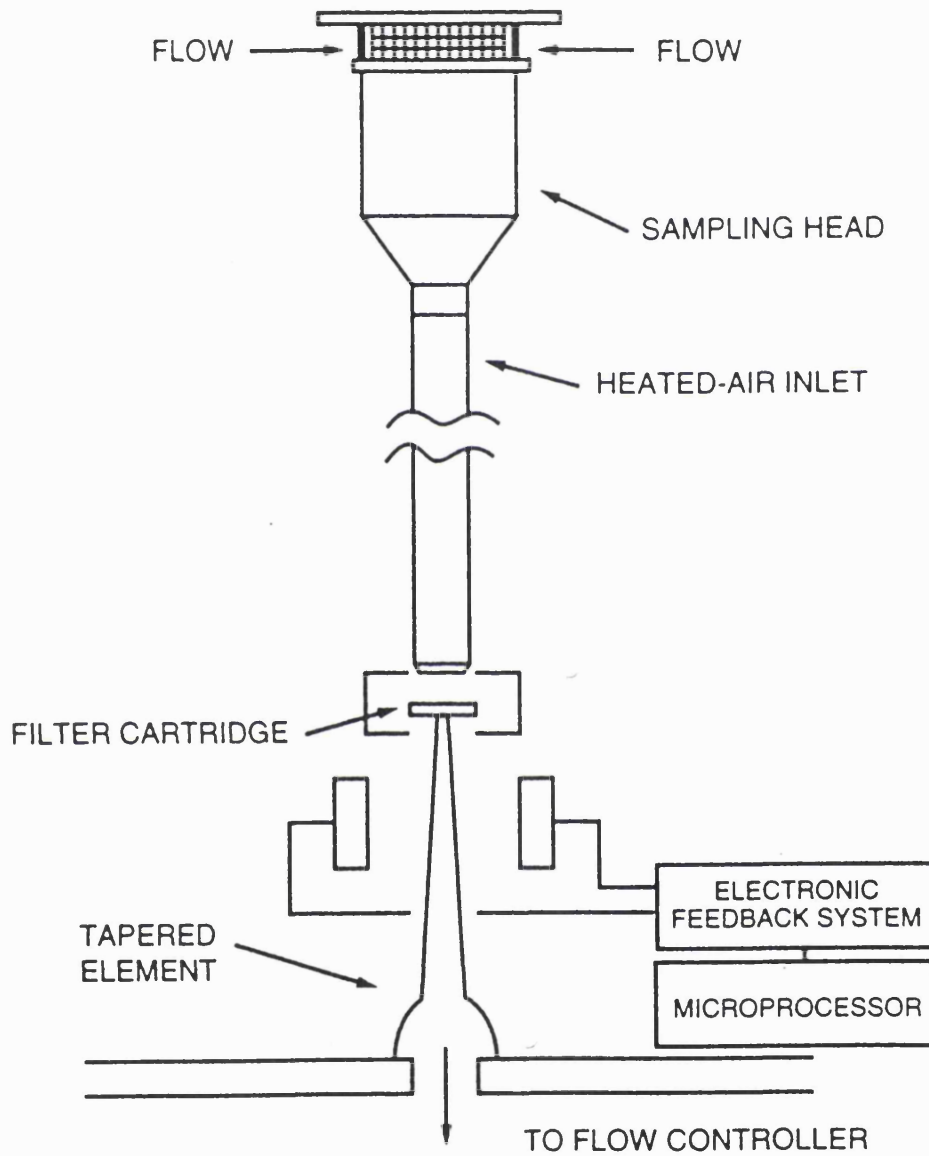
Figure 3.8. Schematic diagram of the TEOM ambient aerosol monitor.
(QUARG, 1996).

3.3.3.4. Beta Radiation Attenuation

This measuring technique is based on the fact that when beta rays emitted by a nuclear source impinge on matter, some are absorbed, some are scattered and some are transmitted. The reduction of the incident beam intensity, known as beta radiation attenuation is proportional to the mass concentration of the material (Allen, 1997).

The most popular system that uses beta attenuation is basically an automatic tape sampler (as described in 3.3.2.5) where a promethium 147 beta source is fitted directly above the filter tape, and a Geiger Muller type detector measures the absorption of beta radiation. The instrument can be set to operate from ½ h up to 24h cycles with intermediate averages if selected. It automatically takes a sample and feeds it into the radiation measuring path where the attenuation of the deposited material is measured.

3.3.3.5. Light Scattering

Light scattering by particles suspended in a fluid has been widely used in developing instruments for the in-situ continuous measurements of particle concentrations. These instruments employ the interaction between suspended particles and visible light within a sensing region (QUARG, 1996). In all applications, the samples have to be diluted with fresh air to ensure that the particles pass through the sensing volume in single file. Thereafter, the radial distribution of scattered intensity is a function of particles size, shape and refractive index as well as the wavelength of the incident radiation. Therefore, these instruments require a complicated calibration procedure in order to give results in terms of mass concentration. Furthermore, the calibration is valid provided that the nature of particles does not change. This fact makes ambient particulate measurements using this type of technology rather uncertain (QUARG, 1996).

The two types of instruments mainly used are: the right-angle light scattering systems and the near forward light-scattering system. The main difference between these two

instruments is the angle of scattered light. In the first application the light is scattered in near forward direction (1-20°) whereas in the second, the angle of the scattered light is 90° (Allen, 1997). As a result they have different performance characteristics. The former has a very broad size range of application (0.3-60 μm) and is very sensitive. However it is very much dependant on the particle refractive index making it unreliable for use with mixed aerosols. On the other hand, the near forward scattering system is slightly affected by the refractive index but has limitation on the particle size range that it can measure (1.5-6.5 μm) (Lundgren, 1979; Allen, 1997).

Finally, it should be noted that there are similar optical techniques for continuous measurement of airborne particulates based on light absorption rather than scattering. However the light absorbing measuring methods have two major drawbacks. First is that only particles of absorbing material can absorb light, by contrast all particles scatter light. Second the opacity is a function of the projected surface area of particle and not of its mass, and that limits the applications of the measurement. Despite these problems this technique is still used for continuous smoke measurements (Allen, 1997).

3.4. Systems for Monitoring Particulates Emitted from Mobile Sources

Monitoring aerosols emitted from mobile sources is a difficult task due to a number of reasons. For example vehicular emissions contain particles with diameters varying from few nanometers up to several microns. Furthermore, the temperature of the exhaust gases is rather high and the exhaust flow is unsteady and non-uniform (Harrison, 1986).

As indicated earlier traffic pollution has been a major public concern and several measuring techniques have been developed for this purpose. These either use the full or the partial flow of the exhaust gas (ISO 11614, 1994). In case of partial flow, it is important to ensure that the taken sample is representative of the exhaust aerosol. This will require that the gas velocity inside the sampling probe must be equal to that of

the main gas stream at the inlet of the probe. This technique is called isokinetic sampling (Hinds, 1982).

Furthermore, the sampled stream is usually diluted in a tunnel with dry filtered air in order to simulate the equivalent process that particles undergo after they are emitted into the atmosphere and to prevent condensation of the hot vapours (Habibi, 1970, Ahlvik et al., 1998). The latter can also be achieved by maintaining the exhaust gas and the measuring equipment in elevated temperatures (60-120 °C) (ISO 3173, 1974).

A brief review of the most frequently used instruments for measuring diesel aerosols is given below followed by a summary of their main features in Table 3.1.

3.4.1. International Standard Method : Opacimeter (ISO 11614/ 94)

Opacimeters along with filter-type smokemeter are the earliest methods used to measure the total amount of black smoke in diesel exhausts. Even though these methods are considered to be outdated, they are still the official methods used for inspection and maintenance purposes (Ahlvik et al., 1998). The operational characteristics of the filter-type smokemeter (ISO 10054) are similar to those of the BS smokemeter used for ambient sampling and therefore will not be discussed further (see 3.3.2.1. and 3.3.3.2.)

In opacimeters, smoke is directed through a parallel visible light beam of specific length where it absorbs some of the light and thereby diminishing the intensity of the beam (Hinds, 1982). The fraction of the transmitted light which is absorbed through the smoke obscured path is called opacity and is measured in opacity units. The latter is used as an indication of the particulate concentrations in the exhaust gases (ISO 11614, 1994).

The instrument comprises a light source (lamp with colour temperature between 2800 to 3250K), a photoelectric receiver (photocell or photodiode) and a smoke chamber. The latter constitutes the casing of the instrument where the light source and the

receiver are embodied. All the instrument's internal surfaces are painted in matt black in order to minimise reflection and/or diffusion of stray light which may otherwise result in measurement errors (ISO 11614, 1994).

The biggest disadvantage of the technique is that many such instruments of established design cannot achieve a response time less than 0.5 sec (ISO 11614, 1994).

3.4.2. Electrical Analysers

Electrical analysers have been the most common instruments used in the US for diesel particulate measurements. These are based on the particle's electrical mobility Z, which is the ability of a charged particle to move in an electric field (Kittelson et al., 1999). More specifically, the velocity of a charged particle V_{TE} towards the opposite charged terminal of an electric field of strength E is given by:

$$V_{TE} = ZE \qquad (3.1)$$

Figure 3.9.a demonstrates the operational principle of the device. It consists of two opposite charged plates of a certain length, retained at a constant voltage. The aerosol particles are introduced into the constant electric field along a centre line. Equation 3.1 indicates that all particles with mobility greater than a certain value will be attracted and consequently captured onto one plate whereas those with less mobility will pass through the analyser. Therefore by comparing the particles mass entering and leaving the analyser one can determine the particles fraction with a certain electrical mobility (Hinds, 1982).

The particle size distribution measurement is based on the fact that the electrical mobility of a particle is directly proportional to the carried charge which in turn is proportional to the particle's diameter. Therefore, a unique value of electrical mobility is associated with every particle size. The analyser's cut-off mobility and consequently captured particle size is adjusted by varying the applied voltage. Hence, by proper voltage control the particle size distribution can be estimated (Ludgen,

1979). However, this application is feasible only when the particles have been charged under well defined and controlled conditions (e.g. diffusion charging) so that the charge on the particle of a given size is known (Ludgen, 1979; Hinds, 1982) .

3.4.2.1. Electrical Aerosol Analyser (EAA)

A commercial EAA (TSI Inc. Model 3030) used for monitoring diesel exhaust particulate matter is shown in Figure 3.9.b (Baumgard et al., 1992). In this case, the aerosol is drawn into the instrument at about 4 l/min and passes through a unipolar-ion diffusion charger where by using proper control, particles of a given size receive a predictable number of charges. Next, the particles flow to the mobility analyser in laminar flow enveloped by a clean air stream. Depending on the applied voltage on the tubes, the particles with mobility less than the cut-off mobility pass through the analyser and are then collected in a high efficiency filter. An electrometer connected to the filter continuously monitors the accumulated charge carried by the particles. The particle numbers can be calculated from the measured charge and the predetermined cut-off size. The instrument operates with preset voltages to provide the number of particles in each of 10 cut-off sizes between 0.003-1 μm (Hinds 1982; Baumgard et al., 1992).

There are three major problems associated with using EAA for sampling diesel emissions. First, EAA requires nearly constant aerosol concentration ($\pm$ 10%) during an operating cycle (1-3 minutes). However under typical driving conditions aerosol concentration varies more than one order of magnitude within few seconds (Ludgen, 1979). Second, EAA is adversely affected by vapours condensation. However during short period of acceleration/deceleration the exhaust fumes become supersaturated with vapours which results in condensation (Ludgen, 1979). Finally, the size and weight of the instrument have caused difficulties in its applications. The model shown in Figure 3.9.b. has a volume of 0.05 m^3 and weights approximately 24 kg.
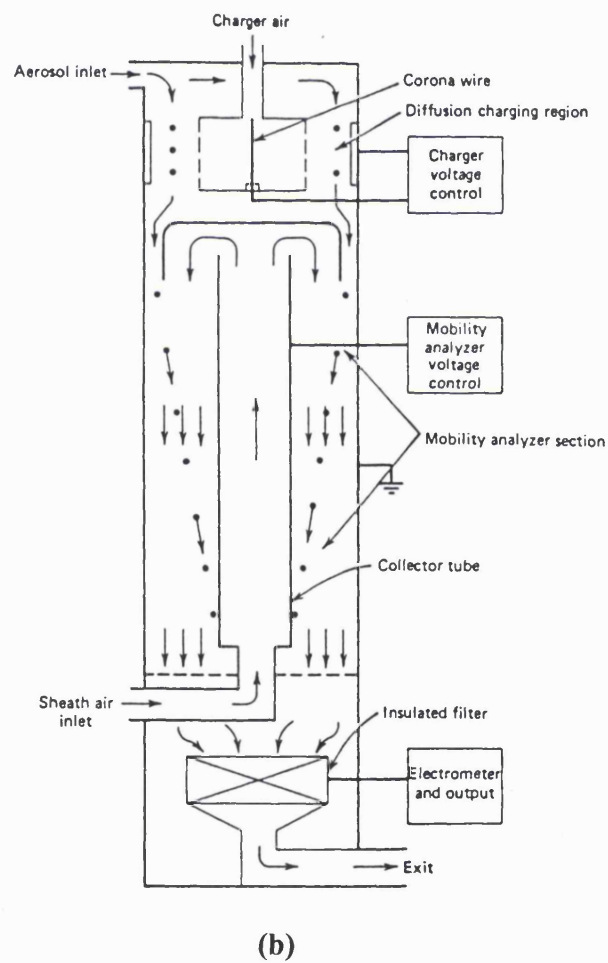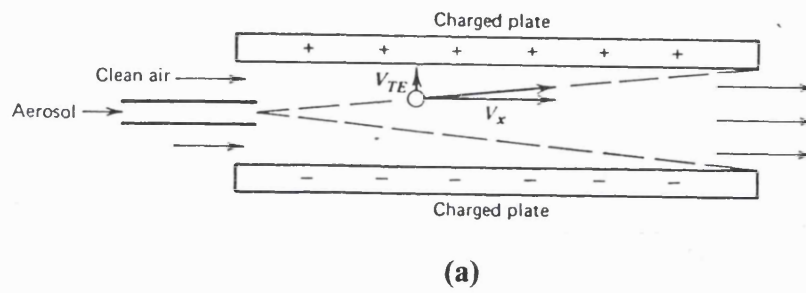
(a)

(b)

Figure 3.9. a) Operational principle of electrical analyser b) Schematic diagram of Electrical Aerosol Analyser (Hinds, 1982).

3.4.2.2. Differential Mobility Particle Sizer (DMPS).

The DMPS has the same operational principle as the EAA with the integral part of the mobility analyser being replaced by a differential type. The instrument employs a bipolar rather than a unipolar charger in order to increase the measurement resolution. The latter is further enhanced by using a condensation nucleus counter instead of an electrometer to count the particles within an electrical mobility range. The measurable size range is between 0.005 and 1 μm (Cohen et al., 1995).

3.4.2.3. Scanning Mobility Particle Sizer (SMPS).

This apparatus has been used by Greenwood et al. (1996) for sampling vehicular particulates. It has proved to be considerably faster than DMPS, since it operates in continuous mode. More specifically, in this instrument, instead of changing the electric field in discrete steps in order to select the cut-off size of the mobility analyser, it scans the electric field continuously. The particles are classified in a time-varying electric field where the applied voltage is ramped exponentially (Wang et al., 1990). Wang et al. (1990) report that this method can complete as many as 100 mobility measurements in 30 seconds without sacrificing measurement resolution. The system can handle particulate concentrations of 10^{14} particles per cubic meter and has an operational size range of 0.01 to 0.7 μm (Greenwood et al., 1996).

3.4.3. Micro-Orifice Uniform Deposit Impactor (MOUDI)

The Micro-orifice Uniform Cascade Impactor (MOUDI) is similar to the conventional cascade impactors described in chapter 3 (see section 3.3.2.7). However, it has been developed (Marple et. al., 1991) so that it can be used in vehicular exhaust sampling and therefore has several features not normally found in a general purpose cascade impactor. These include :

i) Collection of particles as small as 0.056 μm in aerodynamic diameter with moderate pressure drops. This has been achieved by employing a large number of

very small nozzles which allow for small particles to be collected at low jet velocities and consequently low pressure drops. In the particular design the cut-off size of the last stage (2000 nozzles of 52 μm diameter) can be as low as 0.056 μm with a total sampling rate of 30 l/min. In comparison the first stage employs only one nozzle of 1.71 cm diameter resulting to a cut-off size of 18 μm (Marple et al., 1991).

ii) A uniform particle collection on the impaction plates whereas in a conventional impactor, the particles deposit in a mound below the nozzle. This is a result of rotating the impaction plate beneath the nozzles so that the collected particles form annular rings. Furthermore, by drilling the nozzles at specific distances from the centre of rotation, the obtained rings will overlap forming a uniform deposit upon the rotating impaction plate (Marple et al.,1991). The uniform deposition facilitates subsequent analysis of the sample.

iii) Interchangeable impaction plates which can be handled easily and quickly in the field. The foil or filter substrates used for collection of particles are attached upon removable impaction plates. Therefore, after the end of a run, the whole assembly (substrate plus impaction plate) is removed from the impactor and is transported to the lab in special covers equipped with O-rings seals so that contamination is avoided (Marple et al., 1991).

However MOUDI is not suitable for continuous measurements since the operation has to be posed to remove and replace the impaction plates. Furthermore, it does not provide real time measurements and is susceptible to measurement artifacts (Kittelson, 1999).

3.4.4. Electrostatic Low Pressure Impactor (ELPI)

The Electrostatic Low Pressure Impactor is a cascade impactor which provides near real-time measurements of number concentrations of exhaust particles (Ahlvik, 1998). The concept of ELPI was introduced by Keskinen et al. in 1992 as a response to the need of having a cascade impactor that can provide real time measurements.

Initially, the aerosol is sampled through a unipolar charger and thereafter the charged particles pass into a low pressure impactor with electrically isolated collection stages. The current produced by the carried electric charge of the deposited particles is measured at each stage with a multi-channel electrometer. The measured current signals are then converted to size distribution using experimentally determined relations that relate the particle size with the properties of the charger and the impactor stages (Keskinen, 1992). Similar to the EAA, the process of particles charging is very important for the success of the measurement. Therefore, the operation of the system has to be well defined and controlled.

A specially modified cascade impactor with the accompanied electrometer constitute the main body of the instrument. Ahlvik and al.(1998) used a 12 stage Berner multi-jet low pressure impactor with an upper cut-off size of 10 µm and the lowest of 0.03 µm. A schematic presentation is given in Figure 3.10. Each impaction stage is electrically isolated by using rings of dielectric material between successive stages. The outer surface of each impactor stage is connected by a spring loaded contact to an electrometer input cable. The electrometer has as many channels as the impactor stages so it can take simultaneous measurements. Finally, the outer housing surrounding the impactor acts as a shield against electrostatic noise (Keskinen, 1992).

The main disadvantage of this technique is that the calibration of the apparatus is rather complex and tedious. It is based on assumed values for charging probability, particles penetration through the impactor and current measurement and therefore can be problematic (Ahlvik, 1998). Furthermore, there is no calibrating relation that can be generally applied even to impactors of the same type. This means that each individual impactor has to be separately calibrated (Keskinen, 1992).

3.4.5. Photoelectric Aerosol Sensor (PAS).

Photoelectric aerosol sensor (PAS) is an in situ measuring instrument that detects and classifies diesel exhaust particulates according to their polyaromatic hydrocarbons

(PAH) content (Burtscher et al., 1993; Kittelson et al., 1999). The operational principle is based on the fact that particles irradiated with UV light of enough intensity, emit electrons and become positively charged. Subsequently, the positive particles are collected and their charge is measured by an electrometer. This measurement is converted to particle size concentrations using experimentally determined curves. These curves are based on the fact that the photoelectric activity of the particles is directly proportional to the PAH's absorbed onto the particles. Furthermore, the PAH concentration profiles on diesel particles are known and assumed to be fairly constant under well defined sampling conditions. Consequently, the particle concentrations can be inferred from the photoelectric activity (Burtscher et al., 1993).

The main disadvantage of this technique is the assumption that PAH concentration on diesel particles is the same in all occasions as long as the sampling conditions are the same. Furthermore, it has to be kept in mind that other materials absorbed onto the particles' surface may photo-emit electrons and result in error. On the other hand, the technique can take continuous measurements, has a fast response and can detect concentrations as small as 1 ng/m^3 (Burtscher et al., 1993).

3.4.6. Aerosol Time of Flight Mass Spectrometer (ATOFMS).

Aerosol time of flight mass spectrometer can measure the size and determine the chemical composition of individual particles emitted from automobile exhaust (Silva et al., 1997).

Particles are drawn into the sizing region through an inlet nozzle which creates the supersonic expansion of the gas, during which small particles are accelerated to a higher terminal velocity than large particles. In the sizing region, the individual aerodynamic size of the travelling particles can be determined by recording its time of flight between two laser beams set at a known distance.
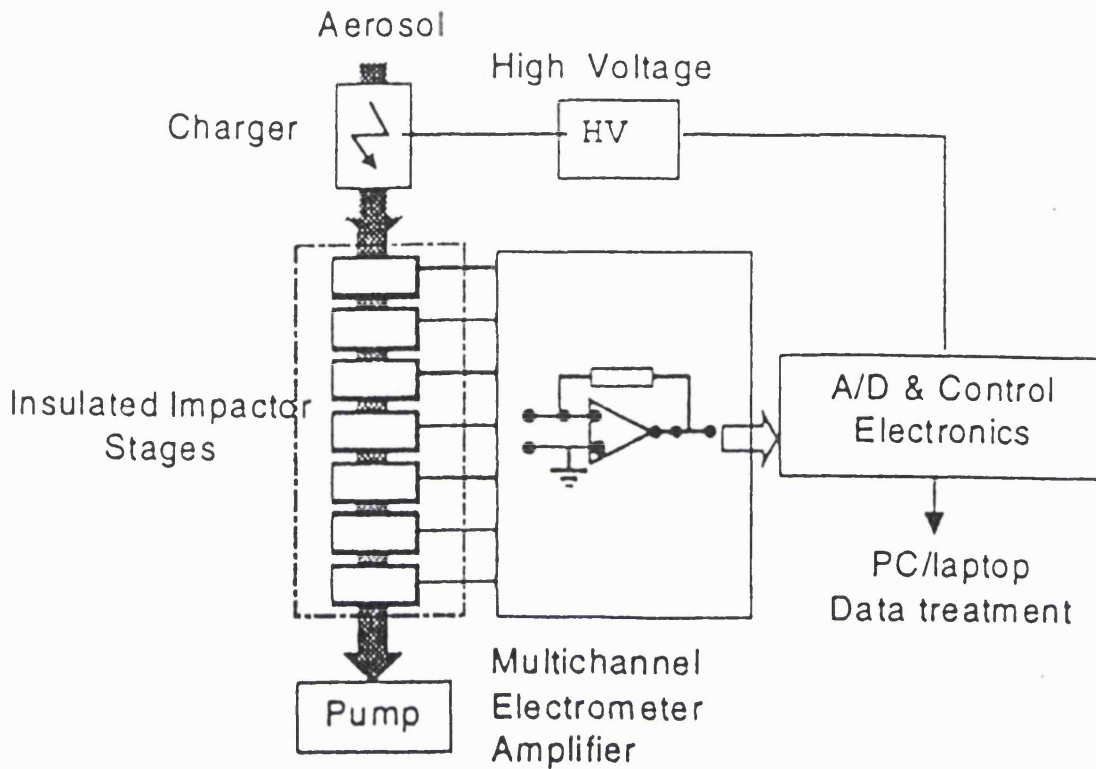
(a)
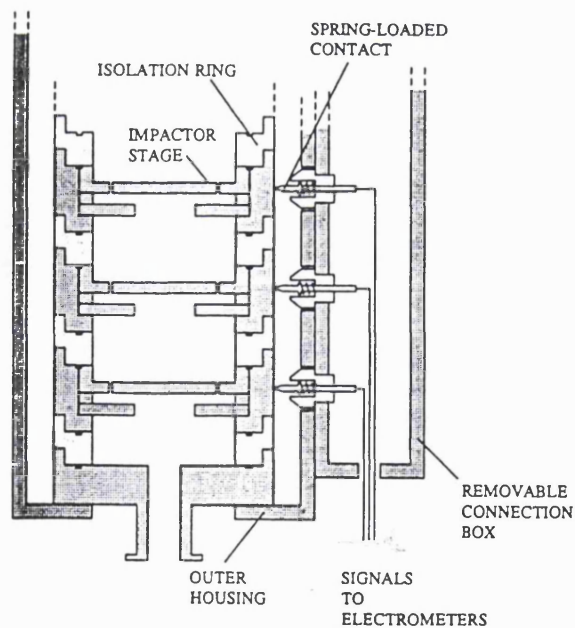
(b)

Figure 3.10. a) Schematic diagram of the Electrical Low Pressure Impactor b) Detail:
Isolation and electrical connections of the impactor stages (Keskinen, 1992)

This time is subsequently compared with predetermined calibration curves created by using particles of a known size. Finally, the particles enter into the ion source region where an Nd:YAG laser with a 266-nm pulse output generates the mass spectra of the individual particles from which composition information are inferred. The operational size range of the instrument is between 0.2 to 10 μm (Gard et al. 1997; Silva et al., 1997).

Preliminary studies suggest that ATOFMS can be used potentially for monitoring vehicular particulates on a continuous basis. However the system dimensions (1.8m long x 0.7 m wide x 1.5 m high and weigh 250 kg) makes it unsuitable for on-board monitoring of automotive emissions (Gard et al. , 1997).

3.4.7. Epiphaniometer

Epiphaniometer is an instrument which continuously measures aerosol surface concentrations. The sampled air is pumped into a chamber containing short lived radioactive lead isotopes (^{211}Pb) produced by an actinium source (^{227}Ac). The lead atoms are attached onto the aerosol particles and are transported through a capillary tube which acts like a diffusion trap for non attached lead particles. At the end of the capillary tube the aerosol particles with the attached lead atoms are deposited on a filter where they are detected by an α–detector which measures the decay of lead. The measured signal is proportional to the exposed surface of the aerosol particles (Gaggeler et al, 1989a; Gaggeler et al., 1989b).

The device requires very small sampling rates (around 1 l /min) and can detect particle concentrations as low as 100 ng/m^3 in the size range between 0.08 to 7 μm. Furthermore due to the relatively short half life of the lead isotopes the system allows continuous monitoring of aerosol without changing or transporting the filter (Gaggeler et al, 1989a ; Gaggeler et al., 1989b).

3.5. Conclusion: Overview of the state of the art, problems identified, way to go!

Over the last two decades, a wide range of instruments have been developed for measuring ambient and source particulate concentrations. Table 3.1 presents a league table of these various techniques.

However, data acquired from the on going research reveal the need for new techniques that respond to new requirements.

The current emissions legislation requires new car models to comply with the correspondent emissions standards. However, it is important to note that for many of these vehicles very little is known about their on-road emissions which can differ significantly from those in lab dynamometers. To obtain realistic emissions data it is necessary to measure emissions from a range of vehicles that are in service. Subsequently valuable information can be inferred about the effect of age of the vehicle as well as poor maintenance on the resulting emissions. Therefore, measuring emissions as vehicles are being driven along public roads provides a test of real emissions. However, in order to achieve this the measuring instrument should be small enough to be portable and capable of taking measurements on line and on real time basis .

Finally, since 1993 smoke tests have been used as random road side test as well as part of the annual MoT inspection. However, a number of car engines in poor conditions were damaged as a result of the test and the test was temporary withdrawn after three months. At the moment, the Department of Transport and Environment has three on going projects (S026F/VB, S140A/VB, S260H/VB) investigating alternative means of testing smoke emissions from exhaust pipes of vehicles, on an on line basis. It should however be borne in mind that the final decision about the suitability of a specific instrument for a defined task should also take into account both physical and economic factors which include:

- the type of measurement

- accuracy, reproducibility and sensitivity of the measurement
- the number and frequency of sampling and analysis operations
- cost of the equipment as well as installation and operational cost.

Table 3.1. Instrument summary (Kittelson, 1999)

Instrument	Parameter	Range	Comments
Cascade Impactors			
MOUDI	Aerodynamic diameter	0.056-10 (μm)	- Not real-time, gravimetric and chemical analysis performed after collection
ELPI	--//--	0.030-10 (μm)	- Near real time with resolution 2 to 15 s - Also used for ambient measurements but with potential volatile particles losses
Electrical Mobility Instruments			
EAA	Electrical mobility equivalent diameter	0.003-1 (μm)	- time resolution : 2-3 mins, 11 size stages - inaccurate results when concentration and size fluctuate during scan - requires high dilution (>200:1) to avoid the saturation of the electrometer - results for particles < 10μm are not very accurate - pre-classification stage required to remove particles < 1μm for diesel aerosol measurements
DMPS	--//--	0.01-0.5 (μm)	- discrete electric field changes makes the whole sampling slower than SMPS - inaccurate results when concentration and size fluctuate during scan - pre-classification stage required to remove particles < 1μm for diesel aerosol measurements
SMPS	--//--	0.01-0.7 (μm)	- 2-4 min scan time for 100 size intervals - time resolution of a few seconds for a single channel - inaccurate results when concentration and size fluctuate during scan - pre-classification stage required to remove particles < 1μm for diesel aerosol measurements
Miscellaneous Instruments			
PAS	surface area	< 1 (μm)	- condensation of vapours on particles interfere with measurement - response time < 1 sec - particles 1 > μm are not charged efficiently
ATOFMS	aerodynamic diameter	0.3 -50 (μm)	- real time measurements of up to 600 particles per min
Epiphaniometer	diffusion mobility	0.01-0.5 (μm)	- slow sampling rates i.e. long sampling times - requires steady state conditions - inaccurate results when concentration and size fluctuate during scan

C H A P T E R   4

CAPACITANCE TECHNIQUE FOR CONCENTRATION MEASUREMENTS

4.1 Introduction

The use of electrical capacitance as a measurement tool in solids-gas systems is based on the principle that the presence of solids between the electrodes of the capacitor, will alter the overall dielectric constant of the mixture and consequently, the measured mean value of capacitance. This technique has been used for various two-phase flow measurements in solids-gas mixtures (Dotson et al., 1949; Irons et al., 1983) and liquid dispersions (Lockhart et al., 1978; Xie et al, 1990).

A complete capacitance concentration measuring system consists of the sensing electrodes (capacitance transducer) and the accompanying measuring electronics (in general, an LCR (abbreviation for L: inductance, C: capacitance, R: resistance-meter).

This chapter contains a brief theoretical overview on the dielectric materials and capacitive systems, followed by a literature review of different applications using capacitance based instruments for concentration measurements. Special attention is given to the design consideration and construction details of the proposed capacitance transducer. The chapter concludes with a brief description of the most commonly used electronic circuits for measuring capacitance.

4.2. Principle of Operation

The main component of any capacitance sensing technique is a sensor which comprises two metal electrodes. The mean value of the sensor capacitance, C_x , can be expressed as:

$$C_x = N_C \, \varepsilon_{eff} \qquad\qquad (4.1)$$

where N_C is a characteristic constant solely determined by the geometry and the dimensions of the sensor and ε_{eff} is the effective dielectric constant of the medium in the sensing volume between the electrodes. If the medium is a mixture of small dielectric spheres randomly distributed in a continuous phase of another dielectric material, then ε_{eff} is determined by the corresponding dielectric constant of the two materials and their volumetric fraction (see Chapter 6) (Sami et al., 1980; Irons et al., 1983).

It is clear that when a mixture of known components is drawn through the sensing volume of a capacitor with specific design and dimensions, N_C as well as the dielectric constants of the mixture's components are constant. Consequently, any change in the sensor's capacitance is entirely attributed to a change in the mixture concentration.

In a standard operational procedure, the transducer's capacitance, Cp_{air} with pure air drawn between its electrodes is recorded first, followed by the measurement of the resulting capacitance, Cp_{sol} when the test solids-gas dispersion is passing through the transducer's sensing volume. However, in the first case, ε_{eff} is equal to the dielectric constant of air, ε_{air} which is unity and hence $Cp_{air} = N_C$ whereas in the second case, $Cp_{sol} = N_C \, \varepsilon_{eff}$ (see equation 4.1). Therefore, the effective dielectric constant of the test dispersion is:

$$\varepsilon_{eff} = \frac{Cp_{sol}}{Cp_{air}} \qquad\qquad (4.2)$$

Subsequently, by repeating the above procedure for different solids fractions in the air stream, a calibration curve is produced where the variation of the effective dielectric constant of the dispersion is plotted against the solids volumetric concentration.

4.3. Theoretical background

The following contain the pertinent theoretical background essential for the understanding of the use of capacitance techniques for concentration measurements. Furthermore, it provides the necessary background for the subsequent analysis of the experimental results presented in Chapter 6. The polarisation phenomenon in dielectrics, which is responsible for the increase in capacitance is described first, followed by a discussion on the application of polarisation in capacitors.

To summarise, in the case that the free space between the electrodes of a capacitor is filled with a dielectric material, the resulting capacitance is increased by a factor, ε_r which depends only on the nature of the material. This factor is termed the relative permitivity or dielectric constant of the material. It is greater than unity for all dielectric materials and equal to one for air (Bolton, 1980).

4.3.1. Polarisation

The most important effect of the imposition of an external field on dielectric materials is polarisation due to the fact that electrons in dielectrics, unlike conductors, are not free to move through the material so that there will be a current flow (Scaife, 1989). There are two main mechanisms by which polarisation occurs: electronic and orientation polarisation (Feynman, 1964; Hockey 1972).

a) Electronic polarisation. To illustrate electronic polarisation mechanism, consider a non-polar (neutral) atom with the positive charge on the nucleus surrounded by negative electrons as shown in figure 4.1.a. When this particle is placed in an external electric field, E_0, the latter creates a local electric field inside the particle termed as internal field, E_{int}, which is proportional to E_0, and is given by the Lorentz's equation (Harrop, 1972; Anderson 1964):

$$E_{int} = E_0 \left(\frac{\varepsilon_s + 2}{3} \right)$$ (4.3)

where ε_s is the dielectric constant of the particle.
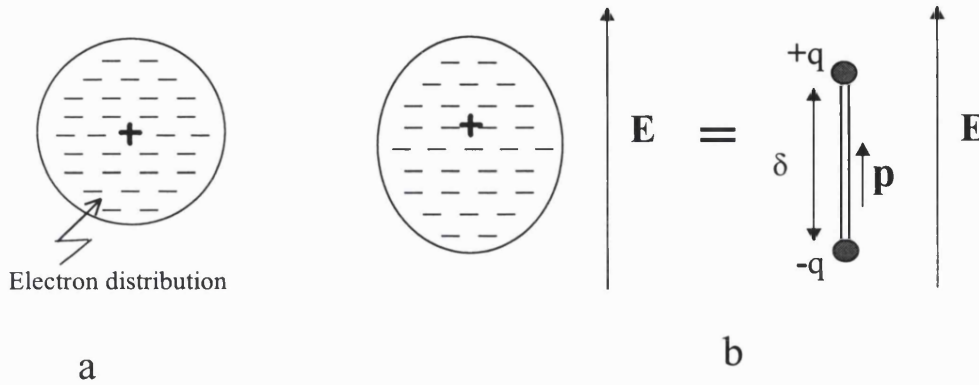
Figure 4.1. Electronic polarisation: An atom in an electric field has its redistribution of electrons displaced with respect to the nucleus (Feynman, 1964).

Under the influence of $\mathbf{E}_{int}$, the nucleus will be displaced relative to the negative charges and the centre of gravity of the negative and positive charges will no longer coincide as illustrated in figure 4.1.b. This neutral configuration is equivalent to an electric dipole i.e two equal charges, $\pm$ q of opposite polarity at a fixed distance, δ. The product of charge and the separation distance is called dipole moment, p and is a vector with a direction along the axis of the dipole pointing from -q to +q and magnitude, $q\delta$ (Feynman, 1964).

If there are N dipoles per unit volume there will be a total dipole moment per unit volume which is represented by a vector $\mathbf{P}$ which is in the direction of the individual dipole moments i.e. direction of the separation distance, δ , and is given by:

$$\mathbf{P} = N\,\mathbf{p} = N\,q\,\delta \qquad\qquad (4.4)$$

Interestingly, P has units of coulombs per square meters i.e. surface density (Feynman, 1964) and therefore P can also be defined by the surface density of charge

which appears on the faces of the dielectric specimen placed in the external field (Braithwaite et al., 1990).

In electronic as well as in orientation (see later) polarisation, the resulting net dipole moment per unit volume or polarisation vector, $\mathbf{P}$ is proportional to the strength of the external applied field, E_0 (Feynman, 1964; Bottcher, 1973; Braithwaite et al., 1990). This is because the induced dipole moment, $\mathbf{p}$ is proportional to $\mathbf{E_{int}}$, which in turn is proportional to E_0 (see equation 4.3) (Harrop, 1972; Bottcher, 1973) Therefore, for a given dielectric material the induced dipole moment $\mathbf{p} = q\delta$ can be written as:

$$\mathbf{p} = \alpha\,\mathbf{E_0} \qquad\qquad (4.5)$$

where α is called the polarisability of the material with dimensions of volume (Harrop, 1972; Bottcher, 1973).

Bottcher (1973) reports that a sphere of radius, r_s , and dielectric constant, ε_S , immersed in a medium of dielectric constant, ε_1, can be represented with an ideal dipole (at the centre of the sphere) surrounded by the dielectric medium. Then the polarisability α of the dielectric sphere is given by:

$$\alpha = \frac{\varepsilon_s - \varepsilon_1}{\varepsilon_s + 2\varepsilon_1} r_s^3 \qquad\qquad (4.6)$$

In the special case of a dielectric sphere immersed in air (i.e. $\varepsilon_1 = 1$), equation 4.6 is reduced to:

$$\alpha = \frac{\varepsilon_s - 1}{\varepsilon_s + 2} r_s^3 \qquad\qquad (4.7)$$

and for conducting particles ($\varepsilon_s \rightarrow \infty$) equation 4.7 becomes:

$$\alpha = r_s^3 \qquad\qquad (4.8)$$

It is worth noticing that generally when polirisable bodies are placed in an electric field the direction of the equivalent induced dipoles are at an angle, θ with E_0 depending on the position of the dielectric body relative to the polarising field (Bottcher, 1973; Van Vlack, 1989).

b) Orientation polarisation. Orientation polarisation on the other hand takes place in polar materials which carry a permanent dipole moment, p_0 because the positive and negative centres do not coincide due to asymmetrical composition (Hockey 1972; Bottcher, 1978). As it shown in figure 4.2.a. without an electric field, the individual dipoles inside the dielectric material are directed randomly, so the net moment per unit volume is zero.

(a)   **(b)**
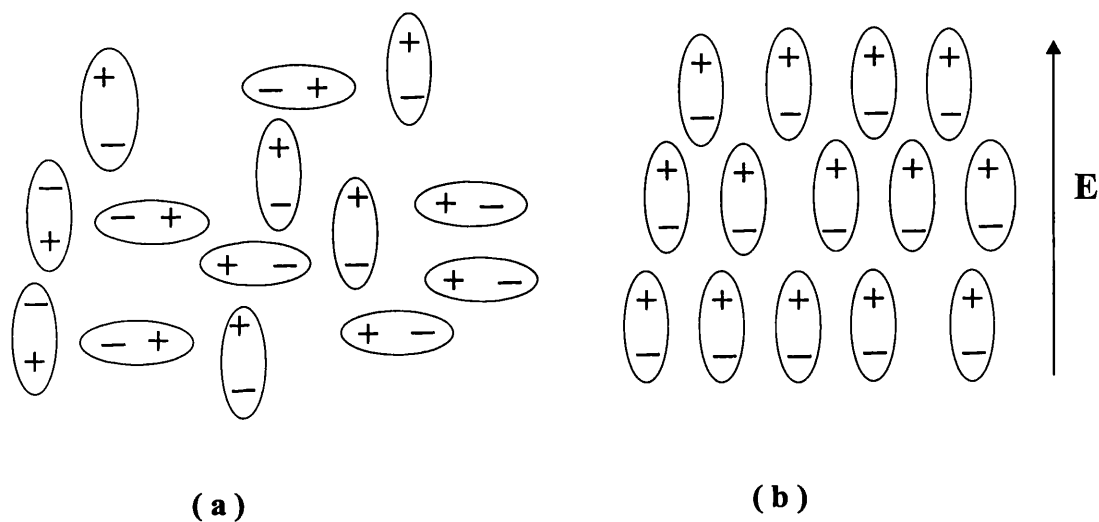
Figure 4.2. Orientation polarisation (a) with no external electric field: random orientation of individual dipoles (b) with external electric field: dipoles rotate into total or partial alignment with electric field (Bottcher, 1978).

When an external electric field is applied, in addition to the electronic polarisation which has been already described, orientation polarisation takes place. As a result, the permanent molecular dipoles align themselves against the external electric field to produce a net dipole moment per unit volume, **P** , as illustrated in figure 4.2.b. For N dipole moments in a unit volume, the magnitude of **P** is equal to the sum of the p_0

components in the direction of the external field in a unit volume (Feynman, 1964; Hockey 1972):

$$P = \sum_{\substack{unit \\ volume}} p_0 \cos\theta_i = N p_0 \cos\theta_i \qquad (4.9)$$

where θ is the angle between the axis of the dipole and the field.

Again, the net dipole moment per unit volume or polarisation vector, P is proportional to the strength of the external applied field, E_0 (Feynman, 1964; Bottcher, 1973; Braithwaite et al., 1990), since a stronger electric field increases the alignment of the permanent dipole moments in the direction of the imposed field. That means that $\cos\theta_i$ in equation 4.9 increases with increasing E_0, until $\cos\theta_i = 1$ when E_0 and p_0 point in the same direction (Richards, 1961; Feynman, 1964). Consequently, polarisation, P can be expressed as:

$$P \propto N, p_0 , E_0 \qquad (4.10)$$

Finally, in case of N spherical particles with radius, r_s, and dielectric constant, ε_s dispersed in a unit volume of air ($\varepsilon_{air} = 1$), a combination of the above mentioned mechanisms determines the total polarisation of the dispersion, P_{dis}. In such a case each particle when polarised by the applied electric field, E_0 can be represented by a dipole of induced dipole moment, p_p (see electronic polarisation above), which is given by:

$$p_p = \alpha\, E_0$$
$$\text{where} \qquad \Rightarrow \qquad p_p \propto r_s^3 , \varepsilon_s, E_0 \qquad (4.11)$$
$$\alpha = \frac{\varepsilon_s - 1}{\varepsilon_s + 2} r_s^3$$

The N individual dipoles at the same time will be aligned under the influence of the external field (orientation polarisation) to produce a total dipole moment per unit volume of dispersion i.e. P_{dis} given by applying equation 4.10:

$$\mathbf{P_{dis}} \propto N, \mathbf{p_p}, \mathbf{E_o} \qquad (4.12)$$

subsequently by combining equation 4.11 and 4.12 the magnitude of the P_{dis} is given by:

$$P_{dis} \propto N, r_s^3, \varepsilon_s, E_o^2 \qquad (4.13)$$

The product of $N\, r_s^3$ represents the total volume of solids particle in unit volume of the mixture. In case of conductive spherical particles (i.e. $\alpha = r_s^3$) equation 4.13. is reduced to:

$$P_{dis} \propto N, r_s^3, E_o^2 \qquad (4.14)$$

It is worth noticing that E_o appears squared because for a given particle the induced dipole moment depends upon E_o as well as the aligning force on the produced dipole is again proportional to E_o.

4.3.2. Dielectric Polarisation in Capacitors.

In the simplest form a capacitor shown in figure 4.3 consists of a pair of parallel metal plates each of area, A separated by distance, d.
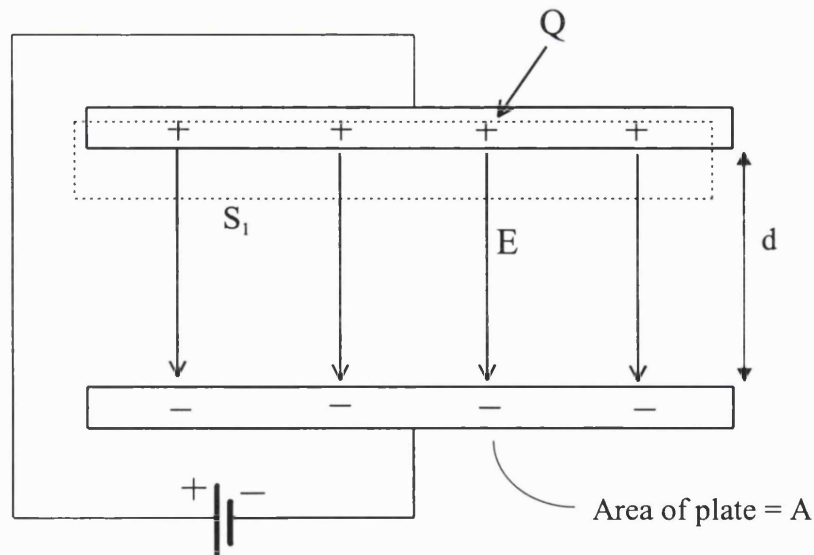

Figure 4.3. Parallel plate capacitor.

The separation distance is taken sufficiently small compared to the plates area so that the resulting electric field, E, will be uniform and fringing effects near the edges can be ignored (Scaife, 1989). By applying a potential difference, V across the plates, charges of equal magnitude Q will spread uniformly on the surfaces of either plates. The ratio of the charge on a plate to the potential difference is the capacitance (Bolton, 1980):

$$C_o = \frac{Q}{V}$$ (4.15)

The potential difference for a uniform field is given by:

$$V = Ed$$ (4.16)

Furthermore, the electric field strength between the capacitor's plates is calculated by applying Gauss law in a closed surface, S_1 as shown in figure 4.3. Accordingly, the field is equal to the surface charge density $\sigma = Q/A$ divided by the dielectric constant of vacuum ε_o (8.85 × 10^{-12} F/m):

$$E = \frac{\sigma}{\varepsilon_o} = \frac{Q}{A\varepsilon_o}$$ (4.17)

Consequently by combining equations 4.15 and 4.16, with air (ε_{air} =1) filling the free space between the plates, the "design" equation of a parallel plate capacitor, is given by:

$$C_o = \frac{\varepsilon_o A}{d}$$ (4.18)

The fact that the presence of an insulating material between the capacitor's plates, increases the capacitance means, that the charge Q on the plates is larger since the voltage remains unchanged (see equation 4.15). In other words the effect of the dielectric material is to increase the charge storage capacity of the electrodes. This is due to the polarisation of the dielectric material. This phenomenon is depicted in figure 4.4 where the formation of dipole chains during polarisation, result in the

appearance of an equal surface charge of opposite polarity on either side of the dielectric (Feynman, 1964; Braithwaite et al., 1990).

The surface density of this charge called surface polarisation charge, σ_{pol}, and is equal to the magnitude of polarisation vector **P** (Feynman, 1964):

$$\sigma_{pol} = P \qquad\qquad (4.19)$$

Subsequently, the polarisation charges neutralise a certain fraction of the initial electrodes' charge, Q which can then be replaced by additional charges from the circuit's voltage source e.g. a battery (Richards, 1961; Feynman, 1964; Braithwaite et al., 1990). The fraction of the initial charge that is neutralised by polarisation, is a characteristic of the dielectric material. More specifically, the ratio of the total charge Q_{tot} (i.e. initial Q, plus the extra charge bounded by the dielectric Q_{pol}) to the initial charge Q is called the relative permitivity or dielectric constant of the material, ε_r:

$$\varepsilon_r = \frac{Q_{total}}{Q} = \frac{Q + Q_{pol}}{Q} \qquad\qquad (4.20)$$

Since Q is always a fraction of Q_{tot}, ε_r is always greater than unity for all the materials apart from air that is equal to unity.

Furthermore, equation 4.20 can be written:

$$\varepsilon_r = \frac{(Q + Q_{pol})A}{QA} = \frac{\sigma + \sigma_{pol}}{\sigma} = \frac{\sigma + P}{\sigma} = 1 + \frac{P}{\sigma} \qquad (4.21)$$

to give:

$$\varepsilon_r = 1 + \frac{P}{\sigma} = 1 + \chi \qquad\qquad (4.22)$$

where χ is a dimensionless number called dielectric susceptibility of the material (Scoot, 1959; Scaife, 1989).

Therefore, by combining equations 4.15 and 4.20, the capacitance with the dielectric inserted between the electrodes can be calculated:

$$C = \frac{Q_{tot}}{V} = \frac{\varepsilon_r Q}{V} = \varepsilon_r C_o$$

and

$$C = \varepsilon_r C_o \qquad (4.23)$$

Finally, by using equation 4.22, equation 4.13 (i.e. proportionality for the polarisation for dispersions of spherical solid particles in air) and bearing in mind that $\sigma = \varepsilon_o E$, then the dielectric constant of a solids/air dispersion, ε_{dis} , is given by:

$$\varepsilon_{dis} \propto N, r^3 , \varepsilon_s/\varepsilon_o, E \qquad (4.24)$$

The above illustrates that the dielectric constant of a suspension of spherical particles in air, depends on the volume concentration of the particles within the capacitor space, their individual dielectric constant, ε_s , and the intensity of the electrical field, E , between the capacitor's electrodes.
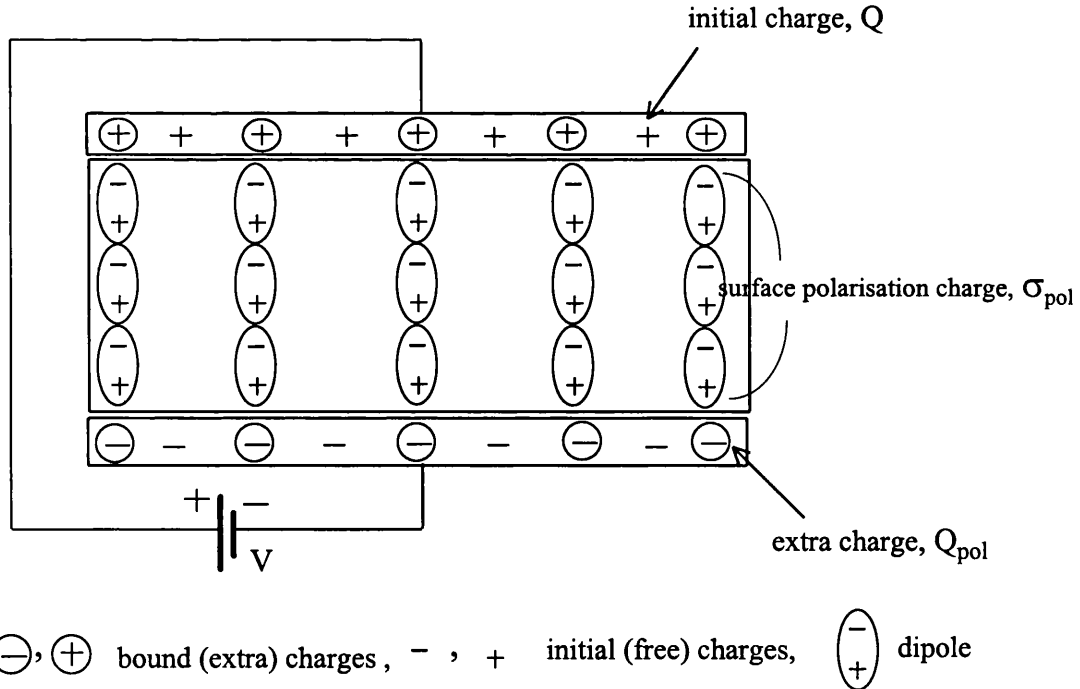

Figure 4.4. Schematic representation of a polarised dielectric in a parallel plate capacitor.

4.4. Literature Review of Capacitance Sensors for Concentration Measurement

Capacitance measurement has been increasingly used in numerous engineering applications for determining the component concentration in two-phase flows. This is because the technique has several advantages compared to alternative measurement techniques. These include:

(i) Safe to operate and does not require specially trained personnel

(ii) Inexpensive to construct and operate

(iii) Rapid response thus making it suitable for in situ, real time measurements applicable for monitoring rapid transients

(iv) Does not involve mechanical or moving parts thus reducing the possibilities for malfunction as well as little maintenance requirements

(v) The output is an analogue signal suitable for process control

Several different types of capacitive sensors have been designed for monitoring the flow of two-phase mixtures in ducts and pipelines (see for example Dotson et al. 1949; Beck et al., 1969a; Lounge, 1996). Dotson et. al., (1949) used a parallel plate capacitive sensor in order to monitor the uniformity of a coal-air mixtures conveyed in pipelines. The sensor comprised two aluminium plates separated by bakelite strips fitted around the conveying line. However, the minimum detectable concentration was only 5% by volume thus rendering the technique unsuitable for particulate emission monitoring. Beck et al. (1969a) designed a flow detector for pneumatic and fluidised conveyors. The method is based on the fact that the flowing powder causes small but significant capacitance changes monitored by an electrode in the wall of the conveyor. In practice, the system employs the main body on the actual conveyor as the one plate of the capacitor (at earth potential) and the other plate is an electrode placed near the flowing material. In a subsequent work, Beck et al (1969b) incorporated two such probes in order to measure the solids conveying velocity of the solids as well as the concentration.

Capacitive sensors have been also used for monitoring the operation of fluidised beds (Morse et al., 1951; Lanneau, 1960; Geldart et al. 1972). These sensors can be inserted within the fluidised bed and monitor its uniformity which is essential for the bed's efficient operation. These probes have to be small so that they cause minimum disruption in the fluidised bed. A typical design incorporates two metal plates (1.3 cm square), 0.7 cm apart attached at the end of 25 cm long tube (Morse et al., 1951).

During the last fifteen years, capacitive sensors have been widely used in tomographic imaging (see for example Huang et al., 1989; Fasching et al., 1991; Xie et al., 1992; Williams et.al., 1993; Reinecke et al., 1997). These techniques allow two or three-dimensional imaging of various processes in chemical engineering. They employ multi-electrode capacitive sensors (4-32 electrodes) mounted flush to the wall of the pipeline or vessel. A sophisticated data acquisition system is required to feed the measured capacitance values into an image reconstruction computer where the cross-sectional image is reconstructed (Huang et al., 1989).

Finally, capacitive sensors have also been used in several other application such as the measurement of density and velocity of flowing snow (Louge et al., 1997), soil moisture content (Shinn et al, 1998), as well as the flowing properties of saturated sand (Campanella et al., 1993).

4.5. Fundamental Requirements for a Capacitance Concentration Transducer

The most important consideration not only for capacitance but generally for all electrical measuring systems is the signal to noise ratio. The term "signal" refers to the change in the sensor's capacitance caused by a change in the concentration of the relevant component of the flow. On the other hand, "noise" corresponds to all the undesirable capacitance changes caused by several factors excluding the actual flow.

It is always desirable to have a signal to noise ratio as high as possible. This is because in many applications, capacitance changes as low as 0.001 pF have to be detected. Such a small signal can easily be masked by noise (Huang, 1988). Therefore it is important to identify and study possible noise sources so that their occurrence can be prevented. However in most cases, these sources are inherent in the process and cannot be eliminated. Their effect has to be quantified and taken into account so that corrections can be made on the final measurements.

Temperature is a potential noise source that has to be accounted for. Temperature fluctuations can cause drift of the baseline capacitance signal (zero flow) that can be misinterpreted as an actual flow. Temperature effect is particularly important in the design of on-line transducers, which have to operate for long periods without recalibration and may be subject to temperature fluctuations.

Another possible source of error is the change in the flow pattern of the components to be measured. For example, in solids pneumatic conveying, depending on the solids loading, size, density and the gas velocity, the flow regime may vary from homogeneously dispersed to creeping flow (see figure 6.42). As a result the solids distribution over the pipe cross section changes. The latter will cause errors in cases that measurement's sensitivity is not homogeneous over the sensor's cross-section. As a result the measured capacitance will be dependent not only on the solids concentration but also on their distribution within the sensor, causing unpredictable errors. Therefore, it is very important that the measurement is independent of the prevailing flow regime.

Electrostatic charges often carried by suspended particles can affect measurements. The extent of the electrostatic effect can be such that the actual measurement becomes impossible due to short circuiting of the capacitor (Huang, 1988). The charging process depends on the particle size, gas velocity and moisture content (Loeb, 1958; Taylor et al., 1994). Although charge generation on powders is well establish phenomenon, the detailed electrification mechanisms are less establish (Gibson, 1982; Singh, 1982). In general, there are two essential factors required for generation and

accumulation of electrostatic charge: a) contact and separation of dissimilar surfaces and b) one of the surfaces has a relative high electrical resistivity (i.e. an insulating surface) (Gibons, 1982). For example, a contact between a clean metal and polymer surfaces usually accumulates a net positive charge in the metal and a negative charge in the polymer (Jones, 1991).

Finally, special attention has to be paid to the presence of humidity since water has a high dielectric constant (ε_r =80). Hence even very small concentrations of water can add appreciably to the measured capacitance.

Summarising, a capacitive transducer designed for concentration measurements should have a minimum and preferably controllable baseline drift, high sensitivity to component concentration changes, homogeneous measurement sensitivity, immunity to electrostatic interferences (external and internal) and measurement stability over a prescribed period of time.

4.6. Proposed Design: Coaxial Capacitance Transducer

4.6.1. Capacitor Electrode Geometry

The most important step in designing a capacitance transducer for concentration measurements is the selection of electrodes' geometry (Huang, 1986; Simons, 1991). This is because it will primarily determine the sensor's range, sensitivity and homogeneity of measurement (NPL, 1969). In the last forty years, several different electrode configurations have been used in an attempt to construct a capacitance transducer suitable for two-phase concentration measurements. Sami et al. (1980) reviewed a variety of such transducers designs used in different applications. Figure 4.5 shows schematic representations of these various designs.

After extensive testing Sami el al. (1980) report that even though all the above configurations gave consistent results, the most promising design in terms of sensitivity and linearity, for all mixtures and flow patterns, is the double helix (see

figure 4.5.d). However, due to their complex design double helix electrodes are difficult to manufacture and be fitted onto a pipeline.
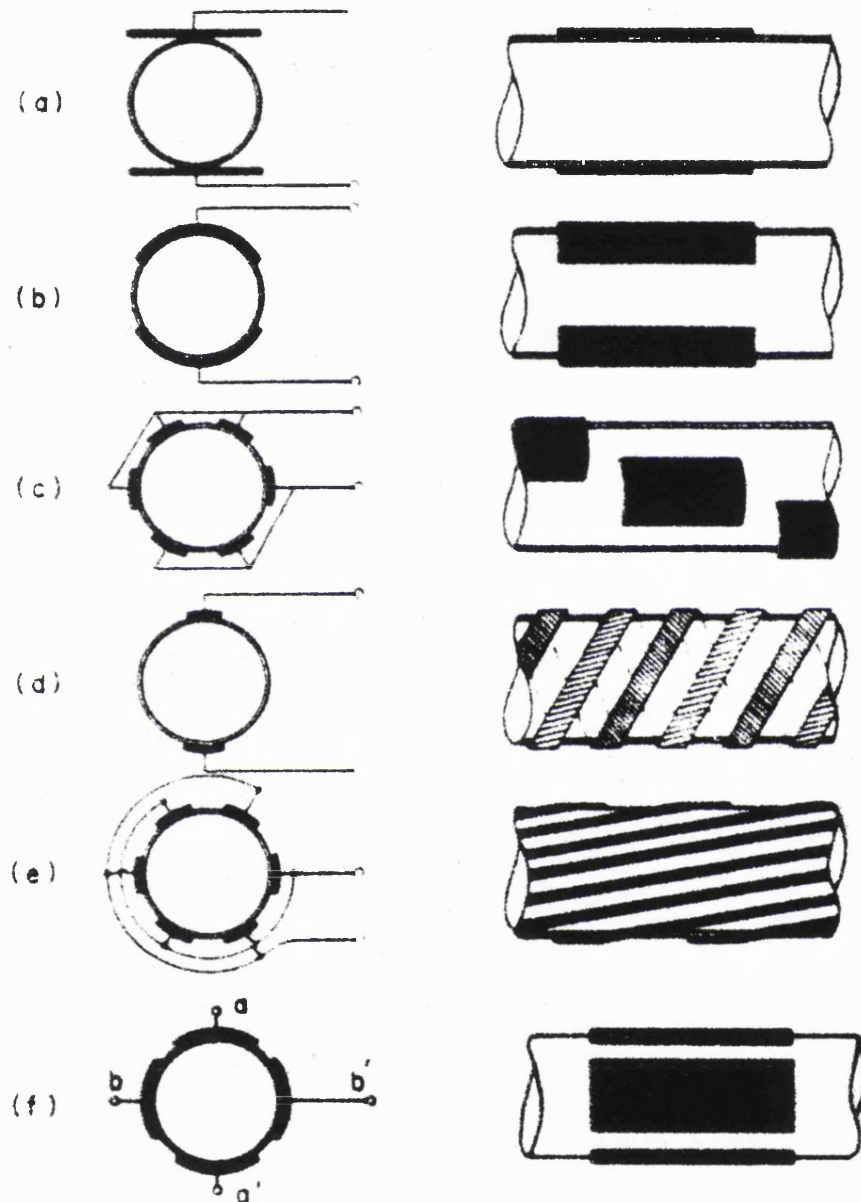

Figure 4.5. Various capacitance concentration transducers: a) parallel plates b) concave plates c) staggered concave plates d) double helix e) multiple helix f) four concave plates (Sami et al. 1980).

As a result concave plate sensors have been the most popular design for practical applications (Huang, 1986). Such configurations which would be ultimately mounted axially around the circumference of the exhaust pipe have been considered for vehicular particulate monitoring and were discounted due to inherent problem of fitting square plates to the circumference of a pipe (Huang, 1986). Furthermore, for similar dimensions, the sensitivity of these arrangements in terms of a change in capacitance are far inferior to a coaxial cylindrical capacitor.

Xie et al., (1992) and Fasching et al., (1991) have designed multiple electrode sensors, involving a sophisticated mechanism that switches among the capacitor pairs within milliseconds so that the whole cross sectional area of flow is scanned at almost the same moment. However, these involve complicated electronics and data acquisition systems resulting in an increase in the cost of the technique.

In the present study, a coaxial cylindrical capacitor has been designed for the measurement of solids concentration in air streams. The principal advantage of using cylindrical electrodes is that the charge density n the electrodes as well as the field between them are better defined than in case of other different geometries (Jonassen, 1998). Also, their simple shape and symmetry result in good capacitance stability (NPL, 1969). Furthermore, in conjunction with the specific application of monitoring exhaust particulates, the cylindrical capacitor has the shape advantage as it can be directly attached to the automobile exhaust tailpipe for on-line measurements.

Figure 4.6 is a basic schematic representation of the coaxial cylindrical capacitor designed and constructed for the present study. The unit basically comprises two conducting cylinders (see later) of different diameters placed coaxially within one another so that an annulus is formed. The length of each cylinder is, L and the inner cylinder of radius, a is separated from the outer cylinder of radius, b with the test dielectric material flowing through the annulus. The separation distance between the cylinders is taken considerably smaller than their length so that the fringing effects near the edges can be minimised and thereby effectively ignored (Scott, 1959; Scaife,

1989). A capacitor is created by application of a voltage, V between the inner and the outer cylinder.
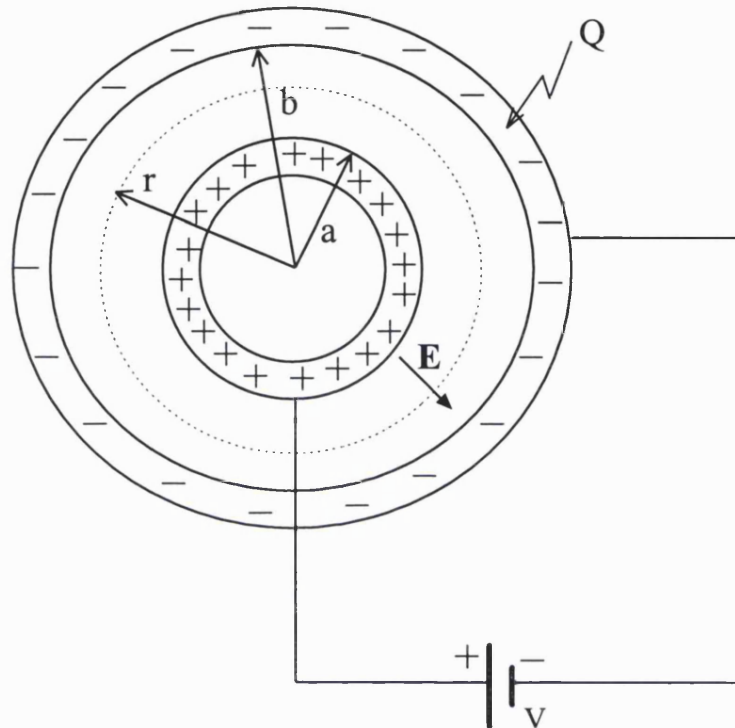
Figure 4.6. Coaxial Cylindrical Capacitor

The capacitance is given by:

$$C = \frac{Q}{V} = \frac{2\pi L\varepsilon_0}{\ln(b/a)} \qquad (4.25)$$

Equation 4.25 gives the capacitance of a cylindrical capacitor when the free space between the two electrodes is occupied by air. In the case of presence of a dielectric material of relative permitivity, ε_r within the annulus, equation 4.25 takes the form:

$$C = \frac{2\pi L\varepsilon_0\varepsilon_r}{\ln(b/a)} \qquad (4.26)$$

Comparing equation 4.26 with the basic capacitance equation, 4.1 ($C_x = N_c\varepsilon_{ff}$) , it follows that

$$N_C = 2\pi L/\ln(b/a)$$ (4.27)

It is clear that the characteristic constant, N_C given by the above equation, is solely determined by the geometry and the dimensions of the sensor (i.e. L, a and b) and ε_{ff} (= $\varepsilon_o\varepsilon_r$) is the effective dielectric constant of the medium in the sensing volume between the electrodes. Therefore in the present study, equation 4.26 will be used as the "basic design equation" for the cylindrical capacitor transducer.

4.6.2. Capacitor Electrode Dimensions

The correct choice of the cylinders length, L and the radii, a and b (see figure 4.6) involves taking into account the general requirements for a capacitive concentration transducer (see section 4.4) particularly those relating to its proposed application for measuring vehicular particulate emissions.

Firstly and most important, the transducer's capacitance should be within the measurement range of the commercial LCR meter (Hewlett Packard 4263B) employed in this study which is between 1 pico-Farad and 1 Farad. Measurements outside this range will require specially constructed LCR meters, which will add to the system's complexity and cost. Equation 4.26 indicates that the measured capacitance of the coaxial transducer increases with the following:

a) an increase in the length, L of the cylinders

b) a decrease in the radii ratio, b/a or the gap between the two coaxial cylinders

Furthermore, the transducer should be sensitive enough to detect very small changes in the solids concentrations. This is especially so in case of monitoring vehicular exhaust particulates as the typical concentrations encountered are relatively small (around 20-200 mg/m^3 i.e. 1.7×10^{-5}-1.7×10^{-3} %, v/v) (Bosch, 1996; Bagyi, 1998).

Also, the effective dielectric constant of the air/solids mixture is expected to be small bearing in mind that 75-85% of the exhaust particulate mass is carbon which has a low dielectric constant of 5.7 (Frey et al., 1967; Bagyi, 1998). Therefore, it is essential to increase the system's sensitivity in terms of maximising the effective dielectric constant for a given solids concentration in the mixture.

Considering, the fact that the dielectric constant of a particle-gas suspension is proportional to the polarisation of its elementary dipole units, which is in turn proportional to the imposed electrical field (see sections 4.3.1-4.3.2), then an increase in the latter will result in an increase in the dielectric constant of the material. Also since the electric field between two electrodes at a constant voltage is inversely proportional to the separation distance between them, then the electric field will be increased by decreasing the separation distance between the electrodes (see Chapter 6). In addition, in order to further increase the electric field the applied voltage used throughout the experimental series is 1 Volt, which the maximum output signal provided by the specific LCR meter.

Another important feature required for a capacitance sensor, is uniform measurement sensitivity over the whole cross sectional area of the sensing volume. This can be achieved by ensuring that the electric field between the capacitor's electrodes is as uniform as possible. In theory, a capacitor with completely uniform electric field is impossible to be constructed. This is because there will always be a small distortion of the field right on the edges of the electrodes (fringing) due to a small increase in the charge density on these areas (Scott, 1959; Feynman, 1964). In practice though, this error can be effectively ignored by reducing the separation distance between the electrodes in comparison with their length (Scaife, 1989; Jonassen,1998). Xie et al. (1990) suggest that in practical measuring systems, electrode lengths about twice the separation distance will be adequate to give high sensitivity and to minimise fringe effects. In other applications (Dotson et al. 1949; Sami et al., 1980; Irons et al., 1983) electrodes lengths varying from 1.8 to 6 times the separation distance have been used.

In case of the coaxial capacitor, the electric field is symmetrical and directed radially outward from the central axis (Jonassen, 1998). Its strength is inversely proportional to the distance, r from the centre and is given by:

$$E = \frac{Q}{2\pi \, r \, L \, \varepsilon_0} \qquad (4.28)$$

where:

Q is the total charge on the electrodes

r is the distance from the centre

L is the electrode length

The electric field even though well defined, is not uniform along the cross-section of the capacitor (Jonassen, 1998). The non-uniformity of the field is characterised by the denser field lines in the centre of the capacitor. However this non uniformity becomes less profound when the separation distance becomes smaller. Therefore, in the case of coaxial capacitors, it is necessary to have the smallest possible separation distance, which will increase the uniformity of the electric field at the main body of the capacitor as well as at the edges.

In conclusion, it is clear that it is advantageous for the coaxial capacitor electrodes to have a small separation distance with relatively long length. However, the minimum separation distance is dictated by two factors. These include the breakdown electric strength of air and the build up of high back pressures.

Air, under normal circumstances, is a good insulator. However, there is a critical value of electric field strength that air can withstand before electrical breakdown occurs and a violent discharge (spark/flashover) takes place. The theoretical breakdown strength of air at atmospheric pressure is 3×10^6 V/m (Bolton, 1980; von Hippel, 1995). For a given electrode separation distance, it is therefore possible to calculate the maximum voltage difference that can be applied before electrical discharge occurs.

Small electrode separations may cause unacceptably high back pressures during flow measurements. In the specific application of monitoring vehicular emissions for example, ISO 10054:1998(E) requires that the maximum back pressure generated by the measuring instrument should not exceed 1 kPa so that the engine's performance will not be affected (ISO 10054, 1998).

Long electrode lengths are desirable since this increases the measured signal (see equation 4.26) as well as reducing fringing effects. The maximum electrode length is however limited by practical considerations such as portability and more importantly, to ensure the homogeneity of the test suspension along the measurement zone (Louge et al., 1996).

Taking all the above mentioned factors into account, the following dimensions were selected for the construction of the coaxial capacitor transducer (see figures 4.7 and 4.8 and plates 4.1-4.3):

- Inside radius of the outer cylinder, b = 1.62 cm
- Outside radius of the inner tube, a = 0.90 cm
- Length of the cylinders, L = 12 cm

The inter-electrode separation distance (i.e. b-a), D_e between the two electrodes is 0.72 cm. This is almost 16 times smaller than the electrode length. Furthermore, at atmospheric pressure the capacitor can withstand a voltage of 33 kV before electrical discharge occurs. In the present study a voltage of maximum 1 Volt is used which is well below the critical value mentioned above. Finally, direct measurements indicate that the resulting back pressure for this design configuration is minimal even at high sampling rates (0.05 kPa for 850 l/min air flowrate).

4.6.3. Construction and Development

Figures 4.7 and 4.8 show dimensioned schematic representations of the coaxial capacitor designed and constructed for the present studies whereas plates 4.1-4.3 show photographs of various views of the capacitance transducer and its components.

The two cylindrical electrodes are constructed from non magnetic grade 316 stainless steel so that magnetic effects inherent in electrical applications can be minimised (Lockhart et al; 1978). Furthermore, such material is homogeneous, free of oxides with clean surfaces thus avoiding the occurrence of "contact" potential difference within the electrodes (Scott, 1959). Additionally, the thickness of the electrodes (0.19 cm) has been taken between one third to one fourth of the air separation distance (Terman 1950) and their surfaces were machined and well polished free of sharp edges in order to prevent corona discharge (Terman 1950; Feynman et al., 1964; Von Hippel, 1995).

The latter occurs in charged bodies with sharp ends where the charge density is much higher than in the surrounding regions. Sharp ends result in very strong electric fields acting outwards that may well exceed the breakdown field strength of air thus resulting in a violent discharge (Feynman et al., 1964; Bolton, 1980).

Both ends of the inner cylinder are fitted with hemispherical stainless steel (grade 316) caps. As well as avoiding corona discharge, the caps block the flow of the test mixture through the inner cylinder and evenly direct and streamline the flow of particles into and out of the transducer's annulus. It is worth mentioning that in the initial design, the end caps were made from an insulating material (Teflon) in order to contain the electric field solely between the two electrodes. However, since the cap's hemispherical surface were directly exposed to the flowing particles, a large build-up of static charge on the insulator occurred due to multiple particle impacts. Since electric charge cannot move freely in insulators, it was concentrated in a small area which eventually lead to a corona discharge (Loeb, 1958). The problem was overcome by constructing the caps from stainless steel with radius of curvature as large as practicable (see figures 4.7 and 4.8 a and plate 4.3).

To measure accurately the capacitance between the two terminals of the capacitor, it is important to keep the two cylinders coaxially aligned so that there is uniform spacing between the inner and outer cylinder. In case of misalignment, the electrical field within the capacitor will not be uniform thus resulting in incorrect

measurements. In the present design (see figure 4.8.b and plates 4.1 and 4.2), the inner cylinder is accurately aligned by adjusting the three metal screws perpendicular to the capacitor body which also keep the cylinder firmly positioned and free from vibrations due to the flow. Three Teflon washers attached on the outer cylinder prevent contact between the metal screws and the cylinder thus avoiding the short-circuiting of the capacitor.

The cylindrical capacitor is securely attached to the pipeline conveying the solid gas mixture to be measured using 4 mm wide Teflon rings fitted on either side of the outer cylinder. Teflon was selected for insulation since it possesses high breakdown strength, negligible dielectric absorption with high melting point essential for high temperature applications (Bolton1980; Lockhart, 1978).The choice of the appropriate dimensions of the insulating material is also important. Insulating surfaces have to be kept to a minimum since they harbour electrostatic build-up thus leading to violent discharge. On the other hand, sufficient insulation must be provided in order to prevent spark discharge across the insulating surface between the outer electrode and the attached pipeline (Kuwenhoven, 1933).

Two "spade" connectors were fitted to the capacitance probe for the connection of the test leads via Kelvin clips to the LCR meter. One of these connectors is welded to the middle of the outside surface of the outer cylinder whereas the other is fitted to one of the supporting screws connected to the inner electrode.

Finally, the whole transducer is enclosed in a metallic earthed screen which protects the capacitor from any interference from external electric fields. The use of the screen is recommended regardless of the cleanliness of the surroundings (Simons, 1991; Xie, et al., 1990).

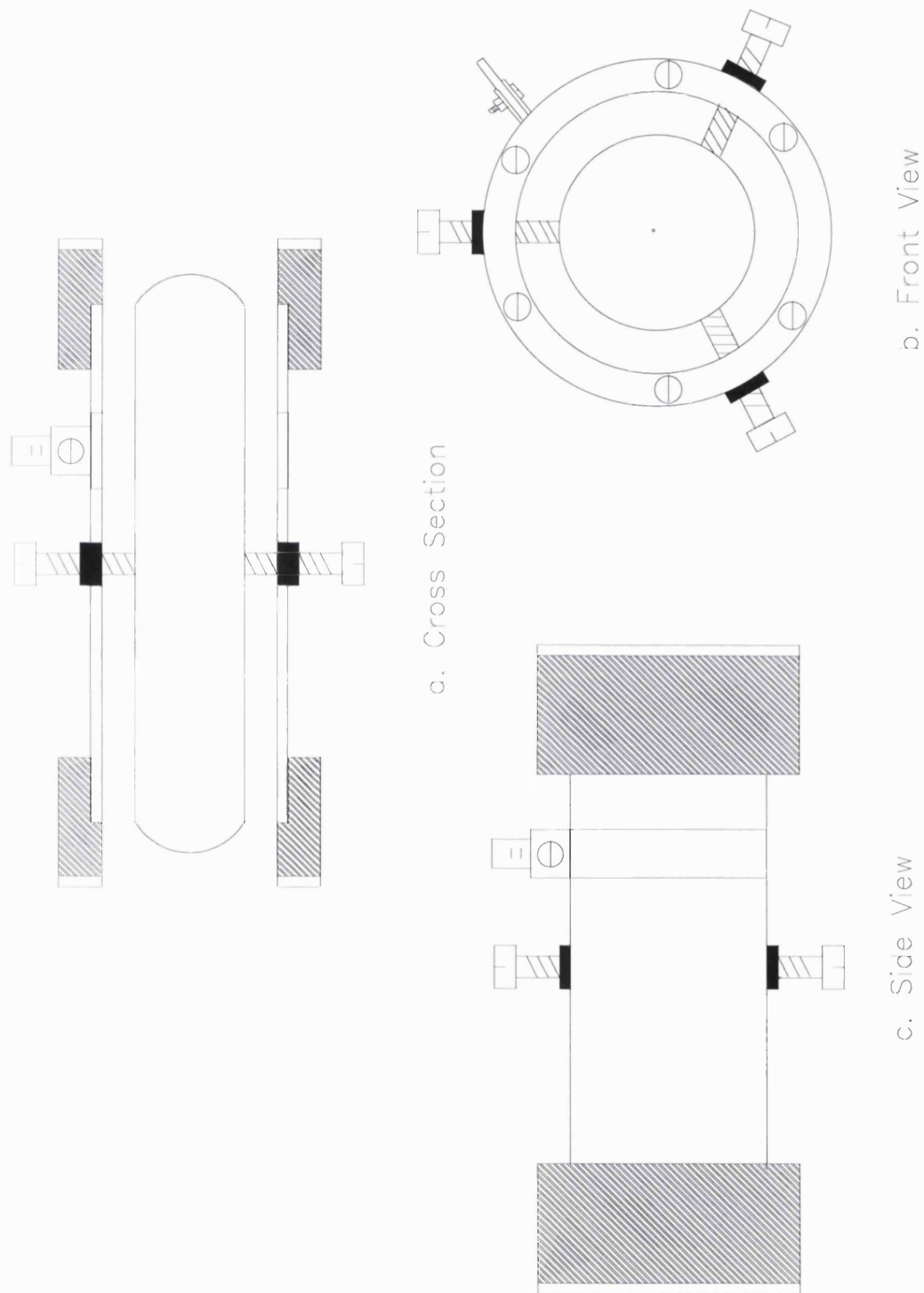b. Front View

a. Cross Section

c. Side View

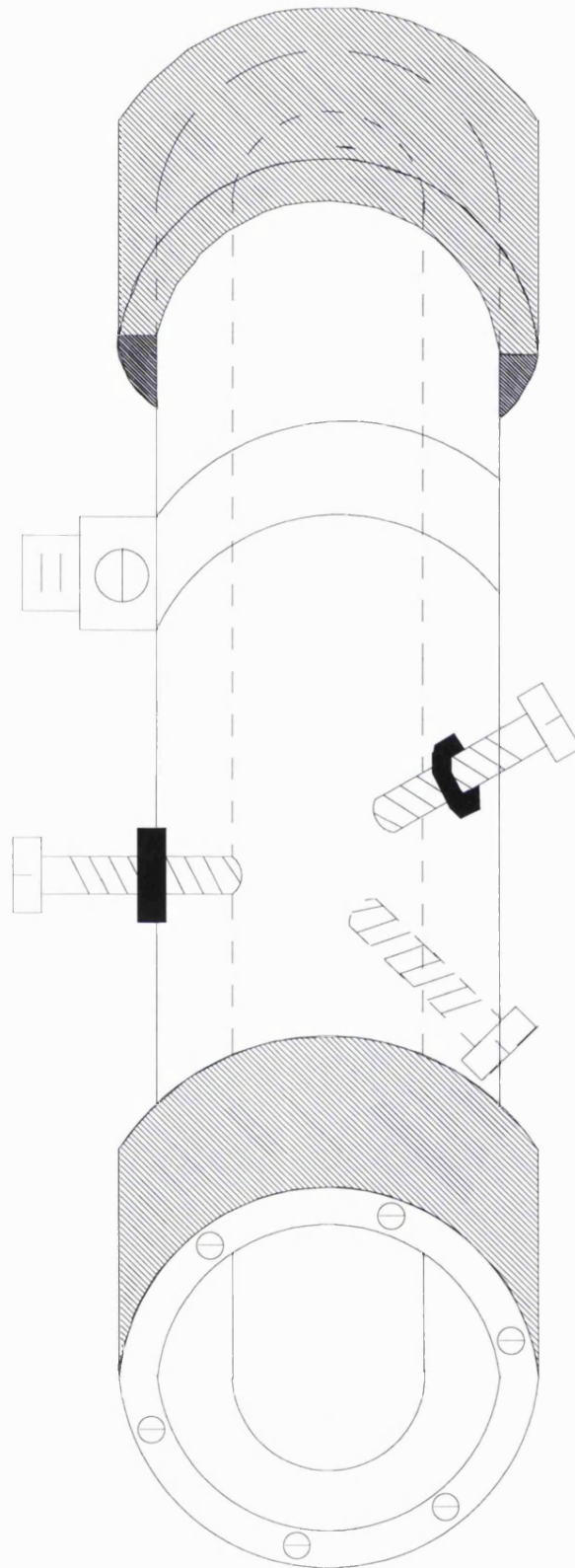Figure 4.7. Various cross-section views of the capacitance transducer

Figure 4.8. Isometric representation of the capacitance transducer.

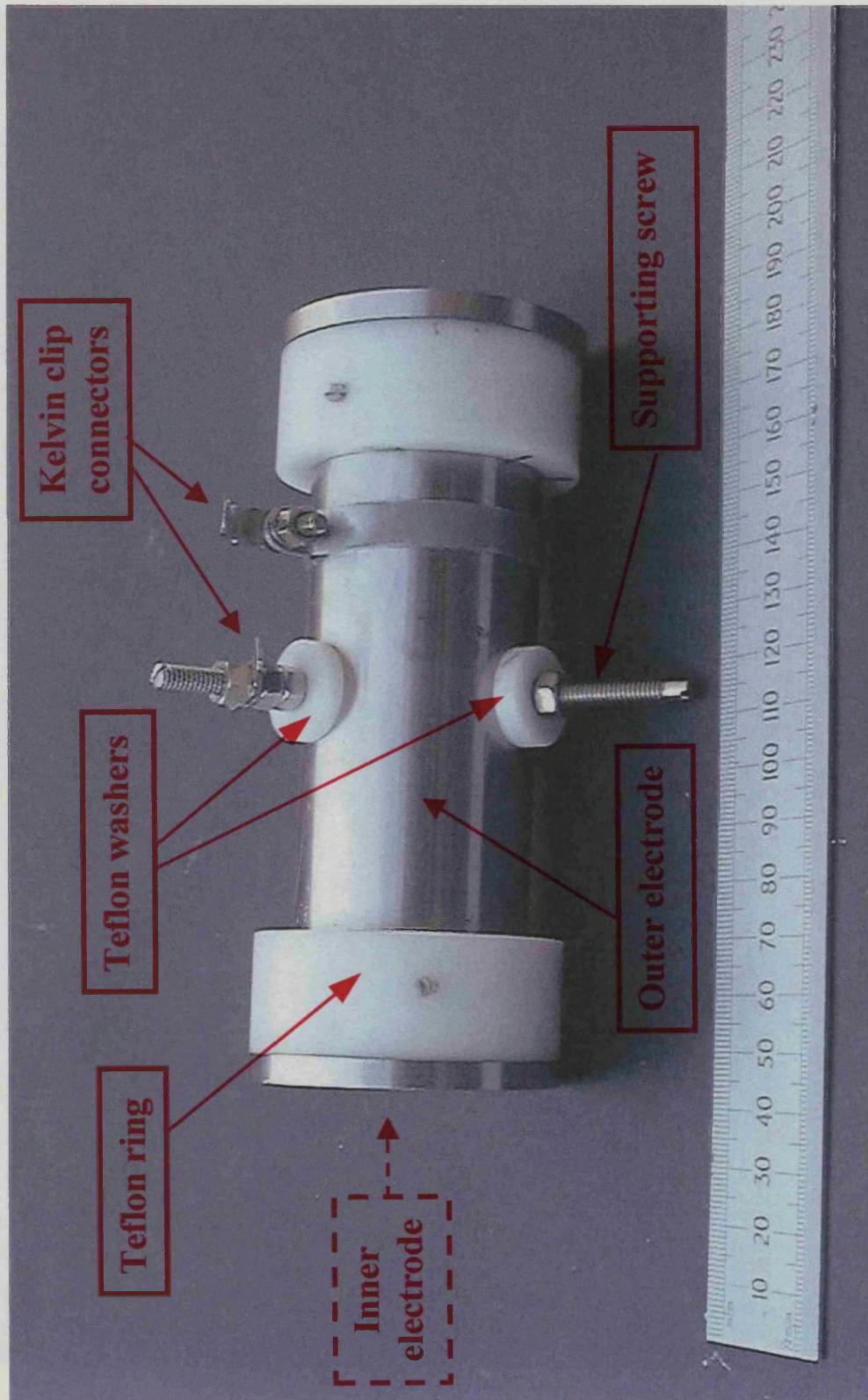Plate 4.1. Photograph showing a side view of the capacitance transducer.
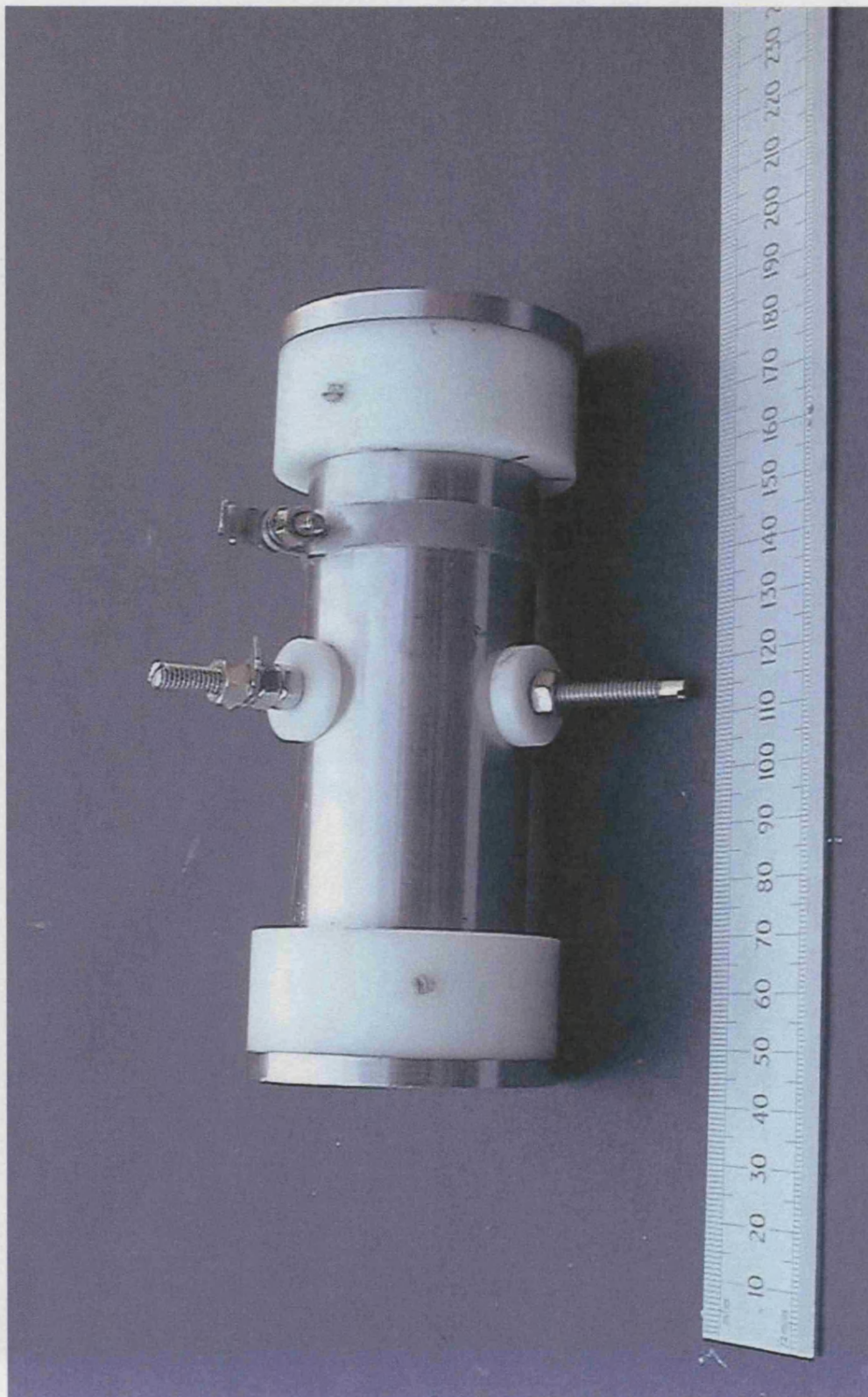
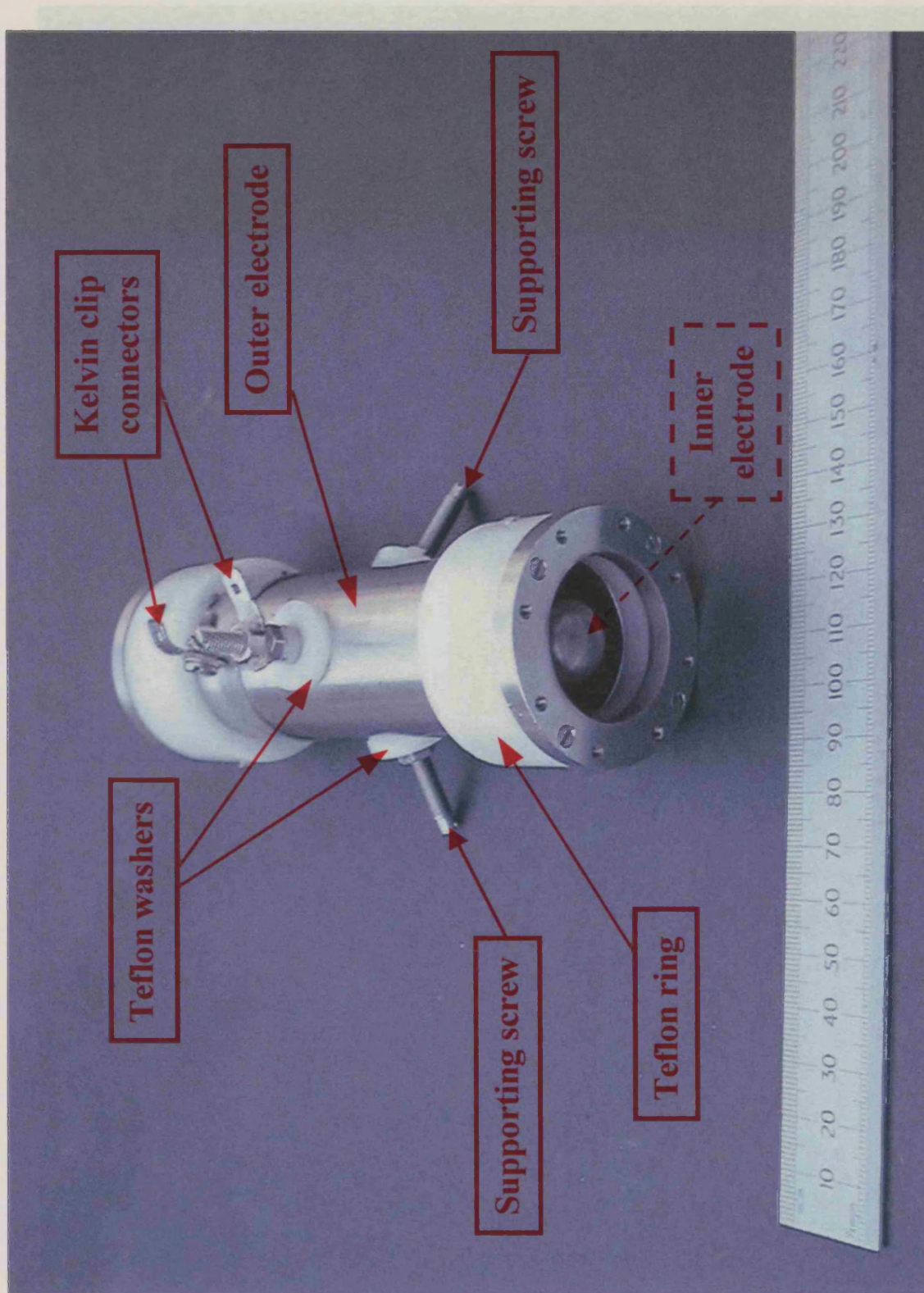Plate 4.1. Photograph showing a side view of the capacitance transducer.

Plate 4.2. Photograph showing a front view of the capacitance transducer.

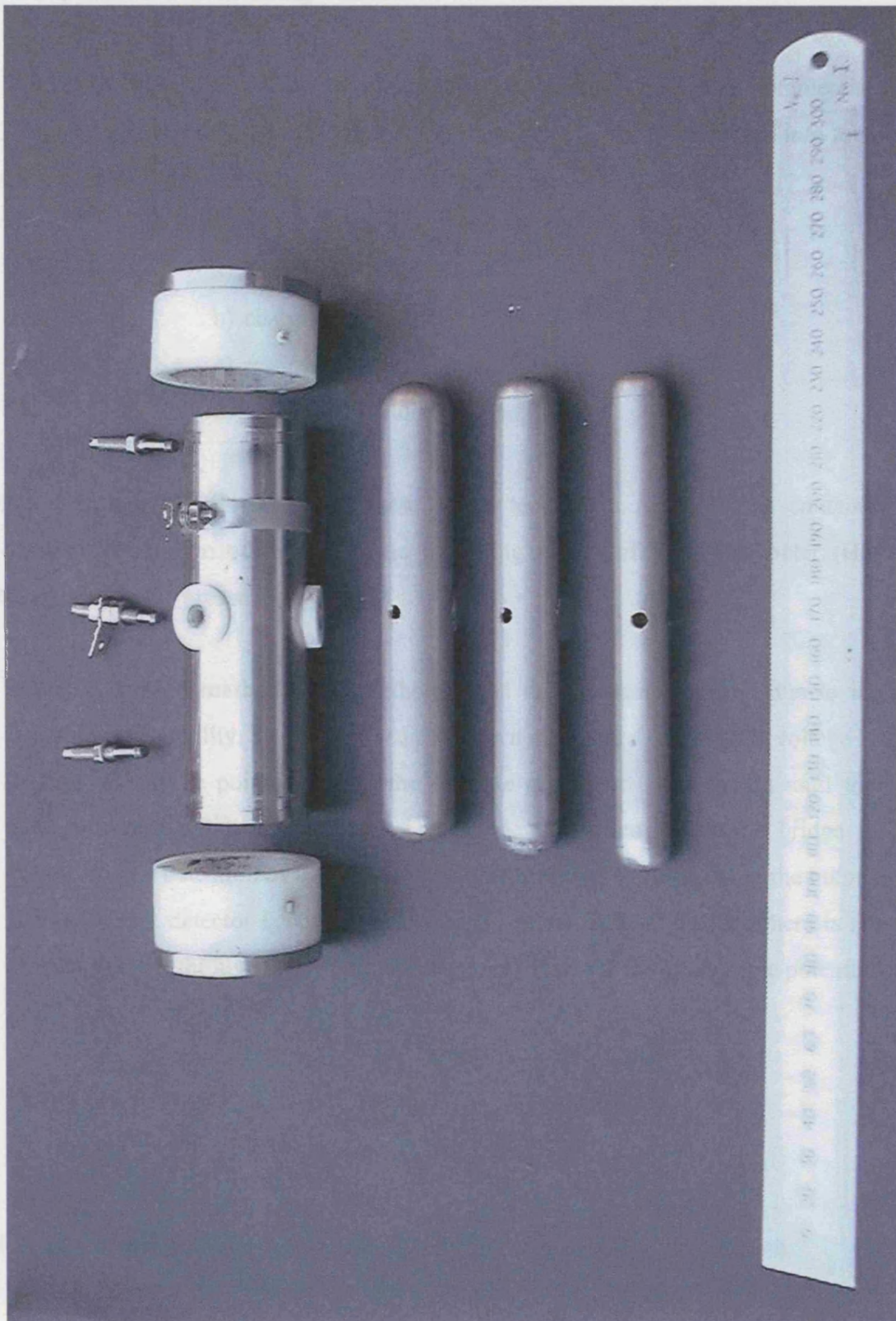Plate 4.2. Photograph showing a front view of the capacitance transducer.

Plate 4.3 Photograph showing the capacitance transducer dismantled, with the various components in isolation.

4.7. Capacitance Measuring Circuits

A wide range of capacitance measuring circuits are employed in various commercial LCR meters. The principle of operation of all these circuits can be classified into four general groups (Wind, 1956; Huang, 1986; Simons, 1991, HP, 1993);

> a) ac bridge method
>
> b) charge/discharge method
>
> c) resonance method
>
> d) oscillation method

The following is a brief overview of these various techniques. Appendix A contains a detailed description of the automatic balancing circuit of the LCR meter (HP 4263B) used in the present study.

e) **The a.c. bridge method.** This method is the most commonly used due to its accuracy and stability. The basic circuit is shown in Figure 4.9.a. An a.c. voltage is applied across the points AC and the variable capacitor, Cv is varied until the voltage across points BD is zero. This is the null point where the bridge is balanced. The detection of the null point can be achieved by monitoring the output with a current detector I_D connected across the points BD. At balance there is no current flowing through BD. Therefore the points B and D are at the same potential and

$$I_1 R_1 = I_2 R_2 \qquad (4.29)$$

$$I_1 C_U = I_2 C_V \qquad (4.30)$$

Dividing the first equation by the second and solving we obtain:

$$C_U = \frac{C_V R_1}{R_2} \qquad (4.31)$$

From the above equation, the unknown capacitance, C_U can be measured.

b) The charge/discharge method. A typical circuit based on this method is shown in Figure 4.9.b. Basically, the unknown capacitance, C_U is charged to a certain voltage, V via a switch S_1 and after a time period, is discharged via another switch S_2 into a current detector. The charge transferred to the current detector from C_U during one charge/discharge cycle is given by the following equation:

$$Q = V \, C_U \qquad (4.32)$$

The above procedure is repeated at a predetermined frequency. The successive discharging pulses are measured by a current detector from where the charge, Q can be determined.

c) The resonance method. The principle of this method is shown in Figure 4.9.c. A sine wave source provides an excitation voltage, V_E of frequency equal to the resonance frequency of the LC (inductance-capacitance) system. This system consists of a known inductance, L and an unknown capacitance, C_U. Any changes in the C_U will result in a change of both amplitude and phase of the output voltage, V_{out} which is in turn measured by a voltage detector.

d) The oscillation method. This method can be applied to either LC or RC (resistance-capacitance) oscillating systems. Figure 4.9.d is a schematic representation of the basic circuit. In both cases, the oscillating system capacitance C, is replaced by the capacitance, C_U , to be determined. Therefore, changes in C_U result in changes of the oscillation frequency which can be measured using a digital counter or a frequency to voltage converter.

The LCR (HP 4263B) meter used in this study like the rest of the general purpose LCR meters, uses an automated version of the bridge method where the basic components are similar to the conventional bridge method with additional circuits for detecting and subsequently rectifying the "unbalanced" bridge.
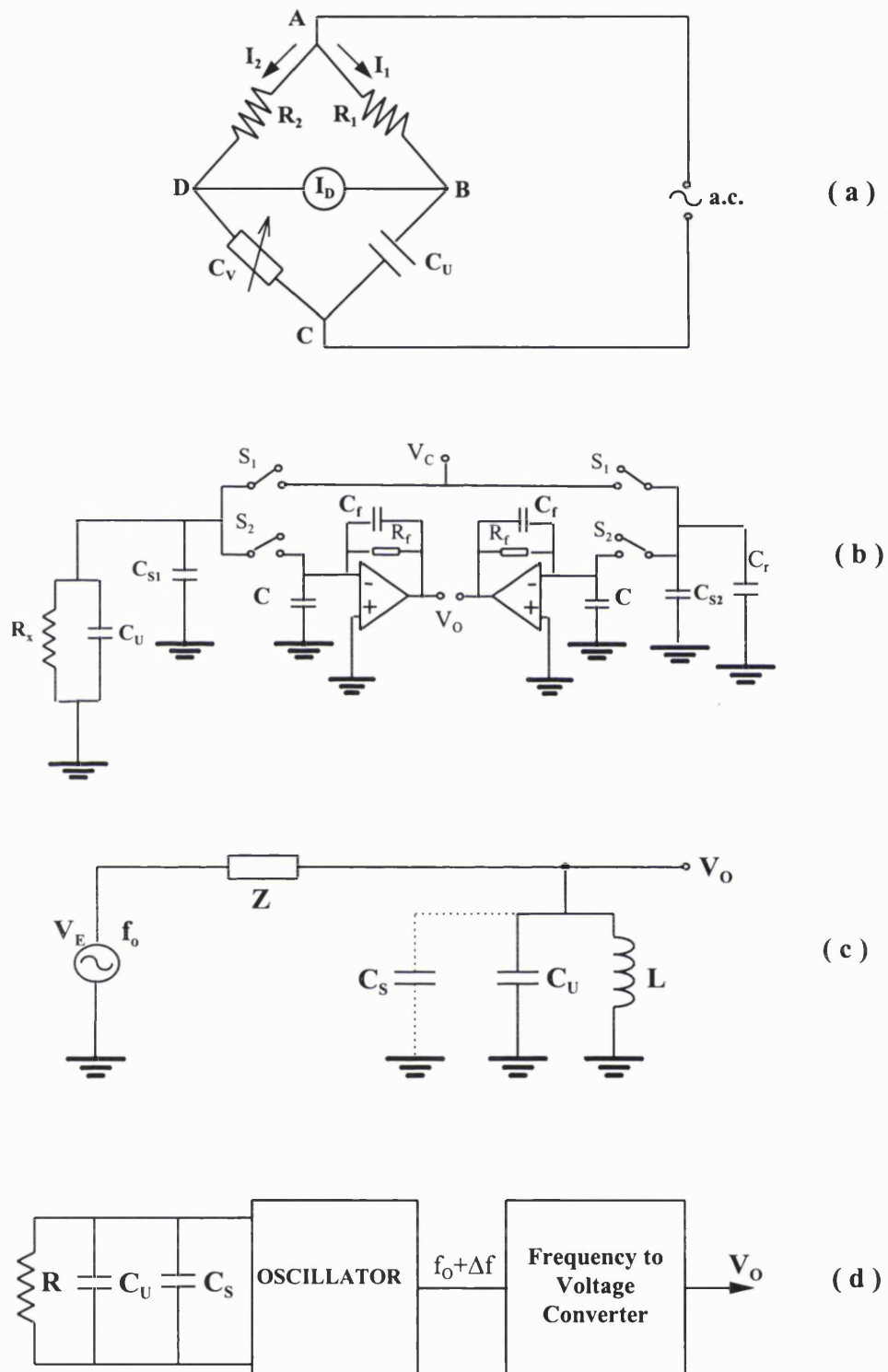
Figure 4.9. Basic capacitance measuring circuits a) ac bridge method b) charge/discharge method c) resonance method d) oscillation method.

The major advantages of this method is wide frequency coverage and high accuracy over a wide capacitance measurement range (HP, 1996). Appendix A contains a description of the automatic balancing circuit of the LCR meter (HP 4263B) as well as its operational specifications.

Finally the LCR meter is connected to the electrodes of the transducer via 1 m long test cables equipped with Kelvin clips (HP 16089B). Their complete operational specifications are given in Appendix A.

CHAPTER   5

DESIGN AND DEVELOPMENT OF SOLIDS DISPERSION UNIT

5.1. Introduction

This chapter describes the design and development of the equipment used for the controlled dispersion of solid particles in an air stream and their subsequent monitoring using the capacitance transducer. Basically, the unit comprises

- An aerosol generation system
- A pneumatic conveying system

A review of the state of the art relating to the currently available technology as well as the pertinent theory is described first, followed by a detailed description and construction details of the unit's distinct modules.

5.2. Literature Review of Aerosol Generation Systems

The most widely used method, for generating solid aerosols is the pneumatic dispersion of a dry powder (Hinds, 1980; Willeke, 1980; Cohen et al., 1995). With this method, finely divided materials with a wide range of particle sizes, shapes, specific gravities, and surface characteristics are readily obtainable in aerosol form. This method of dispersion offers four main advantages compared to other methods of producing aerosols such as those based on nebulisation ,vibrating orifice or spinning disc atomisation (Silverman et al., 1956; Colbeck, 1998). These are

- Its applicability to the majority of materials that can be powdered

- Ability to achieve near-perfect dispersion of the powder to aerosol form

- Almost any amount of dust/unit time can be generated continuously. For example, the dry-dispersion methods can produce feed rates ranging from few milligrams to more than a kilogram per minute to give various dust concentrations

- The produced aerosols do not contain excessive moisture.

The basic elements comprising a dry-dispersion aerosol generator include the powder feeding mechanism for continuously metering and controlling the powder input into the generator at a constant rate together with the means for pneumatically dispersing the powder to form an aerosol (Hinds, 1982).

5.2.1. Powder Feeding Mechanism

The simplest powder feeding mechanisms are based on gravity. The loose powder is fed into the gas stream either solely driven by gravitational force or assisted by vibrators, agitators or pressure head (Hinds, 1982). The main advantage of such systems is that they do not have moving mechanical parts and are very simple in operation (Butters, 1981). However, they tend to give uneven delivery which results in small variations in the concentration of the produced aerosol (Willeke, 1980). Alternatively, more sophisticated designs have been developed where compressed powder is eroded or scraped away at a constant rate resulting to a more stable delivery. These systems employ a variety of gadgets including screw feeders, rotating discs, chains conveyor belts, brushes, troughs and hoppers (Richards, 1966; Hinds 1982; Cohen, 1995; Colbeck, 1998). However, these feeding mechanisms have been regarded far too complicated for the scale and purpose of the specific application.

Figure 5.1 illustrates several gravity-based designs for introducing granular solids into a dilute phase.
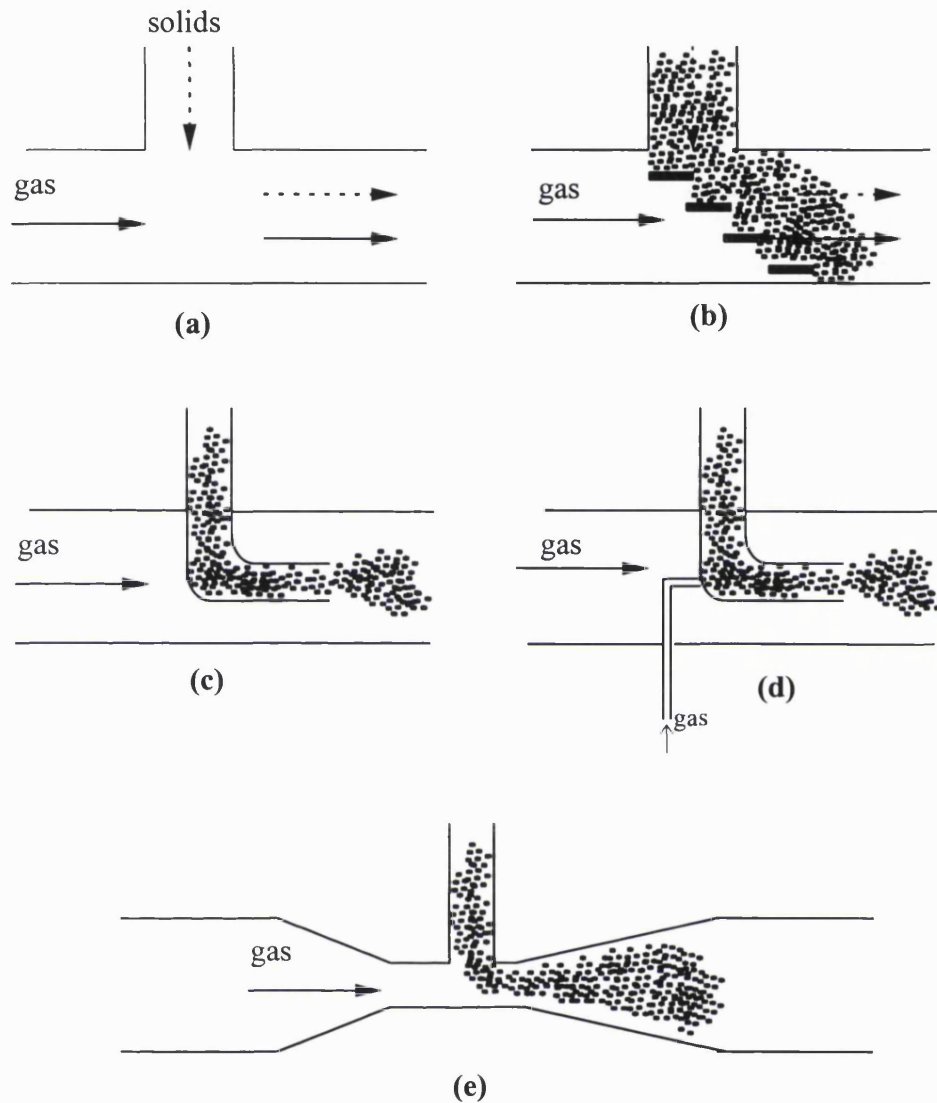
Figure 5.1. Carrier line feeders (Zenz et al. 1960).

Figure 5.1.a shows an ordinary T arrangement which is the most commonly used feeding mechanism. The solids exit from a valve at the base of a bin, through the vertical leg of the T and then swept into horizontal motion by the carrying gas flowing in the horizontal section of the T (Zenz et al., 1960).

However, experiments have shown that solids tend to pile up just below the vertical leg of the T. The extent of the deposition increases with increasing solids feed rate and decreases with increasing gas flowrate. Additionally, solids pile-up decreases

with increasing pipe diameter, under constant solids rate and gas flowing velocity (Zenz et al. 1960). The latter is to be expected since in a pipe of a larger diameter particles have to traverse a longer distance (i.e. the cross section of the pipe) in order to deposit at the bottom of the pipe. Hence, the particles are more likely to be accelerated in the direction of gas flow and not pile up below the feed point (Zenz et al., 1960).

The observation that solids pile-up decreases with increasing pipe diameter initiated the idea of using a cascade type of baffling below the inlet T as it is shown in figure 5.1.b (Jorgensen, 1961). The baffles hinder the downward movement of the particles and therefore giving the gas a better chance to accelerate the particles into horizontal flow.

Zenz et al. (1960) report a variation of the baffling concept as shown in figure 5.1.c. In this design, the vertical leg of T extends further into the conveying pipeline in the form of an elbow. The elbow stretches beyond the horizontal distance determined by the solids angle of repose, so that in the absence of air flow no solids fall from it. A modification of this design as described by Zenz (1960) includes an air jet arranged concentric with conveyor tube (i.e elbow) which directs the solids out of the elbow into the mainstream by producing a velocity component in the desired direction of flow as shown in figure 5.1.d.

Figure 5.1.e illustrates a variation of the original T arrangement as reported by Jorgensen (1961). Here, the vertical leg of the T concludes at the throat of a venturi where the higher velocity provided due to the area restriction, reduces the pressure in the conveying pipe to a value which is below atmospheric pressure. The slight vacuum draws the powder into the dilute air in the conveying pipe avoiding hindrance from reverse air flow as well as preventing solids deposition (Butters, 1981). The gas-solids mixture is subsequently expanded through the divergence section. In this way the "static" pressure needed to support the flow is recovered.

The venturi type of T is considered to be a good solution for feeding powdered material in small scale experimental applications according to Zenz et al. (1960). However, the same authors quote several limitations that make this arrangement unattractive for large scale industrial applications.

One of these limitations is that the vertical leg of the T through which the solids enter the venturi cannot, in effect, be larger than the diameter of the throat of the venturi. Therefore, the dimensions of the throat determines the maximum valve size below the solids hopper which controls the solids intake. This maximum valve size, for instance, may be smaller than the one required for the design range of solids flow, thus limiting the usefulness of such an arrangement lines.

Another complication is that the presence of solids reduces the effectiveness of the pressure recovery in the divergent section of the venturi. However, the latter is important only in long carrier lines (order of hundred meters) and not in small scale operations.

5.2.2. Powder Dispersion

In every aspect of gas-solid operations and as such during powder dispersion, two very important factors are commonly encountered: agglomeration and adhesion. To fully disperse a powder in gaseous media, it is necessary to supply sufficient energy to a certain volume of bulk powder in order to cause agglomerates to be reduced into their components particles and to prevent adhesion in the adjusted surfaces (Hinds, 1982).

Agglomeration occurs during the storage of powdered materials where the individual particles are packed together so close that tend to agglomerates and resist separation. Therefore, it is necessary to use a proper dispersion technique for breaking down the agglomerates into their components particles during the aerosol formation (Silverman et al., 1956).

120

Adhesion on the other hand, is a very common phenomenon during pneumatic transport of the solids (Klinzing, 1981). As particles flow in a pipe some adhere to the surfaces while others settle into small crevices in the system. After the initial deposition of the particles onto the pipe walls, the particles in suspension interact not only amongst themselves but also with those adhering to the wall. Consequently incomplete dispersion occurs which according to Silverman et al. (1956) results in an aerosol with particle size distribution larger than the static size distribution of the initial powder particles.

These two phenomena can be attributed predominately to van der Waals and electrostatic forces, and to a lesser extend to other forces such as capillary and chemical bonding (Klinzing, 1981).

Agglomeration and adhesion of solid particles depend on various factors and conditions such as the type of particle-particle interactions, the surface character of the solid, moisture, particle and surface stickiness, surface roughness, particle size, etc. (Klinzing, 1981; Willeke, 1980). A brief review of these factors will assist the understanding of their effect on agglomeration and adhesion and hence identify possible ways of limiting if not eliminating these undesirable phenomena.

i) Humidity. As the moisture content of the gas increases, the adhesion due to the adsorbed liquid films between the solid particles and adhering surfaces increases (Hinds, 1982). The adsorbed water film forms a bridge between the particles and the surface which keeps them together (Klinzing, 1981). Generally, it can be said that hydrophobic materials (e.g. talc) and dry powders are easier to disperse than the hydrophilic materials (e.g. quartz, limestone) and humidified powders (Willeke, 1980). On the other hand, extremely dry air (i.e. relative humidity < 5%) can cause strong electrostatic forces between particles resulting in reduced dispersibility (Hinds 1982; Colbeck, 1998)

ii) Particle Shape and Size. The shape of the particle is one of the important parameters determining their adhesion properties. Generally, minimum adhesion forces occur for particles of isometric shape, that is, particles that look more like spheres or regular polygons. Planar particles have higher adhesion forces than isometric shapes. One also finds the adhesion forces of needles and fibers to be larger than both isometric and planar particles (Klinzing, 1981). Furthermore, powder's dispercibility increases dramatically with particle size. Moreover, depending on the powder, there is a minimum size below which particles cannot be satisfactorily dispersed (Willeke, 1980).

iii) Temperature. Little work has been done on the effect of temperature on adhesion. Some studies indicate that as the temperature increases, adhesion also increases (Klinzing, 1981). This may be attributed to the fact even though higher temperatures tend to drive off the adsorbed water layers, the electrostatic forces may become more dominant. For painted surfaces, increased temperatures makes the surface sticky and thus increase the adhesion forces (Klinzing, 1981).

iv) Thermophoresis. Thermophoresis phenomenon become important in situations in which the solids-gas suspension is contained by surfaces e.g. during flow of aerosol in a pipe (Boothroyd, 1971). Thermophoresis occurs when temperature gradients are established within the system which in turn result in migration of particles towards the colder region. This is because the gaseous molecules on the warmer side will move faster, colliding with the particles more often and causing greater momentum exchange during each collision. Therefore, a net force is developed pushing the particles away from the warmer area resulting in adhesion of the particles on cold surfaces (Hesketh, 1977). Thermophoretic force is usually very weak, however it becomes rather significant as the particle size decreases. Hence, according to Hesketh (1977), in suspensions of fine or very fine particles in gases, it is increasingly important to utilise these forces in order to enhance or hinder the deposition of particles onto cold surfaces. For instance, it is advisable to maintain the wall temperature of a pipe slightly higher than the flowing aerosol. This will produce

temperature gradients that will induce particle motion away from the walls due to thermophoresis which will reduce the wall/particle losses.

Finally, Zenz et al. (1960) list the following as the important parameters affecting the flow of particulate solids in pipes:

a) The internal diameter of the conduit should exceed five to seven times the diameter of the largest particles when they are present in high proportion.

b) Materials of narrow size distribution exhibit better flow characteristics (wider size ranges particles tend to stick).

c) Mild-steel pipe causes sticking more readily than stainless steel or glass.

d) Surface moisture should be kept around 5 %.

e) Fine materials of particle size less than ca 0.1 μm have a pronounced tendency to stick.

5.3. Solids Pneumatic Transport System

After the dispersion process and the initial suspension of the particles, it is necessary to convey the fully suspended particles in the air stream along a certain pipeline length at the end of which the capacitance transducer is located. This requires the determinations of the minimum air conveying velocity for the suspension of the particles and the minimum pipe length that will allow the solids-gas mixture to reach steady state.

5.3.1. Calculation of Air Conveying Velocity

The conveying velocity is considered as one of the most important parameters in the transport of solid particles in an air stream. Cabrejos et al. (1993) reports that systems designed with excessively high conveying velocities are subject to increased pressure drop, solids degradation and pipe erosion. On the other hand systems designed with too low conveying velocities or extremely high solid loadings are subject either to

erratic operation due to deposition or even complete termination of the operation due to blockage.

In the present study, we are interested in the minimum air velocity required to convey a particular amount of solids without particles 'falling' out of suspension prior to concentration measurement. This velocity is known as "critical velocity". In general, it can be interpreted as the safe gas velocity for the conveyance of solids (Cabrejos et al., 1994).

Other researchers use the term saltation or settling velocity to describe the minimum gas velocity in horizontal flow. The reason is that in horizontal conveying, saltation occurs when the carrier gas velocity is small enough to permit settling of the solids particles within the transport line (Klinzing, 1981; Kraus, 1980). Therefore, keeping the gas velocity above the saltation velocity in all horizontal sections of a pipeline ensures no deposition of solids in the system.

The minimum conveying air velocity depends on a number of factors including material to air ratio, absolute density, bulk density, particle size and shape, and physical characteristics such as abrasiveness, tackiness, moisture content etc. Because of the unknown effect of these variables on the conveyability of a material, there is not a single correlation available for prediction of the minimum conveying velocity (Kraus, 1980) and several have been proposed.

The following is a review of these methods with a view for adopting the most appropriate procedure in the present study.

i) Dallavale (1932)

Dallavale (1932) used various materials (e.g. carbon, anthracite, quartz) of different sizes varying from 1400 µm to 8.1 mm in order to calculate minimum air conveying velocities. The proposed equation has been developed in an empirical fashion and

applies to low and intermediate concentrations of solids in air streams. For transportation of solids in horizontal ducts, it takes the form:

$$V_m = 132 \left(\frac{\rho_s}{\rho_s + 1000} \right) . d_p^{0.398} \qquad (5.1)$$

where :

V_m = minimum carrying velocity , m/sec

ρ_s = density of solid particles, kg/m^3

d_p = average diameter of particles to be conveyed, m

Dallavale (1932) concludes that in practice, the actual conveying velocities used in systems with low solids-to-gas weight ratios (<10) are generally over 15 m/sec. For higher ratios (>20), the actual gas velocities are usually less than 7.5 m/sec.

ii) Davis (1935)

Davis (1935) developed a similar equation to Dallavale (1932) in an effort to give a solution to the practical question of how great fluid velocity is required to pick-up or prevent deposition of particles of particular size and density in a simple piping system. Setting up a pressure balance on a single particle submerged in a flow, and taking into account static and dynamic forces, Davis (1935) developed the following equation :

$$V_m = \sqrt{ \frac{0.038 \ g}{\rho_g} \left(3.25 \ d \ (\rho_s - \rho_g) + 47.88 \ P \frac{\rho_g \left(W_s / W_g \right)}{\rho_s} \right) } \qquad (5.2)$$

where :

g = gravitational constant, 9.81m/sec^2

ρ_g = gas density, kg/m^3

P = static gas pressure, Pa

W_g = gas mass flow rate, kg/sec

W_s = solids mass flow rate, kg/sec

125

iii) Owens (1969)

Owens (1969) has suggested that inspection of the dimensionless ratio (a pseudo-Froude number):

$$\frac{\rho_g u_\tau^2}{\rho_s g \, d_p} \tag{5.3}$$

where u_τ is the friction velocity at the pipe wall.

The above ratio is used as criterion for determining when saltation is likely to occur. Indeed the author suggests that saltation is likely to occur when this ratio varies between 1 and 10^{-2}. Particularly for values less than 10^{-2}, large deposition is anticipated.

iv) Rizk (1973)

Rizk (1973) proposes the use of the following semi-theoretical correlation for the calculation of saltation velocity:

$$\frac{W_s}{\rho_g A V_m} = \left(\frac{1}{10^{(1440 \, d_p + 1.96)}}\right) \cdot \left(\frac{V_m}{\sqrt{gD}}\right)^{(1100 \, d_s + 2.5)} \tag{5.4}$$

where $\dfrac{W_s}{\rho_g A V_m}$ is the solids loading   and $V_m/\sqrt{gD}$ is the Froude number at saltation and by rearranging :

$$V_m = \left(\frac{W_s 10^{(1440 \, d_p + 1.96)} (gD)^{(1100 d_s + 2.5)/2}}{W_g}\right)^{1/(1100 d_p + 2.5)} \tag{5.5}$$

where:

V_m = saltation velocity, m/sec ρ_g = gas density, kg/m^3

W_S = solids mass flowrate, kg/sec d_p = mean particle diameter, m

D = pipe diameter, m g = gravitational constant, 9.81 m sec^{-2}

Rhodes (1990) however, suggests that the above stated correlation gives rise to as much as ± 54% error in saltation velocity when compared to experimental data.

v) Kraus (1980)

Kraus (1980) method for calculating the air velocity required to convey a certain material is based on experimental data obtained in conjunction with cereals, wood chips, sawdust, beans cotton, lint, powders, dust, and iron borings.

The curves in figure 5.2 show average air velocities (ft/min) and volume of air required (ft^3) to convey one pound of material according to the material bulk density (lb/ft^3). Attention should be drawn that in this set of curves, one uses the average bulk weight of a cubic foot of material in the condition which is to be conveyed and not the true density of the material. Despite of the fact that the data being somewhat outdated, they are still considered to be useful and 'safe' for the design of many of the existing conveying systems.

Figure 5.2 also indicates that these curves can be used for conveying systems with bulk densities up to 50 lb/ ft^3 (800 kg/m^3). However, according to Kraus (1980), these curves can be extended by extrapolating Sturtenvant's data for bulk densities up to 120 lb/ft^3 (1922 kg/m^3) and using the approximate formula:

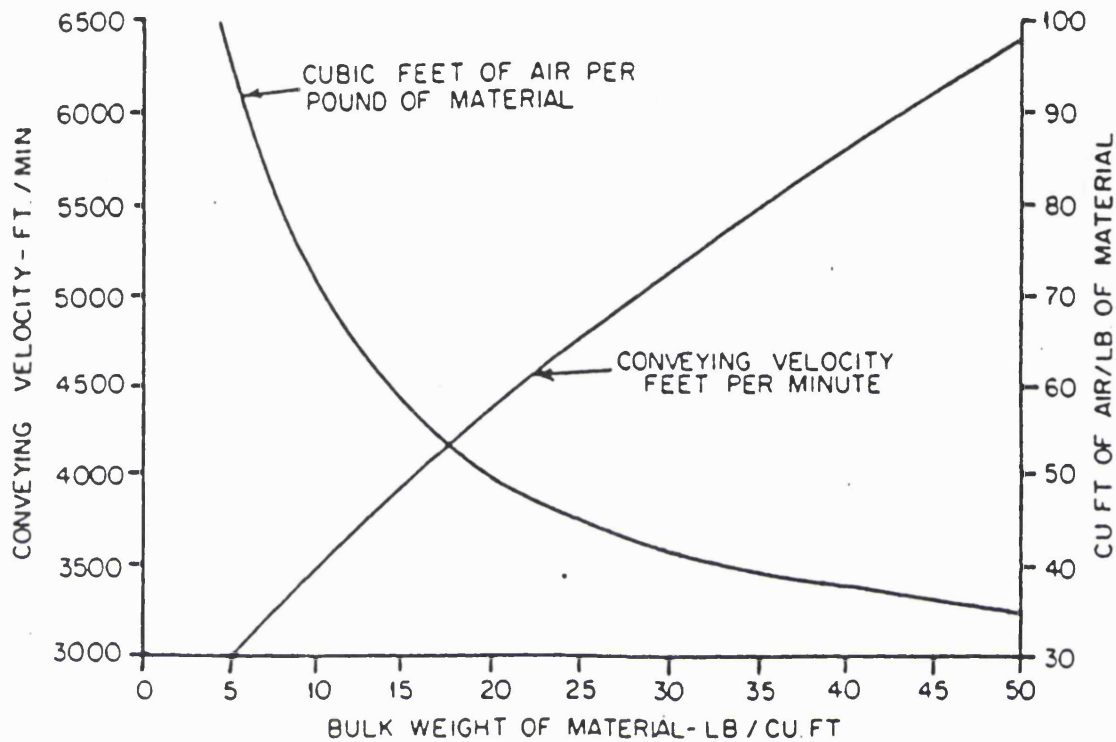$$\text{Velocity} = 920 \cdot \sqrt{\text{bulk density}} \qquad (5.6)$$

Figure 5.2. Average velocities and air volumes for conveying materials

(Kraus, 1980)

vi) Cabrejos et al. (1994)

Cabrejos et al. (1994)'s correlation is a simple equation, useful for predicting the pick up velocity, V_{pu} of particles above 100 μm. Pickup velocity has been defined as the gas velocity required to re-suspend a particle initially at rest at the bottom of the pipe (Cabrejos et al., 1994). The pickup velocity V_{pu}, is given by :

$$V_{pu} = 0.00128 \, Re_p^{0.175} \left(\frac{D}{d_p} \right)^{0.25} \left(\frac{\rho_s}{\rho_g} \right)^{0.75} \sqrt{gd_p} \qquad (5.7)$$

and Re_p is the particle Reynolds number:

$$Re_p = \frac{d_p(V_{pu} - u_p)\rho_g}{\mu_g} \qquad (5.8)$$

where, u_p is the particle velocity which is considered to be a very difficult parameter to determine experimentally (Klinzing, 1981; Kraus, 1980).

However, for fine particles in dilute phase regime Klinzing (1981) proposes the following expression to be satisfactory:

$$u_p = V_{pu} - u_t \qquad (5.9)$$

and u_t is the particle terminal velocity given by :

$$u_t = \frac{0.153 \ g^{0.71} d_p^{1.14} (\rho_S - \rho_g)^{0.71}}{\rho_g^{0.29} \mu_g^{0.43}} \qquad \text{for} \qquad 2 < Re_p < 500$$

This relationship for the pickup velocity is valid for $25 < Re_p < 5000$; $8 < (D/d_p) < 1340$; $700 < (\rho_S/\rho_g) < 4240$.

It is very important to point out that pickup occurs at higher mean gas velocities than saltation (Cabrejos et al., 1994). Therefore operating the solids transport system in velocities higher than the pickup velocity will ensure that the particles are fully suspended.

vii) Graphical Methods & Tabulated Data

In addition to the above methods for calculating the minimum air conveying velocity, some researchers have presented the results of their studies either in tabular or in graphical form. Table 5.1 displays air velocities for conveying coal powder as reported by various authors.

Table 5.1. Comparative air velocities for conveying coal powder.

Material	Conveying Velocity (m/sec)	Reference
Coal, powdered	19.8	Zenz (1960)
Coal, powdered	20.3	Jorgensen (1961)
Coal, pulverised (density =0.56 g /cm^3 & 75% < 76μ)	4.597	Kunii et al. (1969)

Figures 5.3 on the other hand, is a representative plot used for calculating gas velocities required for conveying solid materials of various bulk weight and size as presented by Jorgensen (1961).
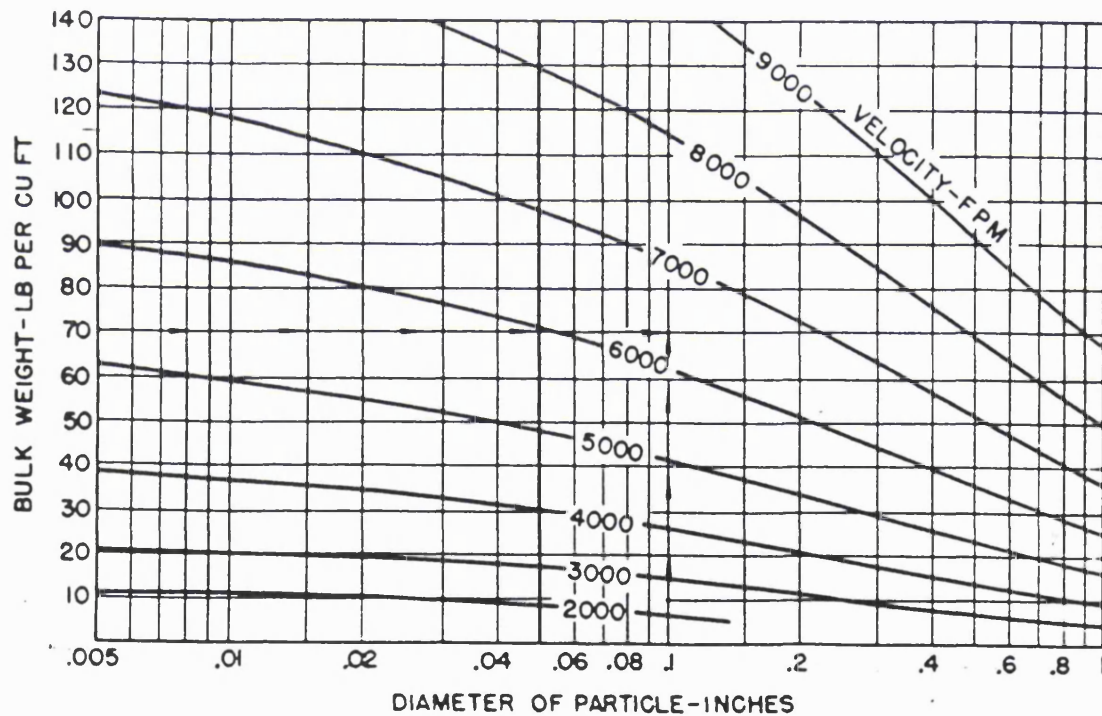

Figure 5.3. Conveying velocities for materials of various bulk weight and size.

130

5.3.2. Case study

In view of the variety of different techniques available for predicting the minimum air conveying velocity, for comparison purposes, the following describes the results of their application to a case study. Here, we consider the transport of spherical coal particles of mean diameter 550 μm and density 1 357Kg /cm^3 through a 3.25 cm ID horizontal pipe. The conveying gas is air (density = 1.29Kg /cm^3) and the dispersion has a solids loading of 0.5 % (v/v). The minimum conveying velocity is required.

Table 5.2 contains the calculated values of the air velocity obtained using the various methods reviewed above:

Table 5.2. Calculated air velocities for transporting a 0.5 % (v/v) dispersion of coal particles (dp = 550 μm and ρ = 1357 kg / m^3) through a 3.25 cm ID horizontal pipe.

Minimum air conveying velocity V_m (m/sec)	Method
3.82	Dallavale (1932)
2.87	Davis (1935)
7.42	Rizk (1973)
3	Kraus (1980)
3.60	Cabrejos et al (1994)

The data in table 5.2 clearly illustrate the diversity of the air conveying velocities obtained by using different calculation methods indicating the absence of a universally applicable equation for designing solids-gas conveying systems.

Indeed, Kraus (1980) and Cabrejos et al. (1993) suggest that best method of determining the conveying velocity is to test the material-flow characteristics in a pilot plant using the type of equipment that is being consider for selection.

5.3.3. Pipeline Acceleration Length

For any pneumatic transport system there is a period after the particles have been injected to the gas stream, over which the particles and gas are not at steady state (Klinzing, 1997). Therefore, it is important for the proposed experimental setup in this study to determine the acceleration length of the pipeline required for the mixture to reach a steady state value. This length depends primarily on particle size (smaller particles require shorter acceleration distance) and on the solids flow rate. It has been observed that it is not significantly affected by the gas velocity or by the solid-gas ratio (Zenz et al., 1960; Marchello et al., 1976).

An analysis by Rose and Duckworth (1968) of experimental results for the transport of various materials for pipes of various angles of inclination upward from horizontal position to the vertical position indicates that the acceleration length, L_A is given by the following equation :

$$L_A = 6D\left[\left(\frac{W_S}{\rho_g g^{0.5} D^{5/2}}\right)\left(\frac{D}{d_S}\right)^{0.5}\left(\frac{\rho_S}{\rho_g}\right)^{0.5}\right]^{1/3} \qquad (5.10)$$

A similar analysis conducted by Klinzing (1981) suggests that the acceleration length may be calculated by using equation 5.11:

$$L_A = \int_{u_{p1}}^{u_{p2}} \frac{u_p}{[0.75C_{DS}\ \varphi_g\rho_g(u_g - u_p)^2\ /\ (\rho_S - \rho_g)d_S] - [(g + 2f_S u_p^2)\ /\ D]} du_p \qquad (5.11)$$

where ϕ_S is voidage of the suspension ($\phi_S = 1 - 4W_S/(\rho_S - \rho_g)\ \pi\ D^2\ u_p$), C_{DS} is the particle discharge coefficient and f_S the solid friction factor.

The upper limit, U_{p2} of the integral in equation 5.11 is the value of the particle velocity at a final steady state whereas the initial value, U_{p1} is the velocity from which the particle accelerates. These values depend on the design of the system.

Equation 5.11 gives the acceleration length for vertical transportation. In case of horizontal transfer, the contribution of gravity is zero and the same equation can be used by omitting the gravitational acceleration, g.

The particle discharge coefficient, C_{DS} in equation 5.11 is highly dependent on the flow regime and is a function of particle's Reynolds number (see equation 5.8). Its value in the intermediate flow regime is determined from (Klinzing, 1981):

$$C_{DS} = \frac{18.5}{Re_p^{0.6}} \qquad \text{for} \qquad 2 < Rep < 500 \qquad (5.12)$$

A number of researchers have suggested various empirical expressions for the calculation of the solids friction factor, f_S in equation 5.11. Klinzing (1981) proposes the use of following expression:

$$f_S = 0.0285 \, (g \, D)^{0.5}/u_p \qquad (5.13)$$

Finally, a more recent work of the same author suggest the two following expressions for the calculation of the acceleration length (Klinzing, 1997):

$$L_A = 0.257 \, D \left(\frac{D}{d_S}\right)^{-1.26} \left(1 + \frac{W_S}{W_g}\right) Re \qquad (5.14)$$

and

$$L_A = (\exp)^{3.32} \left(\frac{d_S}{D}\right)^{0.953} \left(\frac{W_S}{W_g}\right)^{-0.0912} \left(\frac{\rho_S}{\rho_g}\right)^{-0.924} \qquad (5.15)$$

Zenz et al.(1960) cites the observations of several researchers indicating that nearly complete acceleration is achieved within 4.3 m from the solids feed point.

It is noteworthy that for the conditions of the case study cited earlier, and assuming an air conveying velocity of 3 m/sec, the acceleration length calculated using equations 5.10, 5.11, 5.14 and 5.15 are 3.44 m ,1.11 m, 4.3 m and 0.48 m respectively. The significant difference between these two predicted values renders the two estimation methods unreliable and hence a direct measurement based on experimental observation is adopted in this study (see section 5.4.2.2).

5.4. Description & Construction Details of the Experimental Set-up

Figure 5.4 shows a schematic representation of the experimental set up constructed for the present study.

In this arrangement high pressure air is delivered form the main air supply. It is dried prior to entry into the flow control module (4) by passing through an oil trap (2) and a filter (3). The flow control module comprises 3 rotameters (A) for flow rate measurement, control valves, a pressure gage (B) and a buffer chamber (C) for pressure and flow stabilisation.

The system has been previously calibrated and is capable of supplying a wide range of air flowrates through a 6 m long and 0.0325 m i.d. stainless steel (type 304) main pipeline (5).

The introduction of the particles into the air stream from a storage chamber (7) is facilitated by the pressure difference created in a especially designed venturi (6) (see 5.4.1.1) as well as the pressure head generated from a bleed air stream (8). The flow of particulates into the air stream is regulated and controlled using valves (11), (10) and (9). The last valve controls the bleed pressure head.
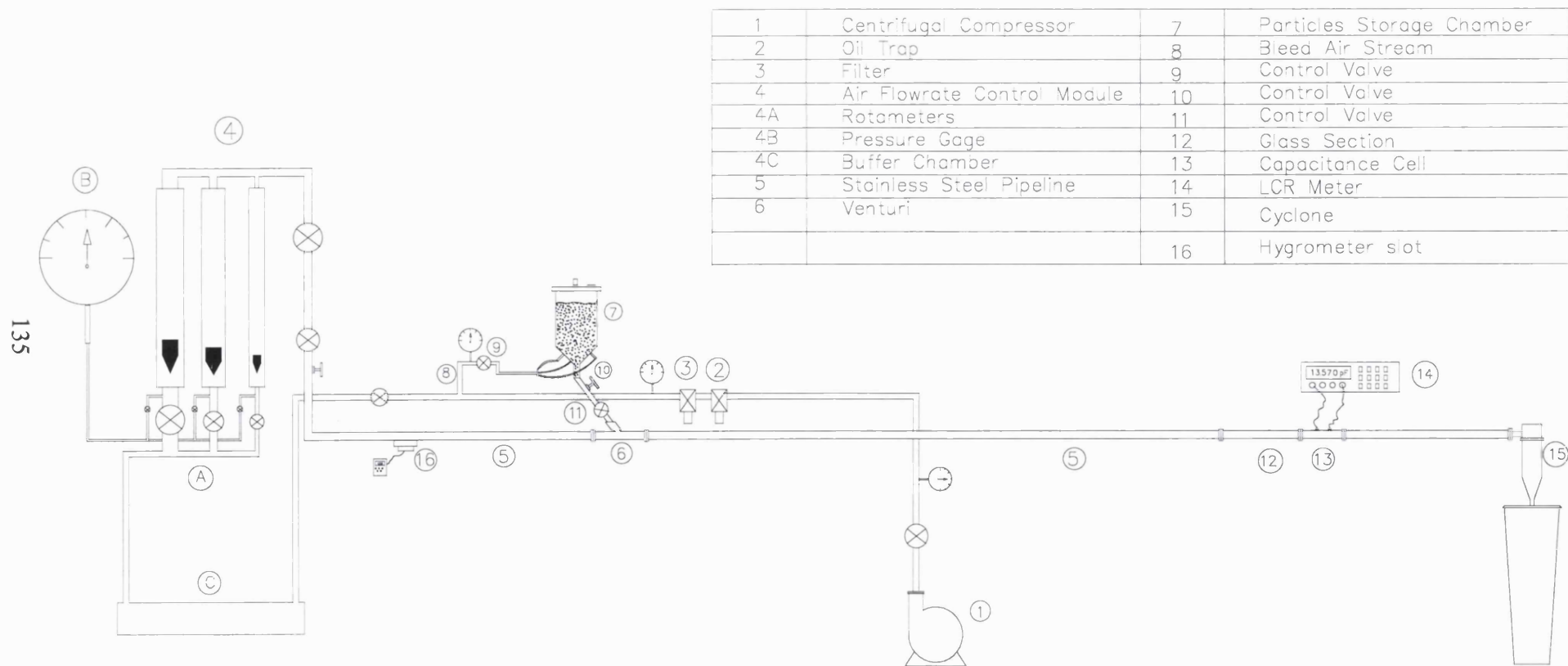
1	Centrifugal Compressor	7	Particles Storage Chamber
2	Oil Trap	8	Bleed Air Stream
3	Filter	9	Control Valve
4	Air Flowrate Control Module	10	Control Valve
4A	Rotameters	11	Control Valve
4B	Pressure Gage	12	Glass Section
4C	Buffer Chamber	13	Capacitance Cell
5	Stainless Steel Pipeline	14	LCR Meter
6	Venturi	15	Cyclone
		16	Hygrometer slot

Figure 5.4. Experimental set—up for the controlled dispersion of solids in an air stream and their subsequent monitoring using the capacitance transducer.

The particles-air suspension is drawn though the 6 m long pipeline, passing through a 0.25 m long glass observation section (12) prior to entry into the capacitance transducer (13) which is in turn connected to the LCR meter (14). Finally, the monitored particles are separated from the air stream with a cyclone (15) and recovered in a collection container.

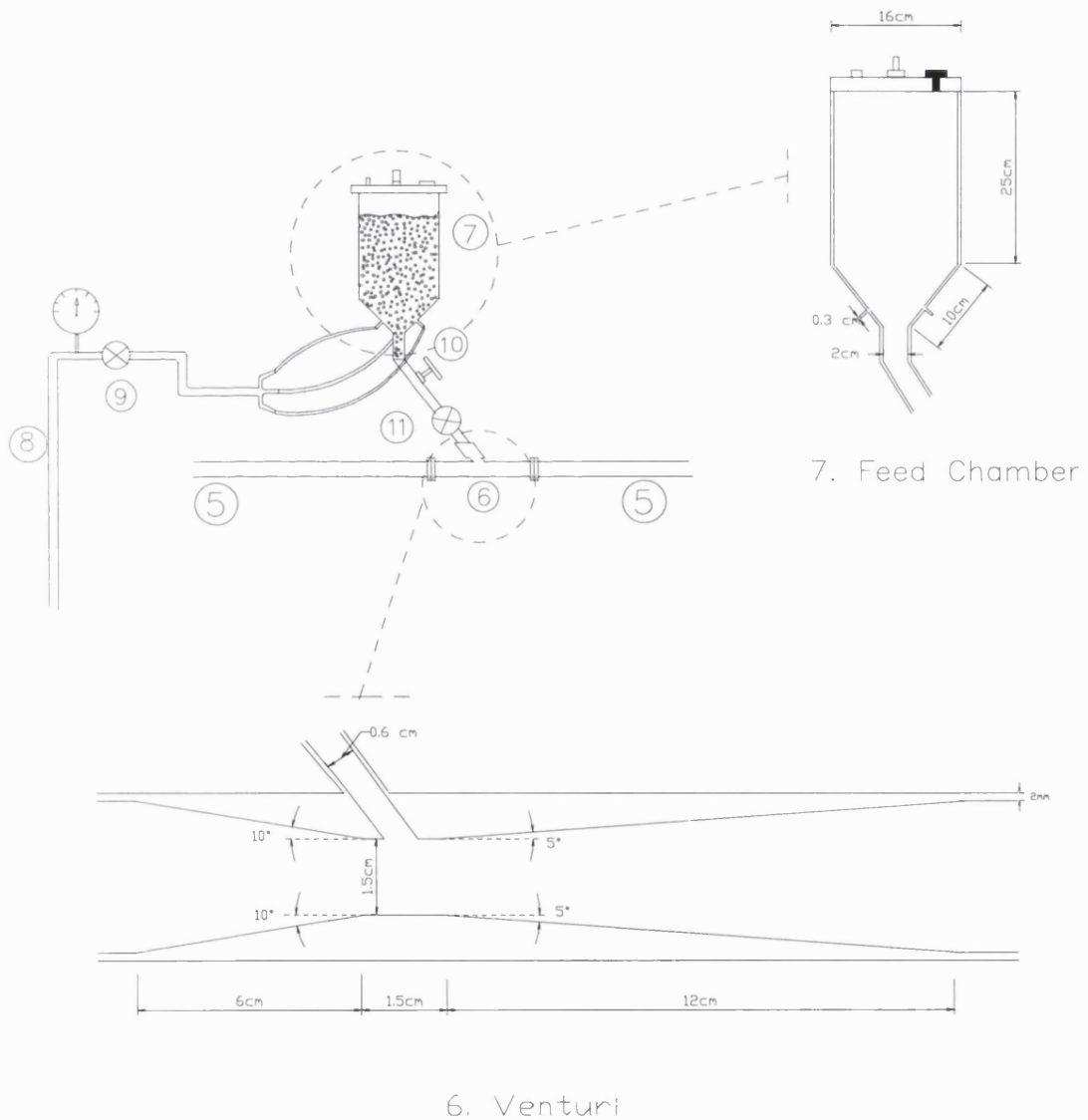Detailed description of the main components of the above experimental set-up is given in the following paragraphs.

Figure 5.5. Detailed view of the feeding arrangement

5.4.1. Aerosol Generation System

The aerosol generation system is shown in figure 5.5. The test powder from the vertical conical hopper is discharged through a rubber standpipe and a venturi feeder to the air stream in the main pipeline.

5.4.1.1. Powder Feeding System

A conventional conical hopper has been selected for storing the test powder during the experiments. In designing mass flow hoppers, one has to ensure that that the discharge orifice is large enough to prevent formation of mechanical and cohesive arches that can stop the flow completely. Also the walls of the hopper should be steep enough to ensure that particles slide along the walls (Shamlou, 1988). Therefore, several steps have been taken in order to facilitate and maintain continuous discharge of the powder during tests. These have taken account of:

a) The orifice diameter of the hopper must be at least six times the average particle diameter in order to avoid formation of arches and obtain an uninterrupted flow (Fayed et al., 1984). Furthermore, it has to be 1.3 times the hoppers diameter so that the flow of the particles will be practically unaffected by the hoppers diameter (Shamlou, 1988).

b) The height of the stored powder (especially when $d_p <$ 500 μm) above the orifice has to be kept low since the discharge rate decreases with increase in the powder's height. This is due to the compression of fine particles and subsequent formation of cohesive arches (Zenz et al., 1960).

c) The attachment of a standpipe just below the discharge orifice, dramatically increases the solids flow (Yuasa et al., 1972). The effect of the standpipe is greater as particle size becomes smaller and as its length increases.

137

d) Injection of an aeration bleed into the region just above the discharge orifice has been found to increase the particle discharge rate (Zenz et al., 1960; Shamlou, 1988). Here, air is pumped though three small nozzles which are welded to the walls around the orifice, fluidising the powder, decreasing its bulk density, and facilitating its discharge (Zenz et al., 1960).

All of the feeding mechanisms shown in figure 5.1 were considered for use in the present study. The vertical T feeding arrangement incorporating baffles (see figure 5.1.b) was unsuitable as it is more appropriate for large diameter pipes (> 10 cm) thus allowing the use of sufficient number of baffles in order to permit adequate dispersion. Furthermore, the use of baffles in the present set up is expected to give rise to high pressure drops due to the relatively small diameter of the main pipe and hence was discounted.

Similarly, the designs, c and d in figure 5.1 are expected to cause large pressure drops due to restrictions on the area available to flow. This is because of the relatively large diameter elbow required to permit free flow of the descending particles, preventing agglomeration and particle jamming in the feed tube.

The ordinary T arrangement shown in figure 5.1.a was not adopted as trials with this design indicated that even relatively low velocities (< 6 m/sec) create a back pressure in the outlet tube of the storage chamber, obstructing and eventually halting the down flow of the particles. This problem becomes more severe in case of fine particles (<100 μm).

The feeding mechanism finally adopted in this study was that comprising a T arrangement with the vertical leg of the T concluding at a venturi as shown in figure 5.1.e. This configuration was used as opposed to the others because it facilitated a controlled delivery of the particulates and did not give rise to backflow. It also resulted in adequate dispersion of the particles in the air stream without the need for excessively high flow rates (Cohen et al., 1995). The venturi is made of brass and has

been designed according to British Standards (BS1042: Section 1:1, 1981). Its dimensions are shown in figure 5.5.

The feeding mechanism must be capable of delivering a controlled amount of material for dispersion at a constant and reproducible rate. In the present arrangement, this was achieved by using a set of two valves (10) and (11) (see figure 5.5) positioned at the middle of the rubber standpipe as well as the pressure head generated from a bleed air stream (8) injected in the powder storage hopper.

The "control" valve (10) regulates the standpipe's cross sectional area available to the particles to descent towards the venturi (6) in a way similar to a conventional diaphragm valve. The stepwise opening of this valve will increase the concentration of particles in the produced aerosol for a constant air velocity. The solids discharge valve (11) is actually a "on - off" clamp placed around the rubber standpipe which when opened releases the particles in to the air stream. Attempts to use conventional valve designs such as ball valve have been found unsuitable because fine particles jammed between the ball and the main valve body.

The bleed air (8), injected via three small nozzles (3 mm in diameter) just above the hopper's discharge orifice facilitates the discharge of the particles. It is found to be especially useful at high air velocities (>19m/sec) in order to overcome back-pressure, and thus maintaining the down flow of the particles. Furthermore, regulating the flowrate of the injected air via control valve (9) contributes to the smooth control of the solids discharge (Shamlou, 1988).

5.4.1.2. Powder Dispersion

To fully disperse the solids fed into the air stream, several features were incorporated in the design of the apparatus in order to overcome or minimise the particle agglomeration and adhesion effects (see section 5.2.2).

The main pipe was constructed from stainless steel (type 304) as opposed to mild steel to reduce particle-wall adhesion. In addition, the internal diameter of the main pipe (5) is 0.0325m which well exceeds the recommended (see for example Zenz et al., 1960; Allen, 1990) safe limit of 5-7 times the diameter of the largest particles to be used ($d_{particle}$(max) = 0.001 mm). The same criterion has been implemented for selecting the dimensions of the standpipe attached below the powder storage hopper (7) which internal diameter is 0.02 m.

The compressed air used to disperse is cleaned, dried (relative humidity $\simeq$ 15%) and freed from compressor oil mist by passing through an oil trap (2) and a filter (3) prior to entry into the main pipeline.

Clearly, temperature gradients which were identified as a source of thermophoretic adhesion (see section 5.2.2. (iv)), do not play a role in the present set up due to the relatively small scale of the apparatus. However, precautions have been taken so that heating or cooling elements have been removed from the vicinity of the experimental set-up.

Finally, the venturi (see figure 5.5) does not only facilitate the flow of particles in the air stream but also facilitates the breakdown of the particle clusters formed in the storage hopper (Cohen et al., 1995). The agglomerates breakdown because they are subjected to high impinging and shearing forces as well as mutual collision when they are drawn up into a jet of compressed air (Silverman et al., 1956; Rhodes, 1990). It has been shown that higher air velocities in the jet will produce lower percentage of agglomerates (Silverman et al., 1956) .

5.4.2. Pneumatic Conveying System

The first priority that one has to tackle while designing a pneumatic conveying system is the determination of the gas velocity since it determines whether or not the particles are carried as a suspension (Butters, 1981). Secondly the necessary pipe length

required for ensuring steady state flow of the suspension has to be determined. Finally, special precautions have to be taken in order to minimise the build up of electrostatic charge on the particles generated by frictional and contact electrification between the particles as well as between the particles and the walls of the conveying system (Taylor et al., 1994, Jonansen, 1998). This is necessary since charge accumulation on powders constitutes an operational hazard (i.e. powder explosions, operator electrostatic shock) as well as affecting the subsequent capacitance measurement. The extent of the electrostatic effect can be such that the actual measurement becomes impossible due to short circuiting of the capacitor (Huang, 1988).

5.4.2.1. Minimum Air Conveying Velocity

As indicated previously (section 5.3.1), the correlations proposed by various authors for calculating the minimum air conveying velocity gave different results for the same experimental conditions. In the present study, minimum air conveying velocities for different size powders and various solids concentrations were obtained form direct visual observation using a 25 cm glass observation section (item 12 in figure 5.4) positioned in close vicinity of the capacitance transducer.

From a practical point of view, it is important to bear in mind that the minimum air conveying velocity depends greatly on the solids loading. Since, the aim of this experimental set-up is to produce a wide range of solids concentrations, it is necessary to have the ability to vary and control the air velocity in order to maintain the particles fully suspended in all cases. Therefore, an air flow control module (item (4) in figure 5.4) has been constructed which provides air flow rates in the range of 0.0045-1.3 m^3/min (i.e. velocities between 0.1-25 m/sec). It comprises:

Three rotameters (4A) (Rotameter MFG.Co, Ltd, UK) with the following specifications:

- Metric 7×P with stainless steel float, delivery flowrate: 0.0045 - 0.038 m³/min.

- Metric 14×P with stainless steel float, delivery flowrate: 0.015 - 0.130 m³/min.

- Metric 35×P with ceramic float, delivery flowrate: 0.1 - 1.3 m³/min.

A standard test gauge (4B) (Buderberg Gauge Co. Ltd, Broadheath) is used for calibrating the entire system. The calibrating pressure is 10 psi measured at the inlet of the three rotameters.

A cylindrical buffer chamber (4C) of sufficient capacity (volume = 0.007m³, length = 0.74m and diameter = 0.11m) is used to absorb any pressure and flow pulsations.

5.4.2.2. Pipeline Acceleration Length

The pipeline acceleration length was determined experimentally due to the absence of a reliable predictive method in the open literature (see section 5.3.3).

The prime objective is to determine the acceleration length appropriate for all the experimental conditions to be used. This length depends largely on particle size and also on the solids flowrate. Taking into account that larger particles require longer distances to be accelerated, estimating the acceleration length for the largest particles that will be used at the maximum flowrate will ensure that this length will be also adequate for the rest of the experimental conditions. Initially a 6m long pipeline has been used with provision for extending it by attaching various lengths stainless steel pipe sections The main pipe is easily detachable in order to allow its occasional cleaning so as to avoid cross contamination when using different powders.

Finally, it is worth noticing that several measures have been taken in order to ensure that undesirable levels of electrostatic charge will not build up either on the particles or on other components of the experimental set-up (e.g. electrical conductors, non-conducting surfaces). The methods of charge dissipation employed on this experimental rig were:

- The earthing of the electrical conductors of the experimental rig including main transporting pipeline, powder storage hopper, venturi, collection cyclone and collection container (Gibons, 1982; Taylor et al., 1994).

- Insertion of earthed rods with diameter 1-3 mm into the solids flow with their tip directed against the flow. This method removes a portion of the powder charge to the via small energy corona discharges from the tip of the earthed rod (Gibons, 1982; Jones et al., 1991).

- Earthed grids placed perpendicular to the solids flow in order to increase contact between the charged solids and earthed surfaces (especially for particles flowing in the core of the dispersion, away from the earthed walls of the transporting pipeline) (Jones et al., 1991)

5.5. Materials, Equipment and Experimental Procedures

5.5.1. Materials and Equipment

The materials used in this study as well as some of their important physical properties are given in table 5.3.

The density of the particles as well as the bulk density of the powders have been measured using a pycnometer (AccuPyc 1330 Pycnometer, Micrometrics) which determines the density and volume of a particular sample by measuring the pressure change of helium in a calibrated volume. Manufacturer reports an absolute precision of $\pm$ 0.01% of nominal full scale.

The size distribution of each powder which was determined by using a low angle laser light scattering (LALLS) particle size analyser (Sympatec GmbH, type Helos). The operational principle of this instrument is based on the fact that when a light beam strikes a particle, interference phenomena occur such as refraction, diffraction, and absorption which give rise to characteristic scattering patterns. The latter are deconvoluted based on Fraunhofer theory to yield the unknown size distribution

(Allen, 1997). In the particular instrument, the suspension of particles is blown directly through the low power laser and the scattered light is focused by a convergent optical system on to an multi-element solid state detector which records the scattered pattern (Sympatec, 1999). Appendix B gives the particle size distribution data for the various powders used in this study. The data are presented in the form of the cumulative percentage undersize curves.

Table 5.3. Physical properties of various powders used in this study.

Powder	density,ρ (kg/m^3)	average size, d_p (μm)	conductivity, σ_{elec} (1 / Ωm)	Shape	dielectric constant, ε_{sol}
Glass ballotini	2500	90 -1000	10×10^{-14}	spherical	7.2
Bronze	8800	125	8.72×10^6	spherical	∞
Copper I and II	8810	125 (copper I) 180 (copper II)	5.8×10^7	spherical	∞
Quartz	2200	310	5×10^{-16}	spherical	4.1
Steel	7510	110	5.03×10^6	irregular	∞

5.5.2. Experimental Procedures

The experimental procedure basically involves the generation of known concentration of particle suspensions in air streams for calibration of the capacitance transducer. Such data may in turn be used for the subsequent determination of particulate concentrations in unknown test samples.

Figure 5.6 is a schematic representation depicting the appropriate mass balance required in order to produce a particle suspension of known concentration. Two

streams are fed into the unit. One stream is clean dried air of constant volumetric flowrate and the second stream is solids powder of constant mass flowrate. The outlet stream leaving the block is the particle suspension of known concentration. The concentration of particles in the suspension can be calculated if the air and solids input stream flowrates are known.
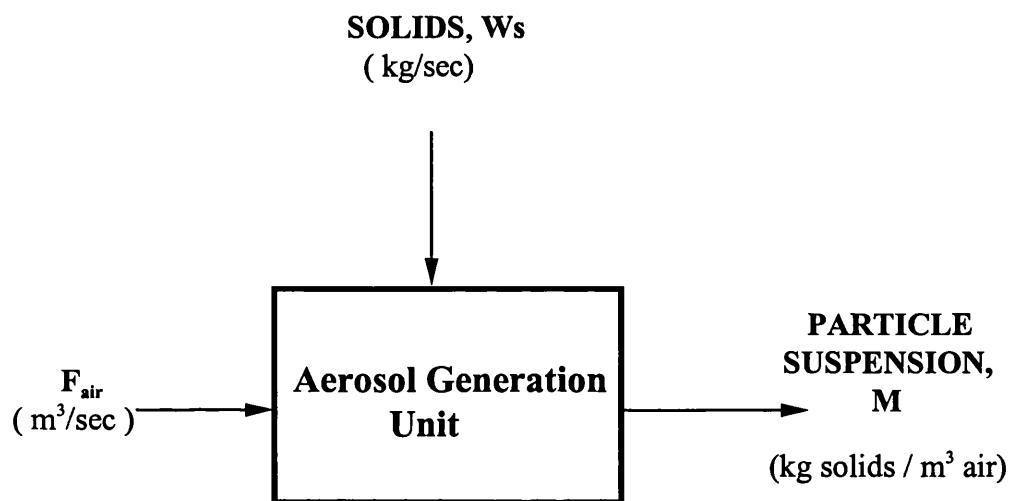
SOLIDS, Ws
(kg/sec)

F_{air}
(m^3/sec) → **Aerosol Generation Unit** → **PARTICLE SUSPENSION, M**

(kg solids / m³ air)

Figure 5.6. Mass balance around the aerosol generation unit.

Applying the mass balance around the aerosol generation unit in figure 5.6 we have:

$$\frac{W_S/\rho_S}{\left(\dfrac{W_S}{\rho_S} + F_{air}\right)} \times 100 = \text{Solids Volumtric Concentration, \%}, \qquad (5.16)$$

where:

W_S = Solids mass flowrate, kg /sec

F_{air} = Air volumetric flowrate, m³/sec

ρ_S = Solids density, kg/m³

The manner in which the solids-gas dispersions are produced in the proceeding experiments is described with reference to figure 5.4. (experimental set-up).

The air flow control module (4) is adjusted in order to provide an air flowrate, F_{air} sufficient to disperse a predetermined quantity of powder stored in the feeding chamber (7). The air flow in the main pipeline (5) is left to stabilise for 1-2 minutes before the powder is fed into the air stream by opening valve (11). The solids mass flow rate, W_S is regulated by using the control valve (10) and the bleed air stream (8) and is calculated by measuring the time required to discharge the specific amount of powder. The time of discharge is measured by using a stop-watch connected with a photo-diode located on the observation window detecting the initiation and termination of the solids flow.

For a series of humidity experiments described in section 6.2.3, the cylindrical (diameter = 0.35m, height = 0.5m) humidifier depicted in figure 5.7 is used. A portion of the air stream leaving the flow control module (4) is split and directed into the cylindrical container, H. which is partially (75%) filled with water. The air, due to the induced agitation is enriched with water droplets, and is drawn back (through valve C) to the main air stream prior to entry into pipeline (5). The extent of humidification is controlled by valves (A) and (B) which determine the volume of the split air directed into the humidifier. The resulting humidity of the air stream is monitored 20 cm upstream of the solids feeding point by inserting an electric hygrometer (Omega, PTH-1X) via a slot (see item (16) in figure 5.4) into the pipeline (5).

The measurement of the capacitance across the cylindrical electrodes of the capacitance transducer is a straight forward operation. The capacitance reading is recorded from the LCR display and is averaged over the time of the experimental run. However, prior to any measurement being taken the LCR meter is switched on and left 15 minutes to warm up, and then the "open circuit" and the "short circuit" correction procedures have to be completed. These procedures are essential in order to

minimise the effect of the inherent stray capacitance of the LCR test cables on the measurement accuracy.
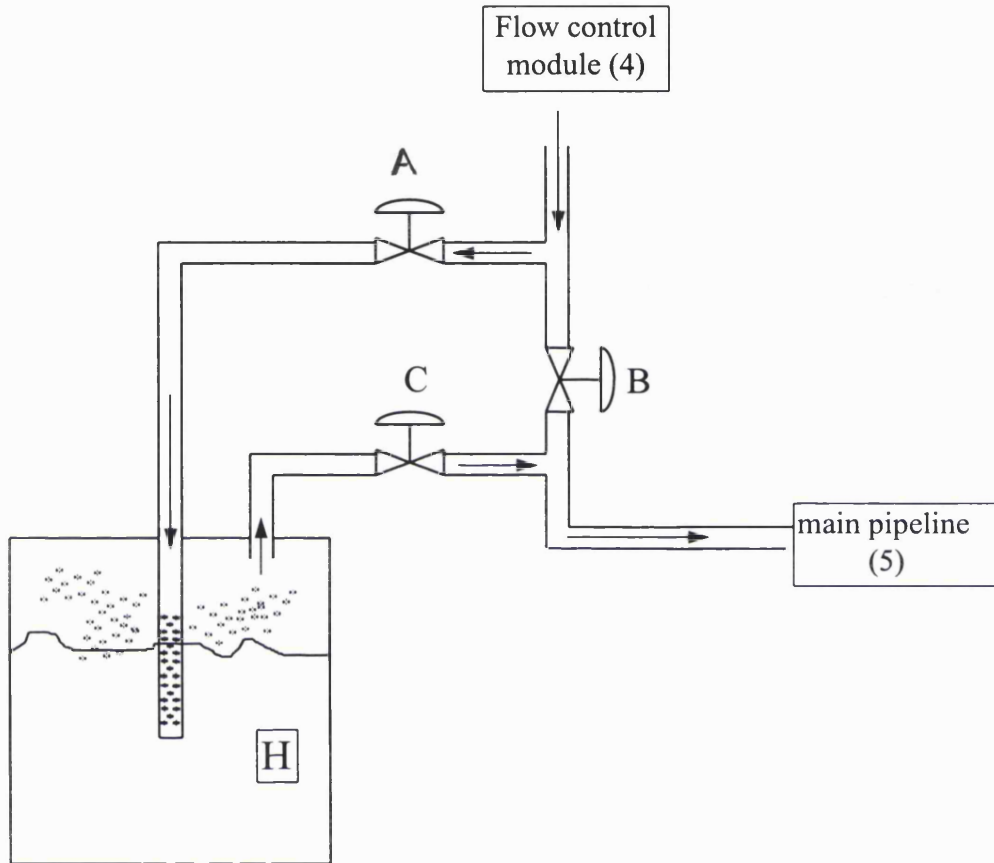

Figure 5.7. Cylindrical humidifier.

CHAPTER 6

RESULTS AND DISCUSSION

6.1. Introduction

This chapter presents and discusses the results of a series of experiments aimed at establishing the feasibility and reliability of the coaxial capacitance transducer in measuring solids concentrations in gas streams. Also, using appropriate experimentation, it sets out to identify the effects of a number of design and operating parameters on the transducer's performance.

The design parameters investigated include the transducer's overall dimensions. The operating conditions on the other hand include air humidity, air stream temperature, air velocity and solids flow pattern as well as the frequency of the applied electrical signal.

The feasibility and reliability of the transducer is evaluated by constructing 'capacitance calibration' curves for dispersions in air of various powders with different dielectric (i.e. insulators and conductors) and physical properties (i.e. density, average particle size and shape). In these curves, the 'effective dielectric constant' of the dispersion, ε_{eff} is plotted against the solids volume fraction, f_S in the air stream. The effective dielectric constant is defined as the ratio of the solids-gas dispersions capacitance, Cp_{Sol} to the capacitance of pure air, Cp_{air} (see section 4.2). Various concentrations of solids in the air streams are produced using the experimental set-up described in chapter 5.

6.2. Solids Concentration Calibration Curves

6.2.1 Insulating Material

Figure 6.1 shows a typical calibration curve for median average, $d_p = 350$ µm soda glass ballotini spherical particles (Jencons Scientific Ltd.) of density, $\rho = 2500$ kg/m^3 and dielectric constant, $\varepsilon_s = 7.2$. The data, showing the variation of the effective dielectric constant of the dispersion, ε_{eff} versus solids volume fraction, f_s, have been obtained by using the coaxial capacitance transducer described in section 4.6.2. For comparison purposes, in figure 6.2 the corresponding calibration curves for quartz ($\rho = 2200$ kg/m^3, $d_p = 310$ µm, $\varepsilon_s = 4.1$) and bronze powder ($\rho = 8800$ kg/m^3, $d_p = 125$ µm, and $\varepsilon_s = \infty$, Makin Metal Powders Ltd.) are plotted along with that of glass ballotini (i.e. figure 2.1). Unless otherwise stated, all data presented above and in the proceeding sections are obtained using an a.c. voltage of 1 Volt and frequency 100 kHz, at 18 °C ambient temperature, using air with a relative humidity of 15% as the dispersion medium.

The following is a summary of some of the main features of the data presented in figures 6.1 and 6.2:

i) The dispersion effective dielectric constant, ε_{eff} is linearly proportional to the concentration of solids drawn through the sensing volume of the cylindrical capacitor. Linear regression of the obtained data indicate a relatively good approximation to straight line with a corresponding correlation coefficients, R^2 varying in the range 0.95-0.998. The linear variation indicates that that the dielectric constant of the solids-air dispersion increases as the fraction of the total volume occupied by the solids (whose relative dielectric constant is always greater than that of air ($\varepsilon_{air} = 1$)) increases. The above is consistent with the theory presented in sections 4.31-4.3.2. as well as the work of other researchers (see for example Beck et al., 1969a; Fasching et al., 1991; Lounge, 1996; Reinecke et al., 1997) who used different electrode designs in several industrial applications (see section 4.4).

ii) The fitting equation for, ε_{eff} as a function of solids volume fraction, f_S is given by:

$$\varepsilon_{eff} = K\,f_S + \alpha'\qquad\qquad(6.1)$$

Where α' is the intercept. The constant, K here termed as the dielectric proportionality constant, represents the rate of increase in ε_{eff} with respect to the solids volumetric concentration, f_S in the dispersion. Figure 6.2. indicates that K increases with the solids dielectric constant, ε_s. The highest value of K corresponds to that for bronze which as a conductor has a dielectric constant theoretically equal to infinity (i.e. very large in practice) (Louge, 1990; Taylor et al., 1994). Similarly, K for glass ballotini is larger than that for quartz since $\varepsilon_{glass} > \varepsilon_{quartz}$. The above trend is in accordance to the theory presented in section 4.3.1 and 4.3.2. where the dielectric constant for a solids-gas dispersion, ε_{dis} depends on dielectric constant, ε_s of the dispersed particles (also see equation 4.24).

iii) The value of the intercept, α' for all the data presented is unity. This is to be expected since for pure air (i.e. $f_S = 0$), ε_{eff} is equal to unity (=dielectric constant of air). Therefore, equation 6.1 can be rewritten as:

$$\varepsilon_{eff} = K\,f_S + 1\qquad\qquad(6.2)$$

The experimentally derived equation 6.2 has the same form as the theoretically defined equation of relative dielectric constant, ε_r for dielectric materials given in Chapter 4 (Section 4.3.2.):

$$\varepsilon_r = \chi + 1\qquad\qquad(6.3)$$

where, χ is a characteristic property of the material called electric susceptibility (Feynman, 1964). Similarly, equation 6.2 can be written as:

$$\varepsilon_{eff} = \chi_{mix} + 1\qquad\qquad(6.4)$$

where $\chi_{mix} = K\,f_S$ can be taken as the electric susceptibility of the dispersion.

A series of experiments were carried out in order to investigate the performance of the transducer in the case of two powders with different dielectric constants homogeneously dispersed in a gas stream. The powders used were quartz (d_p = 310 μm, ρ = 2200 kg/m^3) and glass ballotini (d_p = 350 μm, ρ = 2500 kg/m^3). These were especially selected due to their similar densities and size in order to minimise segregation during their dispersion in air so as to achieve uniform dispersion within the transducer's sensing volume.

Figure 6.3. shows the variation of the effective dielectric constant of the solids/gas dispersions with solids volume fraction for different volumetric ratios of quartz/glass mixture. As before, ε_{eff} increases in a linear manner with the solids volume fraction, f_s. Furthermore, the dielectric proportionality constant, $K_{glass/quartz}$ increases with an increase in percentage volume of the component with higher dielectric constant, in this case glass. Figure 6.4 shows the corresponding variation of $K_{glass/quartz}$ against the volumetric fraction of glass, ϕ in the dispersed phase. The data have been extracted from those in figure 6.3 at a solids volume fraction, f_s of 0.001 . As it may be observed, $K_{glass/quartz}$ increases in a linear manner with an increase in the glass volume fraction in the solids phase. In general, for the mixture:

$$K_{glass/quartz} = K_{quartz}(1-\phi) + K_{glass}\ \phi \qquad (6.5)$$

where K_{glass} and K_{quartz} are the dielectric proportionality constants for pure glass and pure quartz respectively.

In practice, in the case of two powders with different dielectric constants simultaneously dispersed in a gas stream, the capacitance transducer may be used to report the total solids concentration by measuring the dispersion effective dielectric constant, reference to the predetermined calibration curve for the constituent powders (e.g. figure 6.2), knowledge of their volume fraction ϕ, and solving equation 6.5.
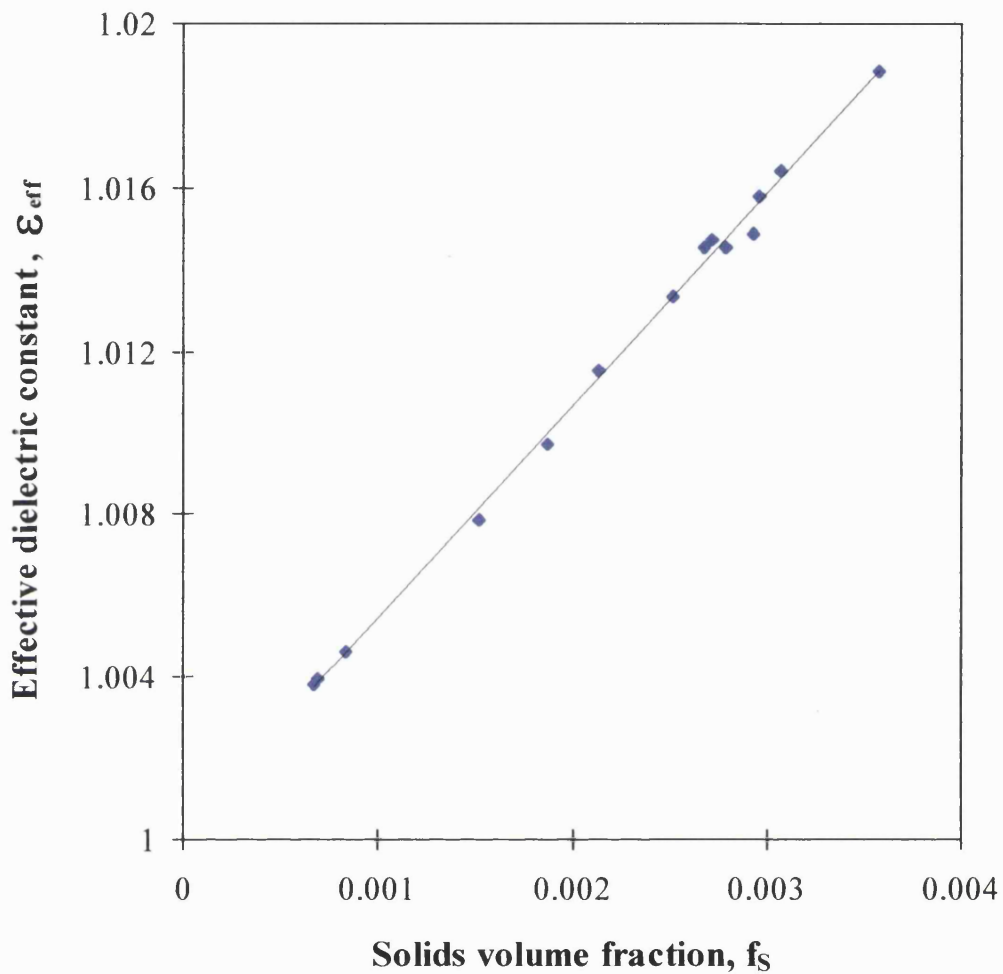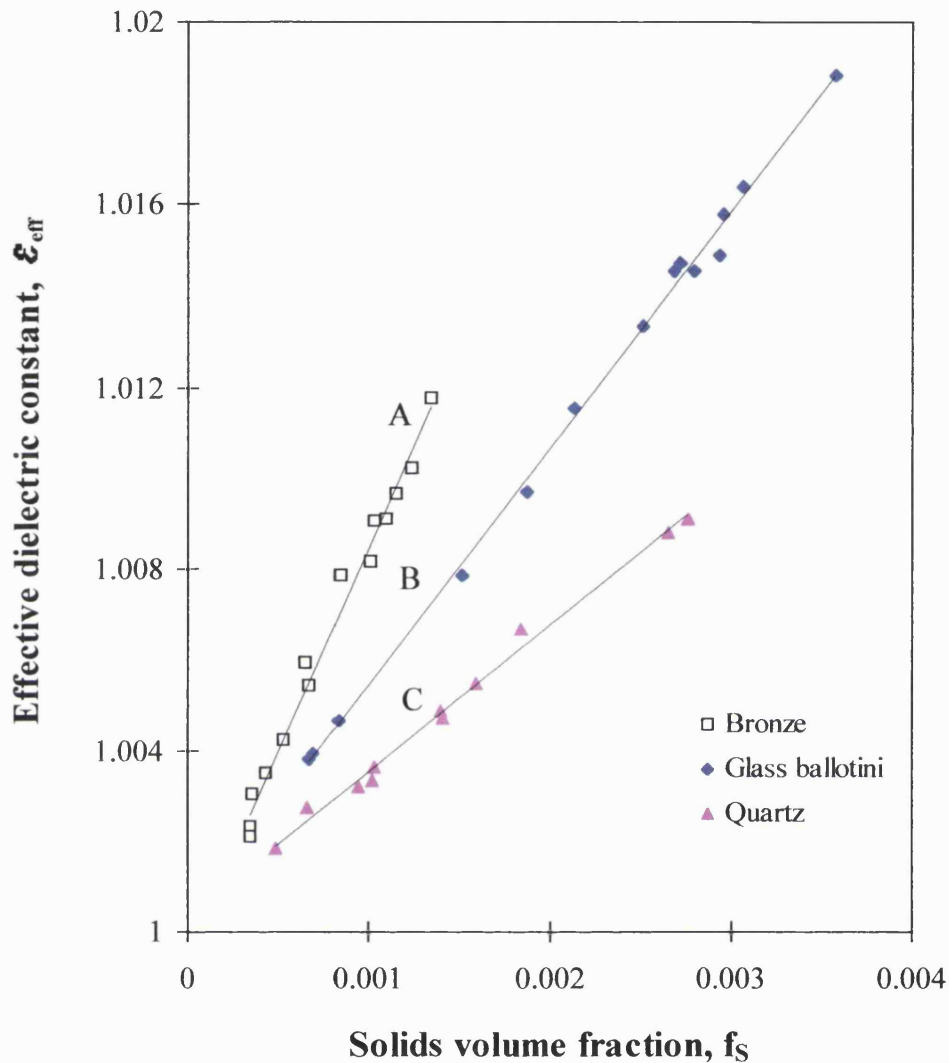
Figure 6.1. Capacitance calibration curve for 350 μm glass ballotini particles (ρ = 2500 kg/m^3) dispersed in air.

Relative humidity: 15%; Ambient temperature: 18 $^{\circ}$C; Transducer T_{1B}; Voltage: 1 Volt; Frequency: 100 kHz .

Fitting equation	Correlation Coefficient , R^2
y = 5.20x + 1.0002	0.997

Figure 6.2. Capacitance calibration curves for various dispersions of solids in air. Curve A, bronze particles (d_p = 125 μm , ρ = 8800 kg/m^3); Curve B, glass ballotini particles (d_p = 350 μm ,ρ = 2500 kg/m^3); Curve C, quartz particles, (d_p = 310 μm, ρ = 2200 kg/m^3).

Relative humidity: 15%; Ambient temperature: 18 °C; Transducer T_{1B}; Voltage: 1 Volt; Frequency: 100 kHz .

	Fitting equation	Correlation Coefficient , R^2
Curve A	y = 8.97x + 0.9995	0.986
Curve B	y = 5.20x + 1.0002	0.997
Curve C	y = 3.01x + 1.0003	0.993
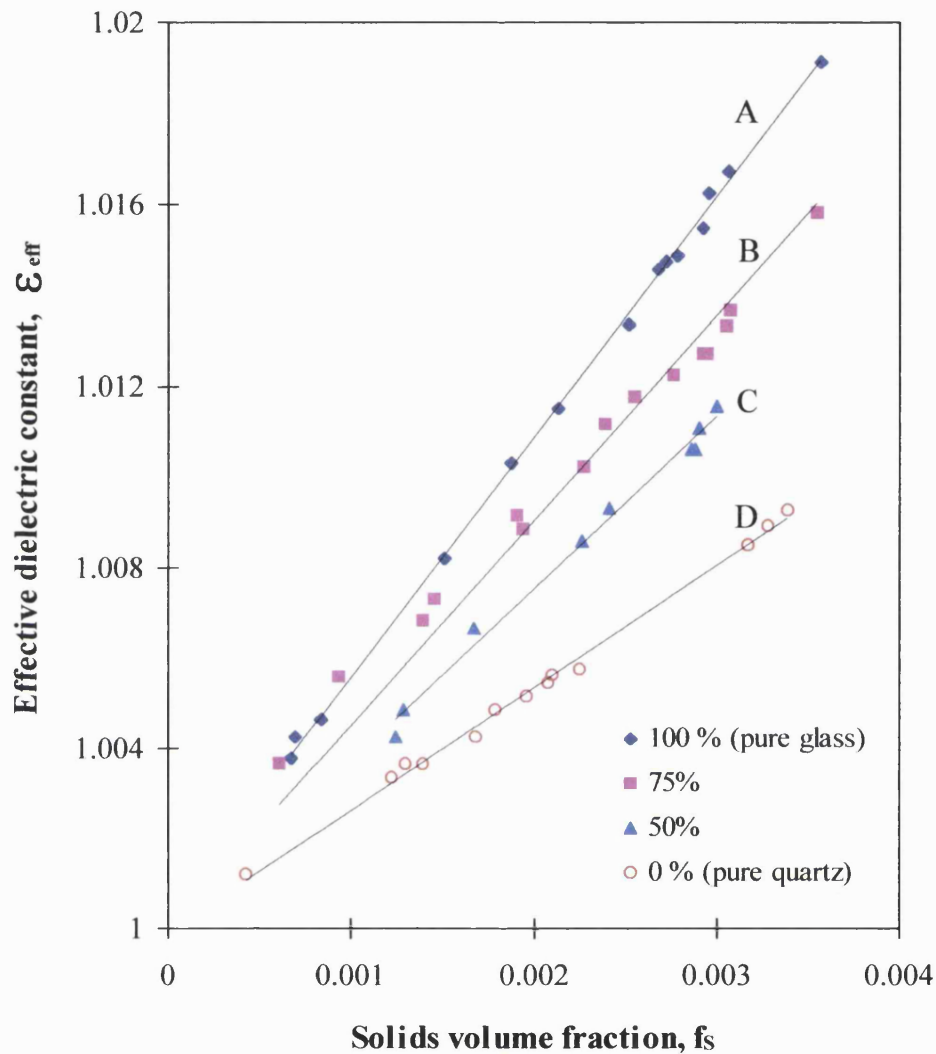
Figure 6.3. Calibration curves for different volumetric ratios of quartz/glass particles dispersed in air. Curve A, 100 % glass ballotini particles (d_p = 350 μm , ρ = 2500 kg/m^3); Curve B, 75 % glass ballotini particles (d_p = 350 μm , ρ = 2500 kg/m^3); Curve C, 50 % glass ballotini particles (d_p = 350 μm , ρ = 2500 kg/m^3); Curve D, 100 % quartz particles (d_p = 310 μm , ρ = 2200 kg/m^3).

Relative humidity: 15%; Ambient temperature: 18 °C; Transducer T_{1B}; Voltage: 1 Volt; Frequency: 100 kHz .

	Fitting equation	Correlation Coefficient , R^2
Curve A	y = 5.20x + 1.0002	0.986
Curve B	y = 4.51x + 1.0005	0.985
Curve C	y = 3.84x + 0.9999	0.993
Curve D	y = 2.85x + 0.9999	0.996
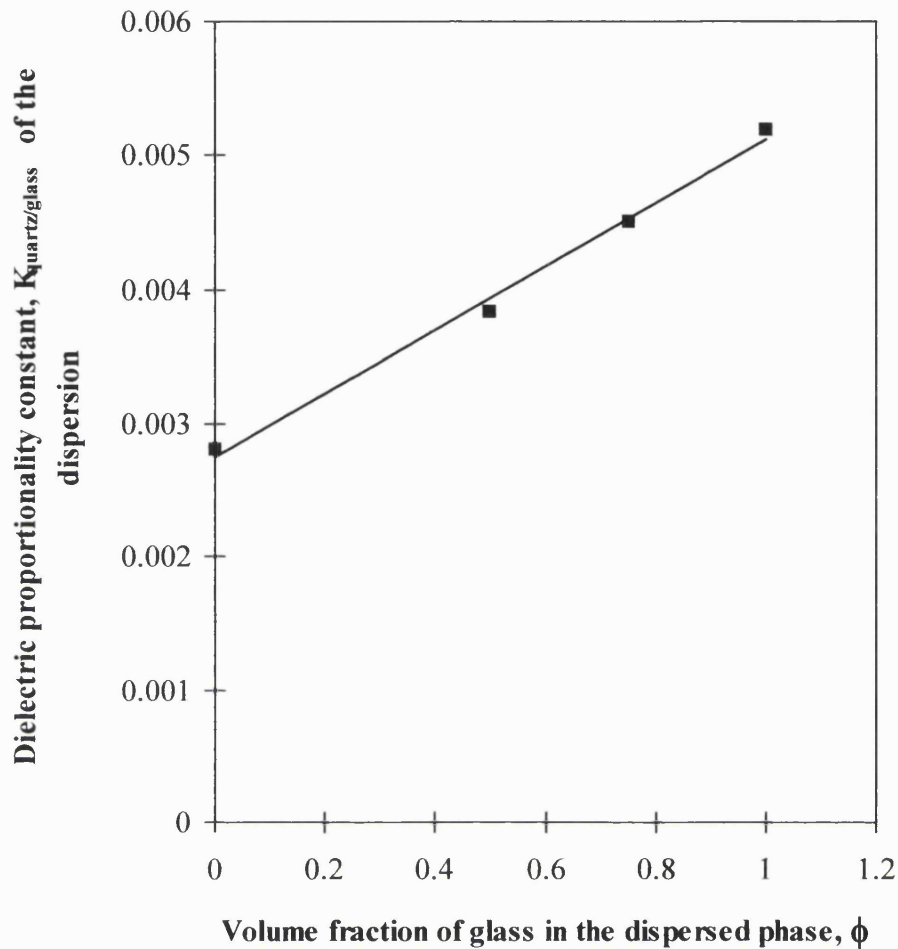
Figure 6.4. Variation of $K_{glass/quartz}$ with glass ballotini volume fraction in the dispersed phase. Total solids volume fraction in the dispersion, $f_S = 0.001$.

Relative humidity: 15%; Ambient temperature: 18 ^{o}C; Transducer T_{1B}; Voltage: 1 Volt; Frequency: 100 kHz .

Fitting equation	Correlation Coefficient , R^2
y = 0.0024x+ 0.0027	0.993

6.2.2. Conducting Materials

Figure 6.5 shows the variation of ε_{eff} with solids volume concentration for various metal powders dispersed in air. A list of these powders along with their pertinent properties are given in table 6.1.

These experiments were carried out in order to investigate the possibility of the capacitance transducer's short-circuiting when conducting particles are dispersed between its electrodes. This is important to establish since the ultimate application of the capacitance transducer is for monitoring diesel particulates. These mainly consist of (approximately 85% wt/wt) carbon black (see section 2.4.2), which is a conductive material. The dielectric calibration curves for dispersions of various metal powders in air, illustrated in figure 6.5, show that dispersed conductive particles can be also monitored using the present technique. Furthermore, the effective dielectric constant for all the tested dispersions, obeys the characteristic equation 6.2, derived for dispersions of insulating powders. However, in this case a single calibration line serves for all the powders tested. The fitting equation is given by

$$\varepsilon_{eff} = 8.54 \ f_S + 1 \qquad (6.6)$$

The above results indicate that perfectly conductive particles (e.g. metallic) when dispersed in an isolating host behave as inclusions of dielectrics in the host medium and therefore the effective conductivity of the dispersion can be ignored (Tinga et al., 1973). This is because, each particle behaves like an individual dipole since it develops an equally charged, positive and a negative side due to the movement of the free electron under the influence of the external field (Richards, 1961; Van Vlack, 1989). The fundamental difference between the polarisation in insulators and conductors is that in the first case every volume element of the material is polarised whereas for the latter, the induced dipole moment arises from movement of "true" surface charges (Richards, 1961).

Table 6.1. Properties of conducting powders used for concentration measurement.

Powder	density, ρ (kg/m^3)	average size, d_p (μm)	conductivity, σ_{elec} (1 / Ωm)	Shape	dielectric constant, ε_s
Bronze	8800	125	8.72x10^6	spherical	∞
Copper I	8810	180	5.8x10^7	spherical	∞
Copper II	8810	125	5.8x10^7	spherical	∞
Steel	7510	110	5.03x10^6	irregular	∞

The fact that a single calibration curve suffices for all powders tested regardless of density or conductivity is in accordance with theory presented in section 4.3.1. The latter predicts that for dispersions of conductive spherical particles in air, polarisation and consequently the effective dielectric constant, depends on the solids volume concentration in the dispersion and not on the relative dielectric constant of the dispersed particles (see equation 4.14) (Meredith et al., 1960; Tinga et al., 1973; Turner, 1976; Louge et al., 1990).

Furthermore, the small deviation observed for the data for steel powder may be attributed to its irregular shape (chips) as opposed to the more spherical copper and bronze particles (Tinga et al., 1973; Louge et al., 1990). Figures 6.6-6.9 show electron microscope photographs for the powders tested. However, further investigations are required to elucidate the effect of particles shape on, ε_{eff}. It is noteworthy that experimental (Irons et al., 1983; Louge et al., 1990;) and theoretical (Tinga et al., 1973; Bottcher, 1973) research work suggest that the shape of the dispersed particles affects the value of the internal electric field which in turn affects the particle's polarisation. For example, in ellipsoidal particles, the internal electric field is predicted to be higher than in spherical particles resulting in higher polarisation and consequently higher, ε_{eff} (Bottcher, 1973).
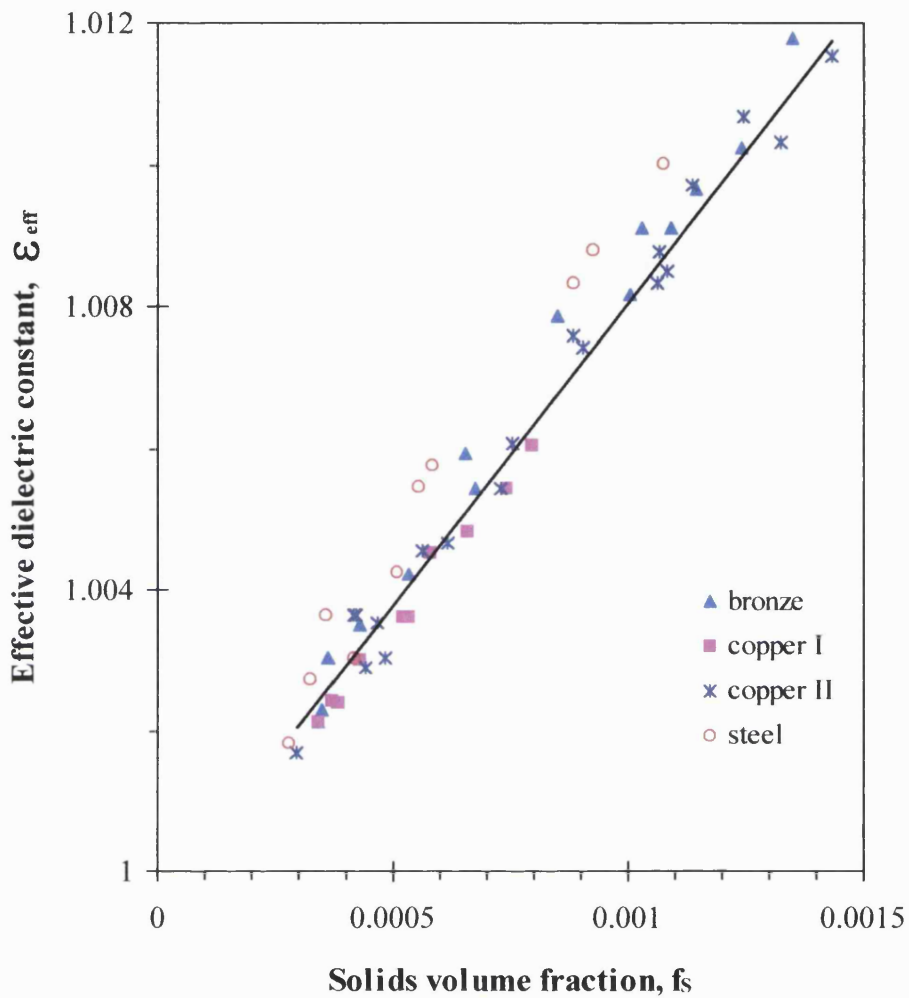
Figure 6.5. Capacitance calibration data for various dispersions of conductive solids in air.

Relative humidity: 15%; Ambient temperature: 17 $^{\circ}$C; Transducer T_{1B}; Voltage: 1 Volt; Frequency: 100 kHz .

Powder	density, ρ (kg/m^3)	average size, d_p (μm)	Shape
Bronze	8800	125	spherical
Copper I	8810	180	spherical
Copper II	8810	125	spherical
Steel	7510	110	irregular

Fitting equation	Correlation Coefficient , R^2
y = 8.54x + 1	0.963

Figure 6.6. Electron microscope photographs of steel particles (ρ = 7510 kg/m^3, d_p = 110 μm).
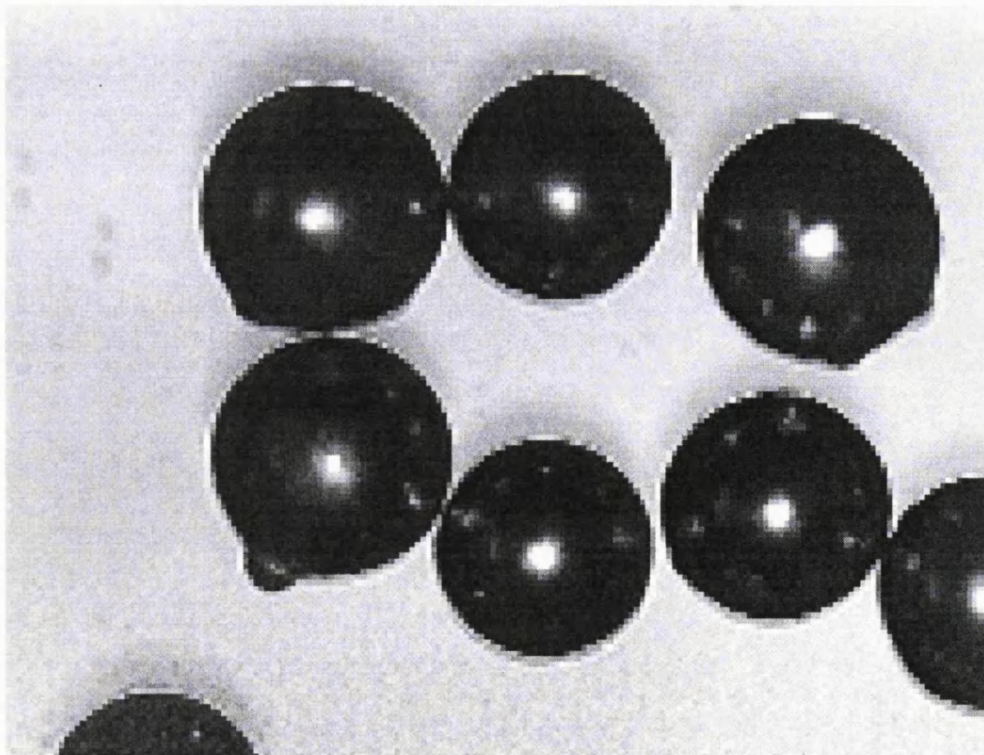
Figure 6.7. Electron microscope photographs of bronze particles (ρ = 8800 kg/m^3, d_p = 125 μm).

159
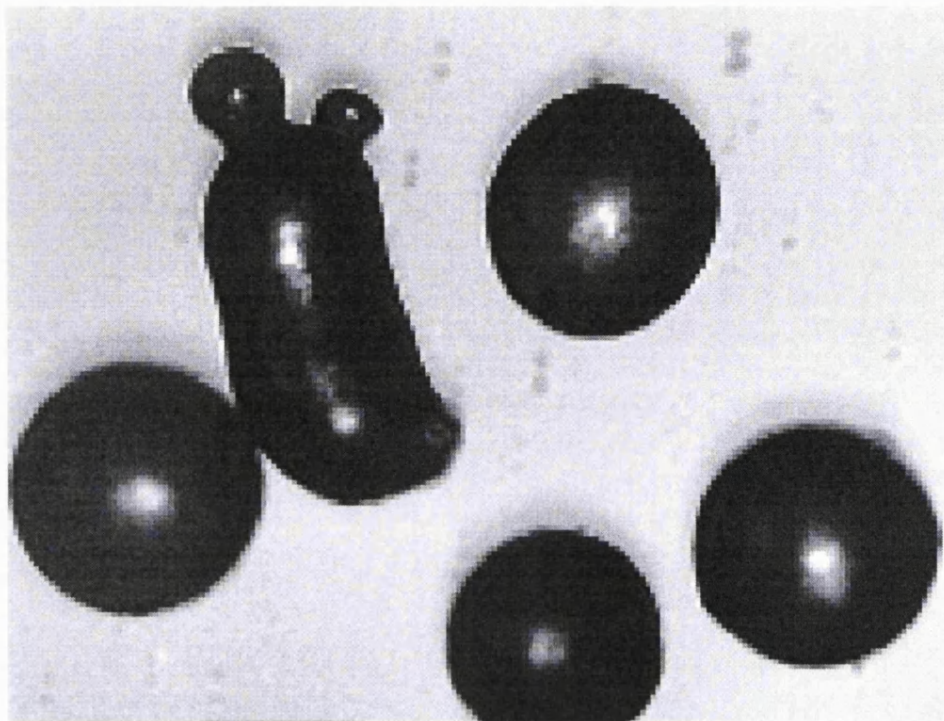
Figure 6.8. Electron microscope photographs of copper particles ($\rho = 8810$ kg/m^3, $d_p = 180$ µm).
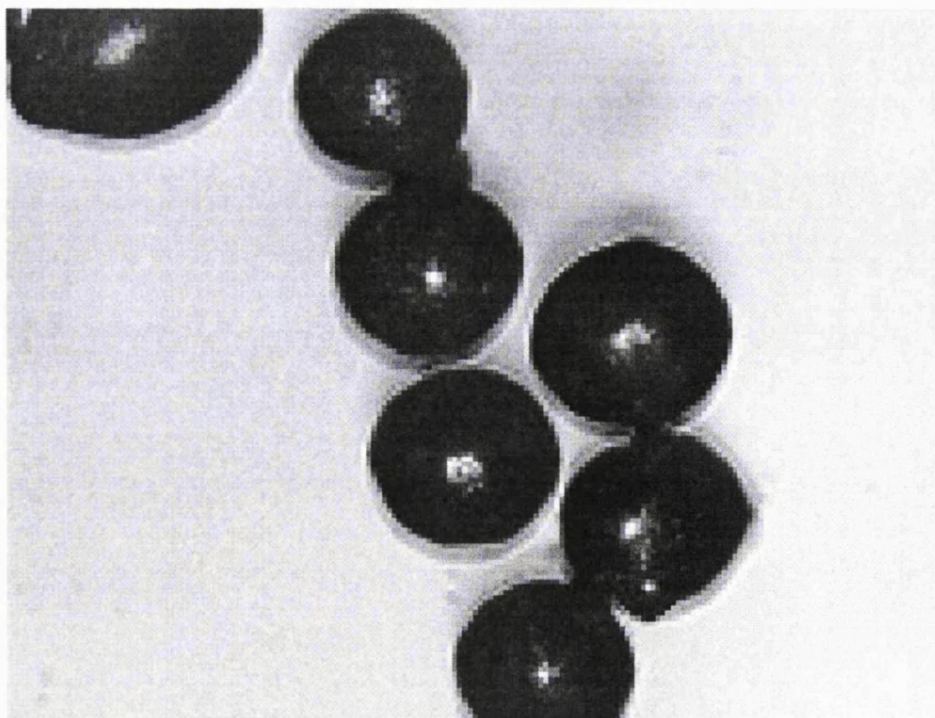
Figure 6.9. Electron microscope photographs of copper particles ($\rho = 8810$ kg/m^3, $d_p = 125$ µm).

However, it is emphasised that the above findings are valid as long as the voltage applied across the dispersion is not large enough to cause an electric discharge between the grains. Also, the average separation distance between the particles must be sufficient so that the effective conductivity of the dispersion can be ignored (Morse et al., 1951; Louge et al., 1990). Failing to comply with the above will result in short circuiting and subsequent discharge of the capacitor.

Finally, it is pointed out that several attempts were made to monitor carbon black particulates since these closely resemble diesel particles. However, due to their brittle nature, extensive attrition during their pneumatic conveying took place. This as well as the accompanying health hazard associated with fine particles made the task of conducting controlled experiments using carbon black impossible.

6.3. Effect of Electrode Dimensions

In Chapter 4 (section 4.6.2) the importance of the electrodes' dimensions on the performance of the coaxial transducer was highlighted. In brief, the electrodes' dimensions are crucial in producing capacitances of sufficient magnitude to be successfully measured by the LCRs as well as providing sufficient sensitivity.

The basic tool used in determining the transducer's dimensions is the "design equation" for a cylindrical capacitor which is recalled here (see section 4.6):

$$C = \frac{2\pi L \varepsilon_0}{\ln(b/a)} \qquad (4.25)$$

The above equation gives the capacitance of a cylindrical condenser when the free space between the two electrodes is occupied by air only. For the purposes of evaluating the effect on performance, two coaxial transducers with different dimensions, T_1 and T_2 were constructed. For each transducer, the inter-electrode separation distance, D_e was varied by using inner electrodes of the same material but with different radius, a. The dimensions of all the configurations used in this study are given in Table 6.2.

Table 6.2. Capacitance transducers dimensions

Transducer	Outer electrode radius, b (cm)	Inner electrode radius, a (cm)	Inter-electrode separation distance, D_e (cm)
T_1	Length, L =12 cm		
A	1.62	1.06	0.56
B	1.62	0.9	0.72
C	1.62	0.75	0.87
T_2	Length, L = 17.5 cm		
A	2.375	1.65	0.725
B	2.375	1.4	0.975
C	2.375	1.15	1.225

The theoretical value of Cp_{air} when pure air is drawn through the transducer can be calculated by inserting the above dimensions in equation 4.25. Therefore, in the case of transducer T_{1B}, for example, Cp_{air} will be given:

$$Cp_{air} = \frac{2\pi L \varepsilon_o}{\ln(b/a)} = \frac{2\pi \cdot 0.12 \cdot 8.85 \cdot 10^{-12}}{\ln(0.0162/0.009)} = 11.35 \cdot 10^{-12} F = 11.35 pF$$

However, the average capacitance Cp_{air}, for T_{1B} measured during the experiments was 17.15 pF which is almost 6 pF larger than the theoretical value. The corresponding theoretical (using the above design equation) and experimentally determined values of Cp_{air} for the rest of the capacitance configurations, presented in table 6.2, are given in table 6.3.

These tabulated results indicate that in all cases the experimentally measured capacitance is almost 6 pF larger than the theoretically calculated value. This extra capacitance is due to parasitic or stray capacitances and it is an expected phenomenon since every single component in the capacitor's 'close' vicinity introduces a stray capacitance (Cimorreli et al., 1967; Taylor et al., 1994).

Table 6.3. Comparison of the theoretical and experimentally determined values of the baseline capacitance, Cp_{air}.

Transducer	Theoretical Cp_{air} (pF)	Experimental Cp_{air} (pF)	$Cp_{air(exp)} - Cp_{air(th)}$ (pF)
T_1			
A	8.65	14.5	5.85
B	11.35	17.15	5.8
C	15.8	21.5	5.7
T_2			
A	13.4	19.2	5.8
B	18.4	24.3	5.9
C	26.8	33.0	6.2

These include the support screws positioned perpendicular to the cylinders (see figure 4.8 and plate 4.1), the screen (even if it is earthed) which contains the capacitance cell to prevent interference from external electric fields, the connecting leads of test fixture, the LCR meter as well as the fringing effect at the edges of the cylindrical electrodes (NPL, 1969; Huang et al., 1988). Although the individual contribution of these components is small, the cumulative result is appreciable especially when the measurement is in the picofarad range. Therefore, since the parasitic capacitances is an inherent phenomenon and cannot be eliminated it is imperative first, to minimise them so that they are smaller than the actual electrode capacitance, and more importantly to keep them constant and reproducible, in order to achieve the accuracy and consistency required (NPL, 1969; Huang et al., 1988). The data in table 6.3 indicate that indeed the stray capacitance is smaller than the actual electrode capacitance with its average value remaining relatively unchanged at around 6 pF.

Figures 6.10 and 6.11 show the effect of the inter-electrode separation distance, D_e on the dielectric calibration data for glass ballotini ($d_p = 350$ μm) for transducer T_1 and T_2 respectively.

From the data, it is clear that the slope of the fitted lines, which is a direct measure of the system's sensitivity, dramatically increases when the separation distance, D_e between the electrodes decreases. Therefore, for the fitting equation:

$$\varepsilon_{eff} = K\, f_S + 1 \qquad (6.7)$$

the corresponding dielectric proportionality constants are:

$$K_A > K_B > K_C$$

where the subscripts A, B and C refer to different inter-electrode separation distances (see table 6.2). This means that a solids-gas dispersion of a specific composition exhibits a higher dielectric constant with decreasing inter-electrode distance. This is due to the fact that for a constant applied voltage, decreasing separation distances result in an increase in the electric field between the transducer's electrodes. The latter increases the total polarisation of the test particles in the dispersion and consequently its dielectric constant. These observations are consistent with the experimental work of other researchers (e.g. Irons et al., 1983) as well as the theory presented in chapter 4, where the derived dielectric constant of the spherical particles dispersed in air was found to be proportional to the external electrical field (see equation 4.24).

The above observations are confirmed from the corresponding data in figures 6.12-6.15 where the results of the same experiments, for two different dispersions of quartz and copper in air using transducers T_1 and T_2, are presented.

Consequently, given the dependence of ε_{eff} on the applied electric filed, it would be expected that for a particular solids volumetric concentration f_S, the magnitude of, (ε_{eff} -1) i.e. the electric susceptibility of the dispersion, χ_{mix} (see section 6.2), divided by the average electric field, E_{avg}, for the three different inter-electrode separation distances should be constant. E_{avg} is calculated by using equation 6.8 given below relating the electric field at any radius, r in the annulus area of the cylindrical capacitor to the applied voltage V (Taylor, 1994).

$$E = \frac{V}{r \ln\left(\frac{b}{a}\right)} \qquad (6.8)$$

The average value of the electric field over the (i.e. between the outer radius of the inner electrode, a to the inner radius of outer electrode, b) will be given by :

$$E_{avg} = \frac{1}{b-a} \int_a^b E(r)dr \qquad (6.9)$$

Combining equations 6.8 and 6.9 :

$$E_{avg} = \frac{V}{b-a} \qquad (6.10)$$

In figures 6.16 and 6.17, the ratio of χ_{mix} to E_{avg} for three different inter-electrode separation distances (A, B and C) are plotted against f_s, for the glass ballotini dispersion using transducers T_1 and T_2. It is clear from the data presented that for both transducers, the corresponding results for the three inter-electrode separation distances, coincide thus verifying the above observation. Furthermore, the corresponding slope of the fitted line for T_1 is 3.43 which is relatively close to that for T_2 which at 3.91. This is to be expected since the dispersed powder in both cases is the same, and strength of the average electric field (see equation 6.10) is independent of the electrode length (electrode length of T_1= 12 cm < electrode length of T_2= 17.5 cm).

The same mathematical manipulations have been repeated for dispersions of quartz and copper in air, for both transducer T_1 and T_2. The corresponding results are presented in figures 6.18-6.21. Again it is worth noting the similarity of the slopes of the data fitting lines for the same powder for the two different transducers T_1 and T_2. From these figures it is clear that for a solids-gas dispersion of a given concentration, the ratio of the dispersion's electronic susceptibility, χ_{mix} to the applied external average field, E_{avg} is constant.
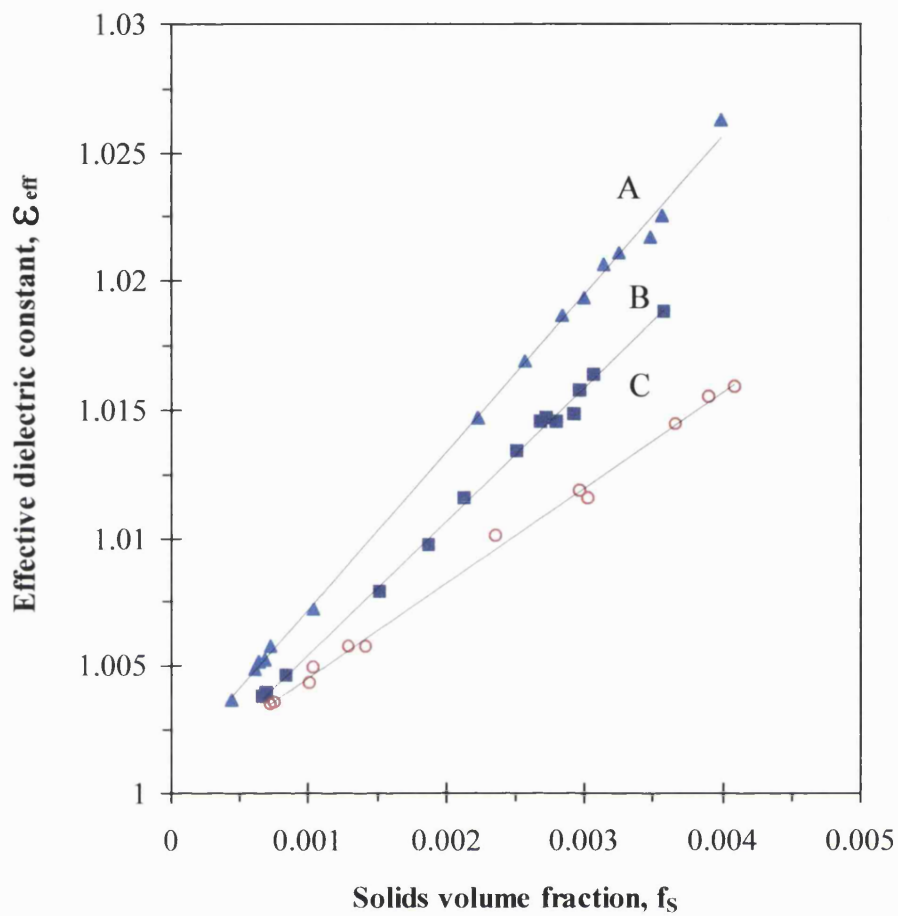
Figure 6.10. Effect of the inter-electrode separation distance, D_e on the capacitance calibration data for glass ballotini particles (d_p = 350 μm , ρ = 2500 kg/m^3) dispersed in air using Transducer T_1 (see table 6.2).

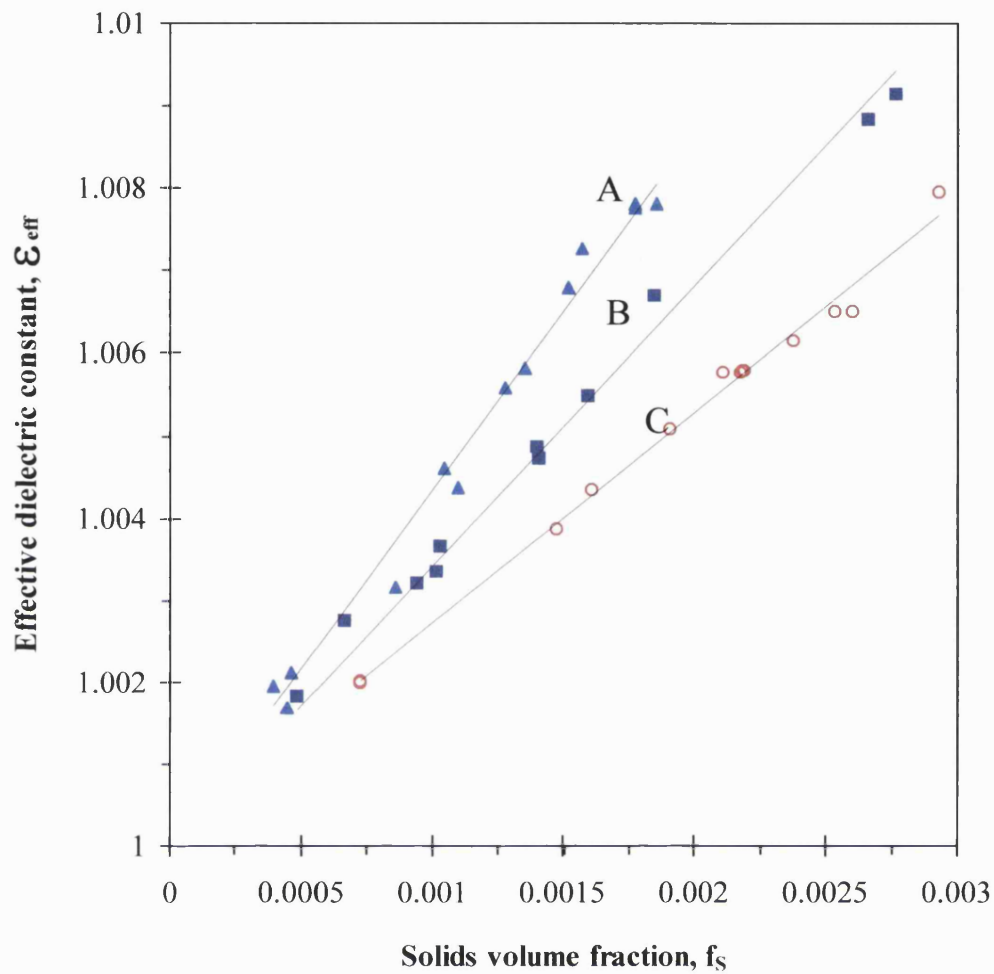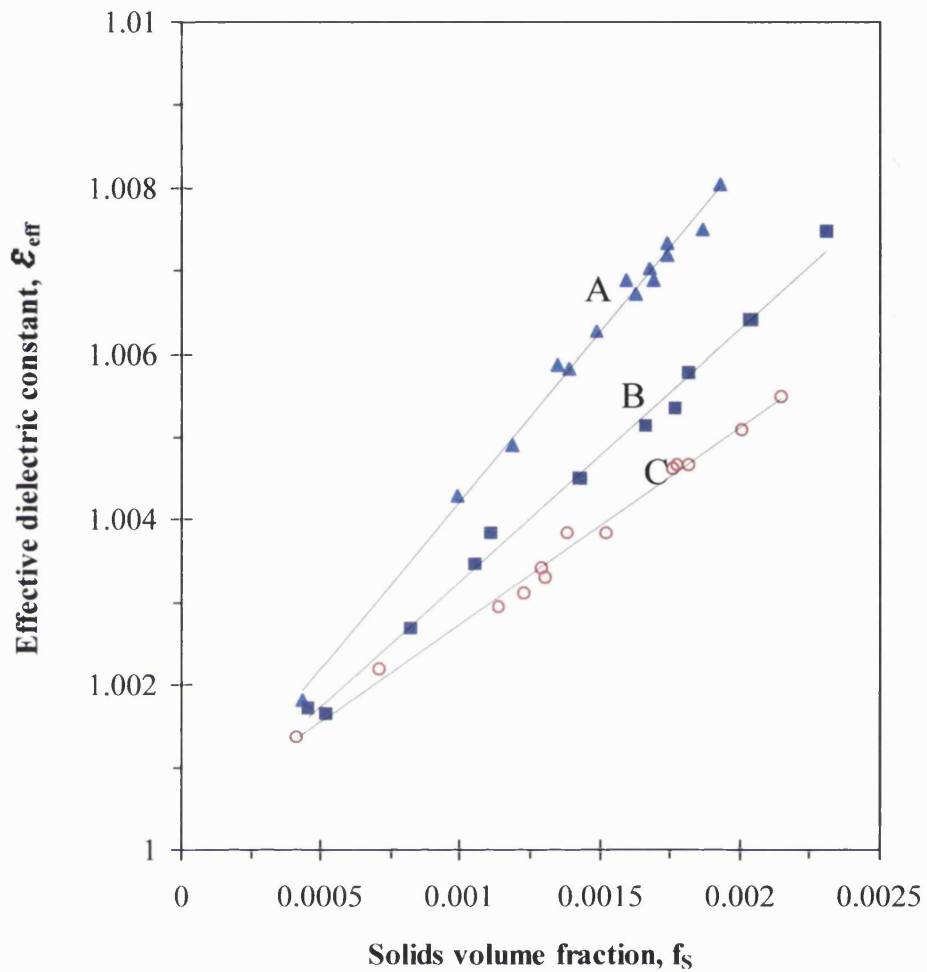Relative humidity: 15%; Ambient temperature: 18 $^\circ$C ; Voltage: 1 Volt ; Frequency: 100 kHz.

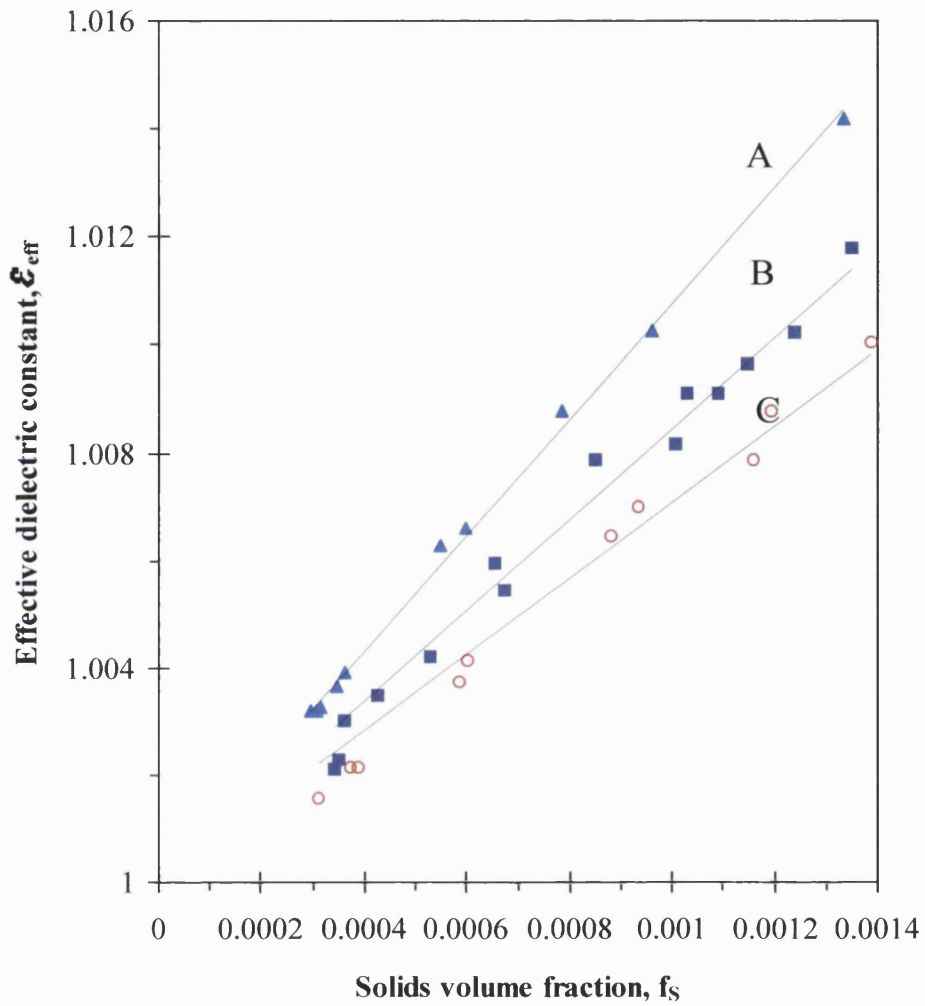| Curve	inter-electrode separation distance, D_e (cm)
A	0.56
B	0.72
C	0.87
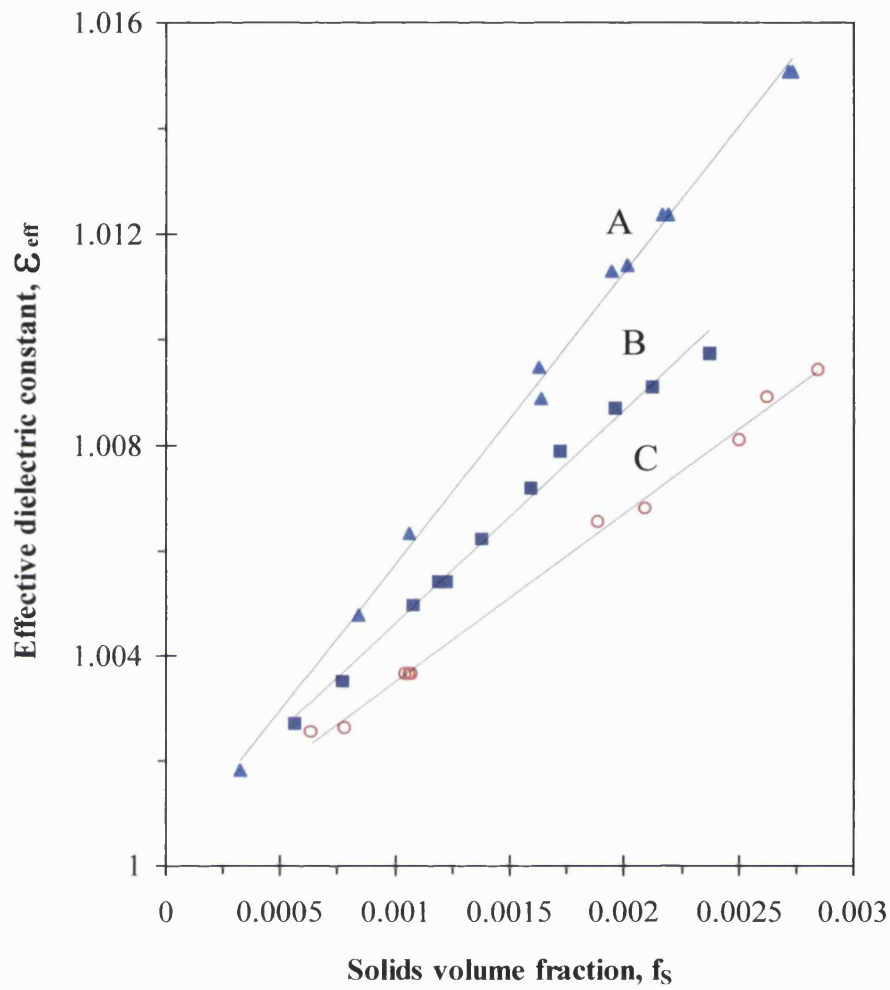
Figure 6.11. Effect of the inter-electrode separation distance, D_e on the capacitance calibration data for glass ballotini particles (d_p = 350 μm , ρ = 2500 kg/m^3) dispersed in air using Transducer T_2 (see table 6.2.)

Relative humidity: 15%; Ambient temperature: 18 °C ; Voltage: 1 Volt ; Frequency: 100 kHz.
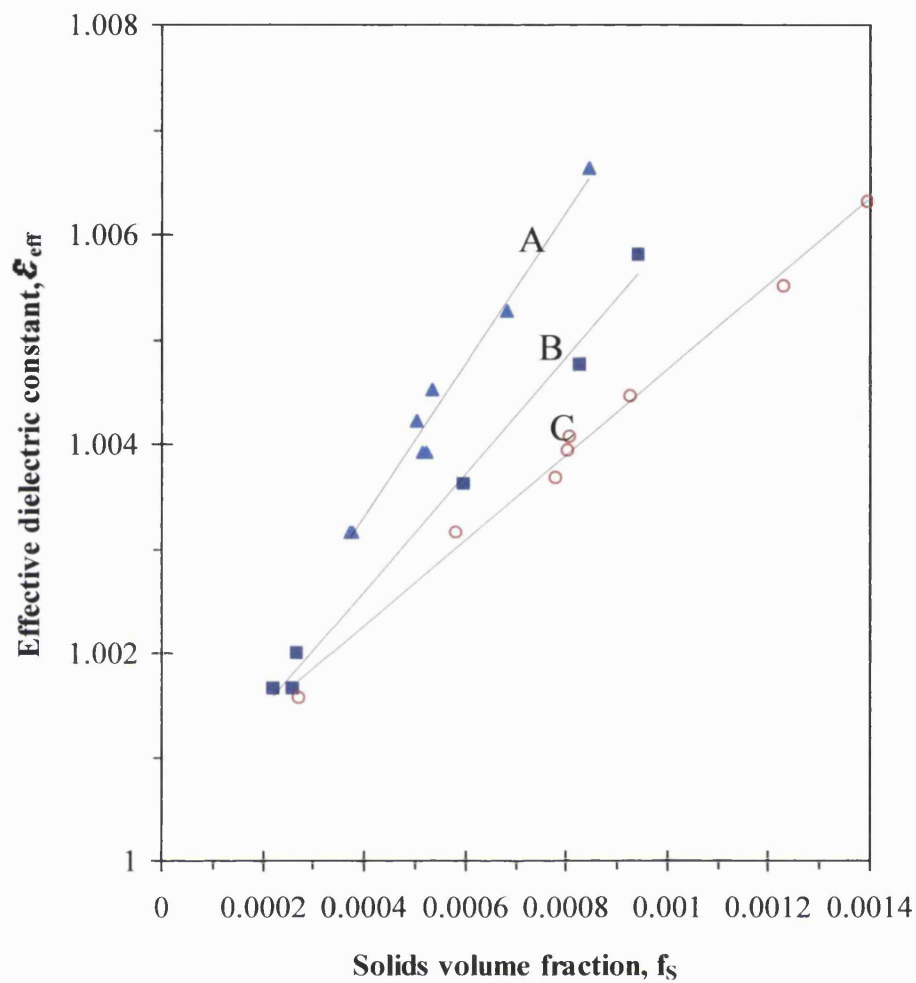
Curve	inter-electrode separation distance, D_e (cm)
A	0.725
B	0.975
C	1.225

Figure 6.12. Effect of the inter-electrode separation distance, D_e on the capacitance calibration data for quartz   particles (d_p = 310 μm , ρ = 2200 kg/m^3) dispersed in air using Transducer T_1 (see table 6.2).

Relative humidity: 15%; Ambient temperature: 18 $^{\circ}$C ; Voltage: 1 Volt ; Frequency: 100 kHz.

Curve	inter-electrode separation distance, D_e (cm)
A	0.56
B	0.72
C	0.87

Figure 6.13. Effect of the inter-electrode separation distance, D_e on the capacitance calibration data for quartz particles (d_p = 310 μm , ρ = 2200 kg/m^3) dispersed in air using Transducer T_2 (see table 6.2.)

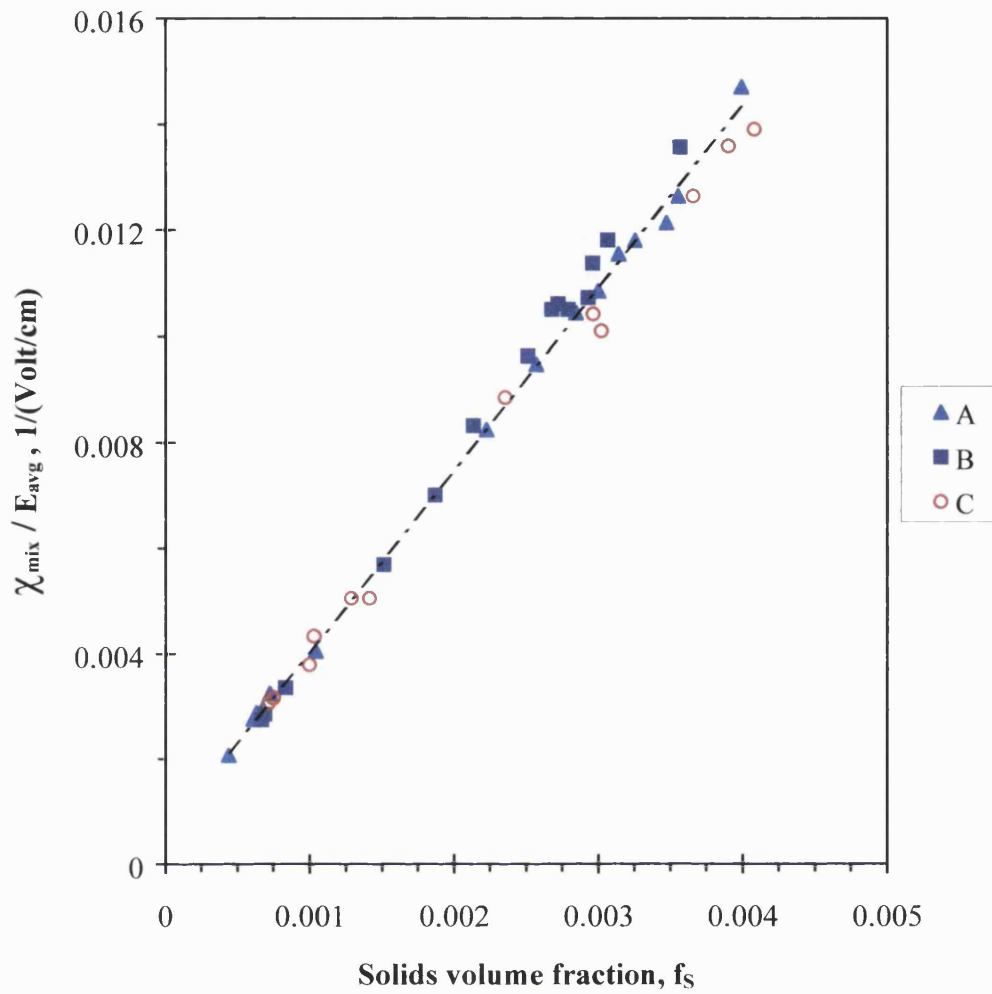Relative humidity: 15%; Ambient temperature: 18 °C ; Voltage: 1 Volt ; Frequency: 100 kHz.

Curve	inter-electrode separation distance, D_e(cm)
A	0.725
B	0.975
C	1.225

Figure 6.14. Effect of the inter-electrode separation distance, D_e on the capacitance calibration data for glass ballotini particles (d_p = 125 μm , ρ = 8800 kg/m^3) dispersed in air using Transducer T_1 (see table 6.2).

Relative humidity: 15%; Ambient temperature: 18 $^\circ$C ; Voltage: 1 Volt ; Frequency: 100 kHz.

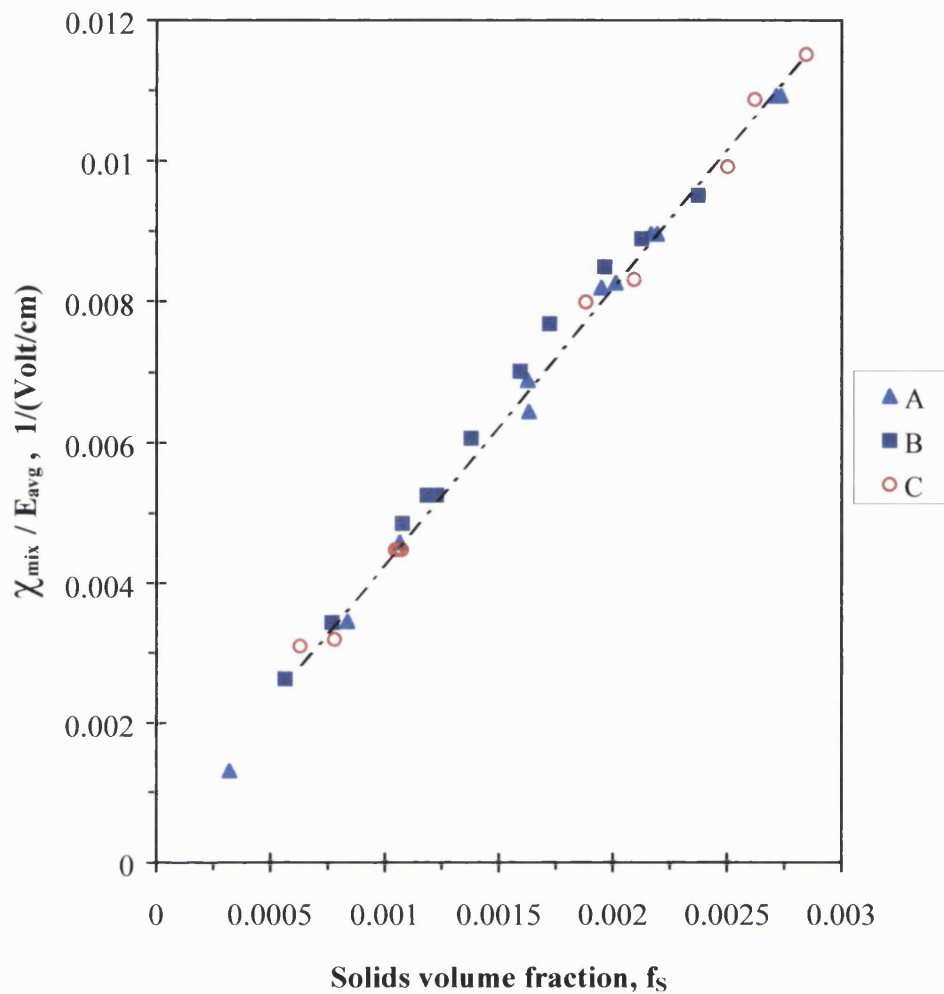| Curve	inter-electrode separation distance, D_e (cm)
A	0.56
B	0.72
C	0.87

Figure 6.15. Effect of the inter-electrode separation distance, D_e on the capacitance calibration data for glass ballotini particles (d_p = 125 μm , ρ = 8800 kg/m^3) dispersed in air using Transducer T_2 (see table 6.2.)

Relative humidity: 15%; Ambient temperature: 18 °C ; Voltage: 1 Volt ; Frequency: 100 kHz.

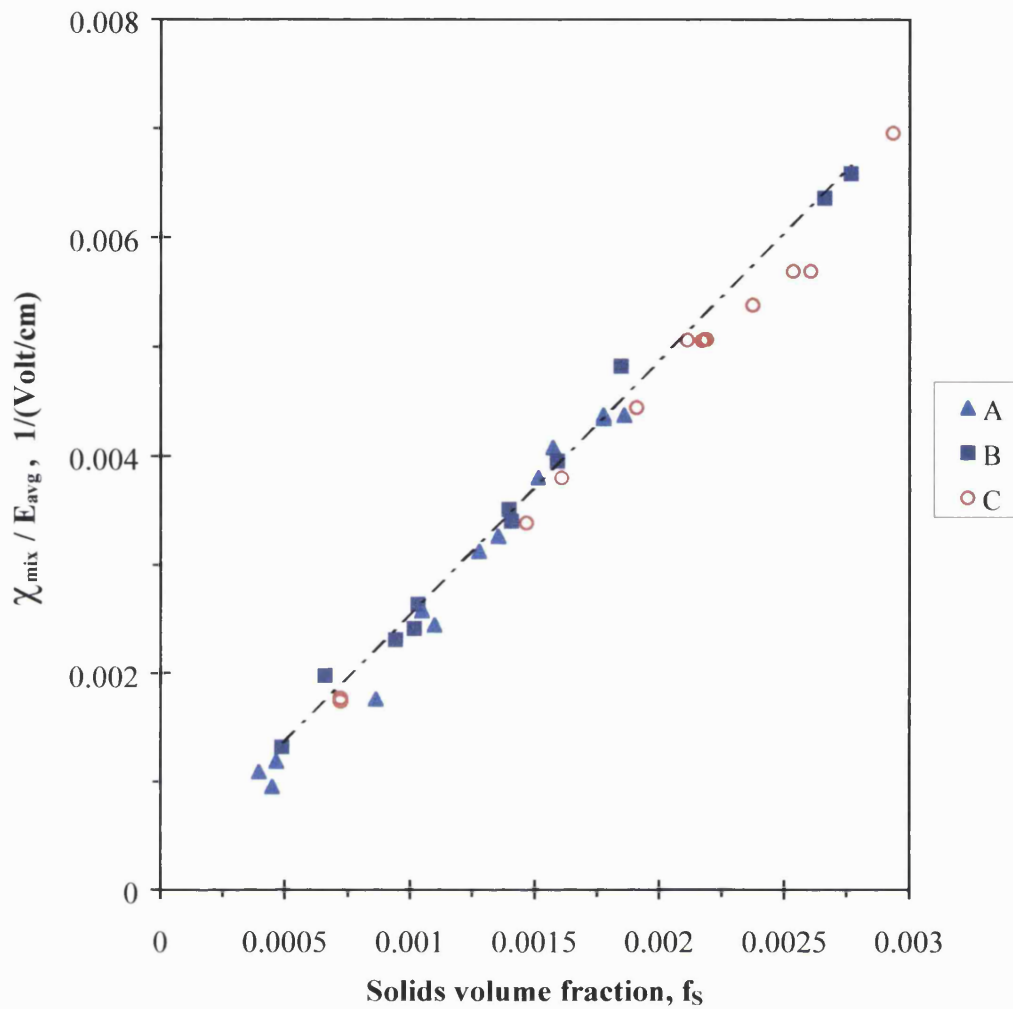| Curve	inter-electrode separation distance, D_e (cm)
A	0.725
B	0.975
C	1.225

Figure 6.16. The variation of the ratio χ_{mix}/E_{avg} with f_S for three different inter-electrode separation distances A, B and C, for glass ballotini particles ($d_p = 350$ μm , $\rho = 2500$ kg/m^3) dispersed in air using Transducer T$_1$ (see table 6.2).

Relative humidity: 15%; Ambient temperature: 18 °C ; Voltage: 1 Volt ; Frequency: 100 kHz.

Curve	inter-electrode separation distance, D_e (cm)
A	0.56
B	0.72
C	0.87

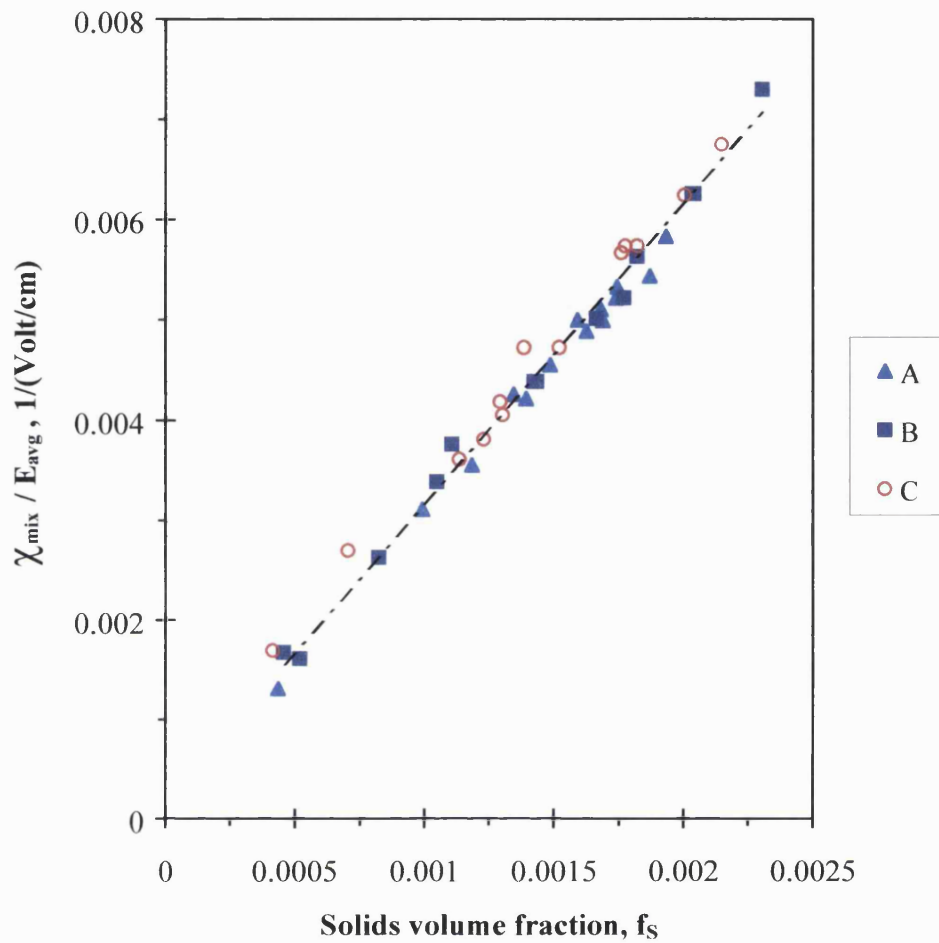| Fitting equation	Correlation Coefficient , R^2
y = 3.43x + 0.0006	0.992

Figure 6.17. The variation of the ratio χ_{mix}/E_{avg} with f_S for three different inter-electrode separation distances A, B and C, for glass ballotini particles ($d_p = 350$ μm , $\rho = 2500$ kg/m^3) dispersed in air using Transducer T_2 (see table 6.2).

Relative humidity: 15%; Ambient temperature: 18 $^\circ$C ; Voltage: 1 Volt ; Frequency: 100 kHz.

	inter-electrode separation distance, D_e(cm)
A	0.725
B	0.975
C	1.225

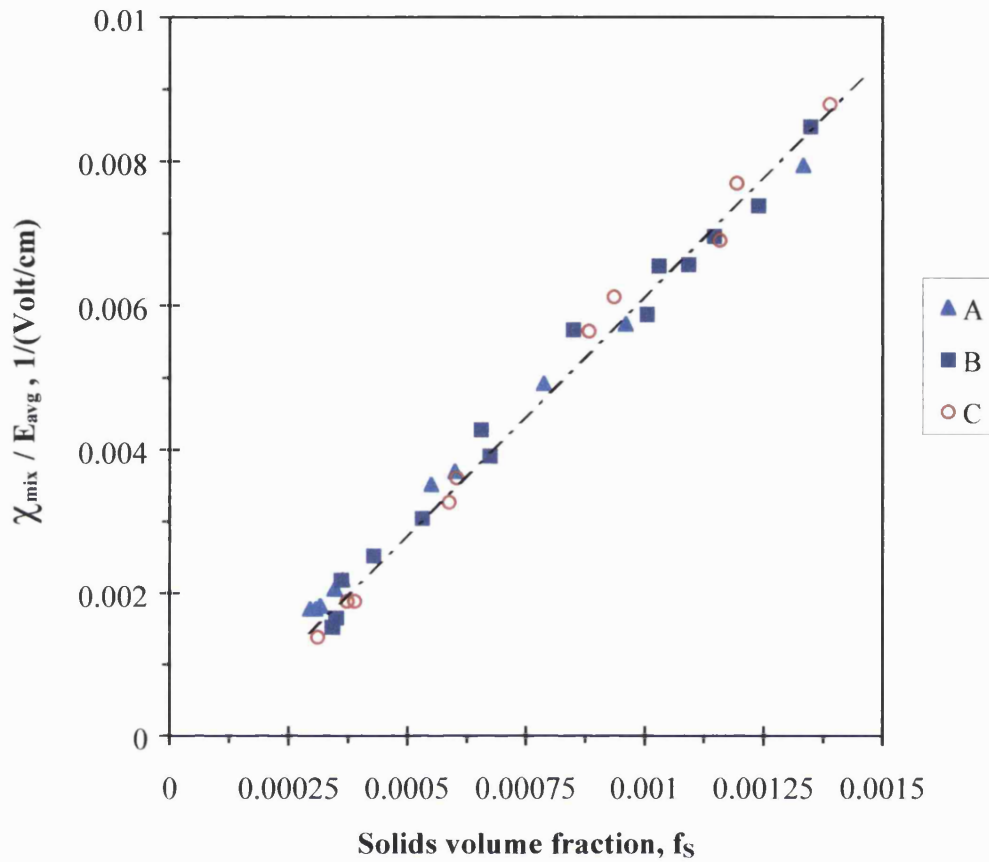| Fitting equation	Correlation Coefficient , R^2
y = 3.91x + 0.0004	0.994

Figure 6.18. The variation of the ratio χ_{mix}/E_{avg} with f_S for three different inter-electrode separation distances A, B and C, for quartz particles ($d_p = 310$ μm , $\rho = 2200$ kg/m^3) dispersed in air, using Transducer T_1 (see table 6.2).

Relative humidity: 15%; Ambient temperature: 18 ^{o}C ; Voltage: 1 Volt ; Frequency: 100 kHz.

	inter-electrode separation distance, D_e(cm)
A	0.56
B	0.72
C	0.87

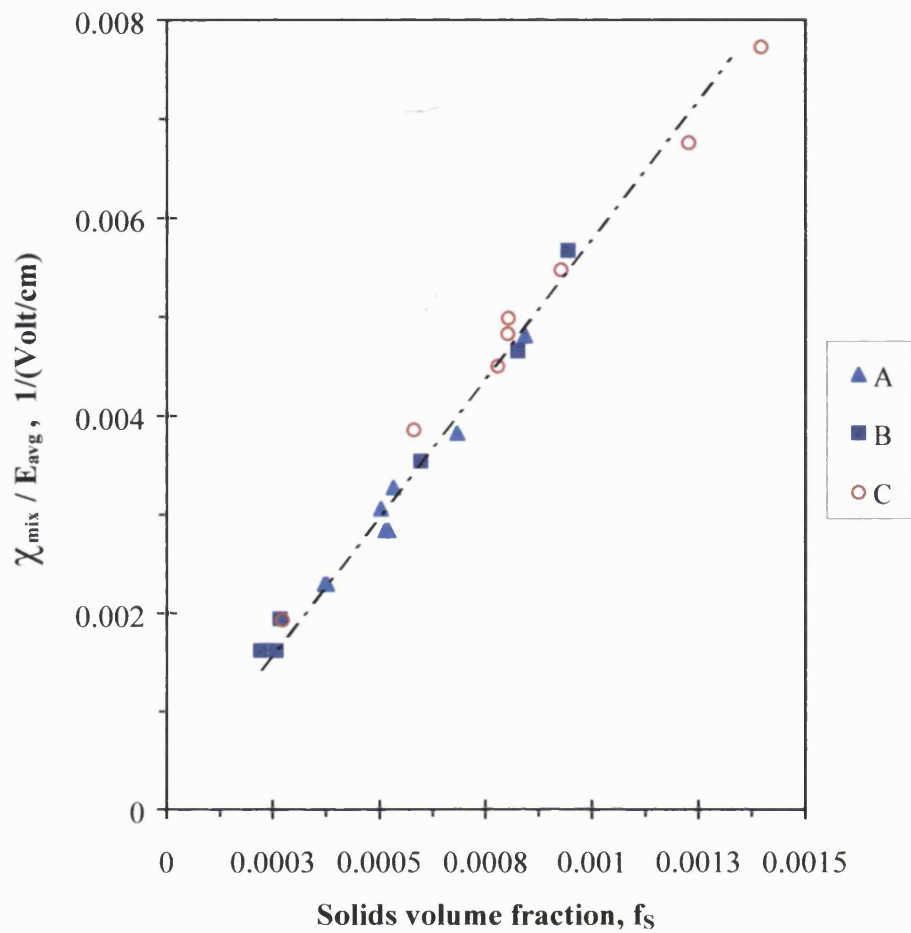| Fitting equation	Correlation Coefficient , R^2
y = 2.3x + 0.0001	0.990

Figure 6.19. The variation of the ratio χ_{mix}/E_{avg} with f_S for three different inter-electrode separation distances A, B and C, for quartz particles ($d_p = 310\ \mu m$, $\rho = 2200\ kg/m^3$) dispersed in air, using Transducer T_2 (see table 6.2).

Relative humidity: 15%; Ambient temperature: 18 °C ; Voltage: 1 Volt ; Frequency: 100 kHz.

	inter-electrode separation distance, D_e(cm)
A	0.725
B	0.975
C	1.225

Fitting equation	Correlation Coefficient , R^2
y = 2.90x + 0.0002	0.989

Figure 6.20. The variation of the ratio χ_{mix}/E_{avg} with f_S for three different inter-electrode separation distances A, B and C, for bronze particles (d_p = 125 μm , ρ = 8800 kg/m^3) dispersed in air using Transducer T_1 (see table 6.2).

Relative humidity: 15%; Ambient temperature: 18 ^{o}C; Voltage: 1 Volt ; Frequency: 100 kHz.

	inter-electrode separation distance, D_e (cm)
A	0.56
B	0.72
C	0.87

Fitting equation	Correlation Coefficient , R^2
y = 6.03x + 0.0002	0.989

Figure 6.21. The variation of the ratio χ_{mix}/E_{avg} with f_S for three different inter-electrode separation distances A, B and C, for bronze particles (d_p = 125 μm , ρ = 8800 kg/m^3) dispersed in air using Transducer T_2 (see table 6.2).

Relative humidity: 15%; Ambient temperature: 18 ^{o}C; Voltage: 1 Volt ; Frequency: 100 kHz.

	inter-electrode separation distance, D_e (cm)
A	0.725
B	0.975
C	1.225

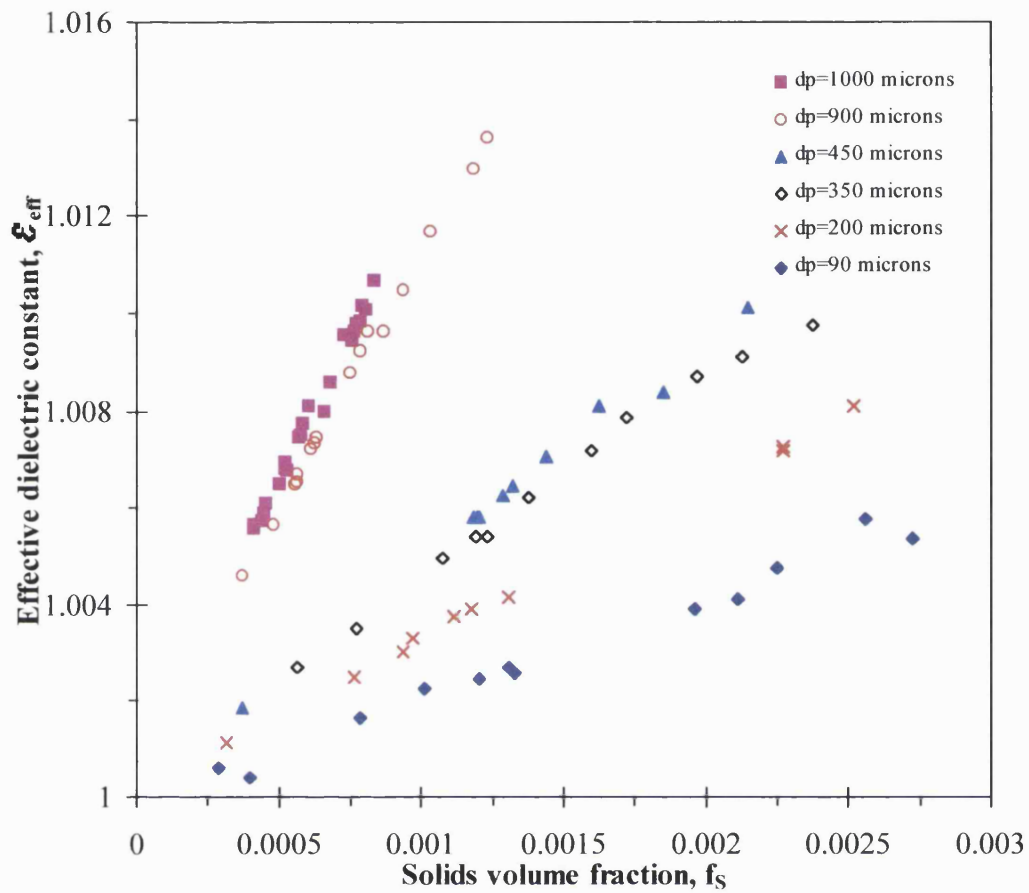| Fitting equation	Correlation Coefficient , R^2
y = 5.95x + 0.0001	0.989

6.4. Effect of Particle Size

Figures 6.22 and 6.23 show the effect of particle size on the effective dielectric constant of glass ballotini dispersions in air, using transducers T_{1B} and T_{2B} respectively (see table 6.2). From the data, it is clear that ε_{eff} decreases with decrease in the particle diameter. This phenomenon is attributed to a decrease in electronic polarisation for smaller particles. It is a consequence of a reduction in the internal electric field, E_{int} inside each particle with decreasing particle size which as described in Chapter 4, is responsible for the relative displacement of positive and negative charges within the particle i.e. electronic polarisation (see section 4.3.1). However, according to Lorentz's equation (equation 4.3, section 4.3.1), E_{int} for a specific material is proportional only to the external electric field, E_0 which in the present experiments, remains constant since the separation distance, D_e between the electrodes as well as the applied voltage remains unchanged. Therefore, it must be concluded that the polarising electric field, E_{int} is smaller inside the smaller particles even though the external electric field remains unchanged.

This can be explained considering the fact that the particles prior to entering the capacitor's sensing volume have been transported through a metal pipeline and as a result acquire electrostatic charge due to contact and frictional charging. The distribution of charge on an insulator is a local phenomenon since the charge on its surface cannot move freely (Jonassen, 1998). As a result the situation, depicted in figure 6.24 arises where a portion of the field lines of the external field are terminated on the surface of the dielectric particle rather going through the dielectric and contributing to the electronic polarisation. Consequently the electronic polarisation is decreased which results in a reduction in the dielectric constant of the spherical particle.
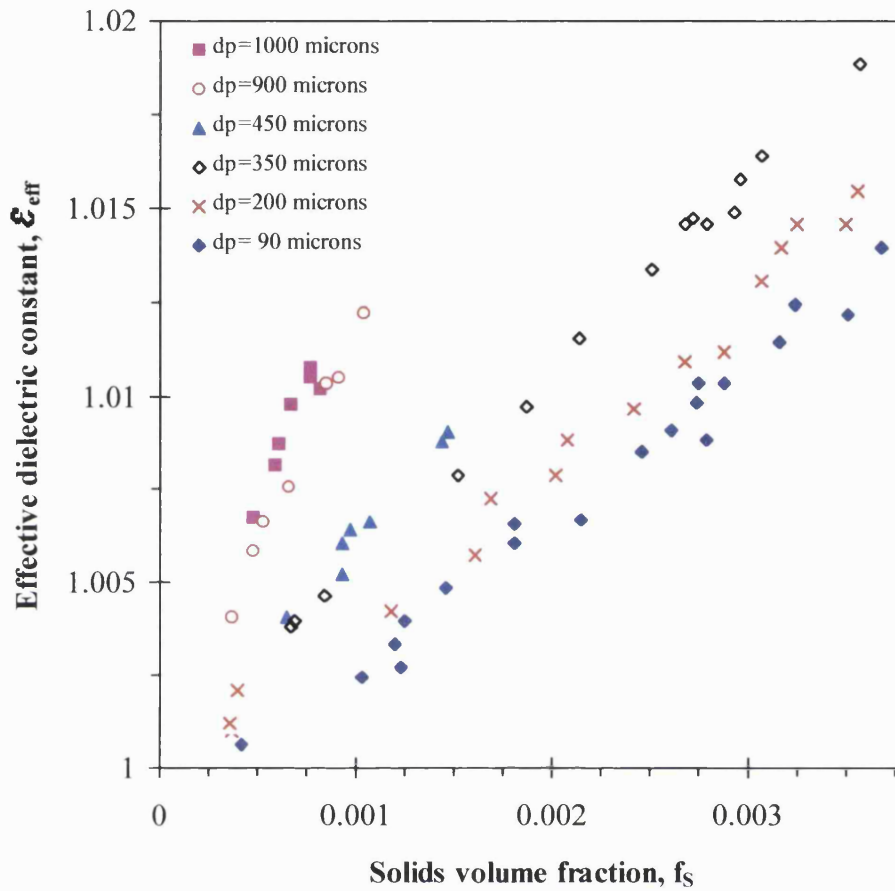
Figure 6.22. Effect of the particle size, d_p on the effective dielectric constant, ε_{eff} for glass ballotini particles dispersion (ρ = 2500 kg/m^3) in air.

Transducer $T_{1\ B}$; Relative humidity: 15%; Ambient temperature: 18 ^{o}C; Voltage: 1 Volt; Frequency: 100 kHz.

Figure 6.23. Effect of the particle size, d_p on the effective dielectric constant, ε_{eff} for glass ballotini particles dispersion ($\rho = 2500$ kg/m^3) in air.

Transducer $T_{2\ B}$; Relative humidity: 15%; Ambient temperature: 18 $^\circ$C; Voltage: 1 Volt; Frequency: 100 kHz.
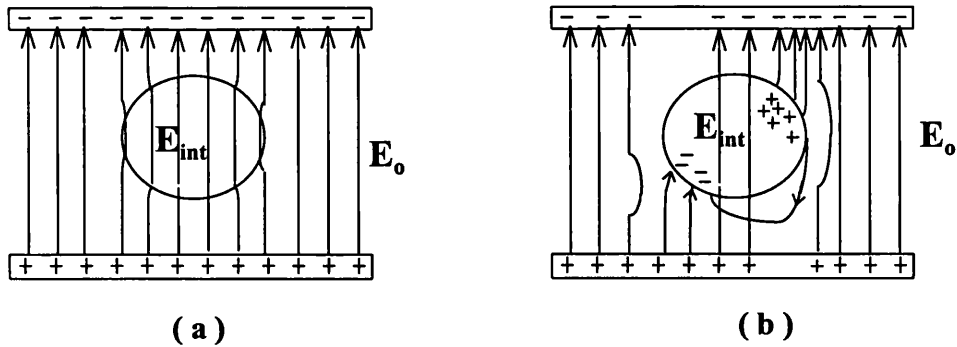
Figure 6.24. A spherical dielectric particle immersed in an electric field (a) without surface charge (b) with acquired surface charge (bipolar).

On the other hand, the acquired electrostatic charge is proportional to the particles' surface area (Rudinger, 1980; Butters, 1981; Taylor et al., 1994). Therefore, in the case of two solids-gas dispersions with the same volumetric concentration, the one with the smaller particle size distribution will carry more electrostatic charge and hence its total polarisation will be lower than the other's. As a result, the former exhibits lower effective dielectric constant for the same solids volumetric concentration, f_s.

To verify the above, figures 6.25 and 6.26 show the product of χ_{mix} i.e. (ε_{eff}-1) and the average surface area per unit volume of the powder plotted against, f_s for the above dispersions of glass ballotini for transducers T_1 and T_2 respectively. It is clear that in both cases, the corresponding data fall on the same fitting line for all the dispersions with different average particle size, apart from those for 90 μm dispersion which are slightly higher. The higher values suggest that actually the 90 μm particles carry less charge than that corresponding to their surface area. This may be attributed to depletion of a portion of acquired charge due to "corona" and "spark" discharges between the charged particles that have acquired a critical value of high charge density that cannot be sustained. Furthermore, the particles interactions are more frequent in solids dispersions of fine particles than in dispersions of larger particles with the same solids fraction because in the former case there are more particles in the

same dispersion volume increasing therefore the possibility of particle-particle interactions. The above phenomenon was manifested during the 90 μm glass ballotini experimental runs with occasional "overload" of the LCR meter due to the occurrence of "conducting string" amongst the particles short-circuiting the electrodes of the transducer. In all the above calculations the average surface area per unit volume of solids for each powder is based on its size distribution presented in Appendix B.

The above observation is consistent with the experimental work carried out by Irons et al. (1982) and Louge et al. (1990). The former evaluated the use of capacitance transducers for concentration measurements in gas-powder streams during pneumatic conveying. The effective dielectric constant was found to be dependent on the particle size. However, no physical explanation was attempted. Louge et al., (1990) used a capacitance transducer to measure the effective dielectric constant of stationary suspensions of particles in petroleum jelly. In this case however, the effective dielectric constant of the suspensions was found to be independent of the particle size. This is justified by the fact that the particles in the suspension are stationary and not moving so they do not acquire any electrostatic charges due to triboelectrification.
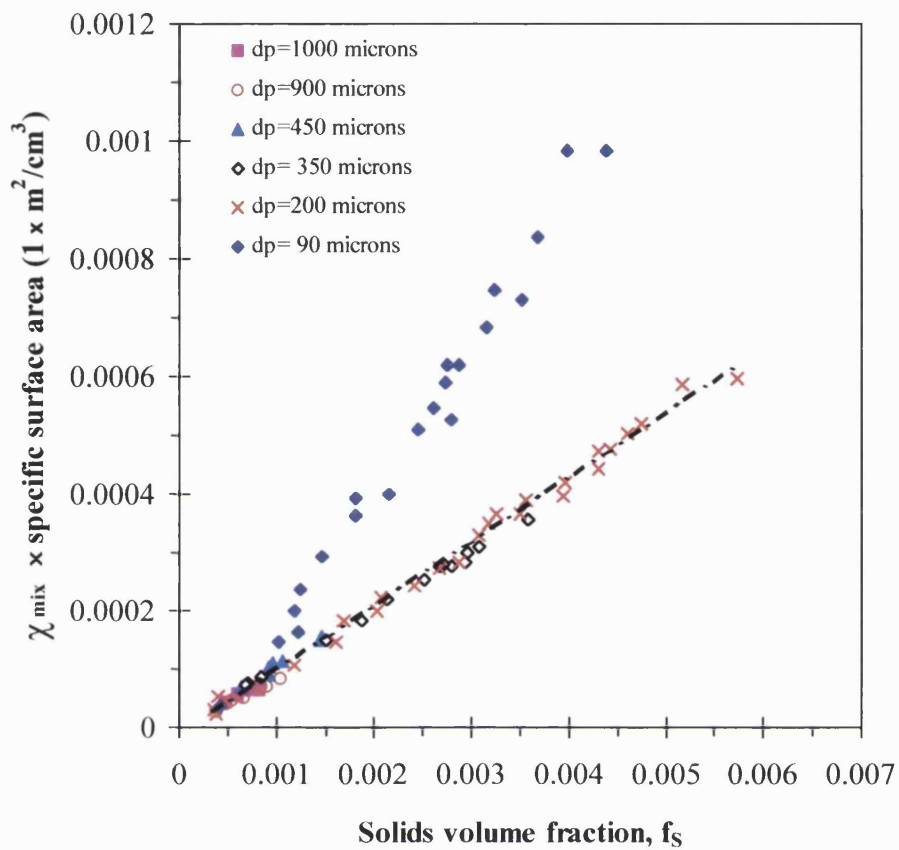
Figure 6.25. The variation of the product of χ_{mix} times the specific surface area of the powder for various size glass ballotini particles dispersions (ρ = 2500 kg/m^3) in air.

Transducer $T_{1\,B}$; Relative humidity: 15%; Ambient temperature: 18 °C; Voltage: 1 Volt; Frequency: 100 kHz.

Fitting equation	Correlation Coefficient , R^2
y = 0.098x + 0.000005	0.995
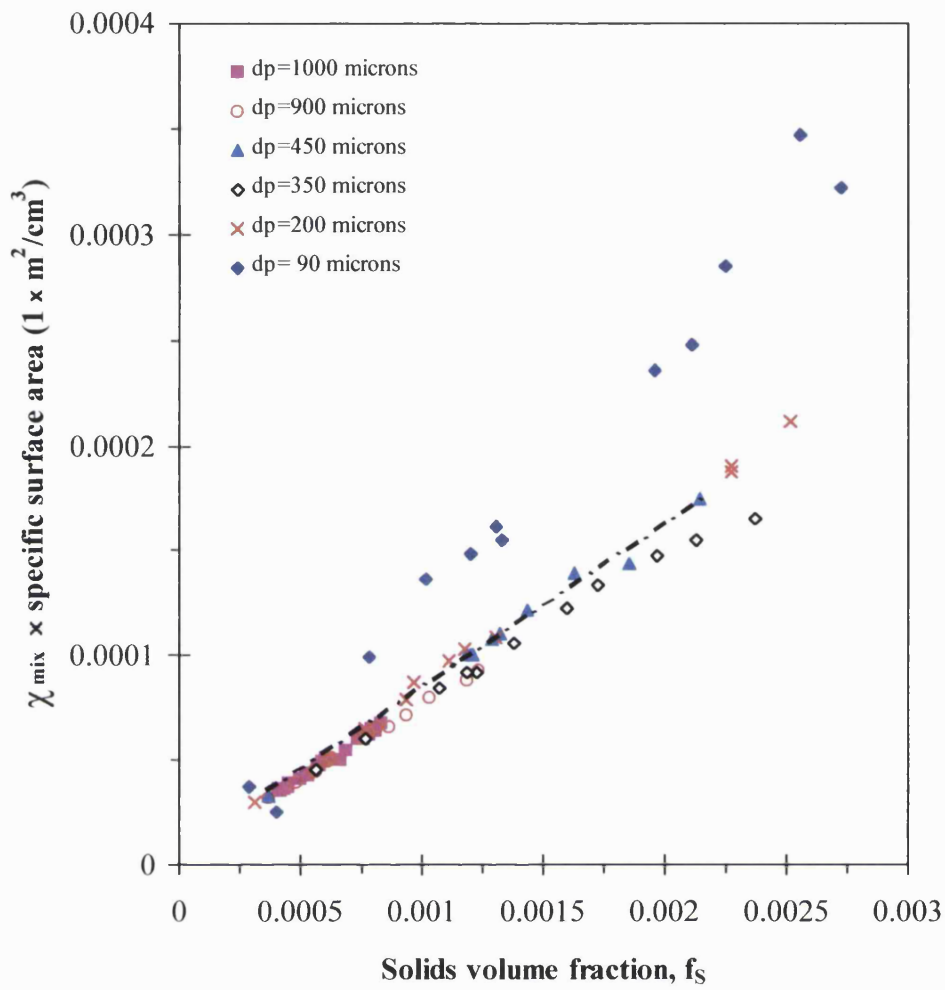
Figure 6.26. The variation of the product of χ_{mix} times the specific surface area of the powder for various size glass ballotini particles dispersions ($\rho = 2500$ kg/m^3) in air.

Transducer $T_{2\ B}$; Relative humidity: 15%; Ambient temperature: 18 °C; Voltage: 1 Volt; Frequency: 100 kHz.

Fitting equation	Correlation Coefficient , R^2
y = 0.082x + 0.000006	0.980

184

6.5. Effect of Humidity

The presence of humidity within the sensing volume of the capacitance transducer may lead to an overestimation of solids concentration in the dispersion. This is because water can add appreciably to the measured capacitance even in very small concentrations due to its high dielectric constant ($\varepsilon_r=80$). In practice, diesel exhaust fumes typically contain water vapour varying in the range 2 to 15 % v/v, (which at 50 °C at the end of the tailpipe is equivalent to 10 - 88% relative humidity) depending on several factors such driving conditions, fuel, car model etc. (see section 2.4.2.2).

The following describes the results of a series of experiments carried out in order to investigate and quantify the effect of humidity on the measured capacitance in the presence and absence of particulates and consequently the resulting changes in, ε_{eff}. Air humidity was controlled using a cylindrical humidifier described in section 5.5.2. and was monitored by an electric hygrometer (Omega, PTH-1X) inserted into the pipeline via a slot, 20 cm upstream of the solids feeding point (see item 16 in figure 5.4).

Figure 6.27 shows the variation of ΔCp_a with relative humidity in the range 8 – 78%. ΔCp_a is defined as the change in Cp_{air} capacitance relative to a reference value corresponding to that for a 'relatively dry' air stream of 5% relative humidity. The data have been obtained using the 17.5 cm long transducer with three different inter-electrode distances namely T_{2A}, T_{2B}, T_{2C} (see table 6.2).

Examining figure 6.27 it is clear that in the case of all three inter-electrode distances, air capacitance, Cp_{air} remains initially unchanged (i.e. $\Delta Cp_a = 0$) with increase in humidity. Therefore, no correction is required for the effect of air humidity on capacitance, in this region. This trend is then marked by a rapid and dramatic rise in Cp_{air} with further increase in humidity. The points at which this transition occurs for the three inter-electrode distances 0.725, 0.975 and 1.225 cm, correspond to relative humidities of 42, 45 and 48% respectively. Examining the above data, it is clear that the 'transition in capacitance' may be effectively delayed with increase in inter-

electrode distance. For example, in the case of an inter-electrode distance of 1.225 cm, no correction for capacitance is required at relative humidities as high as 48%. This is however at a cost of a reduction is sensitivity (see section 6.2.1).
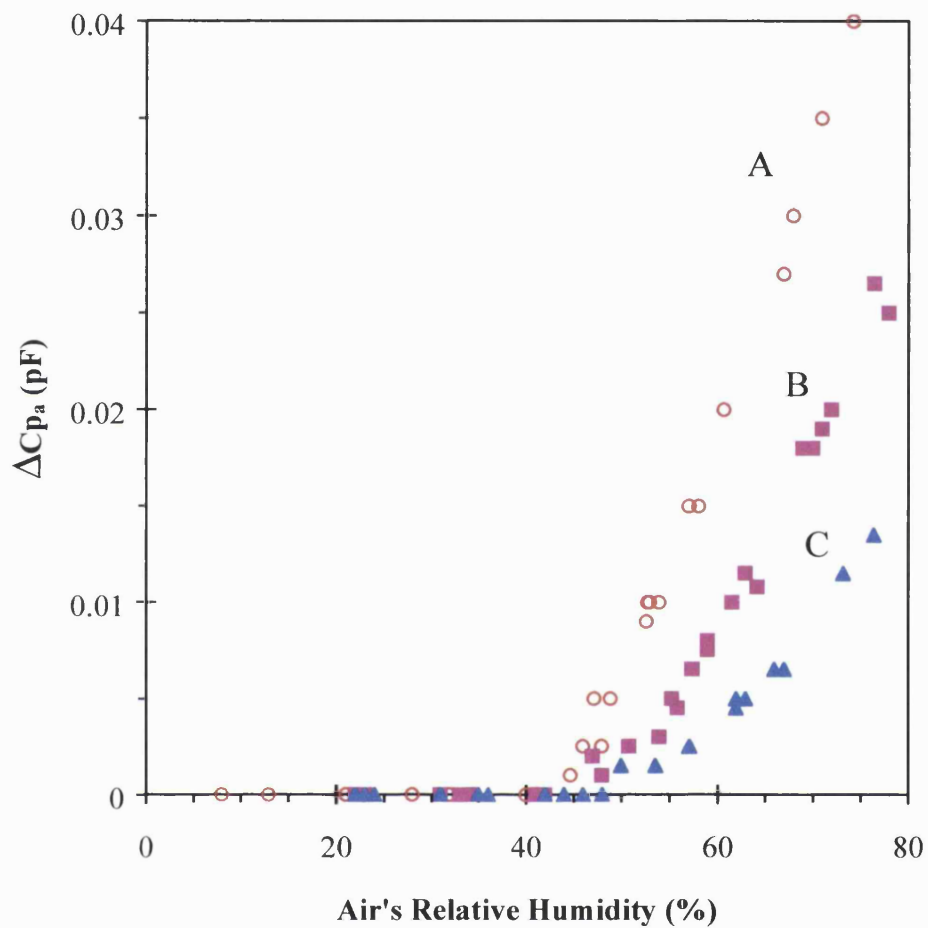
Figure 6.28 shows the variation of the ratio $Cp_{air(RH)}/Cp_o$ with relative humidity for each electrode separation distance. $Cp_{air(RH)}$ is the measured capacitance of air with relative humidity, RH, at and beyond the transition point and Cp_o is the air capacitance at transition point . The data may be approximated by straight lines with the following general equation:

$$\frac{Cp_{air}}{Cp_O} = n \cdot [R.H.] \qquad (6.11)$$

The corresponding slopes as well as the correlation coefficients are given in the table presented in figure 6.28. As expected, the slope of the fitted lines or the transducer sensitivity increases with a decrease in inter-electrode separation distance. Furthermore, equation 6.11 above may serve as "correction equation" for compensating for the effect of humidity on the measured electrical capacitance beyond the transition point.

Returning to the data in figure 6.27, it is important to note that the above mentioned transition points (i.e. 45, 48 and 51% R.H.) can be regarded as the minimum water concentrations which can be detected by the transducer. These values correspond to volumetric concentrations in the range $5.5\text{-}6.5 \times 10^{-4}$ % v/v, which are approximately 10 times smaller than the corresponding threshold "detection value" for glass ballotini (ca. 2×10^{-3} %v/v, see figure 6.22). This is to be expected since the dielectric constant of water is approximately 10 times greater than that for glass (cf. $\varepsilon_{water} = 80$ and $\varepsilon_{glass} = 7.2$).

Figures 6.29 to 6.31 show the dielectric calibration curves for two different size glass ballotini ($d_p = 200$; figure 6.29 and 990 μm; figure 6.30) and bronze ($d_p = 125$ μm; figure 6.31) powder at different air relative humidities varying in the range 18 - 72 %. The data have been obtained using the 17.5 cm long transducer with 0.975 cm inter-electrode distance i.e. T_{2B}.

Figure 6.27. The variation of the ΔCp_a with relative humidity for different inter-electrode distances, D_e. Curve A: 0.725 cm; Curve B: 0.975 cm; Curve C: 1.225 cm.
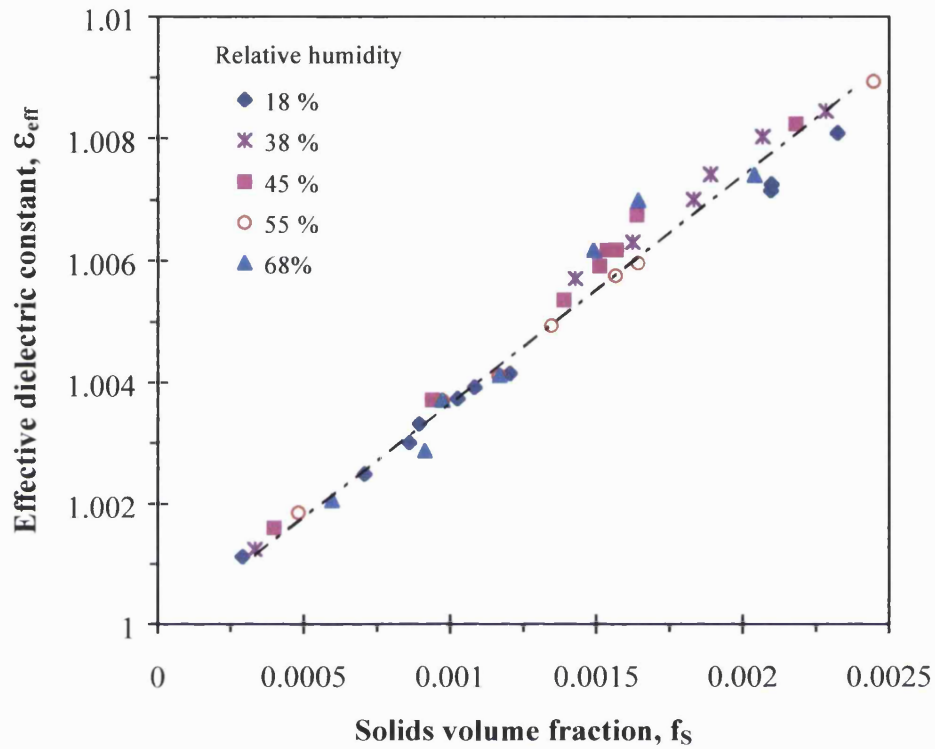
Transducer T_2 ; Ambient temperature: 18 °C; Voltage: 1 Volt; Frequency: 100 kHz .
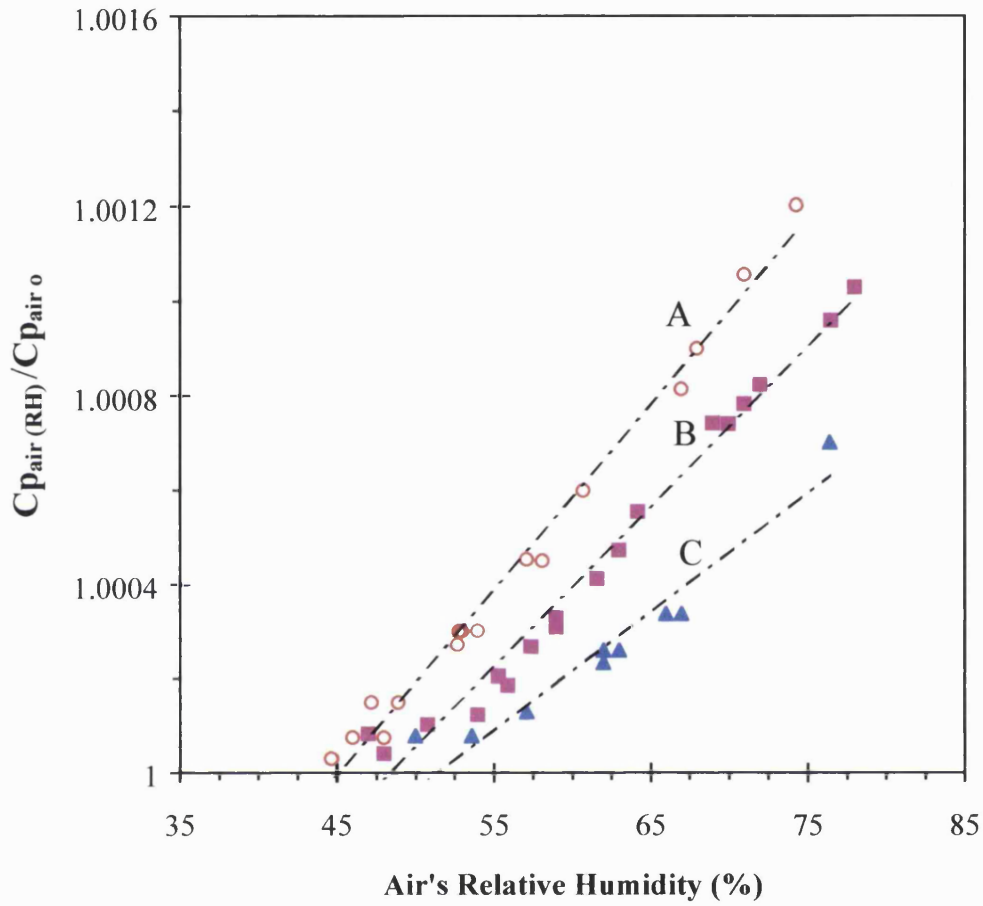
Figure 6.28. The variation of the ratio $Cp_{air(RH)}$ / Cp_o with relative humidity for various inter-electrode separation distances, D_e.

Transducer T_2 ; Ambient temperature: 18 ^oC; Voltage: 1 Volt; Frequency: 100 kHz .

Curve	inter-electrode separation distance, D_e (cm)	Fitting equation	Correlation Coefficient, R^2
A	0.725	$y = 4 \times 10^{-5} x + 0.998$	0.988
B	0.975	$y = 3 \times 10^{-5} x + 0.998$	0.998
C	1.225	$y = 2 \times 10^{-5} x + 0.998$	0.920

Figure 6.29. The variation of the ε_{eff} with f_S for glass ballotini particles ($d_p = 200\ \mu m$, $\rho = 2500\ kg/m^3$) dispersed in air at various relative humidities.

Transducer $T_{2\,B}$; Ambient temperature: 18 ^oC ; Voltage: 1 Volt; Frequency: 100 kHz.

Fitting equation	Correlation Coefficient , R^2
y = 3.84x + 1	0.983
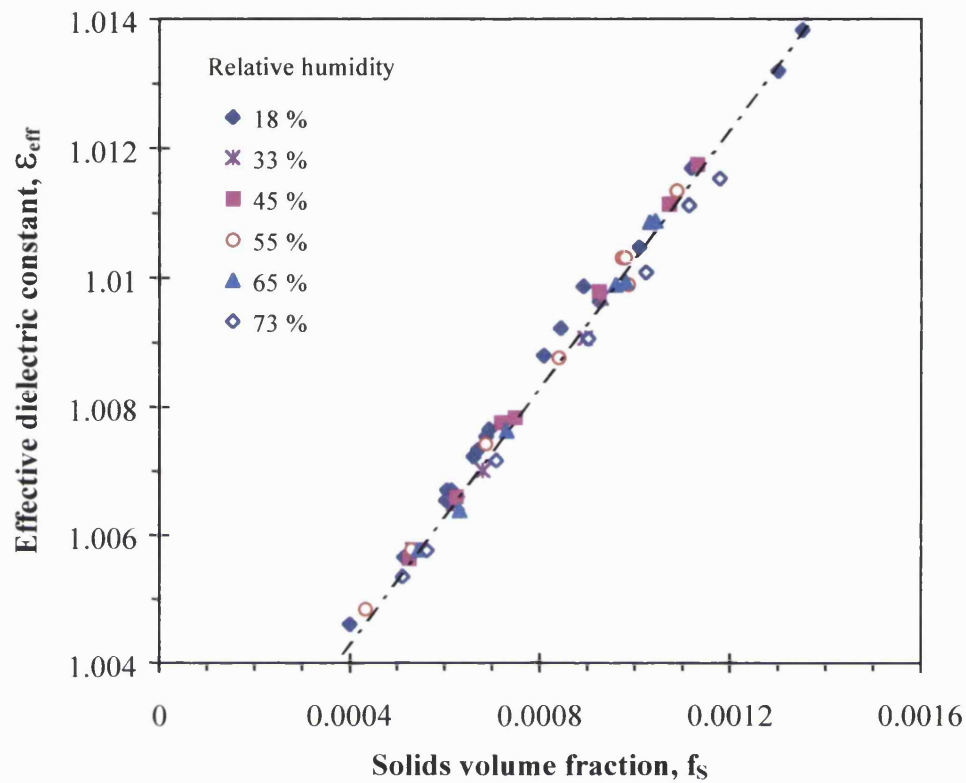
Figure 6.30. The variation of the ε_{eff} with f_S for glass ballotini particles (d_p = 900 μm , ρ = 2500 kg/m³) dispersed in air at various relative humidities.

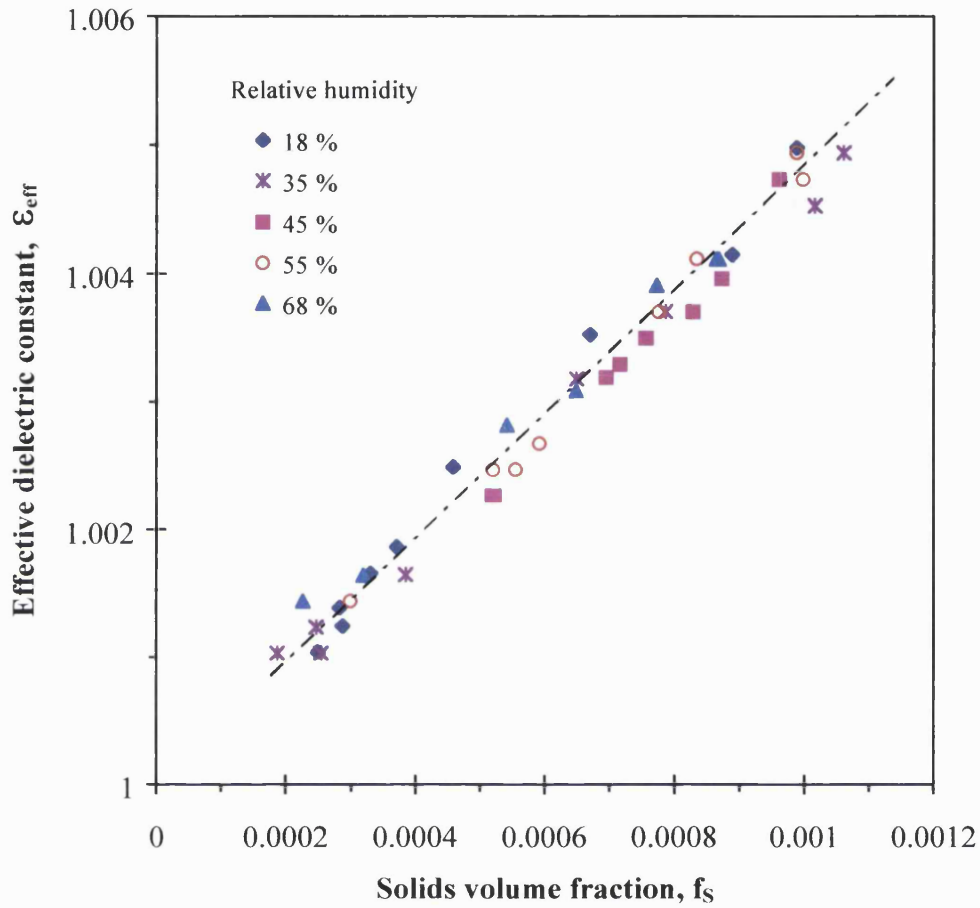Transducer $T_{2\,B}$; Ambient temperature: 18 °C.; Voltage: 1 Volt; Frequency: 100 kHz.

Fitting equation	Correlation Coefficient , R^2
y = 9.83x + 1.0004	0.990

Figure 6.31. The variation of the ε_{eff} with f_S for bronze particles (d_p = 125 μm , ρ = 8800 kg/m^3) dispersed in air at various relative humidities.

Transducer $T_{2\,B}$; Ambient temperature: 18 ^{o}C; Voltage: 1 Volt; Frequency: 100 kHz.

Fitting equation	Correlation Coefficient , R^2
y = 4.62x + 1.0001	0.983

Examining the data, it is clear that in all cases, the presence of humidity does not affect the transducer's response. This is due to the fact that the water vapour behaves like a discrete phase and its effect has been already taken into account in measuring the baseline capacitance, Cp_{air} for the given air relative humidity.

In conclusion, it has been shown that within the ranges tested, air humidity does not affect the dielectric properties of the gas-solid dispersion and as a result, ε_{eff} for the dispersion remains constant. However, attention should be paid in case of zero solids concentration where increase in the recorded capacitance (i.e. Cp_{air}) due to humidity may be wrongly attributed to the presence of solids.

6.6. Effect of Temperature

Temperature is a potential noise source in capacitance measurement and its effect must therefore be studied. Similar, to the humidity effects, temperature fluctuations can cause drift of the baseline signal (zero flow), i.e. Cp_{air}. This phenomenon is particularly important in the case of on-line transducers that have to operate for long periods without re-calibration at higher than ambient temperatures. In the particular application of the exhaust particulate monitor, international standards suggest that the test gas at the instant of measurement should be between 52 -120 °C. Within this temperature range, all the water present is in vapour form and all other uncondensed non-solid particles (i.e. uncondensed/unburned fuel or lubricating oil) are assumed to be insignificant in normal exhaust smoke (ISO 3173, 1974; BS 8178-2, 1997; ISO/DIS 11614, 1994).

Capacitance/temperature experiments were conducted using transducer, T_1 (see table 6.2) with two different inter-electrode separation distances, 0.72 cm (T_{1B}) and 0.87 cm (T_{1C}). An air blower equipped with an 1.3 kW heating coil was located at one end of a 15 cm long stainless steel pipe (i.d. = 3.25 cm, o.d. = 3.27 cm) with the other end connected to the capacitance transducer. The blower supplied air at a flow rate of 500 l/min, regulated at two fixed temperature levels of 15 °C or 100 °C.

It should be noted that the transducer's capacitance may change both due to the temperature dependence of the dielectric constant of air as well as the thermal expansion of the transducer itself. In order to elucidate the relative contributions of each factor, capacitance/temperature experiments both during heating and cooling cycles were conducted. To ascertain the uncertainties associated with the measurements of electrode temperatures by attaching temperature probes to their surfaces, measurements were obtained with the capacitance transducer and the adjoining pipe thermally insulated. The results were then compared against those in the absence of insulation. Also, data during both heating up and cooling down cycles were recorded in order to investigate the possibility of hysterisis.

Finally the results are used to determine a 'capacitance temperature coefficient' which may in turn be used as a temperature correction factor.

The capacitance probe was thermally insulated by wrapping the outer electrode and the adjoining pipe with approximately 10 mm thick layer of flexible foamed polyethylene. All temperatures were recorded using standard BS 1843 type K (NiCr/NiAl) thermocouples. These were glued to the electrode surfaces (at approximately half way along their lengths) using small quantities of (<0.1 g) of super-glue.

Figure 6.32 shows the variation of the mean surface temperature, θ_{mean} of the inner and outer cylindrical electrodes plotted against heating time, for both transducers T_{1B} and T_{1C}. The mean surface temperature is defined as :

$$\theta_{mean} = \frac{\theta_{in} + \theta_{out}}{2} \qquad (6.12)$$

where θ_{in} and θ_{out} are the surface temperatures of the inner and outer electrodes respectively .

Returning to the data in figure 6.32, curves A and C show the data with thermal insulation whereas curves B and D show the corresponding data in the absence of

insulation. The data were obtained using air at 100 °C flowing at approximately 500 l/min through the capacitance probe.

Figure 6.33 on the other hand shows the corresponding variation of the baseline capacitance, Cp_{air}, with time. This variation is expressed as:

$$\Delta Cp_{air} = |Cp_{air(t)} - Cp_{air(t=0)}| \qquad (6.13)$$

where :

$Cp_{air(t=0)}$ = baseline capacitance at time, t = 0 at the reference mean electrode reference temperature, $\theta_o = 26 \pm 1$ °C.

$Cp_{air(t)}$ = capacitance at time, t at the measured mean electrode temperature θ.

A comparison of figures 6.32 and 6.33 shows that, the variation of capacitance with time follows similar trends to that of temperature/time profiles.

Figure 6.34 shows the variation of, ΔCp_{air} against the mean electrode temperature, θ_{mean}. The data have been extracted from figures 6.32 and 6.33. The gradient, T_θ for the fitting line which is equal to 0.0019 pF/°C represents the rate of increase in, ΔCp_{air} with respect to mean electrode temperature.

Figure 6.35 shows the mean electrode surface temperature profiles vs time for transducers T_{1B} and T_{1C} with and without external insulation during a cooling cycle. In this case, measurements were recorded upon the switching off of hot air flowing through the capacitance probes. Figure 6.36 shows the corresponding variation of the baseline capacitance, ΔCp_{air} (with reference mean electrode surface temperature θ_o = 26±1 °C) with time. Finally, in figure 6.37, ΔCp_{air} is plotted against, θ_{mean} by extracting the data from figures 6.35 and 6.36. It is clear that, the decrease in the baseline capacitance is linearly proportional to decrease in the transducer mean temperature. It is noteworthy that the rate of change in, ΔCp_{air} with respect to temperature during the cooling cycle is equal to that for the heating tests (0.0019 pF/°C).
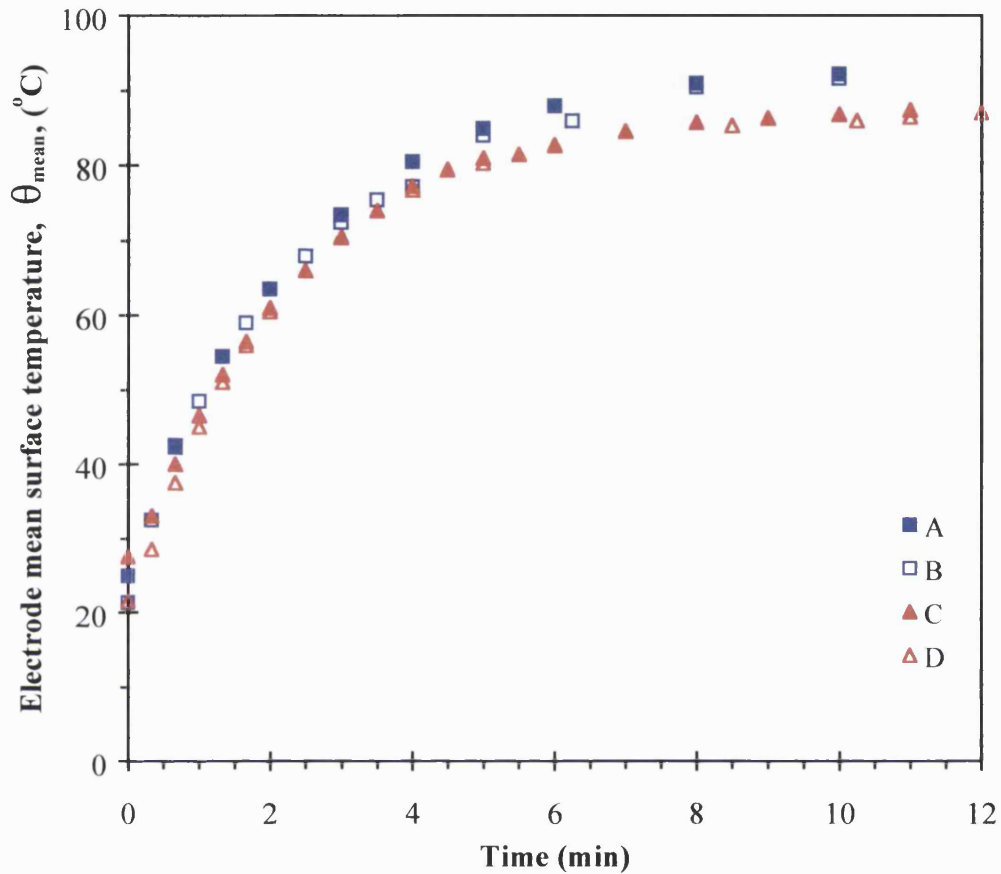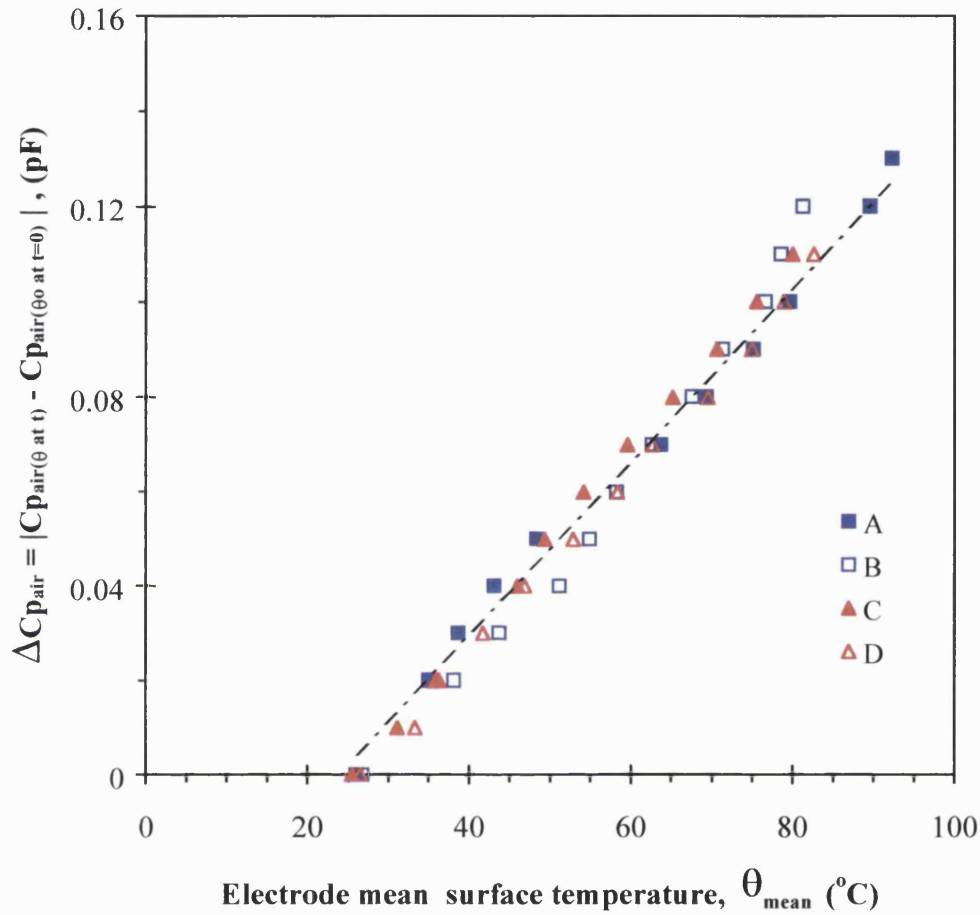
Figure 6.32. The variation of electrode mean surface temperature, θ_{mean} with elapsed time during heating cycle for two different inter-electrode separation distances, D_e with and without thermal insulation . Curve A: D_e = 0.72 cm (insulated) ; Curve B: D_e = 0.72 cm (non-insulated); Curve C: D_e = 0.875 cm (insulated) ; Curve D: D_e = 0.875 cm (non-insulated).

Transducer T_1; Air Relative Humidity : 9%; Flow air temperature: 100 $^{\circ}$C; Voltage: 1 Volt; Frequency: 100 kHz.
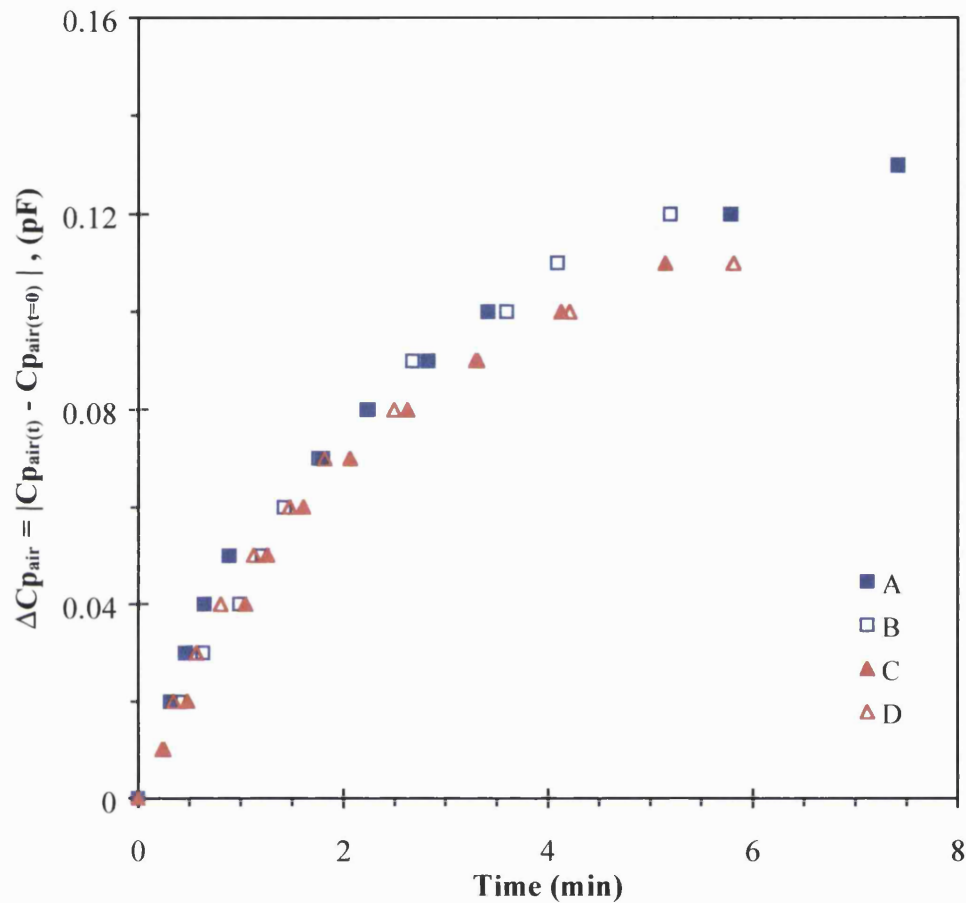
Figure 6.33. The variation of the ΔCp_{air} with elapsed time during heating cycle for two different inter-electrode separation distances, D_e with and without thermal insulation . Curve A: $D_e = 0.72$ cm (insulated); Curve B: $D_e = 0.72$ cm (non-insulated); Curve C: $D_e = 0.875$ cm (insulated); Curve D: $D_e = 0.875$ cm (non-insulated).

Transducer T_1; Air Relative Humidity : 9%; Flow air temperature: 100 ^{O}C; Voltage: 1 Volt; Frequency: 100 kHz.

Figure 6.34. The variation of the ΔCp_{air} with θ_{mean} during heating cycle for two different inter-electrode separation distances, D_e with and without thermal insulation . Curve A: D_e = 0.72 cm (insulated); Curve B: D_e = 0.72 cm (non-insulated); Curve C: D_e = 0.875 cm (insulated); Curve D: D_e = 0.875 cm (non-insulated)

Transducer T_1; Air Relative Humidity : 9%; Flow air temperature: 100 ^{O}C; Voltage: 1 Volt; Frequency: 100 kHz.

Fitting equation	Correlation Coefficient , R^2
y = 0.0019x - 0.0431	0.991
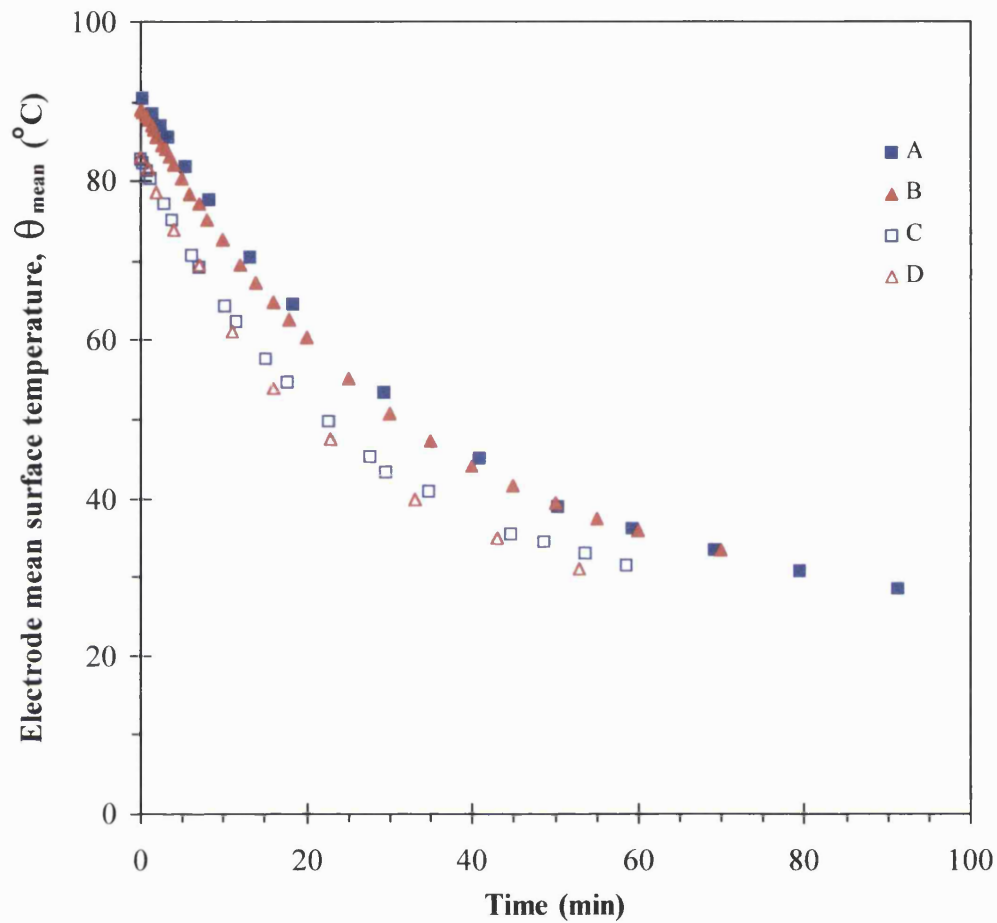
Figure 6.35. The variation of electrode mean surface temperature, θ_{mean} with elapsed time during cooling cycle for two different inter-electrode separation distances, D_e with and without thermal insulation . Curve A: D_e = 0.72 cm (insulated); Curve B: D_e = 0.875 cm (insulated); Curve C: D_e = 0.72 cm (non-insulated) ; Curve D: D_e = 0.875 cm (non-insulated).

Transducer T_1; Voltage: 1 Volt; Frequency: 100 kHz.

Figure 6.36. The variation of the ΔCp_{air} with elapsed time during cooling cycle for two different inter-electrode separation distances, D_e with and without thermal insulation . Curve A: $D_e = 0.72$ cm (insulated); Curve B: $D_e = 0.875$ cm (insulated); Curve C: $D_e = 0.72$ cm (non-insulated); Curve D: $D_e = 0.875$ cm (non-insulated).
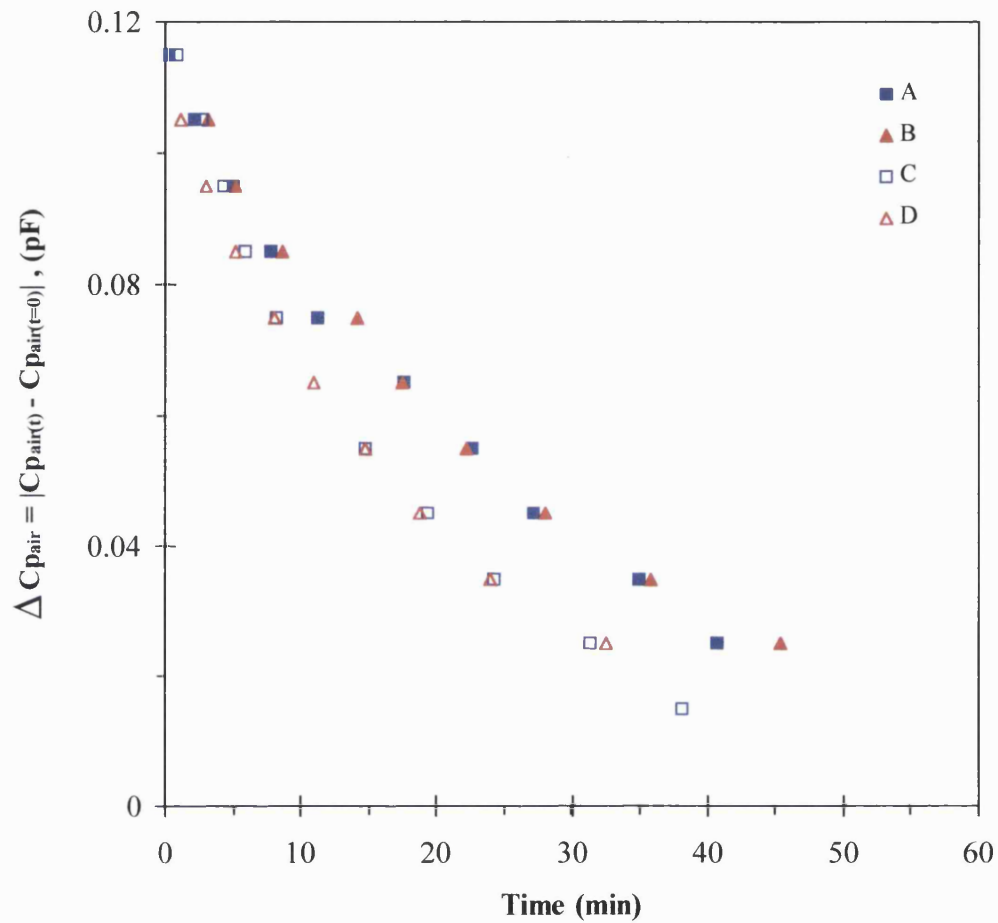
Transducer T_1; Voltage: 1 Volt; Frequency: 100 kHz.
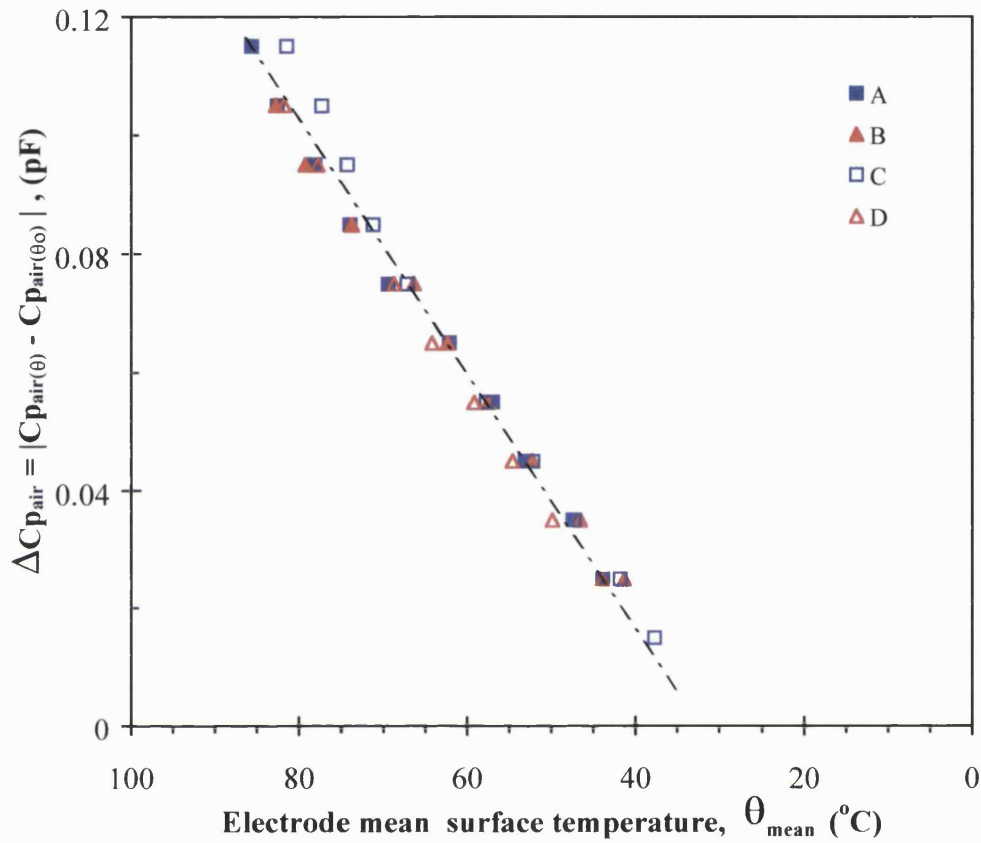
Figure 6.37. The variation of the ΔCp_{air} with θ_{mean} during cooling cycle for two different inter-electrode separation distances, D_e with and without thermal insulation. Curve A: $D_e = 0.72$ cm (insulated) Curve B: $D_e = 0.875$ cm (insulated); Curve C: $D_e = 0.72$ cm (non-insulated); Curve D: $D_e = 0.875$ cm (non-insulated).

Transducer T_1; Voltage: 1 Volt; Frequency: 100 kHz.

Fitting equation	Correlation Coefficient , R^2
y = 0.0019x - 0.06	0.990

The significance of the above data will be explained later. For the time being it is noted that the dielectric constant of gases is inversely proportional to absolute temperature (Feynman, 1964; Hockey, 1972; Van Vlack; 1989). This is because the increased molecular movement due to a rise in temperature results in more misalignment of the individual dipoles due to collisions and therefore reduced polarisation (Feynman, 1964). However, the capacitance/temperature data presented above indicate the opposite trend; capacitance actually increases with a rise in temperature. The observed response is therefore a consequence of the thermal expansion of the capacitance transducer whose capacitance for a given geometry is proportional to its linear dimensions (Terman, 1950; NPL, 1969).

The following conclusions may be made based on the data presented in figures 6.32-6.37:

a) The change in the baseline capacitance, Cp_{air} depends on the mean temperature of the transducer's electrodes and not in the temperature of the medium between the electrodes.

b) Advantageously, for the tested temperature range (25-83 ±1 °C), no hysterisis in the capacitor response is observed with respect to temperature changes since the behaviour during the heating up and cooling down periods are the same. Therefore, the capacity returns to its original value when the temperature comes back to normal.

c) Cp_{air} varies linearly with the mean surface temperature of the cylindrical electrodes. Therefore, for a specific capacitor, a temperature coefficient, C_θ can be experimentally determined, which may in turn be used as a correction factor for accounting for the effect of temperature on capacitance.

Hence, if $Cp_{air(\theta 1)}$ and $Cp_{air(\theta 2)}$ are the baseline capacitances at mean electrode temperatures, θ_1 and θ_2 respectively, then:

$$Cp_{air(\theta 2)} = Cp_{air(\theta 1)}(1 + C_\theta \Delta\theta) \tag{6.14}$$

where C_θ is defined as the capacitor temperature coefficient having units of 1/°C. $\Delta\theta$ (°C) is the corresponding temperature interval.

To calculate, C_θ we use figures 6.38 and 6.39 which show the variation of the fractional change in capacitance expressed as $(\Delta Cp_{air}/ Cp_{air(\theta_0\ at\ t=0)}) = |(Cp_{air(\theta\ at\ t)} - Cp_{air(\theta_0\ at\ t=0)})| / Cp_{air(\theta_0\ at\ t=0)}$ with respect to mean electrodes temperature θ_{mean} for both capacitor electrode distances. Figure 6.38 show the data during a heating cycle whereas the data in figure 6.39 are obtained during the cooling down period. The gradients, C_θ for the corresponding fitting lines are the same and equal to 0.0001/ °C. Interestingly, the above calculated temperature coefficient is the same for both electrode distances and in close agreement with the coefficient of linear expansion for stainless steel (i.e. 0.00012/°C; Perry, 1973), used as the construction material for the capacitance transducer. Hence the change observed in the baseline capacitance with varying temperature is attributed to the linear thermal expansion of the metallic structure.

Advantageously, in the tested temperature range (25-83 ±1 °C) the behaviour of the capacitance transducer with respect to changes in temperature is cyclic i.e. the capacity returns to its original value when the temperature comes back to normal.
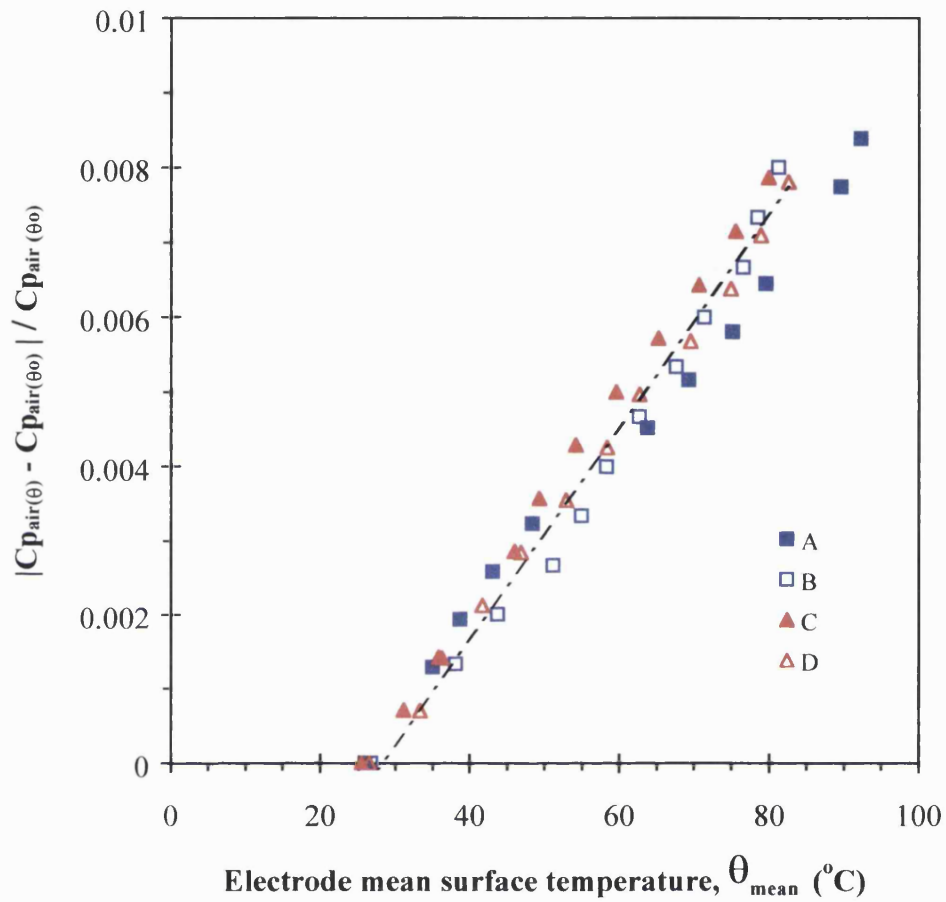
Figure 6.38. The variation of the fractional change in Cp_{air} with θ_{mean} during heating cycle for two different inter-electrode separation distances, D_e with and without thermal insulation . Curve A: $D_e = 0.72$ cm (insulated); Curve B: $D_e = 0.72$ cm (non-insulated); Curve C: $D_e = 0.875$ cm (insulated); Curve D: $D_e = 0.875$ cm (non-insulated).

Air Relative Humidity : 9%; Flow air temperature: 100 $^{\circ}C$; Transducer T_1; Voltage: 1 Volt; Frequency: 100 kHz.

Fitting equation	Correlation Coefficient , R^2
y = 0.0001x - 0.004	0.985
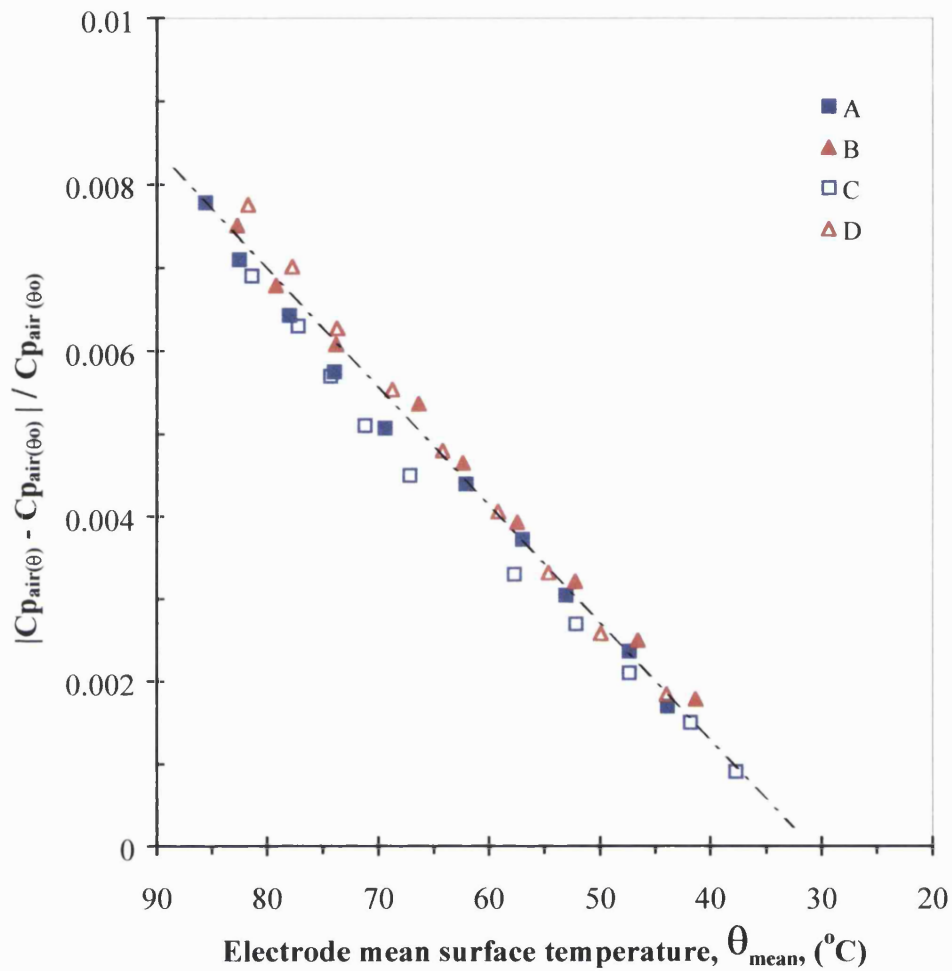
Figure 6.39. The variation of the fractional change in Cp_{air} with θ_{mean} during cooling cycle for two different inter-electrode separation distances, D_e with and without thermal insulation. Curve A: $D_e = 0.72$ cm (insulated ; Curve B: $D_e = 0.875$ cm (insulated); Curve C: $D_e = 0.72$ cm (non-insulated); Curve D: $D_e = 0.875$ cm (non-insulated).
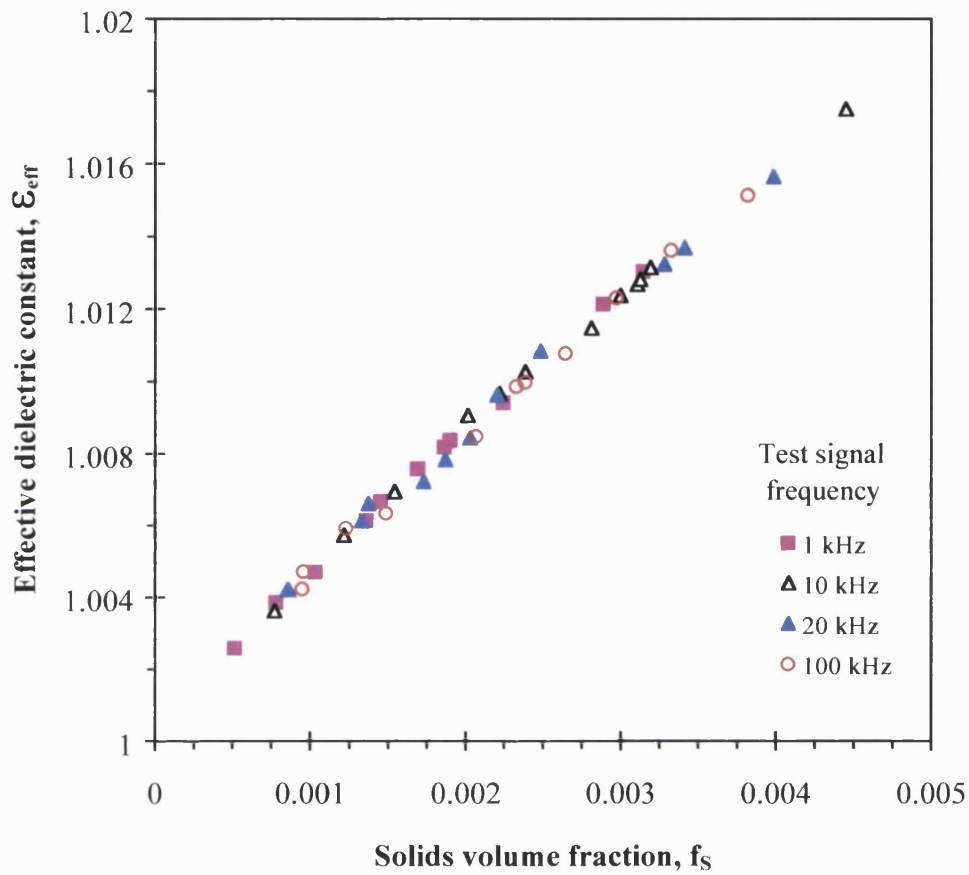
Transducer T_1; Voltage: 1 Volt; Frequency: 100 kHz.

Fitting equation	Correlation Coefficient , R^2
y = 0.0001x - 0.0043	0.986

6.7. Effect of Frequency

Capacitance measuring devices use a.c. voltage circuits and therefore the frequency of the applied voltage is an important factor that can affect the measured capacitance and the subsequent calculation of effective dielectric constant. This is because, the latter depends on polarisation of the dielectric material which in turn is dependent on the applied electric field (Frohlich, 1958; Hockey 1972; Braithwaite et al., 1990).

Figures 6.40 and 6.41 respectively show the variation of effective dielectric constant of glass ballotini ($d_p = 350$ µm) and copper ($d_p = 125$ µm) solid/air dispersions against solids volume fraction in the frequency range 1 - 100 kHz using the LCR meter in conjunction with T_{2B} (see table 6.2) capacitance transducer chosen as an example. From the data, it is clear that for both cases, the frequency of the applied electric field has little effect on the data.

The above observation agrees with the theory predicting that at low frequencies (generally below 10^7 Hz) the dielectric constant of most materials remains unchanged (Richards, 1961; Feynman 1964; Hockey1972; Braithwaite et al., 1990). This is because the dielectric constant depends on polarisation arising through orientation and electronic polarisation (see Chapter 4) which are effective at different frequency ranges (Richards, 1961; Van Vlack, 1989). More specifically, the polar molecules involved in orientation polarisation due to their high inertia have a slower response to the oscillating external field, since it takes a certain amount of time for the heavy molecules to turn towards the direction of the field (Harrop, 1972; Braithwaite et al., 1990). Hence, molecular orientation is limited to maximum frequency of approximately 10^8kHz. In contrast to this, electronic polarisation has a much faster response because it involves electrons which have much smaller inertia (due to smaller mass) and therefore electronic polarisation can occur even in optical frequencies ($< 10^{15}$ Hz). As a result, in high frequencies (generally above 10^{11} Hz) any permanent dipoles in the dielectric medium will not respond at all, resulting in a decrease of the dielectric constant which will depend only on the electronic polarisation of the material due to a zero contribution of the orientation polarisation (Feynman 1964; Hockey1972; Braithwaite et al., 1990).

Figure 6.40. The variation of the ε_{eff} with f_S for dispersion of glass ballotini particles (ρ = 2500 kg/m^3 , d$_p$ = 350 µm) in air, for various frequencies.

Transducer $T_{2\ B}$; Ambient temperature: 18 ^{o}C; Relative humidity: 15%; Voltage: 1 Volt.
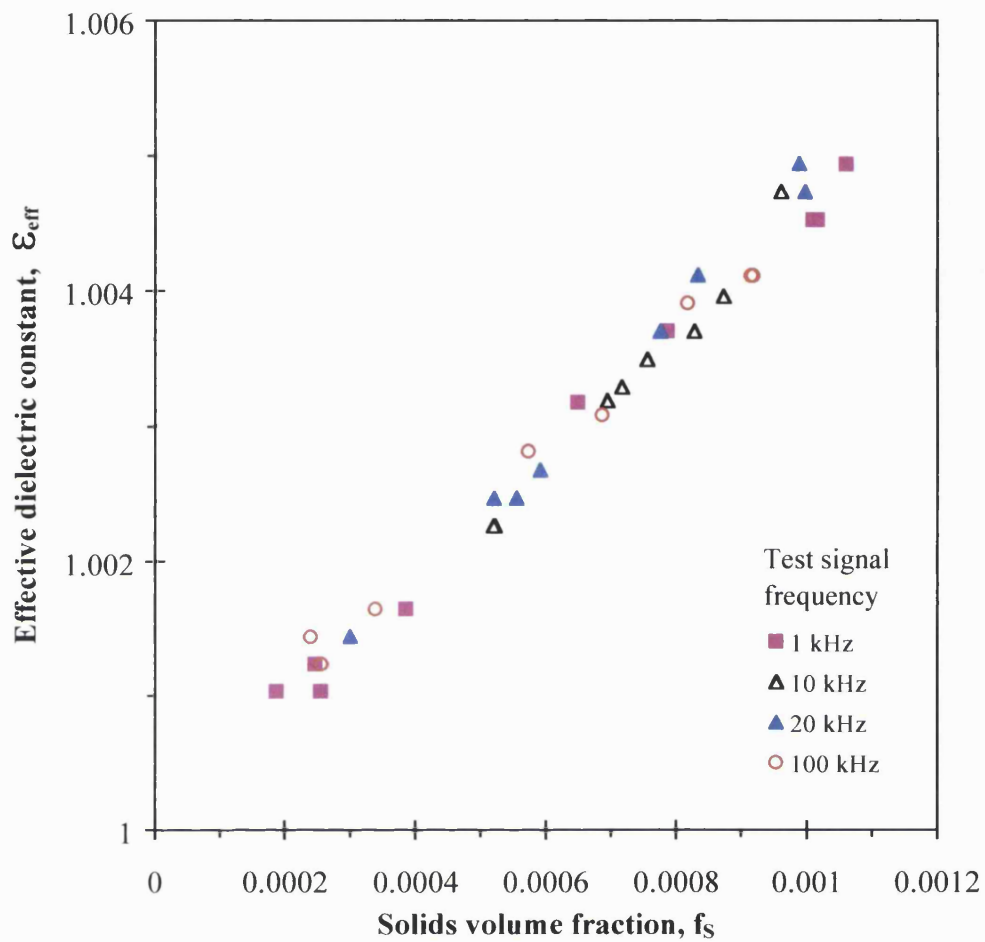
Figure 6.41. The variation of the ε_{eff} with f_S for dispersion of copper particles (ρ = 8810 kg/m^3, d_p = 125 μm) in air, for various frequencies.

Ambient temperature: 18 ^{O}C; Air relative humidity: 15%; Transducer $T_{2\,B}$; Voltage: 1 Volt.

Figure 6.42 shows a typical response for the variation of the dielectric constant with frequency for a hypothetical material (Van Vlack, 1989).
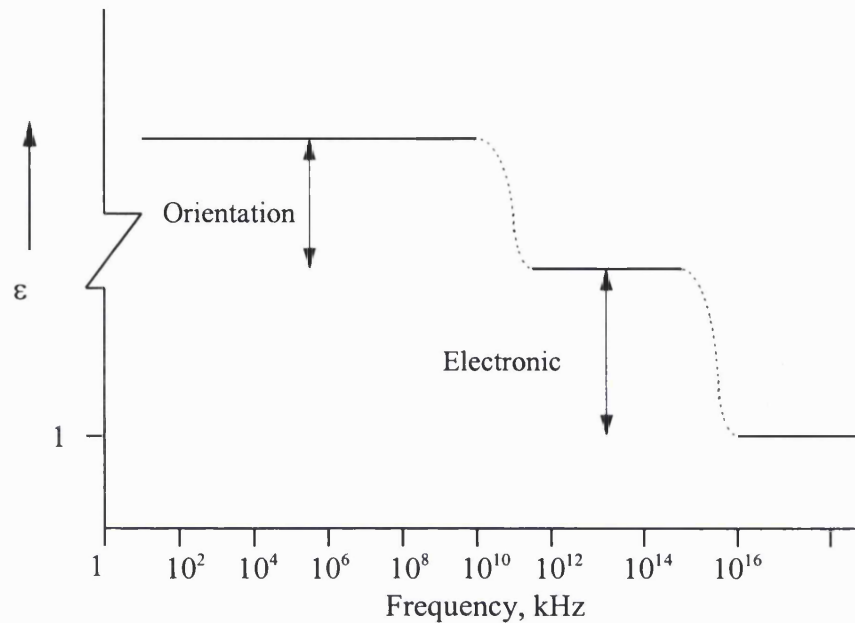
Figure 6.42. Variation of dielectric constant for simple dielectrics.
(Van Vlack, 1989)

6.8. Effect of Flow Regime

The following investigates the effect of the flow conditions prevailing in the pneumatic pipeline on capacitance concentration measurement. The flow regime directly affects the spatial distribution of the dispersed particles within the transducer's sensing volume. This may in turn alter the measured capacitance. Furthermore, for a powder of a specific size distribution, the electrostatic charge acquired during its transportation depends on the conveying velocity (Loeb, 1958; Taylor et al., 1994) which may also affect the measured capacitance (see section 6.2.2).

This investigation was conducted by comparing the effective dielectric constants of a solids-gas dispersion when the velocity of the particles carrying air stream varied in the range 6.5 to 15 m/sec thus resulting in different flow patterns. Generally, for

suspensions of particles of given size, density and mass loading, the flow pattern changes from dilute phase to dense phase flow with decreasing air velocity, as depicted in figure 6.43.
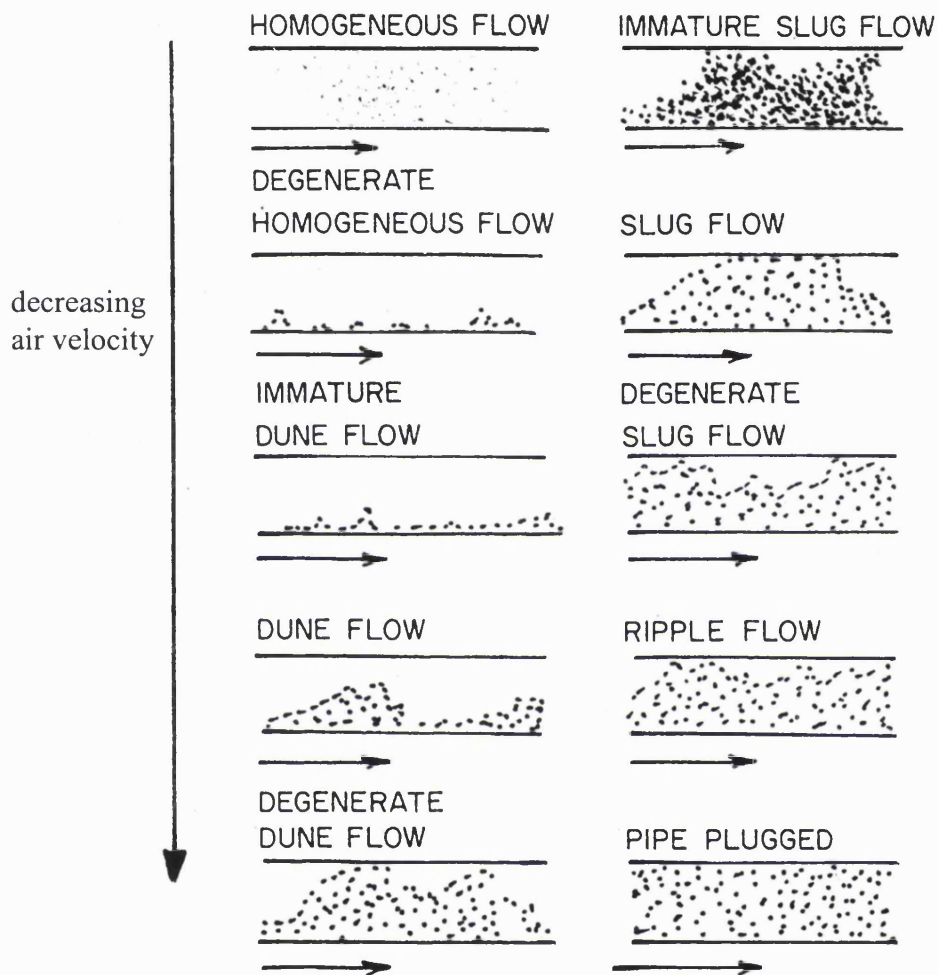
Figure 6.43. Flow patterns in a horizontal pipe((Klinzing, 1997)

The boundary between these flow regimes is not clear cut and there is as yet no universally accepted equations predicting dense phase and dilute phase flow (Klinzing, 1981; Rhodes, 1990). In the present study the prevailing flow regime was varied by changing the air velocity and in each case was confirmed by visual observation of flow through the glass section of the conveying pipe. Furthermore, measurements of Cp_{sol} were taken and compared at three different points (0.2 m, 1.5 m and 6 m downstream from the solids feeding point) along the pipeline, since the

solids flow pattern as well as the total electrostatic charge may vary depending on the distance between the particles feeding point and the transducer.

Figure 6.44 show the effect of the air stream velocity on the dielectric calibration data for glass ballotini (d_p = 1000 μm) using transducers T_{1A}, T_{1B} and T_{1C} (see table 6.2). It is clear that the variation in air velocity, which results in different solids flow regimes - observed though the glass section (see item No. 12 in figure 5.4 in chapter 5)- has no effect on the obtained results. This result is to be expected since the effective dielectric constant of a solids-gas dispersion with a specific size distribution depends on the total volume occupied by the solids in the capacitance measurement zone. These results are consistent with the experimental work of Morse et al. (1951) and Sami et al. (1980) who used capacitance sensors of different design to the coaxial capacitor for concentration measurements in multi-phase pipelines.

On the other hand figures 6.45 and 6.46 show the calibration curves of glass ballotini (d_p = 900 μm) and copper (d_p = 125 μm) obtained by transducer T_2 for three inter-electrode distances (i.e. A, B and C in table 6.2) in three different positions (positions 1,2 and 3) along the conveying pipeline. Similarly, in all cases the calibration curves coincide regardless the location of the used transducer. This indicates that the maximum charge acquired by a particle of certain size due to contact and frictional charging does not change along the conveying pipeline. Furthermore, it indicates that this maximum charge it is reached in very early stage since the first set of measurements were taken only 20 cm downstream of the solids feeding point. The latter coincides with the work of Butters (1981) Gajewski (1994) who suggest that a pneumatically conveyed powder acquires the maximum charge acquired within few inches of pipe length.
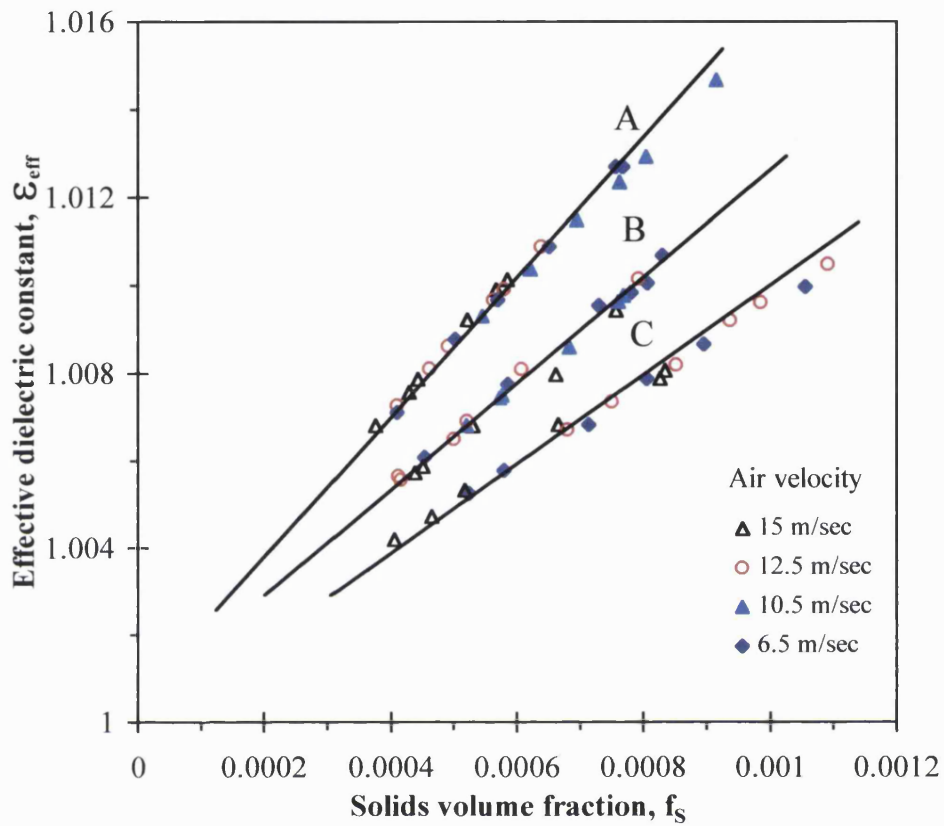
Figure 6.44. The variation of the ε_{eff} with f_S for dispersion of glass ballotini particles (d_p = 1000 μm, ρ = 2500 kg/m^3) in air streams of various velocities for three inter-electrode separation distances, D_e: Curve A: D_e = 0.725 cm; Curve B: D_e = 0.975 cm; Curve C: D_e = 1.225 cm.

Ambient temperature: 18 °C; Air relative humidity: 15%; Transducer T_2; Voltage: 1 Volt; Frequency: 100 kHz.
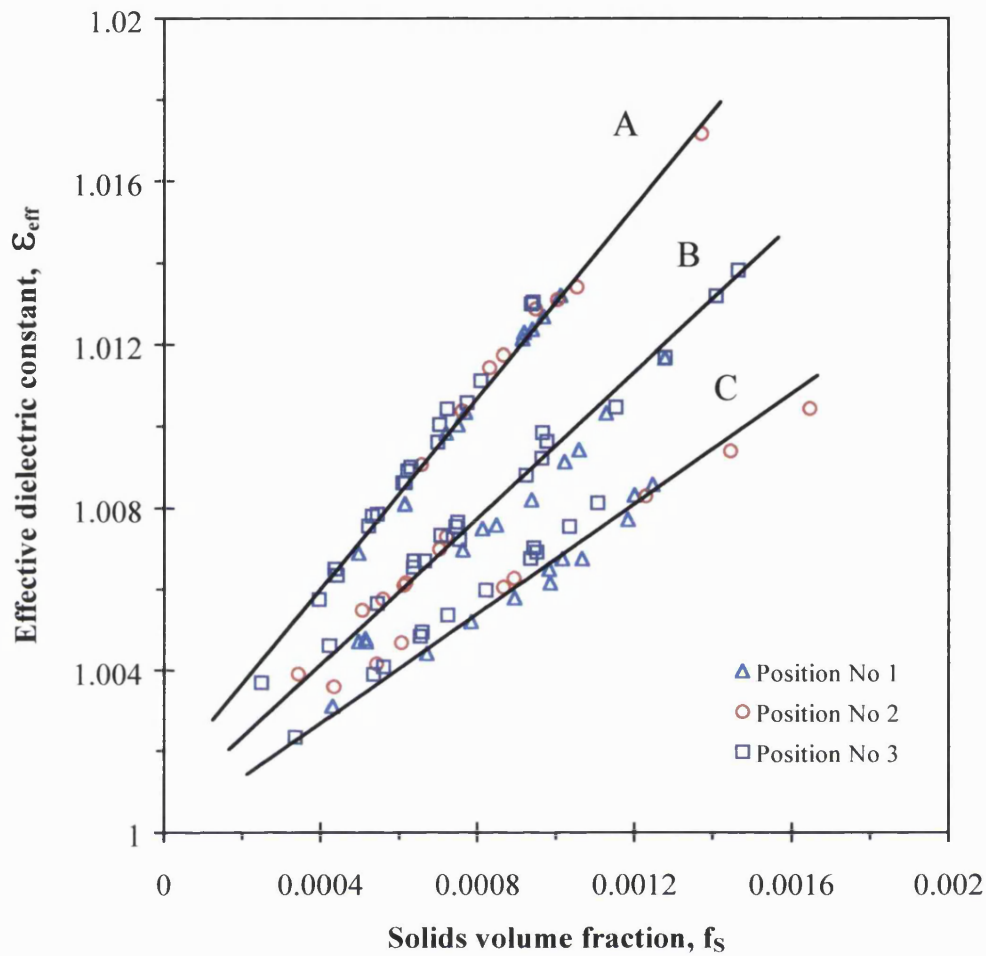
Figure 6.45. The effect of the transducer position along the conveying pipeline on the calibration data for dispersion of glass ballotini particles (d_p = 900 μm, ρ = 2500 kg/m^3) in air for three inter-electrode separation distances, D_e: Curve A: D_e = 0.725 cm; Curve B: D_e = 0.975 cm; Curve C: D_e = 1.225 cm.

Air relative humidity: 15%; Ambient temperature: 18 $^\circ$C; Transducer T_2; Voltage: 1 Volt; Frequency: 100 kHz.

Position	Distance downstream of the solids feeder (m)
1	0.2
2	1.5
3	6
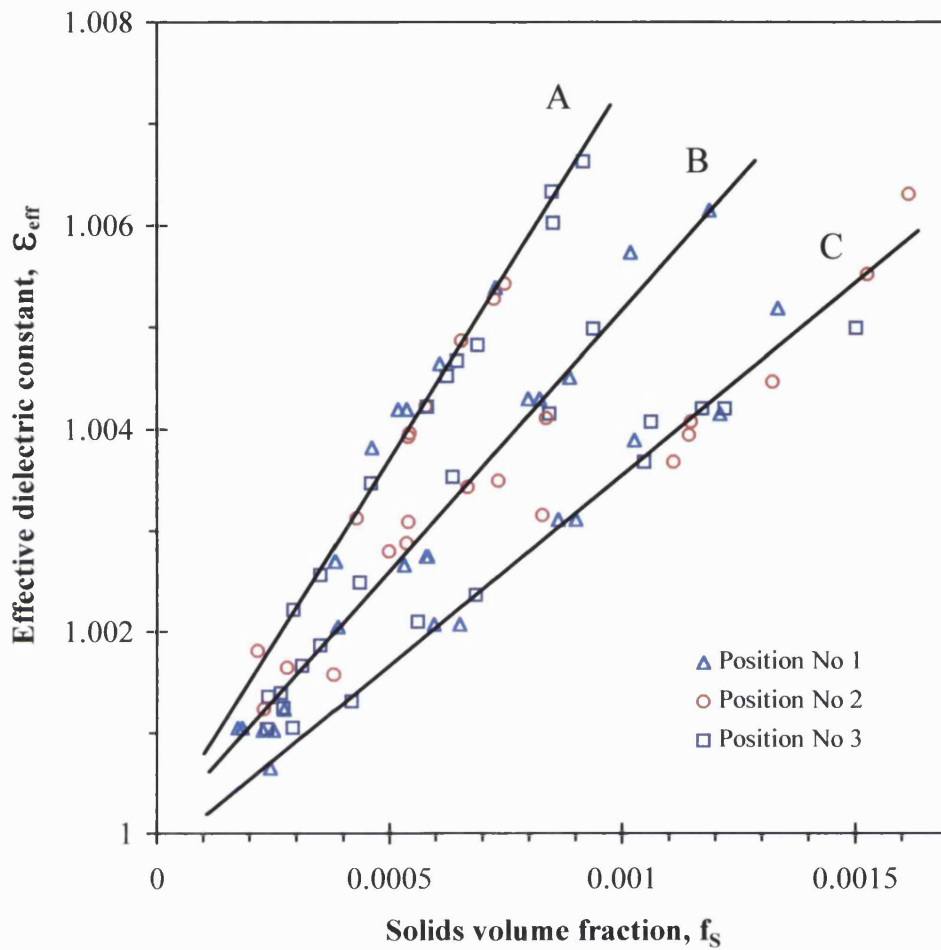
Figure 6.46. The effect of the transducer position along the conveying pipeline on the calibration data for dispersion of copper particles ($\rho = 8810$ kg/m^3, $d_p = 125$ μm) in air for three inter-electrode separation distances, D_e. Curve A: $D_e = 0.725$ cm; Curve B: $D_e = 0.975$ cm; Curve C: $D_e = 1.225$ cm.

Air relative humidity: 15% ; Ambient temperature: 18 ^{o}C; Transducer T_2 ; Voltage: 1 Volt; Frequency: 100 kHz.

Position	Distance downstream of the solids feeder (m)
1	0.2
2	1.5
3	6

CHAPTER 7

CONCLUSIONS AND SUGGESTIONS FOR FUTURE WORK

7.1 Conclusions

This thesis describes the design and development of a transducer for the on-line measurement of particulates concentration in air in real time basis. The technique works on the basis of the fact that the effective dielectric constant, ε_{eff} of a solids-gas dispersion driven through a capacitance cell is directly related to the concentration of the entrained particulates. This measurement technique has been selected due to several advantages including:

- Safe to operate and does not require specially trained personnel
- Inexpensive to construct and operate
- Rapid response thus making it suitable for in situ, real time measurements applicable for monitoring rapid transients
- Does not involve mechanical or moving parts thus reducing the possibilities for malfunction as well as little maintenance requirements
- The output is an analogue signal suitable for process control

The primary application of the device is for the on-line concentration measurement of particulates emitted from diesel engine exhausts although the reported experimental results also evaluate and establish its feasibility for monitoring solids/gas dispersions during their pneumatic conveying.

The transducer basically comprises two different diameter metallic cylinders placed coaxially within one another so that an annulus is formed. The latter constitutes the sensing volume of the capacitance transducer following the application of a voltage between the inner and the outer cylinder. The transducer is placed inline, onto the

214

pipeline conveying the test solid/gas dispersion via Teflon rings fitted on either side of the outer cylindrical electrode thus providing electrical insulation as well as mechanical support.

The principal advantage of using cylindrical electrodes is that the charge density on the electrodes' surface as well as the field between them are better defined compared to other electrode geometries (Jonassen, 1998).

A critical literature review of the air particulate pollution problem with special reference to diesel powered vehicles was presented in chapter 2 whereas several analytical techniques used for ambient and source monitoring were described in chapter 3.

Chapter 4 dealt with a brief theoretical overview on the dielectric materials and capacitive systems, followed by a description of the design considerations and construction details of the capacitance transducer. The chapter concluded with an overview of the most commonly used electronic circuits for measuring capacitance.

More specifically, optimum length and diameter of the cylindrical electrodes were specially selected so as to provide a capacitance signal of sufficient magnitude and sensitivity enabling its measurement using conventional ancillary electronic equipment. Other considerations dictating the design of the capacitance transducer included the dielectric breakdown strength of air, the build up of back-pressure and the unhindered flow of dispersion through the annulus.

For example, a main difficulty encountered during the design of the capacitance transducer was the occurrence of electrostatic discharges within the transducer sensing volume which resulted in short-circuiting of the capacitor. The generation of electrostatic charges was primarily a consequence of particle/particle and particle/wall interactions. The problem was overcome through a combination of design changes, the most important of which included:

- Replacement of the 'pointed' insulating caps of the inner electrode with hemispherical metal caps. This prevented corona discharge of the accumulated electrostatic charge from the tip of the insulating caps.

- Minimising the length of the capacitor Teflon supports. This significantly reduced electrostatic charge built up on their surface due to particle/wall impacts.

- Polishing and hence removing any surface imperfections on the inner electrode walls. This reduced the opportunity for corona or spark discharges.

Considerable time and effort was devoted to the design and construction of the ancillary experimental set up, described in chapter 5, for the production of solid aerosols of a given concentration for calibrating the capacitance transducer. Basically, the unit comprises an aerosol generation system and a pneumatic conveying system.

The basic elements comprising a dry-dispersion aerosol generator include the powder feeding mechanism for continuously metering and controlling the powder input into the generator at a constant rate together with the means for pneumatically dispersing the powder to form an aerosol

After the dispersion process and the initial suspension of the particles, it is necessary to convey the fully suspended particles in the air stream along a certain pipeline length at the end of which the capacitance transducer is located. This requires the determinations of the minimum air conveying velocity for the suspension of the particles and the minimum pipe length that will allow the solids-gas mixture to reach steady state.

Finally, it is worth noticing that several measures have been taken in order to ensure that undesirable levels of electrostatic charge will not build up either on the particles or on other components of the experimental set-up (e.g. electrical conductors, non-conducting surfaces). This was achieved by incorporating several features for charge dissipation such as earthing all the metallic parts of the set-up and inserting earthed rods and grids into the flow. The chapter concluded with a description of the experimental procedures and materials.

The results of extensive experiments elucidating the performance characteristics of the capacitance transducer were presented in chapter 6. These formed the basis for establishing the feasibility and reliability of the capacitance transducer for measuring particulate concentrations in gas streams.

The main findings based on the results obtained using the capacitance probe may be summarised as follows :

• In general, for all the solids-gas dispersions (solids concentrations 0.035 to 0.35 % v/v) investigated, the effective dielectric constant is directly proportional to the solids concentration. The results are consistent for a variety of powders with different dielectric properties (i.e. insulators and conductors) and physical properties (i.e. density and size distribution). Therefore, the system is capable of providing solids volume concentration data.

In the case of dielectric powders suspended in air, the effective dielectric constant of the dispersion was found to be dependent on the respective dielectric constant of the solid phase as well as the particle size. Therefore, for dispersions of different powders of the same size distribution, the resulting, ε_{eff} of the gas-solids dispersions will be greater in the case of the suspended material with the larger individual dielectric constant. Furthermore, ε_{eff} for a given solids-gas dispersion decreases with decreasing average size of the suspended particles. This is attributed to the total charge accumulated on the particles' surface, due to triboelectrification during its pneumatic conveying. This charge is proportional to the powder total surface area (i.e. smaller average particle size). The acquired charge on the particle surface reduces the electric field inside the particle with subsequent reduction of the material's polarisation. Therefore, in the case of two solids-gas dispersions with the same volumetric concentration, the one with the smaller particle size distribution will carry more electrostatic charge and hence its total polarisation will be lower than the other's. As a result, the former exhibits lower effective dielectric constant for the same solids volumetric concentration. However, experimental data for dispersions of the 'fine' particles (ca. 90 µm) exhibit a small deviation from the

217

above trend. It is postulated that such particles carry less charge than that corresponding to their surface area. This may be attributed to depletion of a portion of the acquired charge due to "corona" and "spark" discharges between the charged particles having accumulated a critical value of high charge density which cannot be sustained. Furthermore, particle/particle interactions are more frequent in solids dispersions of very fine particles compared to dispersions of larger particles with the same solids fraction. This is because in the former case, there are more particles in the same dispersion volume thus increasing the opportunity for particle-particle arch discharges.

For conducting solids/air dispersions on the other hand, the effective dielectric constant of the dispersion is independent of the type of constituent materials. This is because the electric field within all conductors is zero. Furthermore, experimental data indicate that particle size has no appreciable effect on the measured capacitance. It is however noted that this study was limited to only two different size fractions of copper. Further investigations are required in order to establish the applicability of the above observation for a range of different size powders.

• The transducer's dimensions have a profound effect on the system's sensitivity. More specifically, a decrease in the separation distance between the two cylindrical electrodes results in an increase of the transducer's sensitivity. This is attributed to the increased polarisation of the suspended particles due to an increase of the applied electric field between the electrodes when the distance between them decreases. On the other hand, the length of the electrodes has no appreciable affect the transducer's sensitivity since the strength of the average electric field is independent of the electrode length (see equation 6.10).

• The transducer's baseline capacitance (zero solids concentration) is linearly proportional to the average surface temperature of the cylindrical electrodes. In order to account for this effect, a temperature coefficient, C_θ was experimentally determined. Interestingly, C_θ was found to be almost the same as the coefficient of

linear expansion of stainless steel (c.f. 0.0001/°C with 0.00012/°C) used for the construction of the capacitance transducer.

- For all solids-gas dispersions tested, relative humidity does not affect the effective dielectric constant of the dispersion. However, the baseline capacitance (Cp_{air}) although remains initially constant, rapidly increases in a linear manner upon further increase in humidity. This is due to the fact that water vapour behaves like a discrete phase which can be detected in the transducer's sensing volume only after reaching a minimum concentration. The corresponding threshold humidity depends on the transducer's dimensions. In the present study it has been found to be in the range 42 - 48%.

- Variations in the frequency of the applied electric field in the range 1-100 kHz has no effect on the effective dielectric constant of the solids/gas dispersion. This is because the selected frequency range (limited by the LCR meter) is not sufficiently large to affect the polarisation process. Previous studies (Hockey, 1972; Braithwaite et al., 1990) set a threshold value of 10^7 Hz (depending on the material) above which the dielectric constant of a material begins to decrease with further increase in frequency.

- Variations in the air conveying velocity (6.5-15 m/sec) as well as the measurement point along the conveying pipeline have no effect on ε_{eff} of the gas-solids dispersion. This indicates that within the ranges tested, the measured capacitance is independent on the spatial distribution of the suspended particles within the transducer's sensing volume which changes depending on the flow conditions (mainly conveying air velocity) prevailing in the pipeline. The fact that changes in the location of the measurement point along the conveying pipeline have no effect on the effective dielectric constant of the gas-solids dispersion, suggests that the maximum charge acquired by a particle of certain size due to triboelectrification, does not change along the conveying pipeline. Furthermore, it indicates that this maximum charge is reached at a very early stage since the first set of measurements were taken only 20 cm downstream of the solids feeding point.

7.2. Suggestions for Future Work

Prototype Development

So far, the results of this study have established the feasibility of operation of the capacitance transducer for monitoring particulate concentrations. Translation of the existing technology into a fully functional prototype for direct attachment onto automobile exhaust tailpipe will require:

- Extending the operation capability of the technique to fine particles particularly those in the range 0.1-10 μm. (see section 2.5). To achieve this, two main problems have to be tackled. First, requires the production of stable dispersions of the fine particles in a controllable manner. During the course of this work, several attempts were made to achieve this task using the existing experimental set up. However, such dispersions could not easily be pneumatically conveyed due to the distinctive flow characteristics of fine powders. Therefore, a new set-up has to be designed for the reproducible production of dispersions of fine particles where a representative sample may be drawn through the capacitance transducer. Second, the electrostatic charging for very fine particles is more prominent than for courser particles. This may result in violent discharges of the excess charge as well as recurrent interferences between the particles within the transducer's sensing volume and short-circuiting of the electrodes (Huang, 1986; Louge et al., 1990). This problem was observed during the present work with very fine insulating powders such as glass ballotini (0.1 <dp<50 μm and occasionally 90 μm) and was successfully dealt by increasing the relative humidity of the air above 40-50%. The effect of increased air humidity is to increase the thickness of the moisture layer present on (and possibly in) all surfaces, which will provide a sufficiently conductive path for charges to leak away (Jonassen, 1998). However, further work is required in order to fully understand such phenomenona as well as developing means of eliminating it using various means such as particle charge neutralisers (radioactive or field ionisation) or antistatic agents (Gibson, 1982; Jonassen, 1998).

- Investigation of the effect of temperature during the actual solids concentration measurements. In the present work, the effect of temperature on the baseline capacitance in the absence of particulates was studied. However, it is necessary to investigate the effect of temperature on the measured capacitance when the solids dispersion is drawn through the transducer, Cp_{sol} since temperature is expected to affect the dielectric constant of the dispersed particles and consequently, ε_{eff}. This will require the construction of the necessary equipment that will produce and maintain gas-solids dispersions at temperatures above 54 °C (as stipulated by international standards for measuring automotive particulates (e.g. ISO 3173, 1974).

- Determination and improvements in accuracy and sensitivity of the current system in terms of solids concentration measurements. This will require further research and experimentation in the design of the capacitance cell as well as its material of construction. For example, addition of two "guard" electrodes at either end of the capacitance probe oscillating at the same frequency as the measuring capacitor will eliminate fringing effects thus resulting in a better defined sensing volume thus improving performance (Reinecke et al., 1997; Huang, 1986).

In the present study, stainless steel electrodes are used. Von Hippel (1995) proposes aluminium as an alternative material for electrode construction as well as the use of metallurgical conditioning procedures that improve their operational characteristics. Furthermore, development of an automatic data acquisition system for on-line monitoring and analysis is expected to improve the accuracy of the results by allowing more rapid and frequent measurements.

Measurement of the average solids velocity in pneumatic conveying systems using cross-correlation techniques

For the flow of solids such as powdered or granular material flowing in pneumatic conveyors, there is a need for automatic, rugged field instruments for measuring average solids velocity.
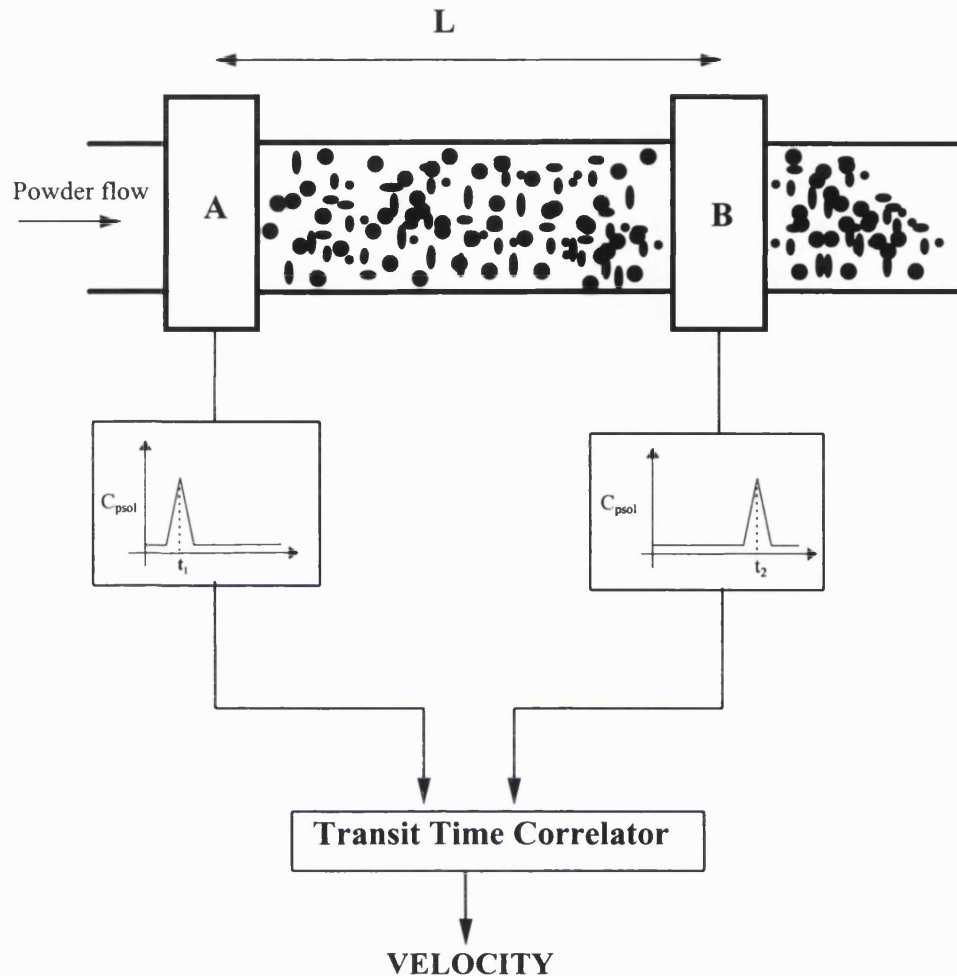
Figure 7.1. Schematic representation of a cross correlation system for measuring particle velocity.

The transit-time correlation method offers a good solution to this problem (Mesch et al., 1972; Rudinger, 1980; Schneider et al. 1982). This method is based on the observation that powder flow in a pneumatic conveyor exhibits local random variations in the concentration of the suspended solids. The latter is expected to result in fluctuations in the measured capacitance, which may for example be monitored using the present capacitance probe. Since these variations travel in a coherent form down the conveyor, it is possible to determine the powder velocity from the transit time of detecting the inherent flow variations between two capacitance transducers say A and, B axially spaced at a distance, L in the flow direction as depicted in figure 7.1. A special correlator is then required for cross-correlating the transducers' output signals and for automatically tracking the transit time. This method is very simple,

has a quick response, does not use moving parts and is independent of the air carrying velocity.

Solid/liquid or liquid/liquid systems

The use of the coaxial transducer in the present form for measuring component volumetric concentration in systems where the continuous phase is a liquid can prove to be a difficult task. This is because conductive liquids will cause short-circuiting of the capacitance transducer. An alternative design that will prevent direct contact of the sensor electrodes with the two-phase dispersion is required. In such a configuration, the outer electrode will be mounted outside an insulating pipe whereas the inner electrode will be coated with a thin layer of insulating material.

N O M E N C L A T U R E

C H A P T E R   3:

E	Electric field strength, V m^{-1}
V_{TE}	Velocity of charged particle, m sec^{-1}
Z	Particle electrical mobility, cm^2 V^{-1} sec^{-1}

C H A P T E R   4:

A	Surface area, m^2
a	Outside radius of the coaxial capacitor inner electrode, m
b	Inside radius of the coaxial capacitor outer electrode, m
C	Capacitance, F
Cp_{air}	Capacitance of pure air or baseline capacitance, F
Cp_{sol}	Capacitance of test solids-gas dispersion, F
C_U	Unknown capacitance to be measured, F
C_V	Variable capacitance, F
C_x	Measured capacitance in equation 4.1, F
d	Electrode separation distance in a parallel plate capacitor, m
De	Coaxial capacitor inter-electrode separation distance, m
E_{int}	Particle internal electric field, V m^{-1}
E_o	External applied electric field, V m^{-1}
I_1 , I_2	Electric currents, A
L	Length of cylindrical electrode, m
N	Number per unit volume
N_C	Constant of proportionality in equation 4.1
p	Dipole moment or elemental dipole, C m
P	Total dipole moment per unit volume, C m^2
P_{dis}	Total dipole moment per unit volume of solids dispersion, C m^2
p_o	Permanent dipole moment, C m

p_p	Particle individual dipole moment, C m
q	Electric charge, C
Q	Capacitor charge, C
Q_{pol}	Capacitor's extra charge due to polarisation of the medium, C
Q_{tot}	Capacitor total charge in equation 4.20, C
R_1, R_2	Resistance, Ω
r_s	Radius of a sphere, m
S_1	Closed surface in Gauss law, m^2
V	Electric potential difference or Voltage, Volt
V_E	Excitation voltage with frequency equal to the resonance, V

Greek Letters

α	Polarisability of a material, m^3
χ	Dielectric susceptibility
δ	Dipole separation distance, m
ε_1	Relative dielectric constant of a dielectric medium
ε_{dis}	Dielectric constant of solids dispersion
ε_{eff}	Effective dielectric constant
ε_o	Dielectric constant of vacuum, 8.85×10^{-12} Fm^{-1}
ε_r	Relative permitivity or dielectric constant of a material
ε_s	Particle dielectric constant
σ	Surface charge density, C m^{-2}
σ_{pol}	Surface polarisation charge density, C m^{-2}

CHAPTER 5:

C_{DS}	Particle discharge coefficient in equation 5.11
D	Conveying pipe diameter, m
d_p	Particle median mean diameter, m

d_S	Average diameter of conveying particles, m
F_{air}	Air volumetric flowrate, $m^3 s^{-1}$
f_S	Solids friction factor in equation 5.11
L_A	Particle acceleration length, m
μ_g	Gas kinematic viscosity, $kg\ m^{-1}\ sec^{-1}$
P	Static gas pressure in equation 5.2, Pa
Re	Reynolds number
Re_p	Particle Reynolds number
u_p	Particle velocity in equation 5.8, $m\ sec^{-1}$
u_τ	Friction velocity at the pipe wall in equation 5.3, $m\ sec^{-1}$
u_t	Particle terminal velocity, $m\ sec^{-1}$
V_m	Minimum carrying velocity of air, $m\ sec^{-1}$
V_{pu}	Particle pick-up velocity, $m\ sec^{-1}$
W_g	Gas mass flow rate, $kg\ sec^{-1}$
W_S	Solids mass flow rate, $kg\ sec^{-1}$

Greek Letters

ϕ_S	Suspension voidage
σ_{elec}	Electrical Conductivity, $\Omega^{-1} m^{-1}$
ρ_g	Carrying gas density, $kg\ m^{-3}$
ρ_s	Solids particles density, $kg\ m^{-3}$

CHAPTER 6:

f_s	Solids volume fraction
K	Dielectric proportionality constant in equation 6.1
E_{avg}	Average electric field in equations 6.9 and 6.10, $V\ m^{-1}$
ΔCp_a	Change in baseline capacitance Cp_{air} relative to the

	corresponding Cp_{air} value at 5% humidity, F
Cp_o	Capacitance at humidity transition point defined in figure 6.27, F
n	Proportionality coefficient in equation 6.11
R.H.	Relative humidity of air in equation 6.11, %
$Cp_{air(t=0)}$	Baseline capacitance at time, t = 0 at the reference mean electrode surface temperature , θ_o = 26±1 °C, F
$Cp_{air(t)}$	Baseline capacitance at time, t at the measured mean electrode surface temperature θ, F
t	Time, s
C_θ	Capacitor temperature coefficient in equation 6.14, $°C^{-1}$
$\Delta\theta$	Temperature interval in equation 6.14, °C
$Cp_{air(\theta 1)}$	Baseline capacitance at mean surface electrode temperatures, θ_1, F
$Cp_{air(\theta 2)}$	Baseline capacitance at mean surface electrode temperatures, θ_2, F

Greek Letters

α'	Intercept in equation 6.1
χ_{mix}	Electric susceptibility of the dispersion in equation 6.4
θ_{mean}	Mean surface temperature of the coaxial transducer's cylindrical electrodes defined in equation 6.12, °C
θ	Measured mean surface temperature of the coaxial transducer's cylindrical electrodes, °C
θ_{in}	Surface temperatures of the transducer's inner electrode, °C
θ_{out}	Surface temperatures of the transducer's outer electrode, °C
θ_o	Reference mean surface temperature of the coaxial transducer's cylindrical electrodes = 26±1 °C
ρ	Dispersed particle density, $kg\ m^{-3}$

227

R E F E R E N C E S

AEA Technology Plc., UK Smoke and Sulphur Dioxide Monitoring Network, Summary Report (1997-1998),1998.

Ahlvik,P., Ntziachristos,L., Keskinen, J., Virtanen, A., Real Time Measurements of Diesel Particle size Distribution with an ELPI, SAE Paper No: 980410, 1998. *Society of Automotive Engineers (SAE)*

Allen,T., Particle Size Measurement, 5th Edition, Chapman and Hall, 1997.

Anderson,H.R., Limb,E.S., Bland,J.M., Bower,J., Pence de Leon,A., Starchan,D.P., Health Effects of an Episode of NO_2 in London in December 1991, Thorax, 50, pp 1188-1193, 1995.

Anderson, J.C., Dielectrics, Chapman and Hall Ltd., London, 1964.

Bagyi, I., Personal communication, Dept. of Chemical Engineering, New Jersey Institute of Technology, USA, 1998.

Baird,C., Environmental Chemistry, W.H. Freeman & Co. N.York, 1995.

Baumgard, K.J., Johnson, J.H., The Effect of Low Sulphur Fuel and Cramic Particle Filter on Diesel Exhaust Particle Size Distributions, SAE, Paper No. 920566, 1992.

Beck, M. S., Drane, J., Plaskowski, A., Wainwright, N., Particle Velocity and Mass Flow in Pneumatic Conveyors, Powder Technology, Vol. 2., pp. 269-27, 1969b.

Beck, M.S., Wainwright, N., Flow-failure Detector for Powdered and Granular Materials, Control, January, 1969a.

Benarie, M.M., Atmospheric Pollution, Proceedings of the 12th International Colloquium, May 5-7, Paris, France, 1976.

Bolton,B., Electromagnetism and its Applications, Van Nostrand Reinhold Co.,1980.

Boothroyd, R.G., Flowing Gas-Solids Suspensions, Chapman and Hall Ltd., London, 1971.

Bosch GmbH, Automotive Handbook, 4th Edition, Germany, Oct. 1996.

Bottcher, C.J.F., Theory of Electric Polarisation, Volume 1. : Dielectrics in Static Fields, Elsevier Scientific Publishing Company, London, 1973.

Bower, J.S., The UK national Urban Air Monitoring Networks, Proceedings : Conference at the Environmental Change Research Centre, UCL, pp 21-27, September, 1994.

Braithwaite, N., Weaver, G., Electronic Materials, The Open University, Butterworths, UK, 1990.

Bretschneider, B., Kurfurst J., Air pPollution Control Technology, Elsevier, Amsterdam, 1987.

BS 1042, "Methods of Measurement of Fluid Flow in Closed Conduits., Section 1.1, 1981.

Buffle, J., Van Leeuwen, H.P., Environmental Particles, Volume 1, Lewis Publishers, London, 1992.

Burtscher, H., Siegmann, H.C., Photoemission for In situ Analysis of Partisulate Combustion Emissions, Water, Air, and Soil Pollution, Vol. 68, pp 125-136, 1993.

Butters, G., Plastic Pneumatic Conveying and Bulk Storage, Applied Science Publishers Ltd., UK, 1981.

Cabrejos, F.J., Klinzing, G. E., Dibble, M.L., Experimental Determination of Minimum Conveying Velocity of Solids Particles In Horizontal Pneumatic Transport, ASME, 5th Inernational Symposium, June, 1993.

Cabrejos, F.J., Klinzing, G. E., Pickup and Saltation Mechanisms of Solids Particles in Horizontal Pneumatic Transport, Powder Technology, 79, pp 173-186, 1994

Campanella, R.G., Kokan, M.J., A New Approach to Measuring Dilatancy in Saturated Sands, Geotechnical Testing Journal, GTJODJ, Vol. 16, No. 4, pp. 485-495, 1993.

Cimorelli, L., Evangelisti, R., The Application Of The Capacitance Method For Void Fraction Measurement In Bulk Boiling Conditions, International Journal of Heat and Mass Transfer, Vol. 10, p.p. 277-288 , 1967.

Clarke, A.G., Panagiotopoulou I., Optical and Chemical Properties of roadside Aerosols, Sci. Tot Environ, 59, pp 131-140, 1987.

Clayton, P., Davis, B.J., Jones, K., Jones, P., Toxic Organic Micro-pollutants in Urban Air, Warren Spring Laboratory, Report LR90(PA), Stevenage, UK, 1992.

Cohen, B.S., Hering, S.V., Air sampling Instruments for Evaluation of Atmospheric Contaminants, American Conference of Governmental Industrial Hygienists Inc., 8th Edition, 1995.

Colbeck, I., Physical and Chemical Properties of Aerosols, Blackie Academic and Professional, London, 1998.

Collier, A.R., Organic Emissions from Light-Duty Vehicles Diesel Engines, Proceedings : Conference at the Environmental Change Research Centre, UCL, September, 1994.

Couling, S., Measurements of Airborne Pollutants, Butterwoth Heinemann Ltd, UK, 1993.

Coulson, J.M., Richardson, J.F., Sinnott, R.K., Chemical Engineering: Design, Vol.6., Pergamon Press, 1991.

Dallavalle, J.M., Heating , Piping and Air-conditioning, November 1932, 639-641.

Davis, R.F., Engineering, Vol 140, p.p. 1, 1935.

Department of The Environment , (DTE), Digest of Environmental Protection and Water Statistics No14 1991, HMSO, London, 1992.

Department of the Environment, Transport and the Regions (DETR), Expert Panel on Air Quality Standards Report : Particles, 1998.

Department of the Environment, Transport and the Regions (DETR), Expert Panel on Air Quality Standards Report : Source Apportionment of Airborne Particulates Matter in the United Kingdom, UK, 1999.

Dockery, D.W., Pope, C.A., Xu, X., Spengler, J.D., Ware, J.H., Fay, M.E., Ferris, B.G., Speizer, F.E., An Association Between Air Pollution and Mortality in Six U.S. Cities, New England Journal of Medicine , 329, pp 1753-1759,1993.

Dotson, J.M., Holden, J.H., Seibert, C.B., Simons, H.P., and Schmidt, L.D., New Method Measures the Solid : Gas Ratio in High- Solid Flow, Chemical Engineering, p.p. 149 , October 1949.

Eggleston, H.S., Pollution in the Atmosphere: Future Emissions from the UK. Warren Spring Laboratory, Report LR 888. UK, 1992.

Elsom, D.M., Atmospheric Pollution : A Global Problem, Blackwell Publishers, UK, 1992.

Farrow, I.K., Cudworth, R.S., Savage, C.A, Simmonds, A.C., Legislated Emissions from Seven Diesel Vehicles from the Large Scale Survey (Report NO. LR931), Regulated Emissions from Three Gasoline Vehicles With Catalysts from the Large Scale Survey (Report No. LR 932), Regulated Emissions from Forty Gasoline Vehicles Without Catalysts from the Large Scale Survey (Report No ;LR 933), Warren Spring Laboratory, UK, 1993.

Fasching, G.E., Smith, N.S.Jr., A Capacitive System fir Three-Dimensional Imaging of Fluidised beds, Review of Scientific Instruments, 62 (9), p.p. 2243, 1991.

Faulkner, M.G., Dismukes, E.B., McDonald, J.R., Pontius, D.H., and Dean, D.H. Assessment of Diesel Particulate Control : Filters, Scrubbers, and Precipitators. EPA Report 600/7-79-232a, Alabama, 1979.

Fayed, M.E., Otten, L., Handbook of Powder Science and Technology, Van Nostrand Reinhold Company Inc., US, 1984.

Feynman, P.R., Leighton, B.R., Sands, M., The Feynman Lectures on Physics, Vol 2. Addison-Wesley Publishing Company Inc., 1964.

Frey, J.W., Corn, M., Physical and Chemical Characteristics of Particulates in Diesel Exhaust, American Industrial Hygiene Association Journal, Sep-Oct. 1967.

Frohlich, H., Theory of Dielectrics : Dielectric Constant and Dielectric Loss, Clarendon Press, Oxford, 1958.

Gaggeler, H.W., Baltenspreger, U., Emmenegger, M., Jost, D.T., Nageli, W., Applications of The Epiphaniometer to Environmental Aerosol Studies , Journal of Aerosol Science, Vol. 20, No 8, pp 1225-1228, 1989b.

Gaggeler, H.W., Baltenspreger, U., Emmenegger, M., Jost, D.T., Schmidt-Ott, A., Haller P., Hofmann, M., The Epiphaniometer A New Device For Continuous Aerosol Monitoring, Journal of Aerosol Science, Vol. 20, No 5, pp 557-564, 1989a.

Gajewski, J.B., Measuring Probes, heads and System for the Non-contact, Electrostatic Measurements of the Two-Phase Flow Parameters in Pneumatic Transport of Solids, Journal of Electrostatics, Vol. 32, p.p. 297-303, 1994.

Gard, E., Mayer, J.E., Morrical, B.D., Dienes, T., Fergenson, D.P., Prather, K.A., Real Time Analysis of Individual Atmospheric Aerosol Particles : Design and Performance of a Portable ATOFMS, Analytical Chemistry, Vol. 69, pp 4083-4091, 1997.

Geldart, D., Kelsey, J.R., The Use of Capacitance Probes in Gas Fluidised Beds, Powder Technology, Vol. 6., pp. 45-50, 1972.

Gibons, N., Electrostatics Hazards Associated With Powder Processing, International Conference on Charged Particles, Southampton, UK, 6-8 Sept. 1982.

Green, R.G., Kwan, H.K., John, R., Beck, M.S., A Low Cost Solids Flowmeter for Industrial Use, Journal of Physics, E: Scientific Instruments, Vol. 11, pp. 1005, 1978.

Greenwood, S.J., Coxon, J.E., Biddulph, T., Bennett J., An Investigation to Determine the Exhaust Particulate Size Distributions for Diesel, Petrol, and
Society of Automotive Engineers (SAE)
Compressed Natural Gas Fuelled Vehicles, SAE, Paper No: 961085, 1996.

Habibi, K., Characterisation of Particulate Lead in Vehicle Exhaust : Experimental Techniques, Environmental science and Technology, Vol. 4., No 3., pp.239, 1970.

Hamilton, R.S., Mansfield, T.A., Airborne Particulate Elemental Carbon: Sources, Transport and Contribution to Dark smoke and Soiling, Atmospheric Environment Vol. 23, pp 1591-1599, 1991.

Harrison, M.R., Perry, R., Handbook of Air Pollution Analysis, Chapman and Hall Ltd., 1986.

Harrison, R.M., Urban Air Pollution and Public Health, Proceedings : Conference at the Environmental Change Research Centre, UCL, September, 1994.

Harrop, P.J., Dielectrics, Butterworth and Co., London, 1972.

Heck, R.M., Farrauto, R.J., Catalytic Air Pollution Control: Commercial Technology, Van Nostrand Reinhold, 1995.

Hesketh, E.H., Fine Particles in Gaseous Media, Ann Arbor Science Publishers Inc., Michigan, 1977.

Hewlett Packard, Operational Manuals of HP 4263B LCR Meter and HP 16089B Kelvin Clip Leads, 1996.

Higgins, B.G., Francis, H.C., Yates, C.J., Warburton, C.J., Fletcher, A.M., Reid, J.A., Pickering, C., Woodcock, A.A., Effects of Air Pollution on Symptoms and Peak Expiratory Flow Measurements in Subjects with Obstructive Airways Disease, Thorax, 50, pp 149-155, 1995.

Hildemann, L.M., Markowski, G.R., Jones, M.C., Cass, G.R., Submicrometer Aerosol Mass Distributions Of Emissions from Boilers, Fireplaces, Automobiles, Diesel Trucks, and Meat-Cooking Operations, Aerosol Science and Technology Vol.14., pp. 138-152, 1991.

Hinds, W.C., Aerosol Technology : properties, behaviour and measurements of airborne particles, John Wiley and Sons, 1982.

Hockey, S.W., Fundamentals Electrostatics, Methuen Educational Ltd., UK, 1972.

Hodges.,L., Environmental Pollution, Holt, Rinehart & Winston, N.York, 1977.

Howitt, J.S., Particulate Control Technology for Light and Heavy Duty Powered Vehicles, Corning Glass Works, USA, 1987.

Huang, S.M., Capacitance Transducers for Concentration Measurement in Multi-component Flow Processes, PhD Thesis, UMIST, Manchester, 1986.

Huang, S.M., Plaskowski, A.B., Xie, C.G., Beck, M.S., Tomographic Imaging of Two Component Flow Using Capacitance Sensors, Journal of Physics E: Scientific Instruments, Vol. 22, pp. 172-177, 1989.

Huang, S.M., Scott, A.L., Green, R.G., Beck, M.S., Electronic Tansducers for Industrial Measurement of Low Value Capacitances, Journal Of Physics, E: Scientific Instruments, Vol. 21., p.p. 242-250, 1988.

Irons, G.A., Chang, J.G., Particle Fraction and Velocity Measurement in Gas-Powder Streams by Capacitance Transducers, International journal of Multiphase Flow, Vol. 9., No. 3, pp. 289-297, 1983.

ISO 10054, Internal Combustion Compression- Ignition Engines: Measurement Apparatus for Smoke from Engines Operating Under Steady-state Conditions-Filter Type Smokemeter, 1998.

ISO 3173, Road Vehicles: Apparatus for Measurement of Opacity of Exhaust Gas from Diesel Engines Operating Under Steady state Conditions, 1974.

ISO/DIS 11614, Reciprocating Internal Combustion Compression-Ignition Engines, Apparatus for Measurement of Opacity and for Determination of the Light Absorption Coefficient of Exhaust Gas, May 1994.

Jonassen, N., Electrostatics , International Thomson Publishing, 1998.

Jones, B.T., King, J.L., Powder Handling and Electrostatics, Lewis Publishers, US, 1991.

Jorgensen, R., Fan Engineering, Buffalo Forge Company, Buffalo, N. York, 1961.

Keith, L.H., Principles of Environmental Sampling, American Chemical Society III Series, US, 1996.

Keskinen, J., Pietarinen, K., Lehtimaki, M., Electrical Low Pressure Impactor, Journal of Aerosol Science, Vol. 23, No. 4., pp 353-360, 1992.

Kittelson, D.B., Megan, A., Winthrop, W.F., Final Report : Review of Diesel Particulate matter Sampling Methods, University of Minnesota, 1999.

Klinzing, G.E., Gas-Solid Transport, McGraw-Hill Inc., 1981.

Klinzing, G.E., Marcus, R.D., Rizk, F., Leung, L.S., Pneumatic Conveying of Solids: A Theoretical and Practical Approach, Chapman & Hall, UK, 1997.

Kouwenhoven, W.B., A Standard of Low Power Factor, Transactions of American Institute of Electrical engineers, pp. 521-536, June 1933.

Kraus, M.N., Pneumatic Conveying of Bulk Materials, McGraw-Hill Publications Co., N. York,1980.

Kunii, D., Levenspiel, O., Fluidisation Engineering, John Wiley & Sons Inc., 1969

Lanneau, K.P., Gas-Solids Contacting in Fluidised Beds, Transactions Institution of Chemical Engineers, Vol. 38, pp. 125-143, 1960.

Lardner, T.J., Archer, R.R., Mechanics of Solids : An Introduction, McGraw-Hill Inc, 1994.

Larson, S.M, Cass, G.R. and Gray, A.H., Atmospheric Carbon Particles and the Los Angeles Visibility Problem, Aerosol Science and Technology, 10, 118-130, 1989.

Lee, D.O, Regional Variations in Long-term Visibility Trends in the UK, 1962-1990, Geography, 79, pp 108-121, 1994.

Light, W., Air Pollution Control Engineering : Basic Calculations for Particulate Collection, M. Dekker, Inc., 1988.

Liu, B.Y.H., Fine Particles : Aerosol Generation, Measurement, Sampling and Analysis, Academic Press, Inc., N.York, 1976.

Lockhart, N.C., Snaith, J.W., Apparatus for Dielectric Measurement on Fluids and Dispersions, Journal of Physics E: Scientific Instruments, Vol. 11, pp. 1011-1014, 1978.

Loeb, L.B., Static Electrification, Berlin: Spriger, 1958.

London Scientific Services, London Air Pollution Monitoring Network, 4th Report, London, UK, 1989.

Louge, M.Y., Guarded Capacitance Probes For Measuring Particulate Concentration and Flow, US Patent No. : 5459406, 1995.

Louge, M.Y., Opie, M., Measurements Of Effective Dielectric Permitivity Of Suspensions, Powder Technology, Vol. 62, pp. 85-94, 1990.

Louge, M.Y., Tuccio, M., Lander, E., Connors, P., Capcitnace Measurements of the Volume Fraction and Velocity of Dielectric Solids Near Grounded Wall, Review of Scientific Instruments, Vol. 67, No. 5, pp. 1869-1877, 1996.

Louge, M.Y., Steiner, R., Keast, S.C., Decker, R., Dent, J., Schneebeli, M., Application of Capacitance Instrumentation to the Measurement of Density an Velocity of Flowing Snow, Cold Regions Science and Technology, Vol. 25, pp. 47-63, 1997.

Lundgen, D.A., Harris, F.S., Marlow, W.H., Lippman M., Clark, W.E., Durham, M.D., Aerosol Measurement, University of Florida Press, 1979.

Lynn, D.A., Air Pollution Threat and Response, GCE Technology Division Addison-Wesley, Publishing Company, Philippines, 1976

Mansfield,T., Sources o Building Soiling and a Review of the Stone Cleaning Industry 1991, International conference in Stone Cleaning, Edinburgh, 1992.

Marble, V., Rub, K.L., and Olson, B.A., DieselExhaust/ Mine Dust Virtual Impactor Personal Aerosol Sampler : Design, Calibration and Field Evaluation, Aerosol. Sci. Technol., Vol. 22 , pp.140-150, 1995.

Marchello, J.M., Gomezplata, A., Gas - Solids Handling in the Process Industries, Marcel Dekker Inc., 1976.

Marple V.A., Rudow, K.L., Behn, S.M., A Micro-orifice Uniform Deposit Impactor (MOUDI) : Description, Calibration and Use., Aerosol Science and Technology Vol. 14, pp 434-446, 1991.

Meredith, R.E., Tobias, C.W., Resistance To Potential Flow Through A Cubical Array Of Spheres, Journal Of Applied Physics, Vol. 31, No. 7, pp. 1270-1273, 1960.

Mesch, F., Kipphan, H., Solids Flow Measurement by Correlation Methods, Opto-Electronics, Vol. 4., p.p. 451-462, 1972.

Micrometrics, Operational Manual of AccuPyc 1330 Pycnometer, Part Number: 133-42801-01, Dec. 1989.

Morris, A.S. , Principles of Measurement and Instrumentation, Prentice Hall Int. Ltd, UK, 1993.

Morse, R.D., Ballou, C.O., The Uniformity of Fluidisation - Its Measurement and Use, Chemical Engineering Progress, Vol. 47, No. 4, pp. 199-204, 1951.

National Physical Laboratory (NPL), Standard Capacitors and their Accuracy in Practice, Ministry of Technology, London, 1969.

Nieuwenhuis, P., Wells P., Motor Vehicles in the Environment, John Wiley & Sons, UK, 1994.

Nightingale, C., Private communication, Dept. of Mechanical Engineering, UCL, 1999.

Nuttal, "Gummer unveils strategy for healthier air by 2005", Times, August 21, 1996.

Owen,P.R., Pneumatic transport, Journal of Fluid Mechanics, 39, 2, pp 407-432.

Pepelko, W., US Environmental Protection Agency, www. dieselnet.com, 1999.

Perry, R.H., Handbook of Chemical Engineer, 5th edition, McGraw-Hill Inc, N.York, 1973.

Pope, C.A., Thun, M.J., Namboodiri, N.M., Dockery, D.W., Evans, J.S., Speizer, F.E., Heath, C.W., Particulate Air Pollution as a Predictor of Mortality in A Prospective Study of U.S. Adults, Am J Respir Grit Care Med, 151,pp 669-674, 1995.

Preining, O., Global Atmospheric Chemical Change, Editors: Hewitt CN, Sturges WT, Elsevier Applied Science, London, 1993 .

Quality of Urban Air Review Group (QUARG): Airborne Particulate Matter in the UK: 3rd Report, 1996.

Regulated Emissions from Forty Gasoline Vehicles Without Catalysts from the Large Scale Survey (Report No. LR 933),

Reinecke, N., Mewes, D., Multielectrode Capacitance Sensors for the Visualisation of Transient Two-Phase Flows, Experimental Thermal and Fluid Science, Vol. 15, pp. 253-266, 1997.

Rhodes, M.J., Principles of Powder Technology, John Willey & Sons Ltd, W. Sussex, 1990.

Richards, C.W., Engineering Materials Science, Chapman & Hall Ltd., London, 1961.

Richards, J.C., The Storage and Recovery of Particulate Solids, The Institution Of Chemical Engineers, London, 1966.

Royal Commission of Environmental Pollution , 15th Report : Emissions from Heavy Duty Diesel vehicles, London, 1991.

Rudinger, G., Fundamentals of Gas-Particle Flow, Elsevier Scientific Publishing Co., US, 1980.

Sami, M., Abouelwafa, A., Kendall, J.E., The Use of Capacitance Sensors for Phase Percentage Determination in Multiphase Pipelines, IEEE Transactions on Instrumentation and Measurement, Vol. IM-29, No. 1, pp. 24-27, 1980.

Sauer, B.B., Stock, R., Lim, K.H., Harmon Ray, W., Polymer Latex Particle Size Measurement Through High Speed Dielectric Spectroscopy, Journal Of Applied Polymer Science, Vol. 39, p.p. 2419-2441, 1990.

Sawyer, R.F., University of California , Berkley, Lectures Series, University College London, 1997.

Scaife, B.K.P., Principles of Dielectrics, Oxford science Publications, 1989.

Schneider, G., Bernard W., Mesch, F., Capacitive Sensors For Solids Flow Measurement by Correlation Methods, ACTA IMEKO, Vol. 2., p.p. 187-193, 1982.

Schwela,D., Zali, O., Urban Traffic Pollution, E&FN Spon, London, 1999.

Scott, W.T., The Physics of Electricity and Magnetism, John Wiley & Sons, N. York, 1959.

Shamlou, P.A., Handling of Bulk Solids: Theory and Practice, Butterworth & Co. Ltd, UK, 1988.

Shinn, J.D., Timian, D.A., Morey, R.M., Mitchell, G., Antle, C.L., Hull, R., Development of a CPT Deployed Probe for In Situ Measurement of Volumetric soil Moisture Content and Electrical Resistivity, Field Analytical Chemistry and Technology, Vol. 2, No. 2., pp. 103-109, 1998.

Silva, P.J., Prather K.A., On line Characterisation of Individual Particles from Automobile Emissions, Environmental Science and Technology, Vol., 31, pp 3074-3080, 1997.

Silverman, L., Billings, C.E., Methods of Generating solid Aerosol, Journal of Air Pollution Control Association, Vol.6, pp. 76-83, 1956.

Simons, S.J.R., The Development of Non-Invasive Sensors for Monitoring Concentrated Sedimenting Suspensions, PhD Thisis, Manchester, 1991.

Singh, S., Electrostatics Hazards Associated With Powder Processing, International Conference on Charged Particles, Southampton, UK, 6-8 Sept. 1982.

Speizer, F.A., Studies of Acid Aerosols in Six Cities and in a new Multi-city Investigation: Design Issues, Environmental Health Perspectives, 79, pp 61-68, 1989.

Stoess, H.A., Pneumatic Conveying, John Willey & Sons, Inc., 1970.

Strauss, W., Air Pollution Control . Part III : Measuring and Monitoring Air Pollutants. A. Willey, N. York, 1978.

Sympatec GmbH, Helos Particle Size Analyser: Operation Manual, 1999.

Taylor, D.M., Secker, P.E., Industrial Electrostatics: Fundamentals and Measurements, John Wiley & Sons Inc., UK, 1994.

Terman, F.E., Radio Engineers Handbook, McGraw-Hill, London, 1950.

Tinga, W.R., Voss, W.A.G., Generalised Approach To Multiphase Dielectric Mixture Theory, Journal of Applied Physics, Vol. 44 , No. 9, pp. 3897-3902, 1973.

Turner, J.C.R., Two-Phase Conductivity: the Electrical Conductance of Liquid Fluidised Beds of Spheres, Chemical engineering Science, Vol. 31, pp. 487-492, 1976.

United Nations (U.N.): A Report of the United Nations Economic Commission for Europe: Fine Particulate Pollution , Pergamon Press, N.York, 1979.

U S Environmental Protection Agency (USEPA), Compilation of Air Pollutant Emissions Factors Volume II : Mobile Sources, Ann Arbor , USA, 1985.

van Vlack, L.H., Elements of Materials Science and Engineering, Addison-Wesley Publishing Company, USA, 1989.

von Hippel, A., Dielectric Materials and Applications, Artech House, 1995.

Walters, S., Griffiths, R.K., Ayres, J.G., Temporal Association Between Hospital Admissions for Asthma in Birmingham and Ambient Levels of Sulphur Dioxide and Smoke, Thorax, 49, pp 133-140, 1994.

Wang, S.C., Flagan, R.C., Scanning Electrical Mobility Spectrometer, Aerosol Science and Technology, Vol. 13, pp 230-240, 1990.

Willeke, K., Generation of Aerosol and Facilities for Exposure Experiments, Ann Arbor Science Publishers Inc., Michigan, 1980.

Williams, D.J., Milne, J.W., Quigley, S.M., and Roberts, D.B.. Particulate Emissions from "In-Use" Motor Vehicles-II. Diesel Vehicles. Atmospheric Environment, Vol. 23, No. 12, pp. 2647-2661, 1989.

Williams, R.A., Xie, C.G., Tomographic Techniques for Characterising Particulate Processes, Particle and Particle Systems Characterisation, Vol. 10, pp. 252-261, 1993.

Wind, M., Handbook of Electronic Measurements: Volume 1, Polytechnic Institute of Brooklyn, 1956.

Wolfgang, F.R., Hildenman, L.M., Mazurek, M.A., Cass, G.R., Simoneti, B.R.T., Sources of Fine Organic Aerosol 2. Noncatalyst and Catalyst Equipped Automobiles and Heavy Duty Tracks, Environmental Science Technology, 27, 636-651, 1993.

World Health Organisation , WHO , Selected Methods For Measuring Air Pollutants, Geneva, 1976.

World Health Organisation , WHO , Sulphur Oxides and Suspended Particulate Matter, Geneva, 1979.

World Health Organisation, WHO , Regional Office for Europe. Update and Revision of the Air Quality Guidelines for Europe. Meeting of the Working Group "classical" air Pollutants, Netherlands, October 1994, Copenhagen, 1995.

World Wide Fund for Nature (WWF), Current and Projected Global Warming Potential of Passenger Cars in the UK, UK, 1993.

www.aeat.co.uk/netcen/airqual/emissions/pm10.htm, 2000

www.aeat.co.uk/netcen/airqual/reports/smkso2/fig1.html, 2000

www.dieselnet.com, 2000

Xie, C.G., Huang, S.M., Hoyle, B.S., Thorn, R., Lenn, C., Snowden, D., Beck, M.S., Electrical Capacitance Tomography for Flow Imaging : System Model For Development of Reconstruction Algorithms and design of Primary Sensors. IEE Proceedings, Vol. 139, No. 1., p.p. 89, Feb. 1992.

Xie, C.G., Scott, A.L., Plaskowski, A., Beck, M.S., Design of Capacitance Electrodes for Concentration Measurement of Two Phase Flow, Measurement Science and Technology, Vol. 1, pp. 65-78, 1990.

Yuasa, Y., Kuno, H., Effects of an Efflux Tube on the Rate of Flow of Glass Beads from a Hopper, Powder Technology, Vol. 6., pp. 97-102, 1972.

Zenz, F.A., Othmer, D.F., Fluidisation and Fluid Particle Systems, Reinhold Publishing Corporation, N. York, 1960.

Appendix A

Electronic Circuits And Technical Specifications of the HP 4236B LCR Meter and HP 16089B Kelvin Clip Leads

HP 4236B LCR meter

HP 4236B LCR meter is a general purpose LCR meter designed for component evaluation on the production line as well as bench top applications. A brief description of the operating theory as well as the basic sections of the measurement circuit is given below followed by list of the general specifications of the meter (HP, 1996) .

Figure A.1 shows a simplified block diagram of the analog section of the meter. The measurement circuit is functionally divided into following sections:

The *Signal Source Section* generates the test signal applied to the unknown component, DUT. The frequency of the test signal is variable from 1 to 100 kHz. A microprocessor controlled frequency synthesiser is employed to generate these high resolution test signals. The output signal level, adjustable from 20 mV to 1 V, is adjusted using an attenuator. Figure A.2 shows a diagram of the signal source section. In addition to generating the test signal applied to the DUT, the reference signals for internal use are also generated in this section (HP, 1996).

The *Auto Balancing Bridge Section* balances the variable resistor current with the DUT current to maintain a zero potential at the low terminal. Figure A.3.a shows a simplified diagram of the bridge section. The detector D detects potential at the low

terminal and controls magnitude and phase of the oscillator, OSC 2 output so that the detected potential becomes zero. The actual balancing operation is made as shown in A.3.b when the bridge is "unbalanced", an error current is detected by an I-V converter, and a phase detector is used to separate the 0° and 90° vector components. The output signals of the phase detector are applied to the modulator to drive the 0° and 90° components signals. The resultant signal is amplified and fed back through variable resistor Rr to cancel the current though the DUT and hence no error current flows into I-V converter. The balancing operation is performed automatically over the full frequency range of 1 to 100 kHz (HP, 1996).

The *Vector Radio Detector Section* measures two vector voltages across the DUT (Edut) and variable resistor Rr (Err) series circuit as shown in figure A.4. Since the variable resistor value is known, measuring two voltages will give the inpendance vector Zx of the DUT by using

$$Zx = Rr \times (Edut / Err) \qquad (A\text{-}1)$$

Each vector voltage is separated into its 0° and 90° components by a phase detector and each component is measured using a dual-slope A to D converter. Either the Edut or Err signal is selected by selector S1 so that the Edut and Err signals follow identical paths to eliminate tracking error between the two signals (HP, 1996).

The general specifications of the HP 4236B LCR meter are:

Measurement range: 1 pF - 1F   Basic accuracy: 0.1%

Test signal level : 20 mV - 1 V (5 mV step)   Test frequency: 1,10,20,100 kHz

Measurement speed : 29 ms   Averaging: 1-256

High speed contact check function (5 ms)   Quick test recovery

Front end protection   Built in comparator

Operating ambient temperature, humidity and altitude range: 0 to 45 °C, < 95% RH @ 40 °C, 0 to 2000 m.

Dimensions (cm): 32 (W) by 10 (H) by 30 (D)   Weight: 4.5 kg

HP 16089B Kelvin Clip leads

The HP 16089B tested leads equipped with Kelvin clip connectors are essential in order to measure odd shaped capacitive components that otherwise cannot be measured with conventional test fixtures (HP, 1996). Their general specifications are:

Frequency range: DC to 100 kHz

Operating ambient temperature: 0 to 55 °C

Operating ambient humidity: < 95% RH @ 40 °C

Weight: 0.3 kg

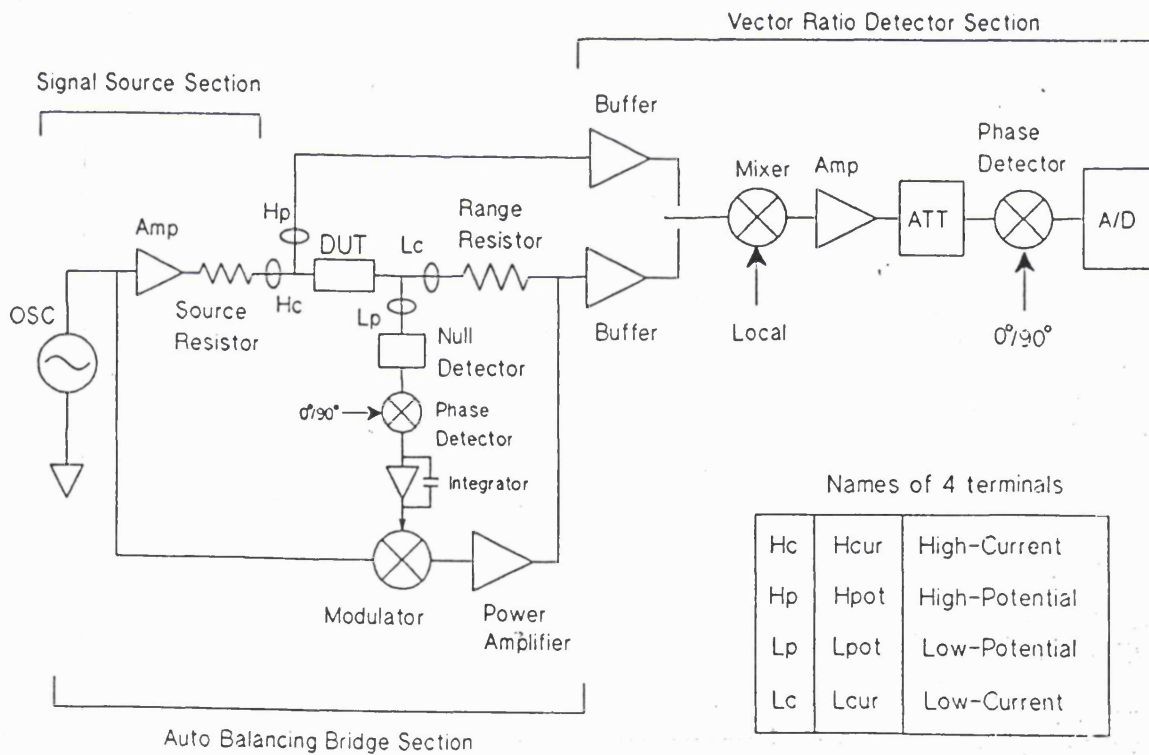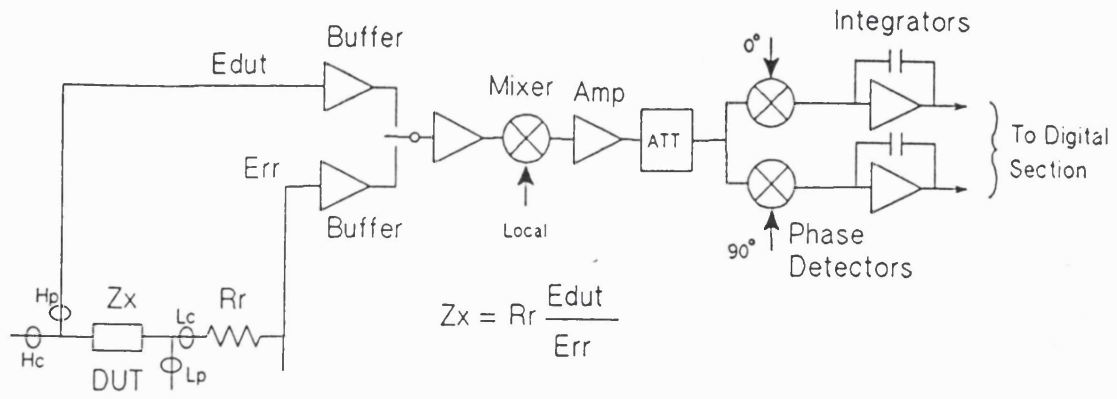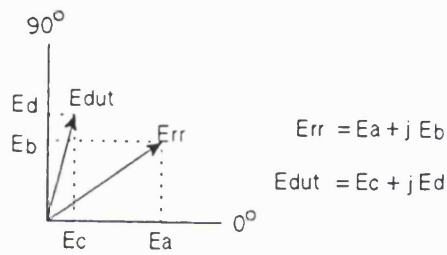Cable length: 0.95m

Minimum required separation distance between the capacitor's terminals: 0.3 cm

Figure A.1. Block diagram of the simplified analog-section for the HP 4236B LCR meter.

Figure A.2. Block diagram of the signal source section.

(a) Simplified Operation of the Auto Balancing Bridge

$$\frac{Edut}{Zx} + \frac{Err}{Rr} = 0$$

(b) Block Diagram

Figure A.3. Block diagram of the auto balancing bridge section.

245

Buffer

Edut

Err

Buffer

Mixer   Amp

ATT

Local

Integrators

0°

90°   Phase
Detectors

To Digital
Section

$$Zx = Rr \frac{Edut}{Err}$$

Hp

Zx

Lc   Rr

Hc

DUT   Lp

(a) Block Diagram

90°

Ed   Edut

Eb   Err

Ec   Ea

0°

$$Err = Ea + j\,Eb$$

$$Edut = Ec + j\,Ed$$

(b) Vector Ratio Calculation

Figure A.4. Block diagram of the vector ratio detector section.

246

A p p e n d i x   B

Particle Size Distribution Data for Powders Used in the

Experimental Study
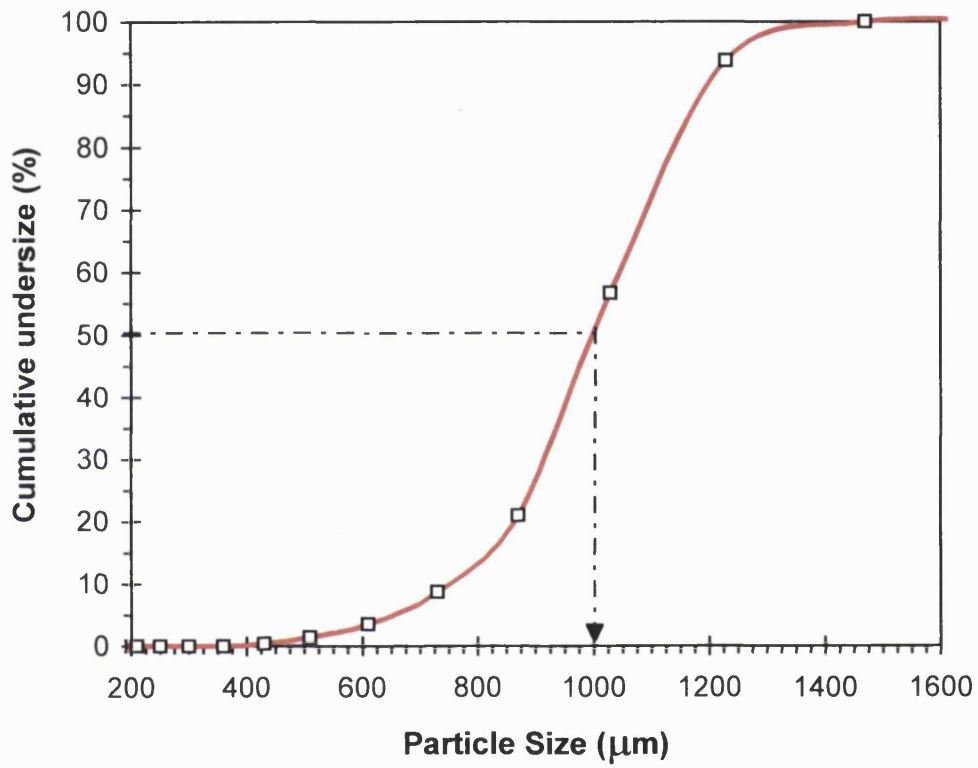
Figure B.1. Particle size distribution for glass ballotini particles ($\rho = 2500$ kg/m^3).
dp(median) = 1000 μm.
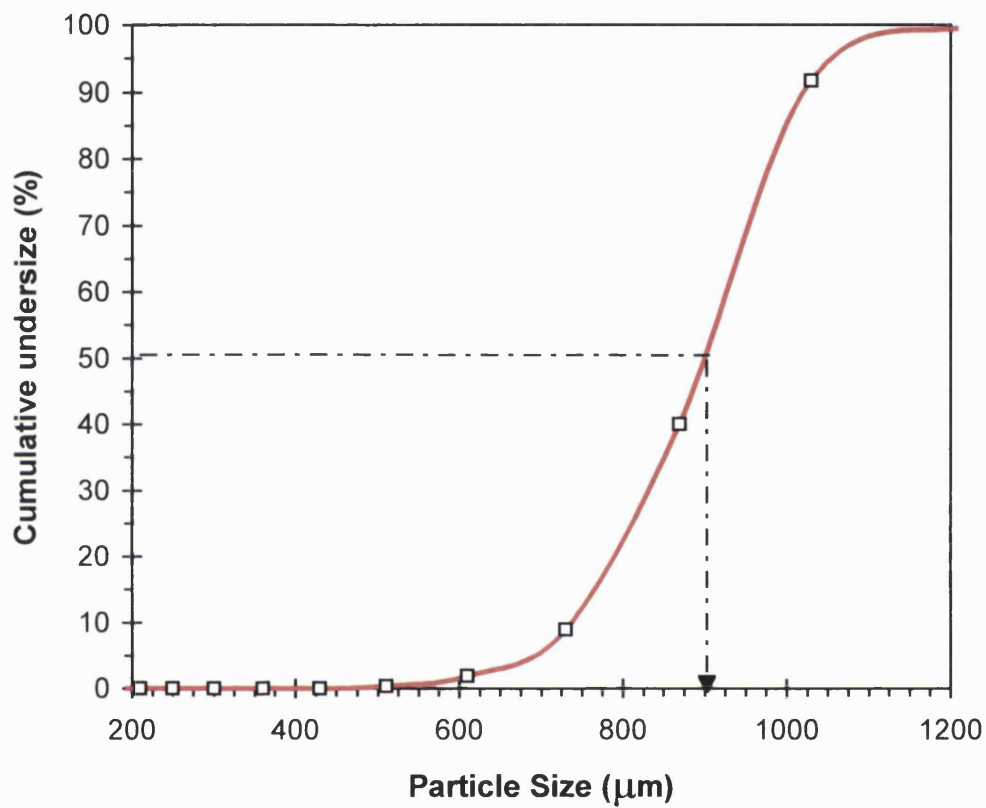
Figure B.2. Particle size distribution for glass ballotini particles (ρ = 2500 kg/m^3).
dp(median) = 900 μm.
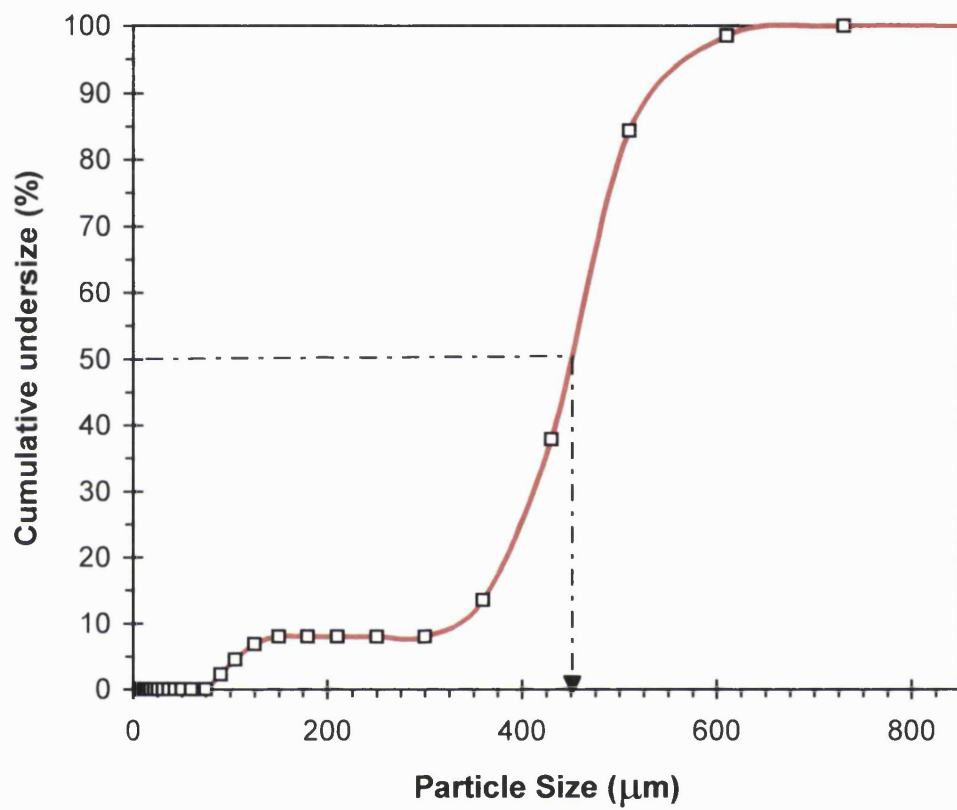
Figure B.3. Particle size distribution for glass ballotini particles (ρ = 2500 kg/m^3).
dp(median) = 450 μm.
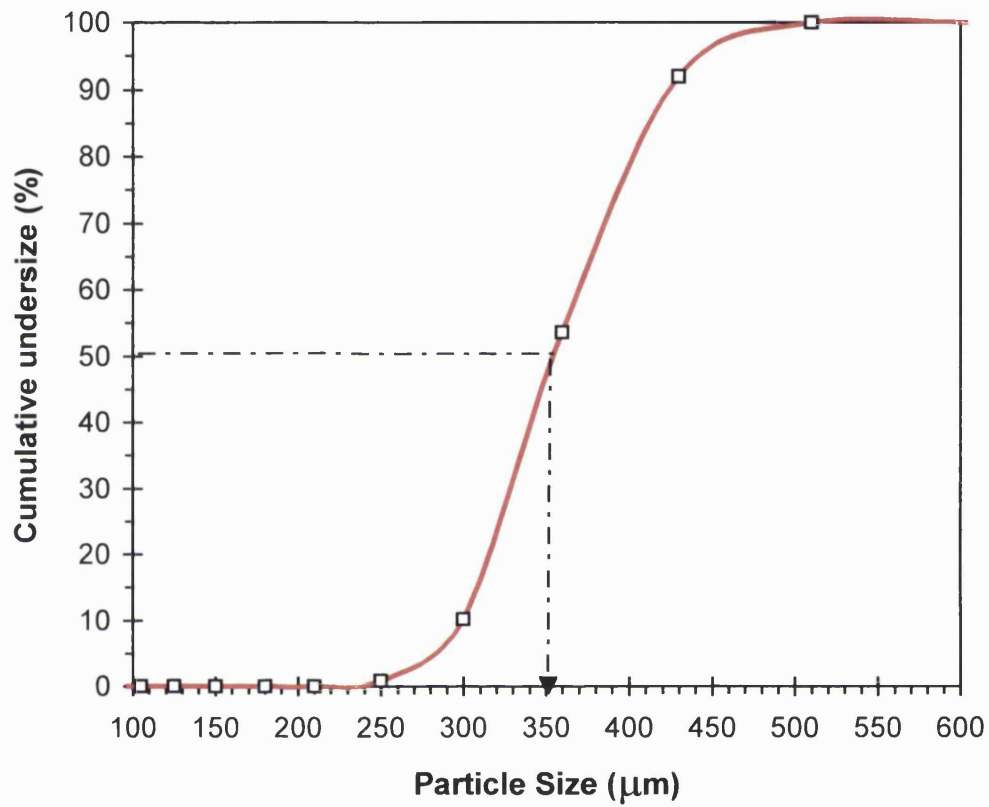
Figure B.4. Particle size distribution for glass ballotini particles (ρ = 2500 kg/m^3).

dp(median) = 350 μm.

252
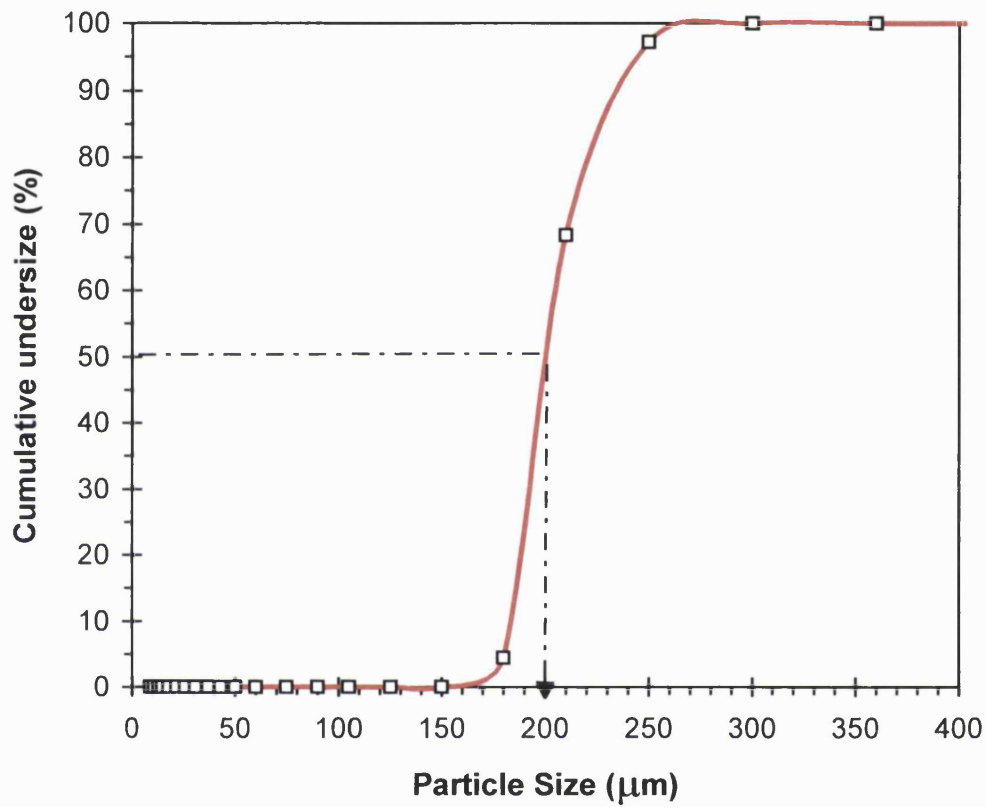
Figure B.5. Particle size distribution for glass ballotini particles (ρ = 2500 kg/m^3).
dp(median) = 200 μm.
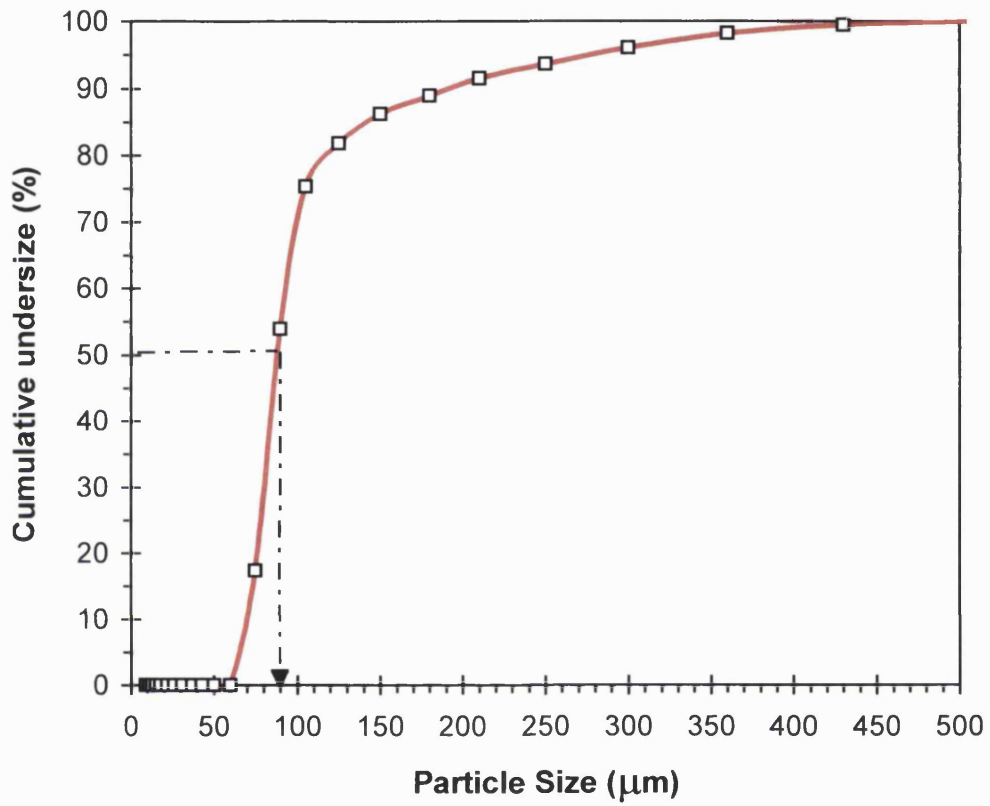
Figure B.6. Particle size distribution for glass ballotini particles (ρ = 2500 kg/m^3).
dp(median) = 90 μm.

254

Figure B.7. Particle size distribution for bronze particles (ρ = 8800 kg/m^3).

dp(median) = 125 μm.
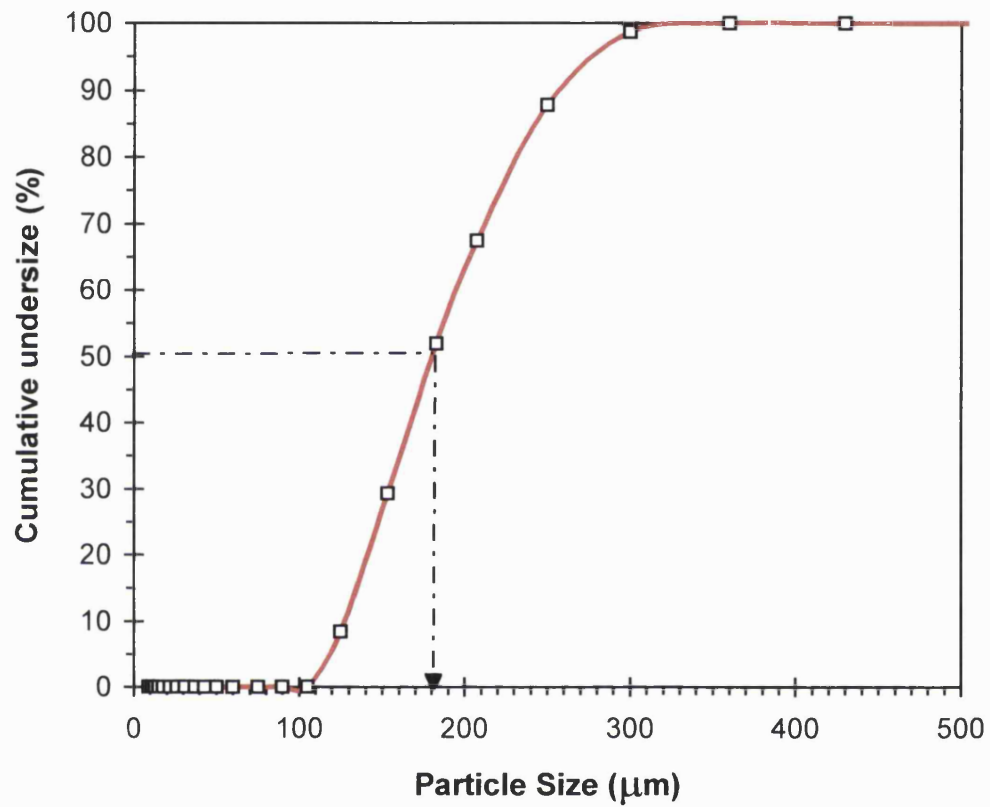
Figure B.8. Particle size distribution for copper I particles (ρ = 8810 kg/m^3).
dp(median) = 180 μm.
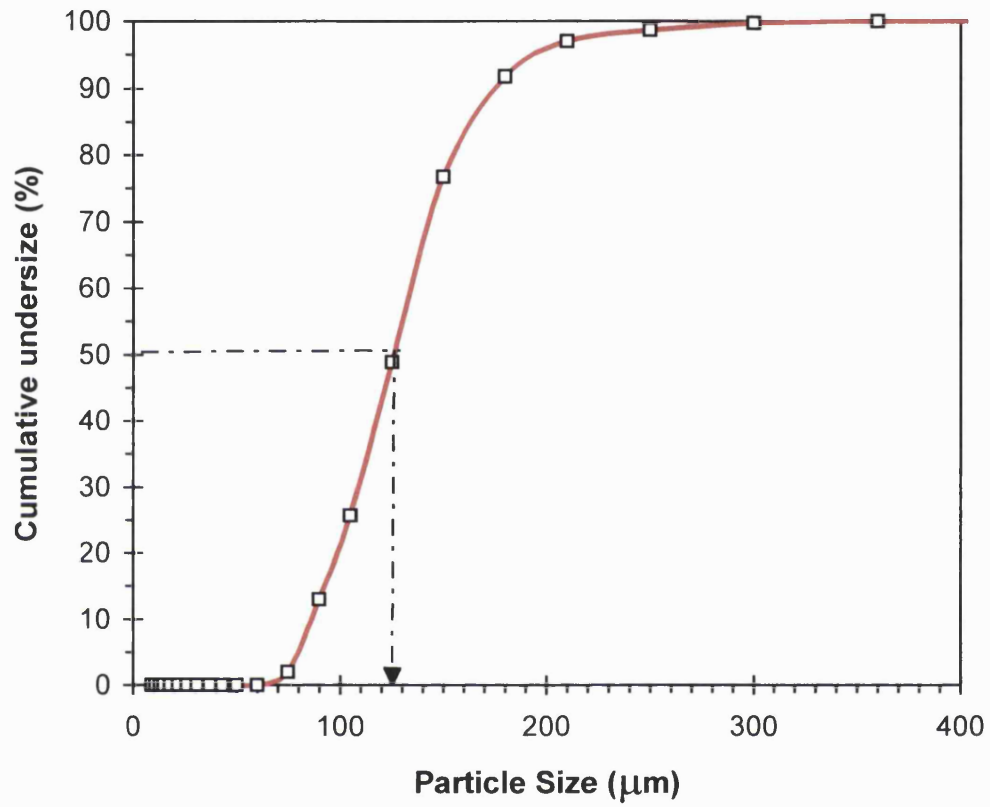
Figure B.9. Particle size distribution for copper II particles ($\rho = 8810$ kg/m^3).

dp(median) = 125 μm.
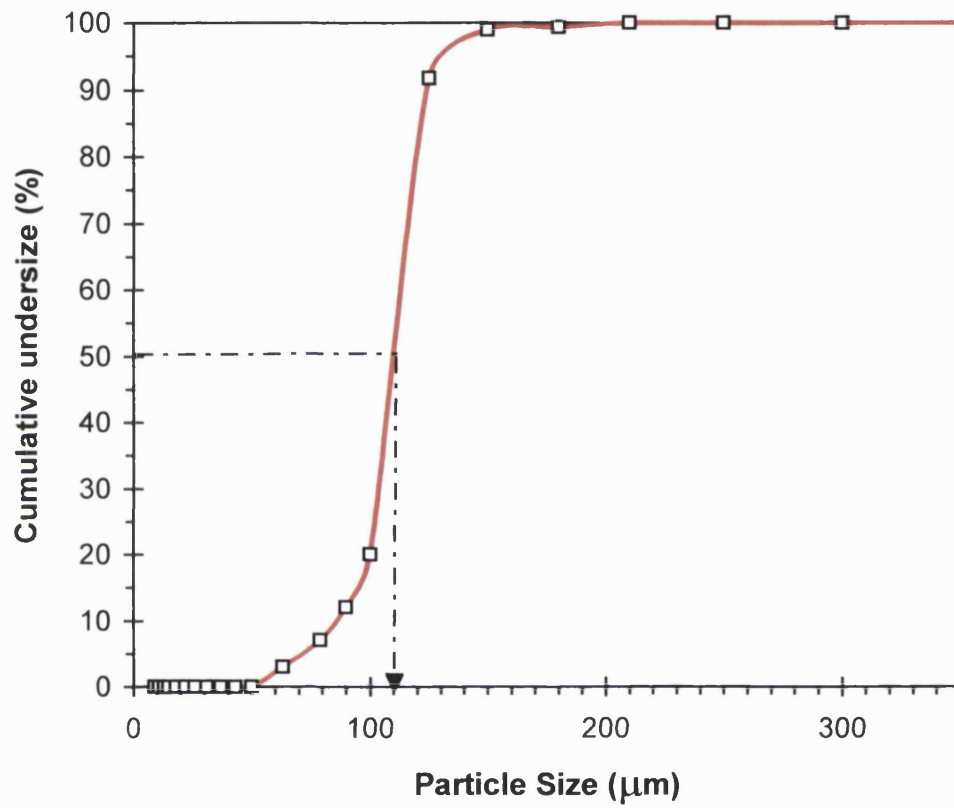
Figure B.10. Particle size distribution for steel particles (ρ = 7510 kg/m^3).

dp(median) = 110 μm.
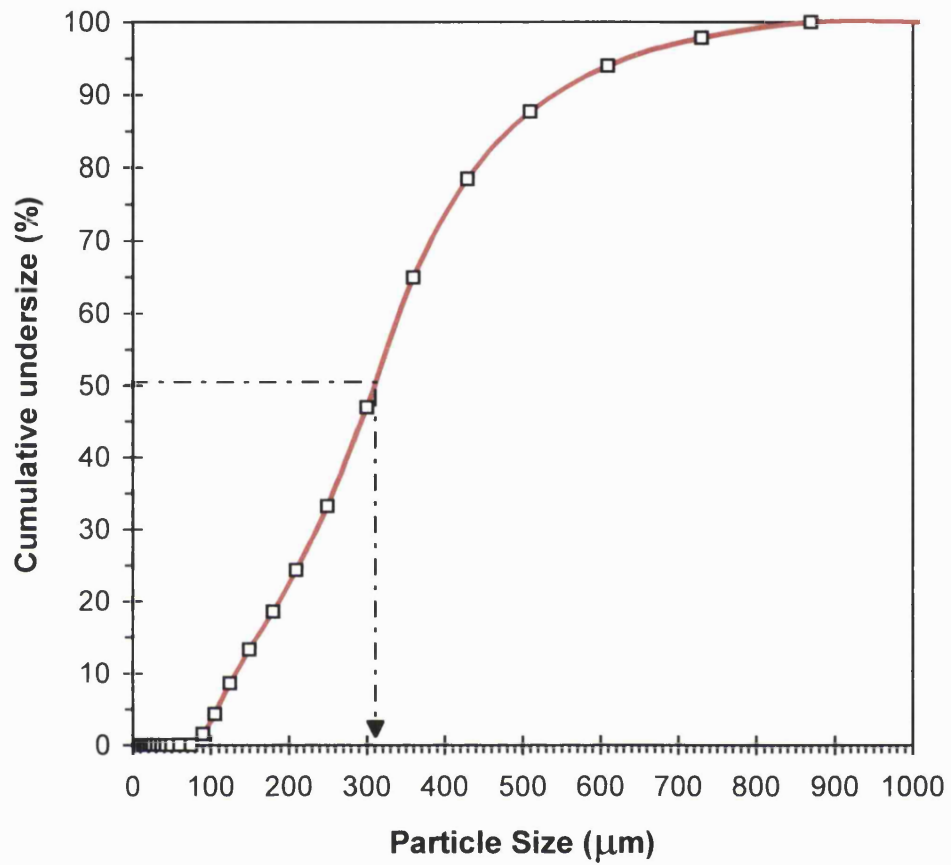
Figure B.11. Particle size distribution for quartz particles (ρ = 2200 kg/m^3).
dp(median) = 310 μm.